University at Buffalo
The State University of New York

Impedance-Matching Control Design for Shake-Table Testing and Model-in-the-Loop Simulations

by

Sai Sharath Parsi, Mettupalayam V. Sivaselvan and Andrew S. Whittaker

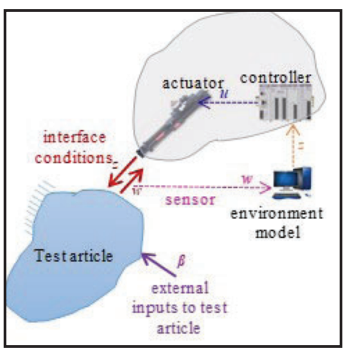

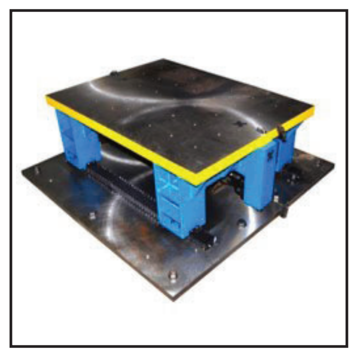

Technical Report MCEER-22-0003

September 30, 2022

MCEER: Earthquake Engineering to Extreme Events

Impedance-Matching Control Design for Shake-Table Testing and Model-in-the-Loop Simulations

By

Sai Sharath Parsi,[1] Mettupalayam V. Sivaselvan[2] and Andrew S. Whittaker[3]

Publication Date: September 30, 2022
Submittal Date: September 3, 2022

Technical Report MCEER-22-0003

Advanced Research Projects Agency – Energy
Award Number DE-AR0000978

1. Graduate Student, Department of Civil, Structural and Environmental Engineering, University at Buffalo, The State University of New York
2 Professor, Department of Civil, Structural and Environmental Engineering, University at Buffalo, The State University of New York
3 SUNY Distinguished Professor, Department of Civil, Structural and Environmental Engineering, University at Buffalo, The State University of New York

MCEER: Earthquake Engineering to Extreme Events
University at Buffalo, The State University of New York
212 Ketter Hall, Buffalo, NY 14260
buffalo.edu/mceer

Preface

MCEER was originally established by the National Science Foundation in 1986 at the University at Buffalo, The State University of New York, as the first National Center for Earthquake Engineering Research (NCEER). In 1998, it became known as the Multidisciplinary Center for Earthquake Engineering Research (MCEER), from which the current name, MCEER, evolved.

Comprising a consortium of researchers and industry partners from numerous disciplines and institutions throughout the United States, MCEER's mission expanded in the early 2000s from its original focus on earthquake engineering to one which addresses the technical and socioeconomic impacts of a variety of hazards, both natural and man-made, on critical infrastructure, facilities, and society.

Model-in-the-loop (MIL) simulation, often referred to as real-time hybrid simulation by earthquake engineers, involves physical testing of structures, systems, or components with the surrounding environment represented virtually using numerical models, and loading devices (actuators) controlled to simulate the effect of the virtual environment at the boundary of the test article. Designing actuator controls that enable accurate imitation of different virtual environments at the interface with the test article is key for executing MIL simulations. This report describes a novel approach for designing such actuator controls, namely, impedance matching control design for an example MIL configuration of 1D base-isolated equipment. Herein, a water-filled cylindrical vessel is the physical test article and a hydraulic shake table, driven by impedance-based MIL controls, is used to simulate acceleration boundary conditions corresponding to different seismic isolation systems at the base of the vessel. Key challenges associated with the design and implementation of MIL controls are identified and practical solutions are proposed. The utility of the solutions is evaluated by extensive testing, and a framework is developed to systematically design such tests as well as identify limitations.

ABSTRACT

Model-in-the-loop (MIL) simulations, commonly referred to as real-time hybrid simulations (RTHS) by earthquake engineers, involve physical testing of structures, systems, or components, with surrounding environment represented virtually using numerical models, and loading devices (actuators) controlled to simulate the effect of the virtual environment at the boundary of the test article. Such testing is appropriate only when the dynamics of the test article is significantly influenced by its interaction with the boundary environment and vice versa. Designing actuator controls that enable accurate imitation of different environments near the interface with the test article is key for executing MIL simulations. This report describes a novel approach for designing such actuator controls, namely, impedance-matching control design, which has been under development by Sivaselvan and his co-workers at the University at Buffalo over the past few years. A key feature of this approach is that actuators are not merely viewed as devices imposing prescribed boundary conditions on the test article but as dynamic systems that are controlled such that their force-motion behavior (impedance/admittance) near the interface with the test article matches closely that of the virtual environment it is representing: a fundamentally different viewpoint from the approaches traditionally used to implement MIL for earthquake-engineering applications.

To date, the impedance-matching approach has been validated predominantly for applications involving force-controlled actuator operation. This report advances this new school of thought by extending it to motion (acceleration)-controlled MIL applications. Specifically, challenges associated with the design and implementation of the impedance-matching MIL controls are identified, solutions are proposed, the usefulness of these solutions is evaluated by extensive testing, and a framework is developed to identify limitations of such testing. These advancements are demonstrated for an example MIL configuration of 1D base-isolated equipment, from conceptualization, through design, implementation, and extensive validation: a cradle-to-grave demonstration.

In this example configuration, a water-filled cylindrical vessel is the physical test article and a uniaxial hydraulic earthquake simulator (hereafter referred to as shake table), driven by impedance-based MIL controls, is used to impose acceleration boundary conditions corresponding to different seismic isolation systems at the base of the vessel. Experiments are performed for a diverse combination of virtual (isolators with different strength and stiffness properties) and physical systems (vessel with different water depths) to validate the MIL controls over a broad range of system parameters. Results show that the shake table

with the designed MIL controls is able to imitate different seismic isolation systems sufficiently accurately up to a frequency of 20 Hz, with reduced accuracy at higher frequencies.

The presentation in this report help: (i) understand nuances of actuator (shake table) control, particularly identifies the key roles of differential pressure (ΔP) feedback and controller sampling frequency in designing robust controls, (ii) extend the techniques of the impedance-matching approach for shake-table testing of structural systems, which involves tracking of a prescribed ground acceleration history at the base of a test article; the controls are shown effective for ground-motion tracking even when the mass of the test article is approximately three times that of the shake table: an outcome that is difficult to achieve using conventional tuning of shake tables, (iii) simplify implementation of MIL by using commercial off-the-shelf controller hardware, thereby making the technology readily deployable at many laboratories, and (iv) standardize (by-and-large) the process of control design, meaning that the controls can be designed and implemented, with few modifications, for a diverse combination of physical and virtual systems: adding significant value and scope to MIL testing.

ACKNOWLEDGMENTS

The work presented in this report was funded by the Advanced Research Projects Agency – Energy (ARPA-E), US Department of Energy, under Award Number DE-AR0000978. This financial support is gratefully acknowledged. The views and opinions of the authors expressed herein do not necessarily state or reflect those of the US Government or any agency thereof.

The experiments described in this report were conducted at the Structural Engineering and Earthquake Simulation Laboratory (SEESL) at the University at Buffalo. The authors acknowledge the technical support provided by the SEESL staff in executing experiments, including Messrs. Mark Pitman, Scot Weinreber, Robert Staniszewski, Christopher Budden, Michael Branch, Jeffrey Cizdziel, and Louis Moretta.

The authors thank the researchers and technical personnel who provided valuable inputs and ideas over the course of this research project, including Professor Michael C. Constantinou, Professor Teng Wu, Mr. Kaivalya Mitesh Lal, Mr. Faizan Ul-Haq Mir, and Dr. Ching Ching Yu of the University at Buffalo, Mr. Ian Sinclair of Hydraulic and Motor Control Inc, and Mr. Sean O'Banion of Delta Computer Systems Inc. The authors gratefully acknowledge the research contributions of past graduate students at the University at Buffalo, including Dr. Katerina Stefanaki, Dr. Vivek Bhasker Kote, and Dr. Mohit Verma, whose work has been of immense help in the development and progression of the impedance-matching pathway for MIL simulations.

TABLE OF CONTENTS

TABLE OF CONTENTS (CONT'D)

TABLE OF CONTENTS (CONT'D)

TABLE OF CONTENTS (CONT'D)

TABLE OF CONTENTS (CONT'D)

TABLE OF CONTENTS (CONT'D)

LIST OF FIGURES

LIST OF FIGURES (CONT'D)

LIST OF FIGURES (CONT'D)

LIST OF FIGURES (CONT'D)

LIST OF FIGURES (CONT'D)

LIST OF FIGURES (CONT'D)

LIST OF FIGURES (CONT'D)

LIST OF FIGURES (CONT'D)

LIST OF TABLES

SECTION 1
PREVIEW OF THE REPORT: SCOPE, OBJECTIVES, AND CONTRIBUTIONS

1.1 Section Prologue

The central theme in this report revolves around designing robust controls for executing model-in-the-loop (MIL) simulations using a novel approach, namely, impedance-matching control design, which has been under development at the University at Buffalo over the past few years (Stefanaki (2017), Kote (2019), Verma and Sivaselvan (2019), and Parsi (2022)). This report advances the impedance-matching MIL theory and develops a standardized framework to design and implement the MIL controls. This section articulates key concepts of the impedance-matching approach, leading to the understanding that the essence of this approach is contained in a single equation, namely, Equation 1-5. The main contributions of this research that led to the successful implementation of this equation are introduced in this first section and are described in much greater detail in the subsequent sections of this report.

Section 1.2 introduces the concept of MIL in a generic setting. Section 1.3 overviews the impedance-matching approach to MIL control design and identifies the main contributions of this report. Section 1.4 contrasts the impedance-matching approach with control algorithms that are traditionally used to implement MIL for earthquake-engineering applications, and highlights the fundamental differences and merits of this new approach. Sections 1.5 and 1.6 describe the scope and organization of the report, respectively.

1.2 Model-in-the-loop simulations

1.2.1 A generic setting

Model-in-the-loop (MIL) simulations, also referred to as real-time hybrid simulations (RTHS) by earthquake engineers, involve physical testing of structures/components for boundary conditions corresponding to one or more of their likely environments simulated by actuators. The environment here broadly corresponds to those elements surrounding the test article (e.g., interconnecting equipment, systems, support structures) that would significantly influence its response under operational or/and accidental loadings (e.g., earthquake, wind, fire). In conventional testing, the test article and its environment are physically constructed, so the loading conditions at the boundary interface are intrinsic, as shown in Figure 1.1b. In the figure, the variable z denotes the condition applied by the environment on the test article, referred to as the *controlled* condition. The *feedback* condition applied by the test article is denoted by w. External inputs to the environment and the test article are denoted by α_i and β_i, respectively.

Figure 1.1c is a conceptual illustration of a MIL simulation wherein the test article is physically constructed with the surrounding environment represented virtually using numerical models. Actuators are controlled to simulate loading conditions corresponding to the simulated environment (i.e., condition z) at the boundary of the test article. The key for executing MIL experiments is designing actuator controls such that the it reproduces the effect of the simulated environment on the test article.

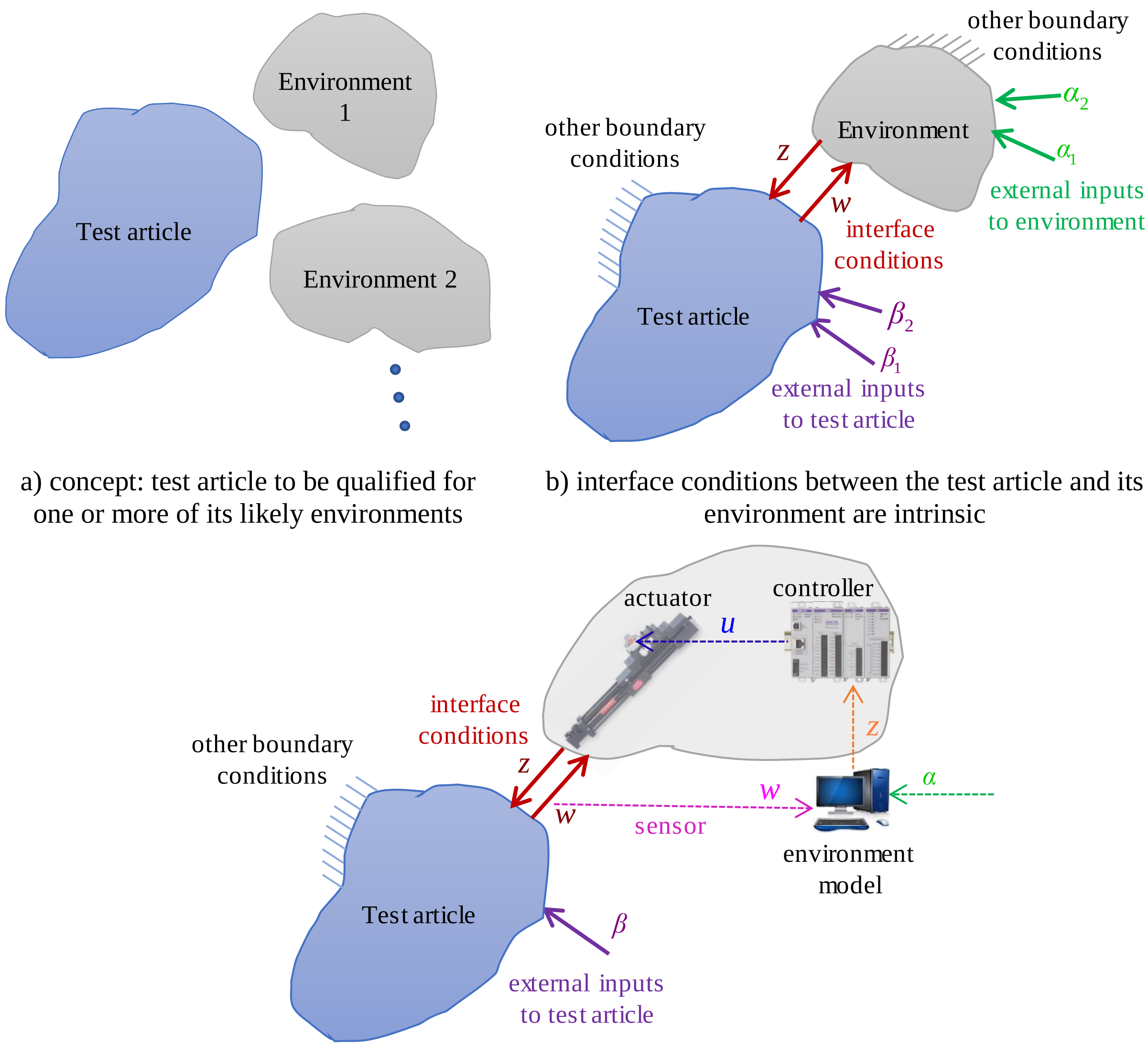

c) MIL testing; solid lines represent physical inputs and dashed lines represent electronic signals

Figure 1.1. Conceptual illustration of model-in-the-loop testing

Presented below are the tasks that are typically concurrently executed in a MIL simulation:

- The feedback condition, w, from the test article, is measured using sensors and input to the numerical model of the environment. This real-time feedback adds value to the experimentation only if the dynamics of the test article is significantly influenced by its environment and vice versa.
- Using the feedback measurement, w, and other inputs, α_{i}, the numerical model of the environment calculates the controlled boundary condition, z, that needs to be applied on the test article.
- A MIL controller uses the calculated z to generate an appropriate control signal, u, to the actuator such that it applies the condition z of the simulated environment on the test article. Put simply, the MIL controller commands the actuator to respond like the simulated environment.
- The test article responds to the applied condition z; the feedback condition, w, is measured and input to the environment model. In the presentation of this report, sensor dynamics are assumed to be sufficiently fast so as not to affect the MIL simulation

Typically, the boundary conditions, z and w, at the interface are taken as power-conjugate quantities, that is, $z^{\mathrm{T}}w$ has units of power (roughly). For example, if a component of z is force[1], then the corresponding component of w is velocity (or displacement/acceleration, and hence the use of word *roughly* above), and vice versa. Note that the notations (e.g., z, w, α, and β) identified in Figure 1.1c are used consistently throughout this report when referring to the respective interface variables and other inputs.

1.2.2 Motivating examples for MIL testing

Structural systems are often required to be qualified for multiple environments, specifically, when the surrounding environment is highly variable, and by extension, the boundary conditions on the test article are not well defined. The interest then is to qualify the test article not for a particular environment but for an envelope of conditions it is likely to encounter during its installation life. Model-in-the-loop testing is an efficient strategy in such cases because a test article can be qualified for multiple environments using one standardized setup by simply switching the properties (and type) of the environment in a computer model. Model-in-the-loop simulations are also beneficial (i) for conducting parametric studies aimed at

---

[1] Whether the test article controls force or motion at the interface depends on its impedance relative to its environment. This is easy to appreciate in a static condition, where the stiffer object controls motion and the more flexible object controls force.

characterizing the dynamic interaction between a test article and its environment and (ii) when a test article exhibits complex dynamics that is/are difficult to capture in a numerical simulation and has to be physically tested. Since only parts or subsystems are physically constructed in a MIL simulation, it leads to reduced costs and efficient use of laboratory space and time. Figure 1.2 presents a few examples from various disciplines (e.g., aerospace, earthquake) where MIL testing is deemed beneficial. Table 1.1 presents an overview of how MIL can be conceptualized for these example cases.

Docking of target and servicing satellites is a critical step for on-orbit servicing and needs to be thoroughly tested before deployment. It is challenging to physically reproduce the 6-DOF on-orbit dynamic motion of a satellite, importantly for the highly variable space conditions. In this MIL configuration, the satellite dynamics, including the microgravity condition, is represented virtually using a real-time model. The docking hardware is connected to the ends of the industrial robots which are maneuvered by the satellite model to physically simulate the docking process. The contact force and moment at the docking interface affecting the satellite dynamics are used as feedback to the satellite simulator in real time.

a) Example 1: industrial robots simulating maneuvering of docking satellites (Ma *et al.*, 2012)

The response of disconnect switch assemblies (and many other substation equipment) is significantly influenced by the configuration and properties of the support structure. A utility company can have several identical switches from the same manufacturer but installed on different support structures. Conducting a series of shake-table tests with multiple support structures is both time consuming and economically unrealistic. Model-in-the-loop simulations can be an effective alternative because the shake table can be controlled to imitate different support structures (represented virtually) at the base of the equipment. Such configurations could be used for virtually iterating the design of the support structure until acceptable performance of the equipment is achieved, a process commonly referred to as virtual prototyping.

b) Example 2: disconnect switch assemblies tested for multiple support structure configurations (Gunay *et al.*, 2015)

Figure 1.2. Examples of MIL testing

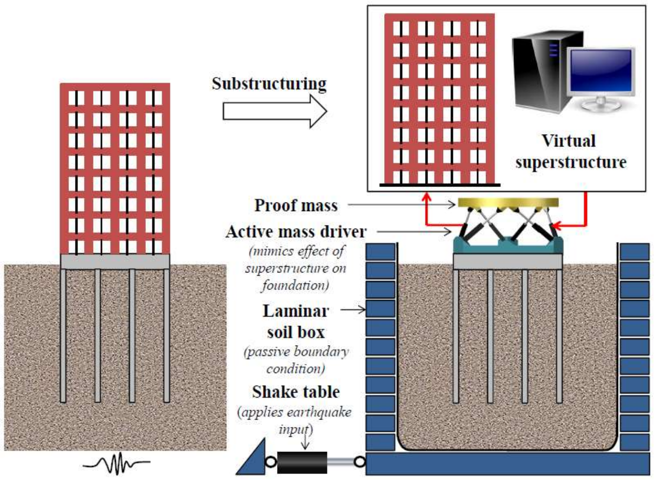

Large-scale laminar box testing of soil-foundation-structure systems is often limited by the laboratory space and sometimes can be cost-prohibitive. Although geotechnical centrifuges can be employed for small-scale testing, they are often challenging due to scaling and similitude requirements. Moreover, testing with different superstructures in a centrifuge would require fabricating a new model for every variant to be tested. By employing MIL, the superstructure is represented virtually, and its boundary conditions are simulated on the physical soil-foundation system using an active mass driver. This way, the effects of soil-structure interaction can be characterized for various superstructure models using a standardized setup. By virtually representing the superstructure, physical space requirements are reduced, and large foundation models can be tested.

c) Example 3: characterizing the effects of soil-foundation-structure interaction (Stefanaki, 2017)

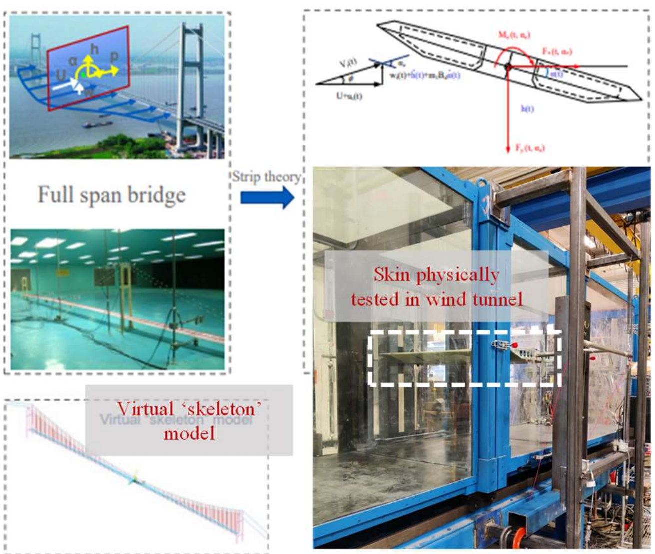

This example is an application of MIL for real-time aerodynamic testing of flexible bridges. Here, the skeleton of the bridge, characterizing the structural dynamics (e.g., mass, damping, and stiffness of the bridge), is represented numerically, while its skin, characterizing the aerodynamic and aeroelastic properties, is physically modeled in a wind tunnel. This configuration is advantageous compared to the conventional fully coupled (aerodynamics and structural dynamics) simulations in a computational fluid dynamic (CFD) environment because a wind tunnel can simulate aerodynamics more accurately than a CFD model. Aerodynamic inputs (gusts) are applied directly on the skin in the wind tunnel, while aeroelastic inputs (motions) are applied using actuators representing the bridge skeleton.

d) Example 4: real-time aerodynamic hybrid simulation for flexible bridges (Wu *et al.*, 2019)

Figure 1-2. Examples of MIL testing (cont'd)

Table 1.1. Overview of implementing MIL for the examples of Figure 1-2

	Example 1 Figure 1-2a (Ma *et al.*, 2012)	Example 2 Figure 1-2b (Gunay *et al.*, 2015)	Example 3 Figure 1-2c (Stefanaki, 2017)	Example 4 Figure 1-2d (Wu *et al.*, 2019)
Problem description	Dynamic maneuvering of two docking satellites	Seismic testing of disconnect switch assemblies for multiple support structures	Laminar box testing of soil-foundation-structure interaction	Real-time aerodynamic hybrid simulation of flexible bridges
Test article (physical)	Docking hardware	Disconnect switch assembly	Soil-foundation system	Skin of the bridge model
Environment (virtual)	Real-time satellite simulator	Support structure	Superstructure	Skeleton of the bridge model
Importance of interaction	Interface forces and moments during docking are critical for satellite maneuvering	Support structure dynamics affects the seismic performance of the disconnect switches	Liquefaction potential in the vicinity of the piles depends on superstructure dynamics	Structural dynamics affects aerodynamic forces (aeroelasticity)
Actuator system	Two 6DOF industrial robots simulating satellite maneuvering	Multi-axis shake table simulating support structure dynamics	Active mass driver (i.e., proof mass with hydraulic actuators) simulating superstructure dynamics	Three electromagnetic actuators simulating aeroelastic inputs
w (*feedback* condition from the test article)	Forces and moments at the docking interface	Forces and moments at the base of the test article	Acceleration of the foundation	Wind-induced forces and moments
z (*controlled* condition on the test article)	6DOF motion of the satellite	Displacement of the support structure	Force applied by the superstructure	Displacement applied to the physical skin model

1.3 Overview of the impedance-matching pathway for MIL simulations

1.3.1 Problem statement

The central problem in MIL testing is designing the controller in Figure 1.1c such that (i) the 'actuator + controller' system has the same effect on the test article as the environment would, and (ii) the actuator-test article feedback system is stable. The problem statement can thus be formulated as follows:

"What should the control input, u, to the actuator be, so that for the measured feedback condition w, the z applied by the actuator on the test article is equal to (or as close as possible to) that of the environment it is representing?"

For Example 3 of Table 1.1, which is a force-controlled MIL configuration, the above problem statement would be written as:

"What should the control input, u, to the actuator be, so that for the measured foundation acceleration, w, the force, z, applied by the active mass driver on the soil-foundation system is equal to (or as close as possible to) that of the superstructure model?"

and for Example 4 of Table 1.1, which is a displacement-controlled MIL configuration, would be:

"What should the control input, u, to the shake table be, so that for the measured wind-induced forces, w, the displacements, z, applied by the actuators on the skin of the bridge is equal to (or as close as possible to) that of the virtual skeleton of the bridge?"

1.3.2 Impedance-matching solution

The above problem statements directly motivate a solution based on 'impedance matching', that is, matching the force-motion behavior (impedance/admittance/immittance) of the actuator system at the interface with that of the simulated environment it is to represent. For ease of explaining the concept, the following two restrictions are considered:

Restriction 1: The actuator system is idealized as a linear system with two inputs: (i) control input, u, which is commanded by the user, and (ii) feedback input, w, which is physically applied by the test article. By linear superposition, the controlled condition, z_{as}, applied by the actuator can be written as:

$$z_{\text{as}} = H_{zu}^{\text{as}} u + H_{zw}^{\text{as}} w \tag{1-1}$$

where H_{zu}^{as} and H_{zw}^{as} are the frequency-domain transfer functions of the actuator system relating the output z with inputs u and w, respectively. The superscript ‘as’ in these transfer functions denotes actuator system. (The controlled and the feedback conditions at the test article-actuator interface can be multiaxial. Although the impedance-matching approach is presented in this report for the uniaxial case, the formulation holds for multiaxial cases too.)

Restriction 2: The environment is modeled as a linear system. One input to the environment is the real-time feedback measurement, w, from the test article. Additionally, the environment model may be subjected to other inputs, α (e.g., earthquake ground motion, wind induced force), which may be known a priori or computed in real time. The interface condition applied by the environment can be written as:

$$z_{\mathrm{vs}} = H_{z\alpha}^{\mathrm{vs}}\alpha + H_{zw}^{\mathrm{vs}}w \tag{1-2}$$

where $H_{z\alpha}^{\mathrm{vs}}$ and $H_{\mathrm{zw}}^{\mathrm{vs}}$ are the transfer functions of the environment relating the output z with inputs α and w, respectively. The superscript ‘vs’ in these transfer function denotes virtual system. Although the first restriction is retained throughout this report, the second restriction is relaxed when the environment exhibits nonlinear response in which case the implementation of MIL is slightly different, as will be discussed in Section 6. With the above two restrictions (i.e., linear actuator system and linear environment), the problem statement for MIL naturally presents a solution by equating Equations 1-1 and 1-2, $z_{\mathrm{as}} = z_{\mathrm{vs}}$:

$$H_{zu}^{\mathrm{as}}u + H_{zw}^{\mathrm{as}}w = H_{z\alpha}^{\mathrm{vs}}\alpha + H_{zw}^{\mathrm{vs}}w \tag{1-3}$$

From above, the control command to the actuator, u, can be calculated as:

$$u = \left(H_{zu}^{\mathrm{as}}\right)^{-1} H_{z\alpha}^{\mathrm{vs}}\alpha \quad + \left(H_{zu}^{\mathrm{as}}\right)^{-1}\left(H_{zw}^{\mathrm{vs}} - H_{zw}^{\mathrm{as}}\right)w \tag{1-4a}$$

$$u = H_{u\alpha}\alpha + H_{uw}w \tag{1-4b}$$

where $H_{u\alpha} = \left(H_{\mathrm{zu}}^{\mathrm{as}}\right)^{-1} H_{z\alpha}^{\mathrm{vs}}$ and $H_{uw} = \left(H_{\mathrm{zu}}^{\mathrm{as}}\right)^{-1}\left(H_{\mathrm{zw}}^{\mathrm{vs}} - H_{\mathrm{zw}}^{\mathrm{as}}\right)$. The above equation is referred to as MIL controller because it enables calculation of the required control input to the actuator that makes it apply the condition z of the simulated environment on the test article.

In the absence of the environmental input, α, Equation 1-4a implies matching the impedance of the controlled actuator system, $H_{zw}^{\mathrm{as}} + H_{zu}^{\mathrm{as}}H_{uw}$, with that of the simulated environment, H_{zw}^{vs}, by suitable controls, hence the approach is termed as ‘impedance matching’. Note that neither here nor in subsequent sections there is any restriction on the test article. The test article does not appear in the control equation and hence it can be of arbitrarily complex nature. Put differently, the MIL controller just utilizes the feedback measurement, w, from the test article and knowledge of the dynamics of the test article is not essential for control design – a prime distinction between the impedance-matching approach and the algorithms traditionally used to implement MIL for earthquake-engineering applications.

Contribution #1: The efficacy of impedance matching control design has been demonstrated by physical testing in Stefanaki and Sivaselvan (2018a) and Verma *et al.* (2019) for the cases where environment controls force at the interface (i.e., w is motion and z is force). In this report, the impedance-matching approach is extended to perform robustly in a motion (acceleration)-controlled setting and is validated by extensive testing. This reverse situation, where the environment controls motion (displacement/velocity/acceleration) at the interface, is more challenging in terms of control design and implementation, for the reasons that come into light in the subsequent sections of the report.

1.3.3 Significance of actuator system modeling

Equation 1-4b is the essence of the impedance-matching approach. However, the usefulness and fidelity of this equation relies on accurate characterization of the actuator transfer functions, H_{zu}^{as} and H_{zw}^{as}. The transfer function related to the control input, H_{zu}^{as}, is commonly used in control design and can be readily measured in the laboratory from the frequency-response measurements of the actuator system. However, the transfer function related to the feedback input, H_{zw}^{as}, is difficult to measure because w is a physical quantity and requires driving the actuator with another, much larger actuator, which is often not feasible in a laboratory setting. This limitation necessitates development of a physics-based model of the actuator system to obtain analytical expressions for H_{zu}^{as} and H_{zw}^{as}, for subsequent use in MIL-related calculations.

While it is well established that servo-hydraulic actuators exhibit nonlinear behavior, approximate linear models are preferred because (i) the nonlinear models typically include more parameters that are difficult to quantify and (ii) to simplify design and implementation of controls (e.g., Equation 1-4b). In this report, a robust mathematical model of a servo-controlled shake table (actuator system) is developed to obtain analytical expressions for H_{zu}^{as} and H_{zw}^{as}. The seminal work of Merritt (1967) is extended herein with some important additions that have shown the linear shake-table model of this report to be simple, beneficial, and highly robust from a control standpoint. Contributions #2, #3, and #4, described below, introduces these key additions. More details are presented in Section 4.

Contribution #2: Servovalve dynamics, an important contributor to the overall response of a servo-actuator system, is typically modeled as pure delay. This is both inaccurate when broad frequency ranges are considered and renders the use of classical transfer function tools inapplicable. Although researchers have developed physics-based servovalve models, their application is limited because manufacturers' technical specifications often do not provide sufficient information on many of the valve parameters, as required by these mathematical models. In this report, servovalve dynamics is characterized using an empirical transfer function deduced directly from the valve specifications. This transfer function, when integrated into the actuator model of Merritt (1967), is shown to predict the response of the servo-hydraulic shake table sufficiently accurately across a broad frequency range. Details are presented in Section 4.3.2.

Contribution #3: A gain on the differential pressure, ΔP, feedback has long been recognized as a stabilizing measure in hydraulic control. However, its benefit in terms of suppressing (damping) the oil-column resonance of the actuator, was not fully exploited. In contrast, it is demonstrated in this report that for a sufficiently large value of ΔP gain, the consequences of nonlinear effects in the actuator system are significantly reduced, and the system exhibits a response close to linear. This then allows for a linear model to predict the actuator response with high fidelity across a broad frequency range, and enables its use in designing the MIL controller. The exact dynamic effects of the ΔP feedback are analyzed theoretically in Section 4.4.3 and validated by experiments in Section 4.5.3.

Contribution #4: It is shown in this report that the bandwidth over which the ΔP gain is beneficial is severely limited by the controller sampling frequency, f_s, even if it is 100 times the oil-column frequency. This outcome is counter-intuitive, but an important consideration when using digital controllers with lower sampling rates, less than 2000 Hz (most commercial shake tables in the Unites States fall in this category). The exact dynamic effects of controller sampling rate on the actuator response are analyzed theoretically in Section 4.4.4 and validated by experiments in Section 4.5.3.

1.3.4 Need for approximations and consequent tradeoffs

The MIL controller of Equation 1-4b cannot be implemented, as-is, in real time as a state-space system because:

- The controller transfer functions, $H_{u\alpha}$ and H_{uw} are often non causal, that is, the order of the numerator is greater than the order of the denominator, making their state-space realization inapplicable and necessitates approximations[2].
- The analytical transfer functions of the actuator system, H_{zu}^{as} and H_{zw}^{as} are characterized based on a linear model (approximation) of a nonlinear system. Often, such linear models poorly represent actuator dynamics at high frequencies, thereby decreasing the fidelity of the MIL controller at high frequencies.
- Another reason for pursuing low controller response at high frequencies is because noise in the feedback measurement, w, is typically greater here. If $|H_{uw}w|$ is not sufficiently curtailed/reduced, noise in w propagates through the feedback system resulting in highly oscillatory response of the actuator, which is not desirable.

The above constraints are addressed in this report by approximating the MIL controller using lowpass filters, namely, $H_{\alpha}^{\text{filter}}$ and H_{w}^{filter}, as shown below:

$$u = \underbrace{\underbrace{H_{\alpha}^{\text{filter}}}_{\text{approximation}} \underbrace{\left(H_{zu}^{\text{as}}\right)^{-1} H_{z\alpha}^{\text{vs}}}_{H_{u\alpha}}}_{\text{approximated controller } H_{u\alpha}^{\text{approx}}} \alpha + \underbrace{\underbrace{H_{w}^{\text{filter}}}_{\text{approximation}} \underbrace{\left(H_{zu}^{\text{as}}\right)^{-1}\left(H_{zw}^{\text{vs}} - H_{zw}^{\text{as}}\right)}_{H_{uw}}}_{\text{approximated controller } H_{uw}^{\text{approx}}} w \tag{1-5}$$

In addition to the above constraints, stability of the actuator-test article feedback system is key for successful MIL simulations. In this report, stability of this coupled feedback system is assessed using the notion of passivity. A system is passive if it cannot generate more energy than what has been input to it. When two passive systems are interconnected, the feedback system is guaranteed to be stable (Brogliato *et al.*, 2007). Typically, most test articles are passive because they cannot generate energy. Therefore, the MIL feedback system will be stable if the controlled actuator is passive: an important constraint for designing the filters $H_{\alpha}^{\text{filter}}$ and H_{w}^{filter}. The advantage of enforcing passivity is that stability of the MIL feedback system can be ensured independent of knowledge of the dynamics of the test article – a key feature of the impedance-matching pathway to MIL. More details on passivity and how it impacts the filter design are presented in Section 9.

---

[2] The relative degree (order of the denominator polynomial minus order of the numerator polynomial) of H_{zu} is greater in a motion-controlled setting, that is, when z is motion and w is force. The greater the relative degree, the more the controller needs to be approximated, thus making motion-controlled (e.g., acceleration-controlled as considered in this report) MIL more challenging than force-controlled. Details are presented Section 6.

Contribution #5: This report describes a rational procedure for designing the controller filters, $H_{\alpha}^{\text{filter}}$ and H_{w}^{filter}, which is shown critical for successful implementation of the impedance-matching MIL. The process identifies explicitly that the filter design is a tradeoff between three design constraints, namely, (i) *performance:* accurate imitation of the VS impedance over a frequency range as broad as possible, (ii) *desired control effort:* low controller response at high frequencies, and (iii) *stability:* assessed using passivity of the controlled actuator system. The tradeoffs are made clearer in Section 6.4 (theoretically) and 9.4 (experimentally).

1.3.5 Time discretization and state-space implementation of MIL controller

After characterizing the actuator dynamics (H_{zu}^{as} and H_{zw}^{as}), the VS dynamics ($H_{z\alpha}^{\text{vs}}$ and H_{zw}^{vs}), and designing the filter approximations ($H_{\alpha}^{\text{filter}}$ and H_{w}^{filter}), the next step is to implement the MIL controller of Equation 1-5 in real time as a state-space system. The controller transfer functions, $H_{u\alpha}^{\text{approx}}$ and H_{uw}^{approx}, are discretized in time, and a state-space realization of this discretization is implemented as a simple mathematical code in a microcontroller (software driving the actuator). When the environment has nonlinear response, that is, when Restriction #2 (Equation 1-2) is relaxed, the implementation of MIL is slightly different, as will be discussed in Sections 6 and 7.

Contribution #6: Model-in-the-loop experiments are typically configured with two distinct controllers, one for hydraulic control (i.e., issuing electrical command to the actuator servovalve) and the other for performing MIL-related calculations (e.g., solving VS equations, implementing Equation 1-5). Such controllers, and their supporting infrastructure, are generally specific to one laboratory. In the MIL experiments described in this report, a single piece of commercial off-the-shelf hardware is used for both hydraulic control and executing MIL code, thus (i) minimizing the controller hardware, (ii) streamlining implementation, and importantly (iii) making the technology readily deployable at many laboratories. Section 7 discusses the aspects related to the implementation of MIL controller.

1.3.6 Application of MIL controller for tracking a prescribed input motion

In the above subsections, the MIL controller is formulated for the actuator to imitate loading conditions of the simulated environment near the test article. There are some special applications wherein the actuator is required to apply a prescribed input, α, as-is, on the test article without any virtual system in the loop. As an example, in shake-table testing, actuators are controlled to directly impose a prescribed ground acceleration motion at the base of the test article. The MIL controller of Equation 1-5 can be used for such applications by considering a virtual environment with zero impedance (i.e., infinite stiffness, meaning $H_{z\alpha}^{\mathrm{vs}} = 1$ and $H_{zw}^{\mathrm{vs}} = 0$). The controller equation can be rewritten as:

$$u = \underbrace{H_{\alpha}^{\mathrm{filter}} \left(H_{zu}^{\mathrm{as}} \right)^{-1} \alpha}_{u_{\alpha} = H_{u\alpha}^{\mathrm{approx}} \alpha} - \underbrace{H_{\mathrm{w}}^{\mathrm{filter}} H_{\mathrm{zw}}^{\mathrm{as}} \left(H_{zu}^{\mathrm{as}} \right)^{-1} w}_{u_{w} = H_{uw}^{\mathrm{approx}} w} \tag{1-6}$$

The first component, u_{α}, is the control input required to drive the actuator to apply prescribed α in the absence of the test article. The second component, u_{w}, compensates for the interaction between the test article and the actuator system, and ensures tracking of α. The heavier the test article, the greater the interaction, and the greater the required compensation, u_{w}.

Contribution #7: Equation 1-6 is a special case of MIL representing a zero-impedance environment, so that the techniques of the impedance-matching control (i.e., measuring the test article's reaction and accordingly adjusting the control command to the actuator through the term u_{w}) can be applied for controlling shake tables. This way of shake-table control is particularly useful when the mass of the test article is comparable or greater than that of the shake table, as will be demonstrated in Section 8.

1.4 Historical context of MIL in the field of earthquake engineering

Within the field of earthquake engineering, model-in-the-loop testing originated as a substructuring strategy, that is, partitioning of structural systems into physical and numerical components. The physical substructure was viewed as an 'experimental finite element', meaning replacing one or more elements of a finite element model with physical elements. Control systems were therefore designed based on applying a target displacement on the test article with restoring force as the feedback, similar to how a finite element is implemented. Figure 1.3a illustrates a conceptual framework of how MIL is traditionally implemented in earthquake-engineering applications, and this has been the core of most studies in the literature. Principally, the 'actuator + test article' is viewed as a combined system that needs to be controlled to track a target displacement command of the environment. The emphasis was therefore on designing tracking controllers. However, actuators, like any other dynamic system, cannot track a reference command accurately across all frequencies. Inaccurate tracking, if not properly accounted for, can result in instabilities, particularly when the test article is lightly damped (e.g., Figure 1.2b). Often, *compensators* are used to address issues related to actuator dynamics, and by extension, compensate for inaccurate tracking.

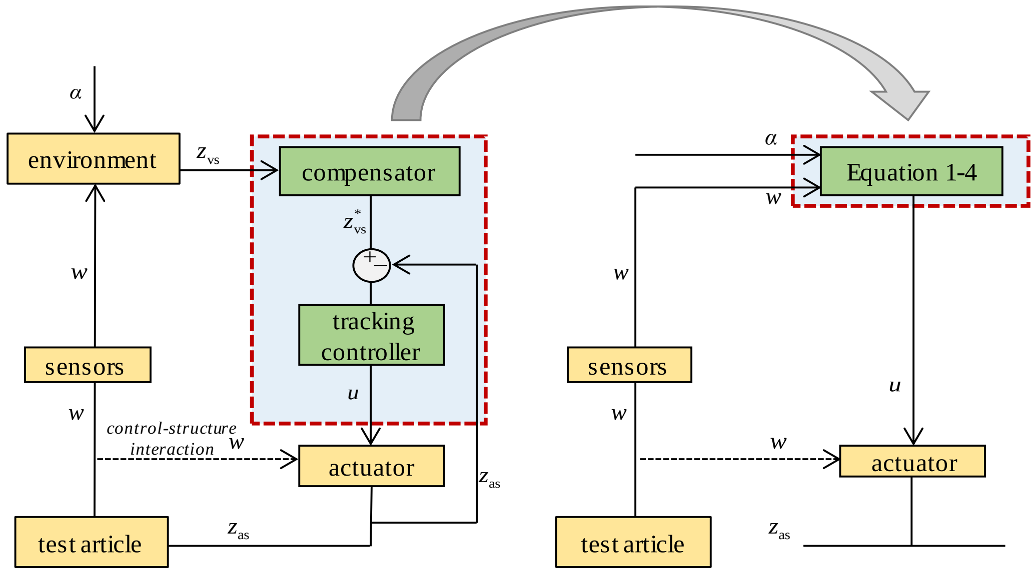

a) conventional approach b) impedance-matching approach

Figure 1.3. Contrasting conventional and the impedance-matching approach to MIL

Another key challenge in MIL testing is the physical feedback between the test article and the actuator system, as indicated by the dashed black line. This physical feedback is inevitable and becomes significant when the inertia of the two systems (i.e., actuator and the test article) is comparable. In the conventional framework of Figure 1.3a, the actuator + test article is viewed as a coupled system. As a result, the force/displacement feedback applied by the test article appears in the path of the displacement/force tracking controller, thus making the knowledge of the dynamics of the test article (i.e., a model of the test article+actuator system) essential for control design. This feedback interaction between the test article and the tracking controller, commonly referred to as control-structure interaction in the literature, makes it difficult to implement MIL for complex test articles (e.g., Figure 1.2) because the dynamics of such systems is not well characterized, which is the very reason they are physically tested. Even if the dynamics of the test article is known a priori, the framework of Figure 1.3a warrant tuning the parameters (gains) of the tracking controller for every test article: major challenge in shake-table testing. Approaching MIL along the lines of tracking controllers, compensators, and specialized time-integration schemes has restricted its application to relatively simple configurations: by contrast, the impedance-matching approach (i) decouples the test article from the control design (see Equation 1-5), (ii) explicitly compensates for the feedback interaction between the test article and the actuator system through the term H_{uw}^{st}, and (iii) simplifies implementation of MIL by replacing the complex blocks of tracking controllers and compensators shown in Figure 1.3a with a few lines of mathematical code.

1.5 Scope of the report and key outcomes

This report is a cradle-to-grave demonstration of the impedance-matching approach, in a motion-controlled setting for a 1D base-isolated equipment. In this demonstration, a fluid-filled cylindrical vessel is the test article and a seismic isolation system at the base, including the basemat, as enclosed by the dashed red lines in Figure 1.4a, constitutes the environment, referred to as virtual system. Herein, the external input, α, to the VS is the unidirectional ground acceleration, denoted by a_g hereafter. In the MIL setup of Figure 1.4b, a uniaxial hydraulic shake table is controlled to imitate the target acceleration of the VS basemat, z_{vs}, at the base of the test article. The reaction force, w, from the vessel is measured using load cells for subsequent use in MIL-related computations.

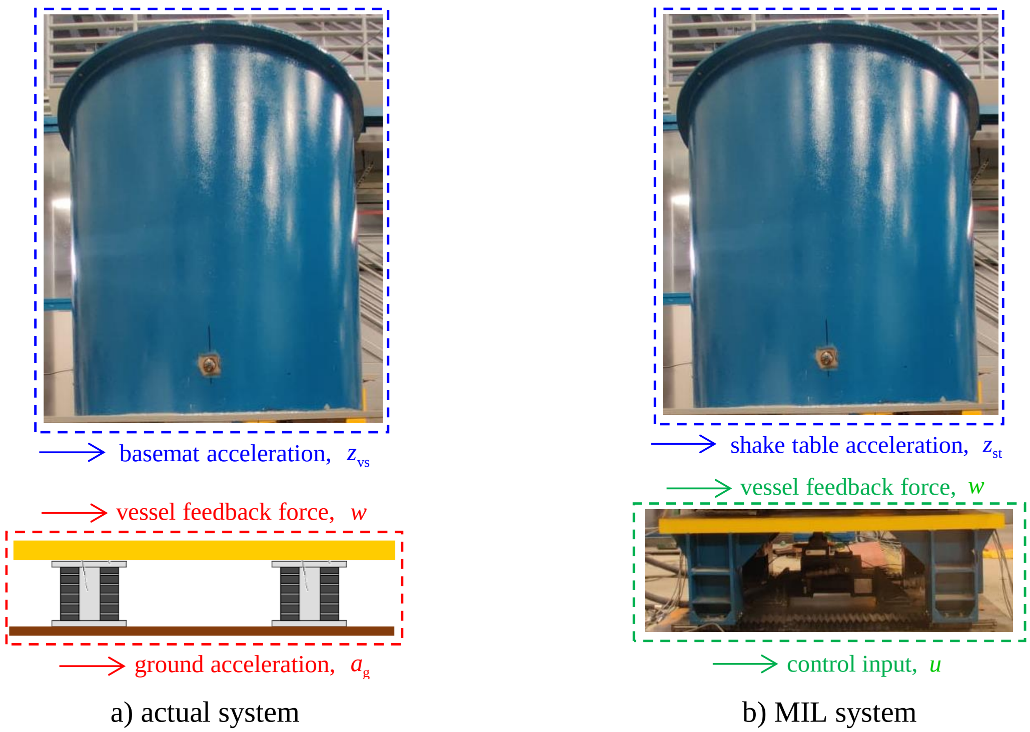

Figure 1.4. MIL conceptualization for 1D base-isolated equipment

Three types of seismic isolation systems are considered in the VS: linear spring-damper (SD) system, and nonlinear lead-rubber (LR) and Friction Pendulum (FP) systems. For the linear SD systems, the implementation of the impedance-matching MIL is straightforward, as discussed in Section 1.3 For the nonlinear LR and FP systems, an alternate implementation is discussed in Section 5. In both cases, the goal is to design a controller by making the impedance of the shake table match, as closely as possible, with that of the isolation system it is to represent.

The MIL experiments described in this report utilizes a digital motion controller hardware from Delta Computer Systems, Model RMC75E (Delta, 2020a) for hydraulic control and execution of MIL programs. Figure 1.5 is an illustration of this feedback interaction loop in the MIL experiments.

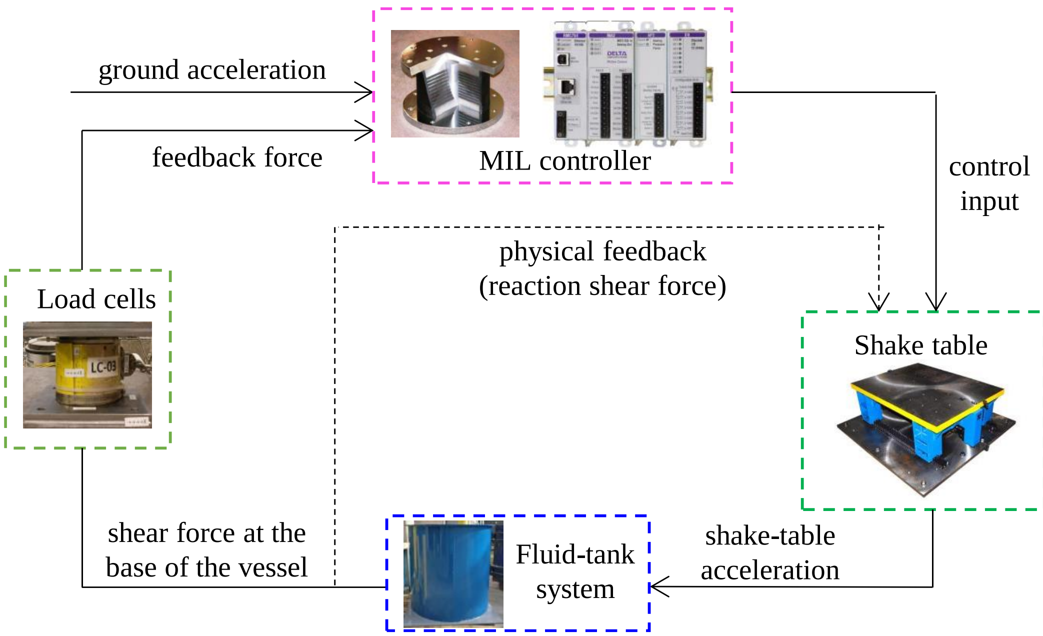

Figure 1.5. Feedback interaction in the MIL experiments

The overarching goal of this report is to develop a standardized (by-and-large) MIL controller that could be used to execute MIL simulations for diverse combinations of virtual systems (bearings with different characteristic strength and stiffness), physical systems (vessel filled with different fluid heights), and input ground motions (acceleration histories with different amplitudes and spectral content), as shown in Figure 1.6. The main contributions of this research, as outlined in Section 1.3, that led to successful execution of the MIL experiments and help achieve this overarching goal are expanded in the subsequent sections of this report in the context of the MIL setup of Figure 1.4b.

Contribution #8: Results show that the shake table with the designed MIL controller is able to imitate acceleration conditions corresponding to different isolation systems sufficiently accurately up to 20 Hz, with reduced accuracy at higher frequencies. Importantly, a standardized controller, $u = H_{a_g}^{\text{filter}}\left(H_{zu}^{\text{st}}\right)^{-1} H_{za_g}^{\text{vs}} a_{\text{g}} + H_{w}^{\text{filter}}\left(H_{zu}^{\text{st}}\right)^{-1}\left(H_{zw}^{\text{vs}} - H_{zw}^{\text{st}}\right)w$, is used to implement MIL for a diverse combination of physical and virtual systems, thereby demonstrating the robustness and versatility of the impedance-matching controls developed herein. Figure 1.7 is a sneak peek of this outcome.

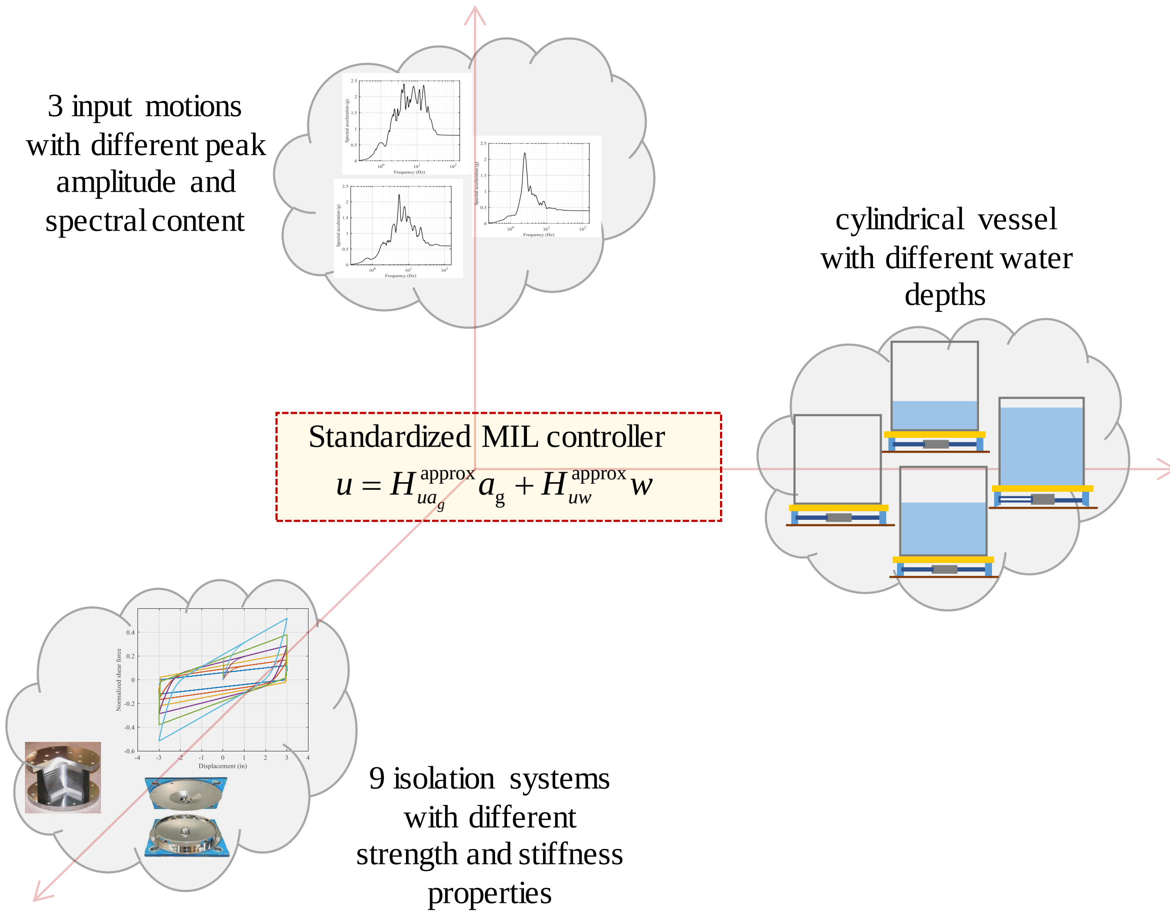

Figure 1.6. Validation of MIL controls for a family of physical and virtual systems

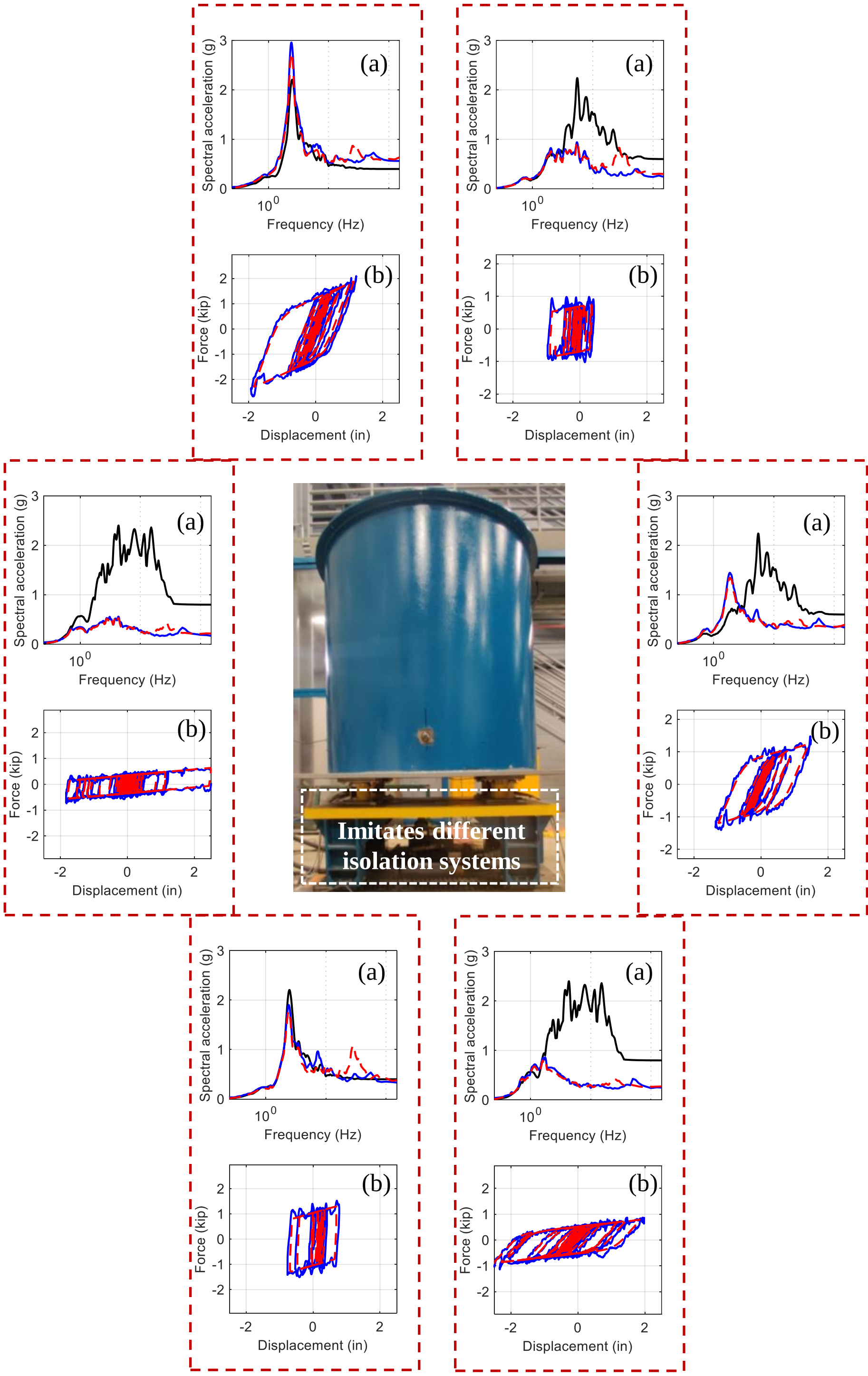

Figure 1.7. Sample test results; panels marked (a) present the acceleration response spectra at the base of the vessel, and panels marked (b) present the force-displacement response of the isolation system to the input motion; solid blue lines are the shake table responses, dashed red lines are the responses of the isolation system model, and the solid black lines are the acceleration spectra of the input ground motion.

1.6 Organization of the report

This report is organized into eleven sections and three appendices as described below:

Section 2 *Literature review on model-in-the-loop simulations*

This section reviews (i) control algorithms traditionally used to implement MIL for earthquake-engineering applications and (ii) some unique and challenging MIL configurations pursued at the University at Buffalo over the last two decades that were the building blocks for the impedance-matching approach.

Section 3 *MIL components for the 1D base-isolated fluid-filled vessel*

This section introduces the components used for executing MIL experiments for the 1D base-isolated setup shown in Figure 1.4. The setup includes a fluid-filled cylindrical vessel (test article), seismic isolation systems (environment represented virtually), a uniaxial hydraulic shake table (loading device), load cells (for feedback measurement), and an RMC75E controller (hydraulic control and implementing MIL code).

Section 4 *Mathematical modeling of the uniaxial servo-hydraulic shake table*

This section discusses mathematical modeling of the uniaxial shake table. A linear model for the shake table is developed by combining the working principles of servo-hydraulic systems and concepts of linear control theory. The linear model is validated through extensive testing of the bare table (without the test article) and of the table with vessel mounted at its top, making explicit Contributions #2, #3, and #4 listed in Section 1.3.3.

Section 5 *Mathematical modeling of the virtual systems*

This section discusses mathematical modeling of the three types of virtual systems considered in the MIL experiments: spring-damper, lead-rubber, and Friction Pendulum isolation systems. These mathematical models enable calculation of the target VS acceleration history that needs to be imitated by the shake table in real time.

Section 6 *Design of the MIL controller*

This section discusses the design of the MIL controller. The technical basis for Equation 1-5 is presented and challenges associated with its implementation are identified. A rational procedure for designing the filters is presented, making explicit the tradeoff between stability and performance, addressing Contribution #5 listed in Section 1.3.4.

Section 7 *Configuring the RMC75E controller and implementation of the MIL codes*

This section describes the configuration of the RMC75E controller hardware and software for the current MIL setup. The MIL controller of Section 6 is discretized in time and a state-space realization of this discretization is implemented as a mathematical code within the RMC controller, addressing Contribution #6 listed in Section 1.3.5.

Section 8 *Validation of the MIL controller for input-acceleration tracking experiments*

This section presents test results for the cases where the shake table is controlled to track a prescribed acceleration, a_g, as-is, at the base of the test article like conventional shake-table testing, addressing Contribution #7 listed in Section 1.3.6.

Section 9 *Validation of the MIL controller for imitating seismic isolation systems*

This section presents results of the model-in-the-loop experiments imitating different seismic isolation systems. The MIL controller is validated for a diverse combination of physical systems (cylindrical vessel filled with different water depths), virtual systems (seismic isolation systems of different types and properties), and input ground motions (acceleration histories with different peak intensities and spectral content), addressing Contribution #8 listed in Section 1.5: the overarching goal of this report. The section also presents a framework to identify the limitations of MIL testing.

Section 10 *Closing the loop*

This section summarizes the merits of the impedance-matching approach to MIL, revisits the key outcomes of this report identified in Section 1, makes some closing remarks on developments made thus far, notes questions that are yet to be answered, and identifies opportunities for future enhancement of the impedance-matching approach.

Section 11 *References*

This section is a list of references used in the report.

Appendix A *Calibration of the feedback measuring load cells*

Appendix B *Configuring RMC75E controller hardware and software with the MIL test system*

Appendix C *Evaluation of goodness of MIL simulation for different sources of feedback measurement*

SECTION 2
LITERATURE REVIEW ON MODEL-IN-THE-LOOP SIMULATIONS

2.1 Section Prologue

This section reviews algorithms that are traditionally used to implement MIL for earthquake-engineering applications. Most researchers have developed control algorithms around three key components: tracking controllers, delay compensators, and specialized time-integration schemes. Algorithms within the framework of these three components are referred to as 'conventional' or 'traditional' in this report. Stefanaki (2017) presented a comprehensive literature review of MIL control algorithms (through 2016) with a focus on earthquake-engineering applications and identified the associated challenges, limitations, and opportunities.

Section 2.1 of this report summarizes Stefanaki's review and identifies developments since 2017. The goal herein is to articulate the key ideas utilized in the traditional MIL algorithms and help the reader contrast them with the impedance-matching approach. Section 2.2 discusses some unique and challenging MIL configurations pursued at the University at Buffalo over the last two decades that were the building blocks for the impedance-matching approach.

2.2 Review of MIL algorithms in earthquake-engineering domain

2.2.1 Historical context

In earthquake engineering, MIL testing originated as a substructuring[3] strategy, that is, partitioning of structural systems into experimental and numerical components. Such testing was seen as replacing one or more elements in a finite element model with physical components (e.g., Mahin *et al.* (1989) and Shing *et al.* (1996)) and actuator controls were therefore designed to apply a target displacement on the test article with reaction force as the feedback.

The early stages of MIL (late 1980s and early 1990s) saw applications of *pseudo-dynamic* testing because the response of the physical elements, although complex and nonlinear, were expected to have no rate dependence. Testing was performed arbitrarily slowly (thus *pseudo-dynamic)*, hence actuator and sensor

[3]Known as real-time hybrid simulation by earthquake engineers, but MIL is used herein for consistency with other sections of the report. Also note that the impedance-matching control design presented herein is broadly applicable to other disciplines.

dynamics were not an issue. The two major concerns at that time were measurement noise and external disturbances, which resulted in inaccurate tracking of the reference command, which could lead to instability if not properly compensated. The issue of inaccurate tracking was addressed using specialized time-integration schemes with dissipative characteristics, similar to how numerical round off and truncation errors are treated in a finite element simulation.

As MIL evolved, rate-dependent behavior of physical systems was considered in the tests. Numerical simulation and physical experimentation were synchronized in time, and the test description transitioned to *real-time pseudo-dynamic* substructuring. Nakashima *et al.* (1992) was the first to execute *pseudo-dynamic* MIL simulations in real time. The next logical step was to extend MIL for *real-time dynamic* testing applications, wherein the physical system had both rate-dependent and inertial effects. Tracking errors were no longer due to measurement noise and disturbances alone; actuator dynamics had to be considered.

Shao and Griffith (2013), McCrum and Williams (2016), Stefanaki and Sivaselvan (2018a), Nakashima (2020), and Tian *et al.* (2020), reviewed MIL control algorithms developed by researchers over the past three decades and identified challenges associated with their implementation. Dyke *et al.* (2020) assembled a collection of manuscripts summarizing contemporary tools and techniques used for executing MIL experiments. Most of these algorithms are based on designing accurate tracking controllers. Because the numerical simulation and physical experimentation are time-synchronized, delay in command generation from the numerical simulation will lead to undesired loading pause on the test article. Additionally, actuator dynamics introduces tracking delays, which are commonly addressed by combining tracking controllers with appropriate delay compensators and specialized time-integration schemes: components seen as the backbone of a successful MIL simulation. Each of these components is briefly discussed next.

2.2.2 Key components for real-time dynamic substructuring

2.2.2.1 Specialized time-integration schemes

During a MIL test, the numerical substructure is solved synchronously with the loading of the test article, meaning, the boundary condition that needs to be imposed on the test article shall be computed and sent to the controller within one time step[4]. This process requires the use of efficient time-integration schemes to

---

[4] This is typically equal to the loop time of the controller. Most operating commercial shake tables in the United States have a loop frequency (inverse of loop time) of less than 2000 Hz.

solve the equations of motion of the numerical substructure within the controller sampling time. Additionally, time-integration schemes with dissipative characteristics are preferred to attenuate tracking delays resulting from measurement errors and actuator dynamics. Over the past few decades, researchers have developed a number of specialized explicit and implicit time-integration schemes for MIL testing, as summarized below in Table 2.1

Table 2.1. Literature on specialized integration schemes, including research post 2016

Nakashima *et al.* (1990); Combescure and Pegon (1997); Wu *et al.* (2006)	Operator-splitting time integration methods for *pseudo-dynamic* and *real-time dynamic* testing; explicit formulations for experimental substructure and implicit formulations for numerical substructure
Nakashima *et al.* (1992); Nakashima and Masaoka (1999)	Explicit time-step staggering approach; larger time step to solve equations of motion and smaller time step to generate actuator commands
Gutierrez and Lopez Cela (1998)	Modal truncation technique; considers low frequency modes where the system has dominant response and attenuates high frequency modes
Zhang *et al.* (2005)	Modified predictor-corrector numerical scheme using state-space formulation
Wu *et al.* (2005)	Explicit central difference method
Chen and Ricles (2008); Chen *et al.* (2009); Gui *et al.* (2014)	Unconditionally stable explicit schemes using techniques of discrete control theory
Bursi *et al.* (2010); Mosqueda and Ahmadizadeh (2011)	Linear and iterative implicit schemes
Bursi *et al.* (2011)	Rosenbrock-based algorithm
Chen and Ricles (2012)	Implicit HHT-α scheme
Kolay and Ricles (2014); Kolay *et al.* (2015); Kolay and Ricles (2016); Kolay and Ricles (2019)	A family of unconditionally stable explicit, parametrically dissipative, model-based algorithms
Ou *et al.* (2015)	Modified Runge-Kutta scheme
Wu *et al.* (2020)	Unconditionally stable, energy-consistent, time integration scheme for nonlinear systems

Implicit time-integration methods, although have desirable properties in terms of dissipative characteristics, are challenging to implement because they require iterations. When the numerical substructure is nonlinear with a large number of degrees of freedom, the number of (and time required for) iterations for the solution to converge is uncertain at each step, and may result in delayed command generation to the controller. On contrary, explicit integration schemes (e.g., central difference method, Newmark method) are most suited for MIL testing because the target boundary condition for the current time step depends entirely on responses in the previous time step. However, explicit time-integration schemes require smaller time steps.

In the impedance-matching approach, actuator control is not viewed from a tracking perspective, and therefore specialized time-integration schemes (focused at attenuating tracking errors) are not required. A time-integration scheme may still be required for solving the equations of motion for nonlinear virtual systems, but that is of secondary concern. For the uniaxial base-isolated MIL case presented in this report, a third-order Runge-Kutta method is employed to solve the equations of motion of nonlinear seismic isolation systems (lead-rubber and Friction Pendulum systems), and the Tustin method is used for the time discretization of the MIL controller (i.e., Equation 1-5). Details are presented in Section 6.

2.2.2.2 Delay compensators

Tracking delays due to actuator dynamics and other factors need to be addressed because they have an effect similar to negative damping in the system and can lead to instability. Delay compensation schemes have been developed by researchers, which can be broadly classified as either polynomial function-based or model-based. The former rely on mathematical expressions, and the latter are based on models of actuator, and in some cases of combined actuator and test article. Table 2.2 summarizes key literature on developing delay compensators.

In contrast with the strategies listed in Table 2.2, the impedance-matching approach explicitly characterizes actuator dynamics in the form of transfer functions (mostly model-based and partly experimentally measured), H_{zu}^{st} and H_{zw}^{st}, which relate the output condition, z, to the control input and the feedback input, respectively. Because the test article is decoupled from the control design, an approximate inverse of the actuator model alone is sufficient for implementing MIL, thus eliminating need for adaptive/inverse/polynomial compensation schemes. The approach also explicitly accounts for the actuator-test article interaction via the term H_{zw}^{st}, which is fundamentally different from the approaches listed in Table 2.2.

Table 2.2. Literature on delay compensation schemes, including research post 2016

Nakashima *et al.* (1992); Nakashima and Masaoka (1999); Horiuchi *et al.* (1999); Wu *et al.* (2005); Zhang *et al.* (2005); Schellenberg *et al.* (2009); Zhu *et al.* (2014)	Polynomial-based extrapolation compensation techniques for attenuating tracking delays
Wagg and Stoten (2001)	An adaptive delay compensation scheme based on the minimal control synthesis concept
Darby *et al.* (2002)	A linear-lead compensation strategy
Wallace *et al.* (2005)	An adaptive polynomial-based forward prediction method
Carrion and Spencer (2007); Lee *et al.* (2007); Narutoshi and Matthew (2014)	Model-based inverse dynamics compensation
Sivaselvan *et al.* (2008); Shao *et al.* (2011)	Adopted the Smith predictor for delay compensation addressing modeling uncertainties and errors
Chae *et al.* (2013)	Adaptive time series compensation with actuator coefficients updated in real time using tracking error
Chen and Tsai (2013)	Dual compensation technique combining an adaptive scheme with a restoring force compensator
Hayati and Song (2016)	Discrete-time compensator based on an Auto-Regressive with Exogenous (ARX) model
Fermandois and Spencer (2017); Galmez and Fermandois (2022)	Adaptive model-based feedforward-feedback controller
Zhou *et al.* (2019)	Combined a Linear-Quadratic-Gaussian controller and a polynomial-based feedforward prediction algorithm to attenuate the effects inaccurate tracking
Palacio-Betancur and Gutierrez Soto (2019)	Conditional adaptive time series (CATS) compensation using the recursive least square (RLS) algorithm
Wang *et al.* (2019)	Adaptive two-stage compensation method combined with polynomial extrapolation and adaptive inverse strategy
Ning *et al.* (2019)	Dynamic compensation using: a mixed sensitivity-based H_∞ controller, a polynomial extrapolation compensation scheme, and an adaptive filter

Table 2-2. Literature on delay compensation schemes, including research post 2016 (cont'd)

Gao and You (2019)	Delay compensation by treating actuator dynamics phase lags and other communication delays similar to negative damping in the real-time hybrid system
Xu *et al.* (2019)	Adaptive windowed frequency-domain evaluation index (WFEI) method; time delay calculated on-line by frequency-domain evaluation index integrated with inverse compensation method
Ouyang *et al.* (2019)	Back-stepping adaptive control to compensate for time-varying lags in the physical setup; little prior knowledge needed about the test article
Najafi and Spencer (2019); Najafi and Spencer (2020); Najafi and Spencer (2021)	Adaptive model-based controller (aMBC) comprising feedforward and feedback links, a reference model, and an adaptation law
Zhou and Li (2020)	Model-based two-stage feedforward compensation method
Tao and Mercan (2021)	Adaptive discrete feedforward delay compensation; includes an outer loop controller to enhance tracking performance and stability

2.2.2.3 Tracking controllers

The early applications of MIL focused on tracking displacement or force at an interface with actuators typically operated in a closed-loop proportional-integral-derivative (PID) control mode. Occasionally, acceleration or force feedforward components were/are used. The PID control with displacement feedback is typically implemented as: $u_{\mathrm{v}} = K_{\mathrm{e}}e + K_{\mathrm{i}}\int e\mathrm{d}t + K_{\mathrm{d}}\dot{e},$ where e is the error between the commanded and the actual condition of the actuator, K_{e}, K_{i}, and K_{d} are the proportional error, integral error, and derivative error gains, respectively, and u_{v} is the electrical signal to the actuator servovalve. The goal is to tune these control gains so that error, $e,$ is minimized and the actuator tracks the reference command accurately in the presence of test article. Table 2.3 summarizes key literature on designing tracking controllers.

The impedance-matching approach does not rely on tracking controllers because the actuator is not simply viewed as a tracking device but rather as a dynamic system that needs to be controlled such that it mimics the impedance of the desired virtual system near the interface with the test article. It will be demonstrated in Section 4 that although the shake table is operated in a closed-loop position control mode in the MIL experiments, the control gains are not tuned for accurate tracking of the reference command but rather to obtain a robust mathematical model of the shake table across a broad frequency range. The key feature of the impedance-matching approach is that the reference command (i.e., control input) to the actuator need not be the desired boundary condition that needs to be controlled at the actuator-test article interface. For example, in the MIL experiments of this report, the control input, u, to the shake table is a displacement command but the condition controlled at the interface is acceleration.

Table 2.3. Literature on specialized integration schemes, including research post 2016

Dimig *et al.* (1999)	Tracking controller with velocity feedforward component to decouple the test specimen from the actuator in a force-control application.
Stoten and Benchoubane (1990); Neild *et al.* (2005)	Adaptive substructure method using minimal control synthesis algorithm; does not require knowledge of dynamics of shake table and test specimen
Seto *et al.* (2002)	Tracking controller using Linear Quadratic with Integral (LQI) approach
Sivaselvan *et al.* (2008); Shao *et al.* (2011)	Similar to the Dimig *et al.* (1999) but using displacement feedforward component
MTS (2010)	A *three variable control* (TVC) method
Carl and Sivaselvan (2011)	A force feedforward approach to approximately decouple the test article from the actuator
Nakata (2013)	A loop shaping controller for force control
Zhou and Wu (2013)	Pressure difference (ΔP) feedback control for reducing the effects of oil-column nonlinearities
Phillips *et al.* (2014)	Model-based multi-metric control method using feedforward and feedback links
Dertimanis *et al.* (2015)	Acceleration-based adaptive inverse control
Yang *et al.* (2015)	Hierarchical control using sliding control technique
Ryu and Reinhorn (2016)	Nonlinear-tracking control based on feedback linearization method; Extended Kalman filter (EKF) accounted for modeling uncertainties
Nakata *et al.* (2017)	Mixed force and displacement control method
Chen *et al.* (2017)	Control framework incorporating a weighted command shaping controller; command shaping was model-based, thus fully capturing control-structure interaction
Rajabi *et al.* (2018)	Sliding mode trajectory tracking control based on online state estimation using Unscented Kalman filter (UKF)
Peiris *et al.* (2020); Peiris *et al.* (2020)	Passivity-based control with adaptive feed-forward filtering

2.3 Conceptualization and evolution of the impedance-matching approach

2.3.1 Background

The impedance-matching approach, as described in Section 1, has evolved through a sequence of unique and challenging MIL configurations pursued at the University at Buffalo over the last two decades. Strategies have been developed to meet the needs of these configurations, and a search for a theoretical support for these strategies revealed connections with some mature concepts in control systems theory, which are less widely known to civil and earthquake engineers. This section describes the beginnings of the impedance-matching approach and its evolution to the form described in Section 1, points out these connections to theory, and sets the stage for the three key criteria that come into light in Section 9. The narrative makes clear that the motivations behind this impedance-based thinking are intuitive and physical rather than abstract and mathematical, although a simple mathematical framework emerges naturally at the end.

2.3.2 MIL configurations by Reinhorn *et al.* (2004) and Carl and Sivaselvan (2011)

A distinguishing feature of the Network for Earthquake Engineering (NEES) facility at the University at Buffalo was to pursue versatile substructuring that combined the use of a shake table and wall-mounted actuators (Reinhorn *et al.*, 2004) for MIL testing of a two-story frame structure. The first story was physically built on the shake table whereas the effect of the second story was simulated using wall-mounted actuators, as illustrated in Figure 2.1a, reproduced from Reinhorn *et al.* (2004).

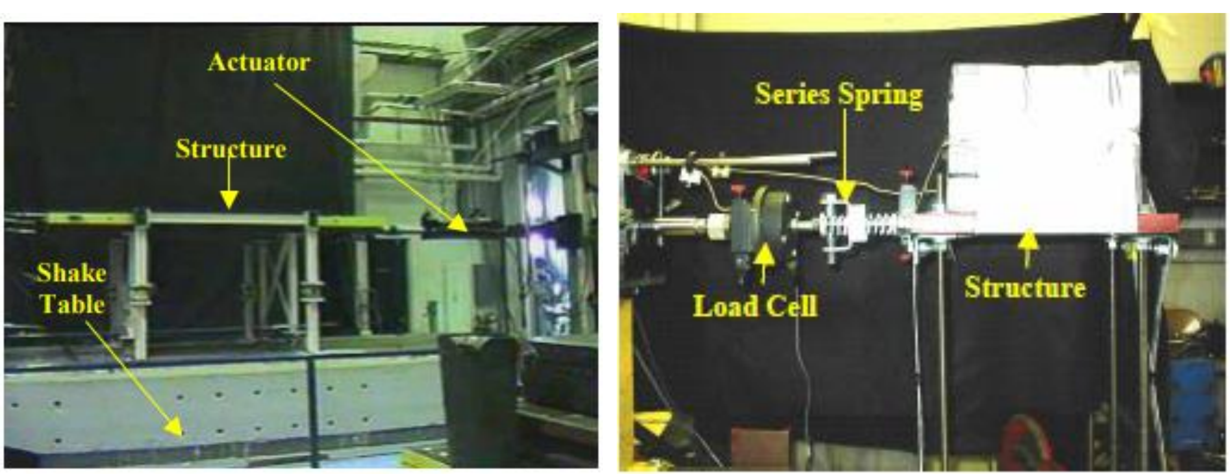

a) MIL setup – shake table and actuator b) small-scale demonstration of force control

Figure 2.1. MIL testing of a two-story frame using shake table and actuators (Reinhorn *et al.*, 2004)

The unique aspect of the MIL configuration of Figure 2.1a was that it required force-based substructuring, which was not common in early 2000s. The shake table induced inertia forces in the test article, and so the actuators were required to be operated in dynamic force control because either actuator force or displacement, but not both, can be controlled at a given interface. Beginning to develop such capability immediately revealed that the actuator needed to act *softly* and *willingly* to follow some of the shake-table motion and not *fight* it for control over the test article. Actuator *softness* was achieved by adding physical compliance between the actuator and the test article using a spring-based system (see Figure 2.1b) – an idea borrowed from series elastic actuators in robotics (Pratt *et al.*, 2002). Actuator *willingness* was achieved by positive feedback of the test article displacement (later understood to what is termed as *disturbance feedforward* in control systems) – an idea borrowed from Dimig *et al.* (1999). This feedforward also has the effect of (approximately) cancelling actuator's interaction with the test article (and the shake table) dynamics when thinking about control alone. This intuitive-based MIL implementation achieved remarkable accuracy (Reinhorn *et al.*, 2004) for a complex configuration, which to this date has not been replicated by others, and may have settled the topic had the appropriate theoretical support been recognized. This support has taken almost two decades and a few other MIL configurations to recognize. This report constitutes a significant step towards establishing this theoretical support.

Using feedforward to cancel actuator-test article interaction was seen as an attractive way of applying displacement control (Carl and Sivaselvan (2011; 2012)). In this case, the feedforward was the interaction force from a stiff test article (a beam) connected to a magnetorheological damper. The notion of actuator *softness* gradually connected thinking with the term *impedance*, and a high-level connection was made between feedforward approach and the seminal work on interaction of robots with their environments by Hogan (1985). The approach of Carl and Sivaselvan, although considering impedance, was still based on tracking a reference command, and conventional strategies were built around it. Carl and Sivaselvan (2011) only used the static (DC) part of what is referred to as H_{zw}^{st} in this report. The theoretical support was right there for the taking but missed. It is now recognized that *MIL = impedance control*.

2.3.3 Impedance-matching MIL for force control (Stefanaki and Sivaselvan, 2018a)

Stefanaki and Sivaselvan (2018a) pursued another unique MIL configuration that included a virtual superstructure on a physical soil-foundation system constructed in a geotechnical laminar box. This study was the first attempt at impedance-matching MIL control for civil engineering applications. A uniaxial active mass driver (AMD)[5], mounted atop the physical soil-foundation system, was controlled to emulate the effect of the superstructure, as illustrated in Figure 2.2. The AMD was operated in force control, that is, it utilized the acceleration motion prorogated through the soil-column as the feedback condition and applied an appropriate force representative of the virtual superstructure on the physical soil-foundation system. Initially, the problem was approached as one of tracking. However, the need to decouple the test article (soil-foundation system + laminar box) from the AMD controls became clear because it was impractical to use a model of this complex test article in control design.

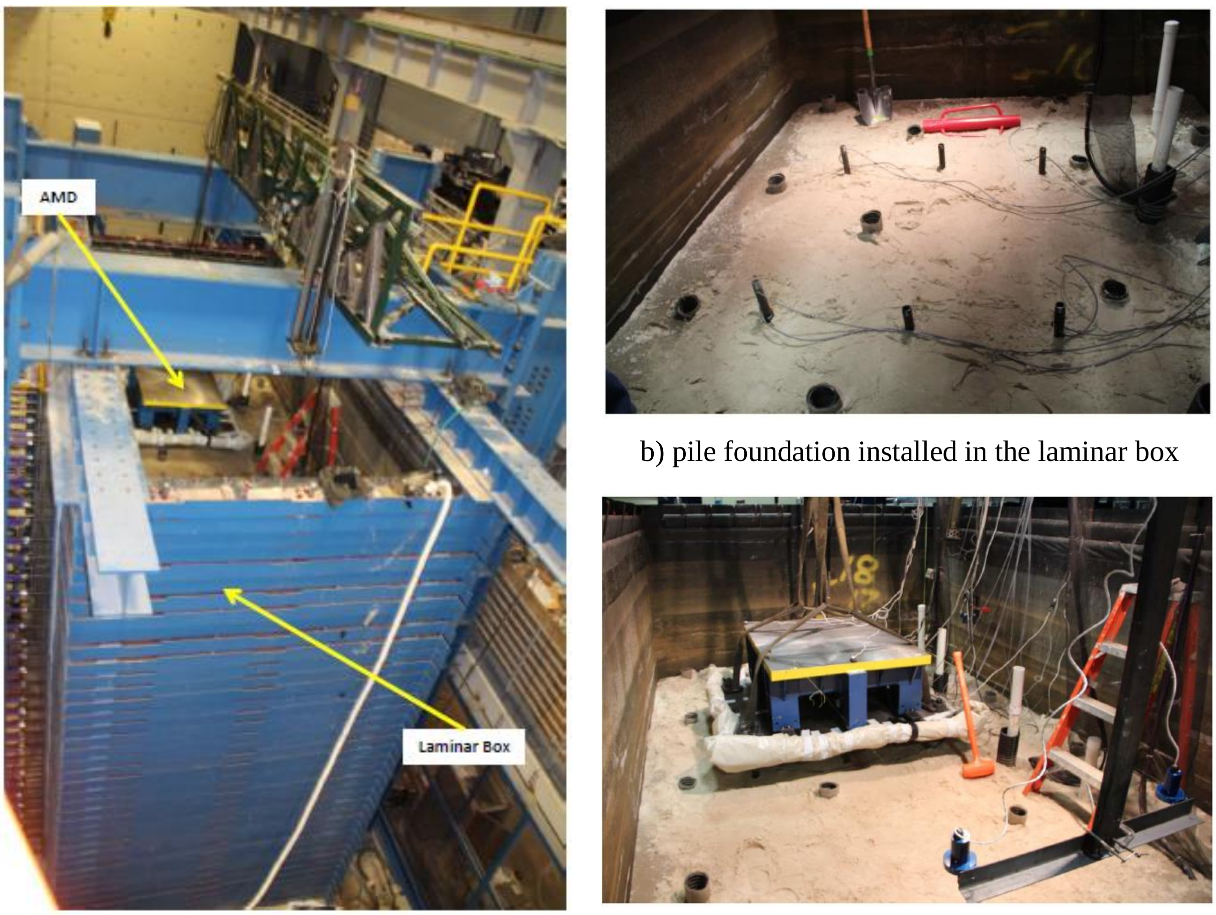

b) pile foundation installed in the laminar box

a) experimental setup

c) AMD mounted on piles

Figure 2.2. MIL test configuration for a physical soil-foundation system with superstructure represented virtually using the AMD (Stefanaki, 2017)

[5] The shake table used in this report.

Stefanaki and Sivaselvan explored an unrelated line of thinking by adjusting physical elements (e.g., resistors and capacitors) in the AMD controller so that its behavior closely resembled that of virtual superstructure without the need for a computational algorithm. These ideas together with prior experience of feedforward cancellation converged to conceptualization of Equation 1-4: a MIL controller based on impedance matching. Stefanaki and Sivaselvan (2018b) demonstrated that this equation could be implemented in real time (as a state-space system) to achieve meaningful MIL simulations, validated the concept of H_{zw}^{st}, and showed that the MIL algorithm could be tested and implemented independently of any test article: fundamentally different from the traditional algorithms and approaches to MIL discussed in Section 2.2. In Stefanaki's configuration, MIL was force-based, which is simpler in terms of implementation due to the smaller relative degree[6] of H_{zu}^{st}, as compared to the motion-controlled MIL setting, tackled in this report.

2.3.4 Impedance-matching MIL for motion control (Kote, 2019)

Kote (2019) developed a unique MIL configuration to investigate the dynamic interaction of electrical substation equipment interconnected through flexible conductors for earthquake loading. Flexible conductors exhibit significant nonlinear dynamics (Fu, 2020) and therefore served as the test article. The boundary conditions corresponding to various pieces of substation equipment were represented by two custom-designed 2-DOF shakers shown in Figure 2.3. In this configuration, MIL was conceptualized as motion-control, that is, the 2-DOF shakers apply displacement at the terminal and the reaction forces and moments from the conductor are taken as feedback conditions.

Although successful MIL simulations were demonstrated, a number of open questions remained, mainly in terms of understanding the tradeoffs between accurate performance (how closely the towers reproduce equipment dynamics) and stability (stability of the feedback system). The issues related to stability arise partly because of the use of an approximated MIL controller (refer to the discussion in Section 1.3.4) and partly because of significant controller response at high frequencies. This report, also utilizing a motion-controlled MIL setup, develops the necessary theoretical framework to understand these tradeoffs (see Section 9.3).

[6] The smaller the relative degree of H_{zu}^{st}, less is the need for approximating the controller equation, and less are the compromises made on the MIL performance. See Section 6.

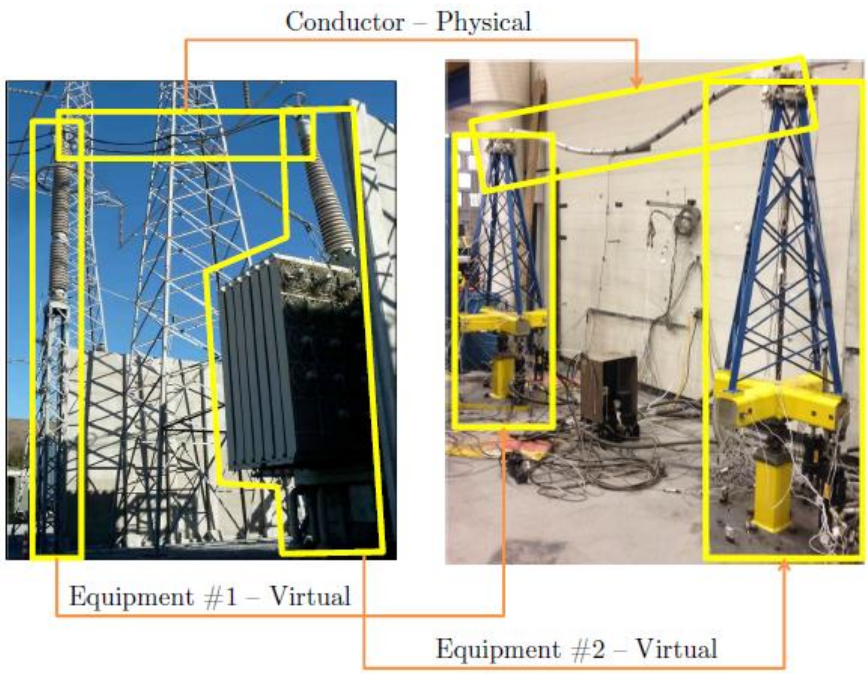

Figure 2.3. MIL test configuration for physical flexible bus conductors with interconnected equipment represented virtually using the 2DOF shakers (Kote, 2019)

2.3.5 Optimization-based approaches to impedance-matching MIL control

2.3.5.1 Linear matrix inequalities, Verma *et al.* (2019)

Verma *et al.* (2019) approached Equation 1-4 from a different perspective. Instead of trying to achieve impedance equality, they posed the question as one of optimization, that is, how closely (and across how broad a frequency range) can the actuator system emulate the virtual-system impedance? Verma *et al.* (2019) formulated the optimization problem from an impedance perspective using linear matrix inequalities (LMI) and validated its application in a force-controlled MIL setting. (Optimization-based thinking was explored in Hauser and Sivaselvan (2009) but from a tracking perspective.)

2.3.5.2 Frequency-domain linear programming, Verma *et al.*, (forthcoming)

Verma *et al.* (forthcoming) systematically approached Kote's MIL configuration of Figure 2.3 from an optimization perspective. The optimization objective was to minimize the difference in the impedances of the controlled actuator system and of the desired virtual system subject to two constraints: (i) the control effort, and subsequently the actuator response, to be limited at high frequencies, and (ii) the controlled actuator system must be passive. Colgate (1988) was the first to use passivity[7] as a framework for assessing stable interaction of a robot with its environment. Verma *et al.* (forthcoming) solved the optimization problem using linear programming in the frequency-domain. The result of optimization was a MIL controller, H_{uw}, in the form of a complex analytic function, which needed to be approximated for implementation, and sometimes led to violating passivity.

2.3.6 Role of this report in advancing the impedance-matching approach

In this report, the impedance-matching MIL is successfully implemented in a motion-controlled uniaxial setting: an intermediary position to the Stefanaki's force-controlled configuration and the Kote's multiaxial motion-controllerd configuration in terms of test-system complexity. A different approach to approximate the MIL controller (i.e., Equation 1-4) is considered and implemented, namely, using lowpass filters, as described in Section 1.3.4. This approach to controller approximation, although different from that of Stefanaki and Verma, has clarified and firmly reestablished the three design criteria for the MIL controller, namely, (i) close resemblance to the VS, (ii) low controller response at high frequencies, and (iii) passivity of the controlled actuator system. A theoretical framework for understanding the design tradeoffs with respect to these criteria is developed and presented Section 9.

2.4 Closing remarks

The traditional strategies for implementing MIL, as listed in Tables 2-1, 2-2, and 2-3, utilize the framework of Figure 1.3a, requiring specialized time-integration schemes, delay compensators, and tracking controllers. In contrast, the impedance-matching approach makes actuator control independent of these components, thus greatly simplifying implementation of MIL. The advantages of this new approach are: (i) controls are stable and easy to implement even for complex substructuring settings, (ii) the virtual-system impedance near the interface with the test article is reproduced accurately across a broad frequency range, (iii) the test article is decoupled from the control design, thus eliminating the challenges associated with control-structure interaction, (iv) controls can be validated using the actuator system alone, that is, the

---

[7] Passivity means a system cannot generate more energy than what has been input to it. When two passive systems are in feedback with each other, the combined system is guaranteed to be stable. The test article typically is passive because it cannot generate energy on its own. Therefore, the coupled test article-actuator system will be stable if the controlled actuator system is passive. Thus, notion of passivity of the controlled actuator system is used in both Verma's work and this report to assess stability. Details are presented in Section 9.3.

ability of an actuator system to reproduce the impedance of a virtual system can be evaluated independently of the test article, and (v) MIL procedures are standardized for qualification testing because they do not rely on tracking controllers, delay compensation schemes, and specialized time-integrations schemes.

The collective effort by Sivaselvan his co-workers over the past decade has resulted in important contributions to the subject of impedance control. Electrical servomotors are most commonly used in robotics applications, for which electrical current directly maps to the motor torque. However, in civil engineering applications utilizing hydraulic actuators, valve opening drives the rate of change of differential pressure and the valve itself has dynamics (see Section 4). Put differently, unlike electric motors where manipulating the current directly affects the desired torque output, in hydraulic systems there are intermediate dynamics between the control variable and the desired actuator output. This makes impedance control more challenging with hydraulic systems, again having to do with the relative degree of H_{zu}^{st}, as briefly discussed in Section 1.3.4. In robotic impedance control, typically the impedances to be matched are relatively simple, most commonly using a spring-mass-dashpot system. For impedance-based MIL in civil and earthquake engineering applications, more complex virtual systems with nonlinear behavior are possible.

SECTION 3
MIL COMPONENTS FOR THE 1D BASE-ISOLATED SYSTEM

3.1 Section Prologue

This section introduces the components used for executing model-in-the-loop (MIL) experiments for the 1D base-isolated fluid-filled vessel. Figure 3.1 is a photograph of the MIL test setup, assembled in the Structural and Earthquake Engineering Simulation Laboratory at the University at Buffalo. The setup includes: (i) a fluid-filled cylindrical vessel as the physical test article, (ii) three different seismic isolation systems, represented virtually using mathematical models, (iii) a uniaxial hydraulic shake table for imposing prescribed boundary condition of the virtual isolation systems at the base of the vessel, (iv) reaction load cells for measuring feedback force from the test article, and (v) controller hardware and software for performing actuator control and MIL-related calculations. Section 3.2 describes the geometrical properties of the vessel. Section 3.3 presents details of the isolation systems considered in the VS. Section 3.4 describes the uniaxial hydraulic shake-table and its instrumentation. Section 3.5 describes the reaction load cells. Section 3.6 describes the hardware and software of the RMC controller.

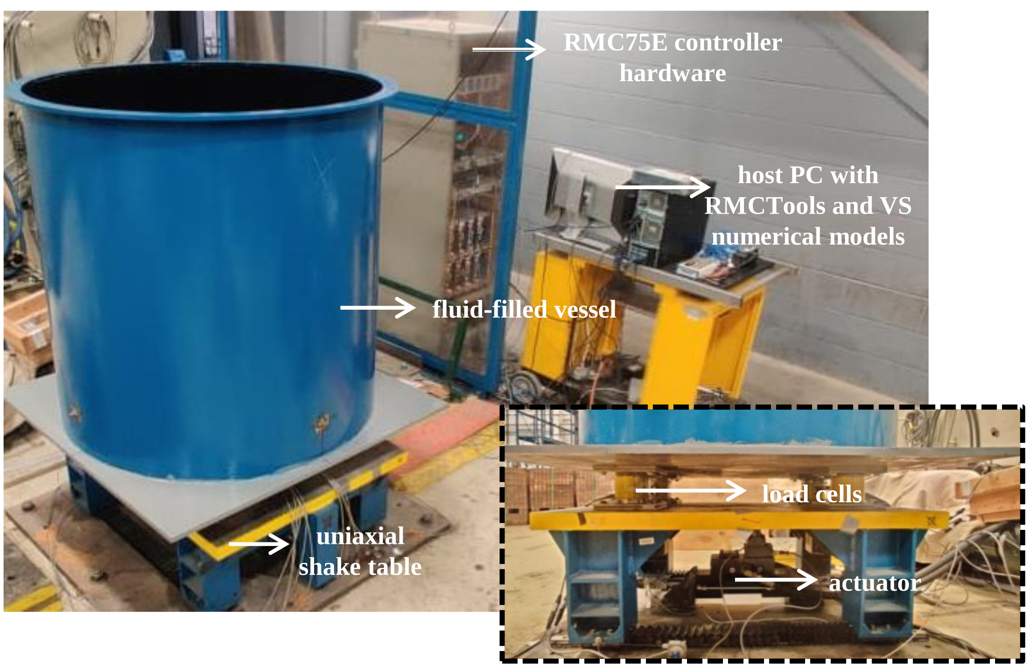

Figure 3.1. MIL test setup for the 1D base-isolated fluid-filled cylindrical vessel

3.2 Physical system: Fluid-filled cylindrical vessel

The cylindrical vessel used in the MIL experiments is 48 inches tall, with a wall thickness of 3/16 inch, and an outer diameter of 48 inches. A 2-inch wide and 0.5-inch thick flange is welded at the top of the vessel to support a 51-inch long and 0.25-inch thick head plate. The bottom of the vessel is welded to a $51 \times 51 \times 0.75$ inches base plate. (All components are constructed of carbon steel.) The load cells are connected to the shake table platform using ½-inch connecting plates, as shown in Figure 3.2a. The total weight of the specimen including the vessel, flange, head, and the base plate is approximately 1.25 kip. The depth of water in the MIL experiments is 36 inches. The total weight of the test article, including the water, is approximately 3.6 kip.

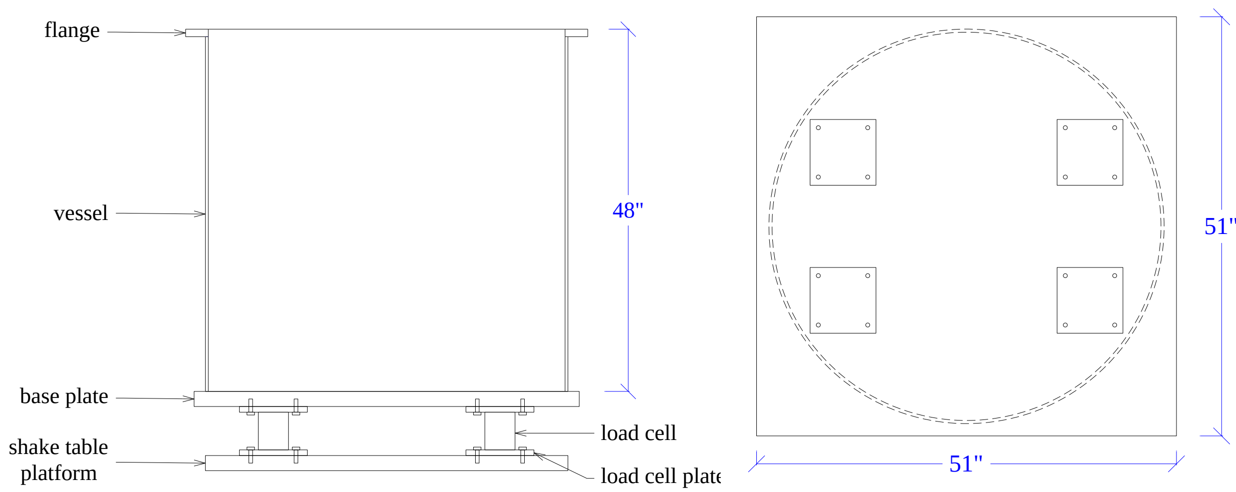

a) elevation view b) plan view of the base plate

Figure 3.2. Elevation and plan views of the test article

3.3 Virtual system: Seismic isolation bearings

Three types of seismic isolation systems are represented virtually in the experiments: linear spring-damper (SD) and nonlinear lead-rubber (LR) and Friction Pendulum (FP) systems. Figure 3.3a is a photograph of a spring-damper isolator unit: a product of the GERB vibration control. The assembly of springs provides horizontal (and vertical) flexibility and the viscous dashpot device accounts for energy dissipation. Figure 3.3b presents a sectional view of an LR bearing. The bearing consists of vertically stacked, alternating layers of bonded rubber and steel shims with top and bottom end plates, and a cylindrical, central lead core. The rubber layers provide horizontal flexibility to the bearing, and the hysteretic yielding of the lead core provides strength and accounts for energy dissipation. Figure 3.3c is a photograph of a single concave FP bearing. The unit consists of a spherical sliding surface, a housing plate, and a slider coated with low-friction, high-load composite, typically a polytetrafluorethylene (PTFE) type composite. The pendulum action of the slider along the spherical surface provides horizontal flexibility, and the coefficient of friction at the PTFE-stainless steel interface governs the strength of the bearing.

Section 5 presents mathematical models for the three virtual systems. These mathematical models enable calculation of the target VS acceleration history, z_{vs}, that needs to be imitated by the uniaxial hydraulic shake table at the base of the test article.

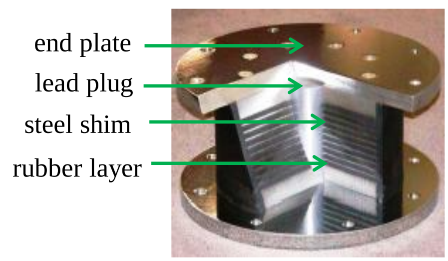

a) spring-damper system (courtesy of GERB) b) lead-rubber system (courtesy of DIS)

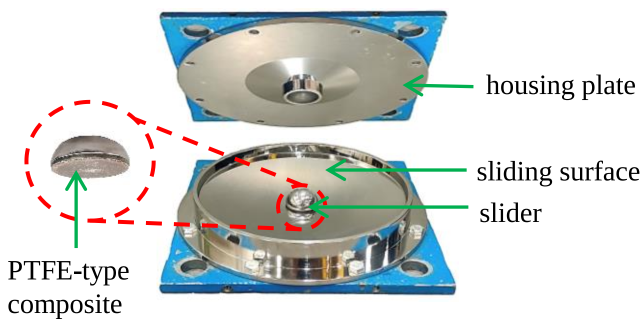

c) Friction Pendulum system (Lal *et al.*, 2021)

Figure 3.3. Seismic isolation systems considered in the VS

3.4 Loading system: Uniaxial servo-hydraulic shake table

Figure 3.4 is a photograph of the uniaxial hydraulic shake-table used in the MIL experiments. The testbed was originally assembled by Stefanaki and Sivaselvan (2018a) for application in MIL testing of a soil-foundation-structure system (see Figure 2.2). Details on the design and construction of this testbed are presented in Stefanaki (2017) and only relevant information is presented here. The shake table consists of a 2-inch thick steel platform that is 48 inches long and 36 inches wide, which is elevated using four W6×

20 columns, each 13 inches tall (see Figure 3.4a). The columns are supported on low-friction recirculating ball bearings (IKOLFHTG30) that slide on rail guides to enable horizontal movement of the shake table. The rails are bolted to a 1.5-inch thick base plate connected to a strong floor. An MTS hydraulic actuator, Model 244.12 (MTS, 2017), is installed beneath the shake-table platform along the 48-inch direction, as shown in Figure 3.4b.

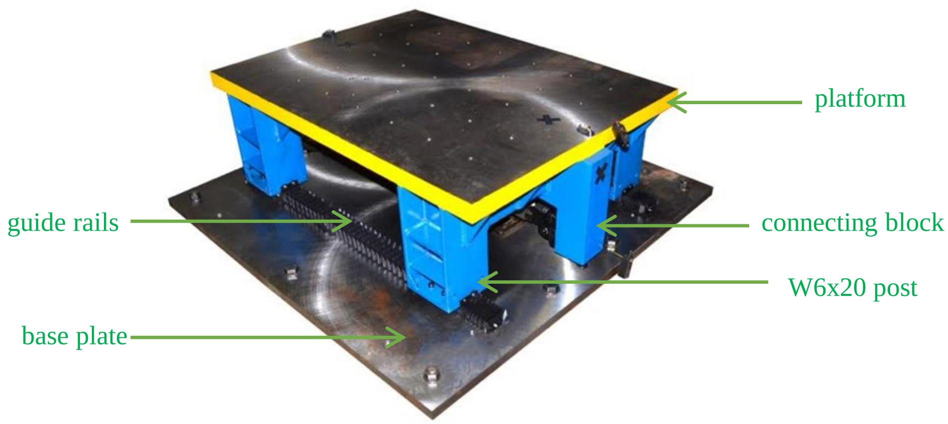

a) isometric view

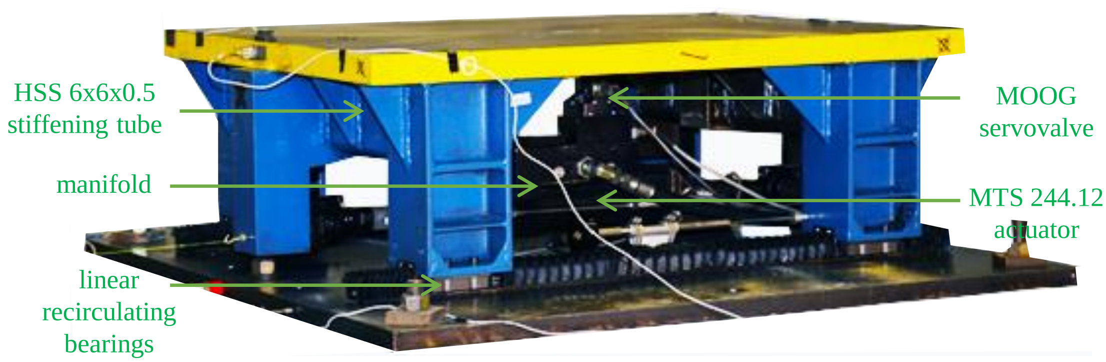

b) side view

c) MTS 244.12 actuator (MTS, 2017)

d) MOOG 760F264A servovalve (MOOG, 2007)

Figure 3.4. Uniaxial servo-hydraulic shake table (Stefanaki and Sivaselvan, 2018a)

The actuator has a nominal force rating of 5.5 kips and an end-to-end dynamic stroke of 6.4 in ($\pm$3.2 in). The body of the actuator is bolted to the base plate using brackets. The actuator is installed with a MOOG servovalve (MOOG, 2007), Model 760F264A, which is a 4-way 2-stage type valve, with a rated full flow capacity of 15 gallons per minute (57.75 in^3/s) at a load pressure of 1000 psi.

3.5 Feedback measuring system: Reaction load cells

The feedback force at the shake table-vessel interface is measured using five-channel reaction load cells (LCs). Four load cells, numbered LC-03, LC-06, LC-08, and LC-14, are selected from the UB SEESL inventory. These load cells are fabricated using a 0.25-inch-thick cylindrical steel tube with squares plates bolted at the top and bottom (Bracci *et al.*, 1992). Figure 3.5 presents a photograph and a schematic of the load cells. Because the current MIL experiments are focused in 1D, the load cells are calibrated only in the unidirectional shear per the procedure described in Appendix A. The calibration factor is set to 0.2 kip/V (i.e., each load cell reads a maximum shear force of 2 kip).

a) load cell unit, LC-03

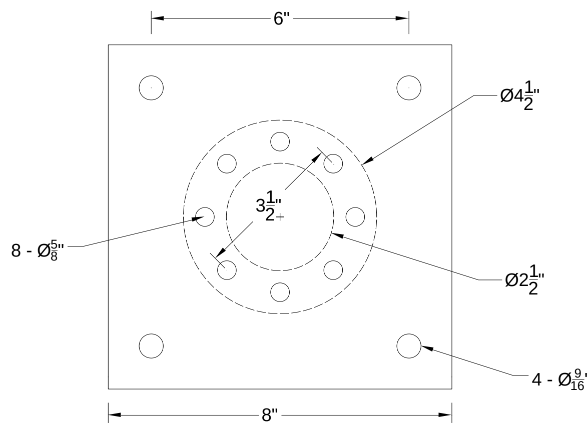

b) schematic of plan view

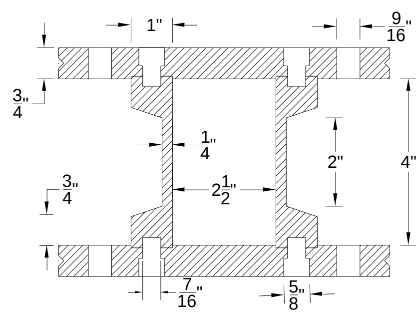

c) schematic of elevation view

Figure 3.5. Reaction load cells for measuring the feedback force (Bracci *et al.*, 1992)

3.6 Controller system: RMC75E digital controller

3.6.1 Introduction to RMC

Typically, MIL experiments are configured with two distinct controller hardware, one for performing hydraulic control (i.e., driving the servovalve in a closed-loop control mode) and the other for performing MIL-related calculations (e.g., implementing Equation 1-5 in real time as a discrete state-space system). Herein, an RMC controller, Model 75E, from Delta Computer Systems (Delta, 2020a) is used to perform both operations. The RMC75E is a deterministic (or digital) controller meaning it reads inputs, performs control actions, and updates outputs at a specific interval called the controller loop time. When the controller finishes calculations for one loop, it waits until the next loop time before performing its calculations again. All commercially available deterministic controllers are structured to operate this way. Section 4.3.4 emphasizes the key role of controller loop time (or frequency) in shake-table control.

3.6.2 Hardware and software of RMC75E

3.6.2.1 RMC hardware

Figure 3.6 is a photograph of the RMC75E controller hardware comprising several individual units referred to as modules. The RMC user manual (Delta, 2021b) lists the different types of modules supported by the RMC75E controller. Only the modules used in the current MIL setup are discussed herein, including a CPU module, an axis module, four expansion modules, and a VC2124 unit.

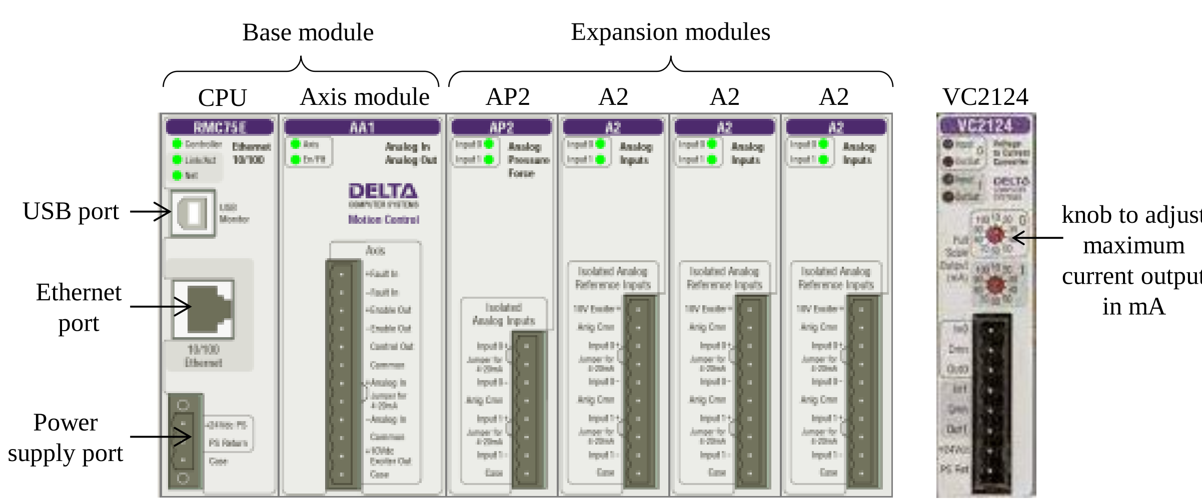

Figure 3.6. RMC controller hardware

1. CPU Module: The leftmost unit in Figure 3.6 is the CPU module, which is the processing unit of the controller. This module contains an Ethernet port for communications, a USB/monitor port to interact with the RMC software on the host computer, and a power supply port. The RMC75E CPU module offers control processing at five different loop times [frequencies]: 250 μs [4000 Hz], 500 μs [2000 Hz], 1000 μs [1000 Hz], 2000 μs [500 Hz], and 4000 μs [250 Hz]. A loop time of 500 μs (loop frequency of 2000 Hz) is used in the MIL experiments.

2. Axis module: An axis module is installed next to the CPU module and is responsible for driving the servo-actuator system. This module is provided with an input slot for receiving transducer feedback (typically displacement) used for closed-loop hydraulic control. The control output slot generates an electrical command to the servovalve, which is a $\pm$ 10V signal, and hereafter referred to as the valve command, u_{v}. The CPU module together with the axis module constitute a complete motion controller called the base module.

3. Expansion modules: These are optional modules that are added to the right of the base module. The expansion modules are added for additional functionality when the actuator control requires interfacing with more than one transducer input, such as for performing position-pressure or position-force control, or for MIL-related applications as considered in this report. The current setup utilizes four expansion modules (one of type AP2 and three of type A2).

4. VC2124: The VC2124 (Delta, 2020b) is an integral part of the RMC75E setup. It receives the valve command, u_{v}, generated by the axis module and drives an appropriate current, u_{i}, through the servovalve coils. The magnitude (and polarity) of this valve current controls the actuator motion. The mathematical relationship between the valve current, u_{i}, and the table acceleration, z_{st}, is derived in Section 4.3. The VC2124 hardware is provided with a knob to adjust conversion scale from voltage, u_{v}, to current, u_{i}. Ideally, the knob should be positioned at the rated full-flow current of the servovalve. For the MOOG 760F264A servovalve, $u_{\mathrm{i,max}} = 25$ mA. Because the settings on VC2124 are available only in the increments of 10 mA, the knob is set to 30 mA in the MIL experiments. This implies that for a maximum valve command of 10 V, the VC2124 drives a current of 30 mA through the servovalve coils. This voltage-to-current conversion gain, $K_{\mathrm{v}} = 3\ \mathrm{mA/V}$, is another key parameter for shake-table control and is revisited in Section 4.

3.6.2.2 RMC software

The RMC controller includes a software component, namely, RMCTools (Delta, 2021a), which is a Windows-based application designed for the user to interact with the physical hardware (i.e., modules) and control all features of the controller such as to configure, troubleshoot, program, plot inputs in real-time etc. The software has several pre-programmed commands to perform actions ranging from simple moves to complex system control. It allows creation of user programs and user functions to execute sequences of commands and perform basic mathematical operations. The user programming feature of the RMCTools enables performing MIL-related computations without requiring intervention from another external logic controller. Section 7 presents details on (i) configuring the RMC75E hardware and software with the MIL test system and (ii) user programs for implementing MIL controller.

SECTION 4
MATHEMATICAL MODELING OF THE UNIAXIAL SERVO-HYDRAULIC SHAKE TABLE

4.1 Section Prologue

The uniaxial shake table in the MIL experiments has two inputs: (i) control input, u, which is a reference displacement command issued by the user, and (ii) reaction force input, w, which is physically applied by the test article. As conceptualized in Section 1.3.2, the control input to the shake table is calculated using the equation: $u = \left(H_{zu}^{\text{st}}\right)^{-1} H_{za_{\text{g}}}^{\text{vs}} a_{\text{g}} + \left(H_{zu}^{\text{st}}\right)^{-1} \left(H_{zw}^{\text{vs}} - H_{zw}^{\text{st}}\right)$, derived by making the impedance of the shake table match that of the virtual isolation system it is intended to represent. The fidelity of such a MIL controller depends on accurate characterization of the shake-table dynamics in the form of transfer functions, H_{zu}^{st} and H_{zw}^{st}. The transfer function H_{zu}^{st} is commonly used in actuator control and can be readily measured from frequency-response experiments performed by setting the control input as a multisine (or whitenoise) broadband signal. The transfer function with respect to the force input, H_{zw}^{st}, is not commonly reported/utilized in the literature but is key to the impedance-matching MIL implementation, as will be demonstrated in Sections 8 and 9. However, w being a physical input, experimental measurement of H_{zw}^{st} requires driving the shake table with another, much larger actuator, and this is generally not feasible in a laboratory setting. This challenge necessitates development of a robust mathematical model for the servo-actuator shake table system to aid derivation of analytical expressions for H_{zu}^{st} and H_{zw}^{st}, which can then be subsequently used for the design and implementation of the MIL controller.

Section 4.2 reviews the working principles of a generic servo-hydraulic actuator system and illustrates key concepts involved in their modeling. A linear mathematical model of the uniaxial shake table is presented in Section 4.3, and analytical expressions for H_{zu}^{st} and H_{zw}^{st} are derived as a function of physical, mechanical, and control parameters of the table. Because H_{zu}^{st} and H_{zw}^{st} are derived from a linear model, the effects of nonlinearities in the servo-actuator system will have to be significantly curtailed for the linear model to predict the table response accurately. Sections 4.4 and 4.5 discuss heuristics[8] of shake-table control that would enable this outcome, and wherein lies some of the key contributions of this research. The

[8] Much of the presentation in Sections 4.2 and 4.3 is well established in literature, but is presented here to support the heuristics of shake-table control discussed in Sections 4.4 and 4.5.

presentation in these last two sections emphasize the key role of two control parameters: (i) ΔP (differential pressure in the actuator chambers) feedback in the hydraulic control and how a sufficiently large value of this gain is highly forgiving of modeling uncertainties and significantly reduces the effects of hydraulic-related nonlinearities in the system, and (ii) the sampling (i.e., loop) frequency of the controller, f_{s}, and its effect on the fidelity of the shake-table model. The exact dynamic effects of the ΔP gain and the controller sampling frequency are analyzed theoretically in Section 4.4 and experimentally in Section 4.5.

4.2 Working principles of a generic servo-hydraulic actuator system

The servovalve is the core of a servo-hydraulic actuator system. It responds to an input current, u_{i}, and regulates the flow of hydraulic fluid in-and-out of the actuator chambers. The description below, on the working principles of a servo-hydraulic actuator system, is based on details presented in Merritt (1967) and Kim and Tsao (2000). Figure 4.1 presents a schematic of a double-acting hydraulic actuator installed with a two-stage servovalve. The first stage, referred to as the *pilot* stage, consists of a motor-driven flapper, a symmetrical double-nozzle, and a feedback spring device for controlling the spool position. The second stage, referred to as the *spool* stage, consists of a four-way control spool[9] assembly.

At the null position (i.e., when the valve current $u_{\mathrm{i}} = 0$), the armature in the pilot stage remains horizontal between the yokes, and the flapper is centered between the two nozzles, as shown in Figure 4.1a. In this configuration, hydraulic fluid continuously flows from the supply ports (operated at a pressure P_{S}) through the fixed inlet orifices (flows Q_{A} and Q_{B}), past the variable nozzles into the flapper chamber (flows Q_{C} and Q_{D}), through the drain orifice (flow Q_{E}), to the return pressure port (operated at a pressure P_{R}). In a symmetrical servovalve, when the flapper is centered between the nozzles, the flows Q_{C} and Q_{D} are equal, resulting in equilibrium for the spool ($P_{\mathrm{A}} = P_{\mathrm{B}}$). During operation, a hydraulic controller (e.g., RMC75E) generates a valve command, u_{v}. This command is passed to a current driver module (e.g., VC2124), which then drives an appropriate amount of current, u_{i}, through the servovalve coils. The resulting magnetic force on the armature rotates the flexural sleeve support, as shown in Figure 4.1b. The rotated flapper assembly partially closes one of the nozzles, increasing the pressure, P_{A}^{*}, at that end of the spool, and decreasing the

[9] The descriptions of the *pilot* and *spool* stages herein are consistent with the MOOG 760F264A servovalve used in this work. Three-stage servovalves, commonly employed in larger shake tables (e.g., 6-DOF shake tables at the University at Buffalo), have a slightly different working mechanism.

pressure, P_B^*, at the other end. This differential pressure across the ends of the spool displaces it by a distance u_s, thus allowing the hydraulic fluid to flow from the supply pressure port to one of the actuator ports (flow Q_1) and from the other actuator port to the return port (flow Q_2).

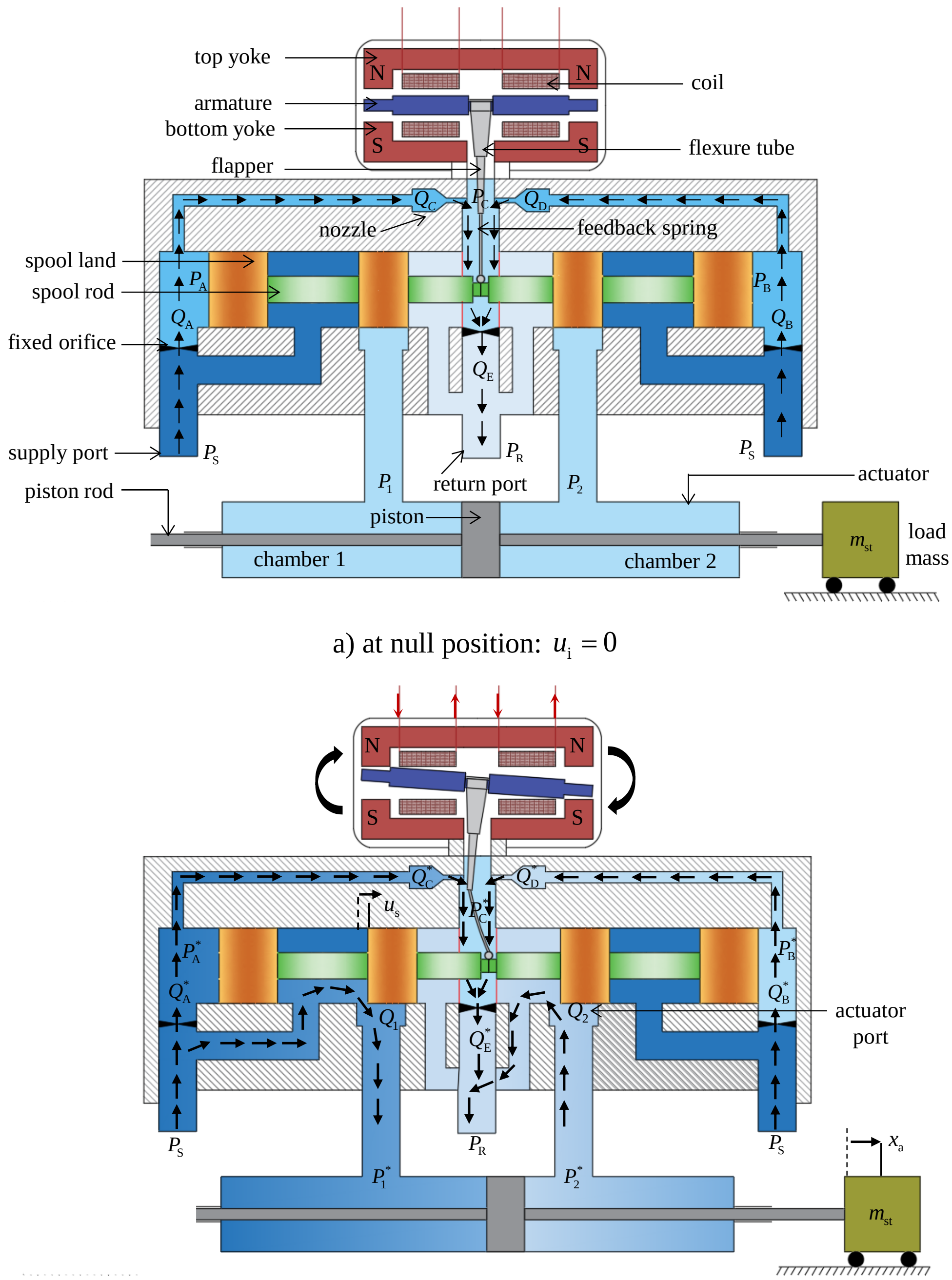

a) at null position: $u_i = 0$

b) valve responding to u_i

Figure 4.1. Working principles of a servo-hydraulic actuator system

The spool moves until the resulting torque from the feedback spring equals the torque produced by the input current. The differential pressure in the actuator chambers, $\Delta P = P_1 - P_2$, drives the load mass, m_{st}, which herein corresponds to the moving mass of the shake table. In this 1D configuration, the actuator force and the reaction force from the test article contributes to the equilibrium of the shake table.

In most control applications, the valve command, u_{v}, and by extension the valve current u_{i}, are not commanded directly. The servo-actuator system is rather operated in a closed-loop control mode with motion (e.g., displacement, acceleration) or force feedback. For the MIL experiments in this report, closed-loop position control is adopted wherein the user command is a reference position to the table. The valve command, u_{v}, is accordingly calculated by implementing the feedback: $u_{\mathrm{v}} = K_{\mathrm{e}} e + K_{\mathrm{d}} \dot{e} + K_{\mathrm{i}} \int e dt$, where the error $e = u - x_{\mathrm{st}}$ is the difference between the commanded, u, and the measured table position, x_{st}, and K_{e}, K_{i} and K_{d} are the proportional; error, integral error, and derivative error gains. Some applications also include ΔP measurement and velocity and acceleration feedforward schemes (Conte and Trombetti, 2000) in the hydraulic feedback. The dynamic response of an actuator system can be controlled by tuning these control gains, which is an important aspect of the impedance-matching approach (and actuator control in general). The next subsection presents a linear mathematical model for the uniaxial shake table, which takes u and w as the inputs and produces the table acceleration, z_{st}, as the output.

4.3 Mathematical modeling of the servo-hydraulic shake table

4.3.1 Overview

The early work on modeling servo-hydraulic actuators dates to mid-1950s. Much credit is attributed to Thayer (1958) and Merritt (1967) for their seminal work in developing the underlying theory. In later studies, researchers (e.g., Rea *et al.* (1977); Hwang *et al.* (1987); Blondet and Esparza (1988); Rinawi and Clough (1991); Muhlenkamp *et al.* (1997); Conte and Trombetti (2000); Kim and Tsao (2000); Stefanaki (2017)) built on Merritt's work and developed mathematical models for servo-hydraulic shake tables for use in earthquake-engineering applications.

It is well documented that servo-hydraulic actuator systems exhibit nonlinear behavior (Merritt, 1967). The nonlinearities arise from several sources, including electrical hysteresis of the torque motor, fluid flow through the orifices and nozzles, leakage through the ports, and sliding friction of the spool. By carefully tuning the control gains (e.g., K_{e}, K_{i}, K_{d}, K_{p}), the effects of these nonlinearities can be significantly curtailed so that a linear model of the table can be used for predicting its response with high fidelity.

The linear shake-table model presented in this report builds on the work of Merritt (1967) and Stefanaki (2017). The Stefanaki model is improved herein by addressing issues related to modeling of servovalve dynamics, tuning of control gains (K_{e} and K_{p}), and including the effect of controller sampling frequency. The improved model is shown to predict the response of the shake table with high accuracy in the frequency range of 0.25 Hz and 80 Hz (in the impedance-matching approach, the accuracy of the linear model is sought over a frequency range as broad as possible due to some fundamental constraints related to the implementation of the MIL controller, as described in Section 6.3).

The linear model is developed in three phases. The servovalve dynamics (i.e., relationship between valve current, u_{i}, and spool displacement, u_{s}) is modeled in the first phase. The second phase involves modeling of the actuator-table dynamics (i.e., relationship between spool displacement, u_{s}, and table acceleration, z_{st}; and between feedback force, w, and z_{st}), which overlaps with the presentation in Stefanaki (2017), but is reproduced here for completeness. The third phase includes modeling of hydraulic control (i.e., relationship between from control input, u, and valve current, u_{i}).

4.3.2 Phase I: Modeling of servovalve dynamics

Merritt (1967), Watton (1989), Lin and Akers (1989), Kim and Tsao (2000), and Liu and Jiang (2014) developed physics-based servovalve models with different degrees of complexity. These models are generally expressed in the form of frequency-domain transfer functions between input valve current, u_{i}, and output spool displacement, u_{s}. Figure 4.2 illustrates the block diagram of a two-stage servovalve model proposed by Merritt (1967). The model incorporates the dynamics of the torque motor, of the armature-flapper assembly, and of the spool valve, and also accounts for their internal force/pressure feedback loops.

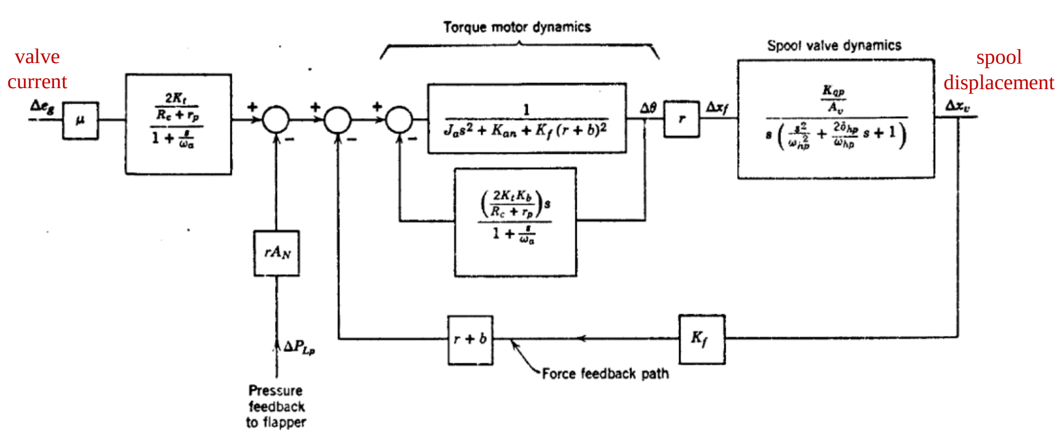

Figure 4.2. Block diagram for a two-stage servovalve model (Merritt, 1967)

The block diagram in Figure 4.2 can be reduced to a third-order transfer function of the form:

$$\frac{u_{\mathrm{s}}(s)}{u_{\mathrm{i}}(s)}=\frac{a_1}{s^3+b_1s^2+b_2s+b_3} \tag{4-1}$$

where the coefficients a_i and b_i are functions of the mechanical and geometrical parameters of the valve, and the properties of the hydraulic fluid. The downside to using physics-based servovalve models is that the manufacturers' technical specifications often do not provide sufficient information on many valve parameters, therefore making it difficult to estimate the model coefficients a_i and b_i. For example, Merritt's model of Figure 4.2 requires information on more than 30 valve parameters. The higher-order models (Kim and Tsao (2000); Liu and Jiang (2014)) require even more, thus limiting the application of physics-based models for representing servovalves.

In some past applications, researchers approximated servovalve dynamics using a constant gain factor (Rea *et al.* (1977); Blondet and Esparza (1988); Rinawi and Clough (1991)), whereas a few others have modeled it as a pure time-delay system (Conte and Trombetti, 2000). These approximations are deemed insufficient when table response is to be predicted over a broad frequency range (> 10 Hz).

In such cases, a practical approach is to measure the response of the servovalve across a broad frequency range and empirically fit the measured response with an approximate transfer function. If experimental valve measurements are not available, manufacturer data (amplitude and phase performance charts) can be used instead, as adopted in this report.

Figure 4.3a presents the performance curves for the MTS 252 Series servovalves (MTS, 2003), wherein the flow to the actuator ports, commonly referred to as the control flow, Q, is the ordinate and the excitation frequency of the valve current is the abscissa. In Figure 4.3b, the specification curve 252.25 corresponding to the MOOG 760F264A servovalve is approximated (see the dashed red line in the figure) using a second-order rational transfer function with two real poles[10] and no zeroes. The two poles are determined by curve-fitting as $\alpha_1=-2\pi 70$ rad/s and $\alpha_2=-2\pi 110$ rad/s. The second-order empirical model is seen to predict the valve frequency response with sufficient accuracy up to 100 Hz, much greater than the frequency range

[10] For a transfer function in the s-domain, $H(s)=n(s)/d(s)$, 'poles' are the roots of the denominator polynomial, $d(s)=0$, and 'zeros' are the roots of the numerator polynomial, $n(s)=0$.

of interest in the current MIL experiments (the oil-column resonance frequency of the shake table is observed around 30 Hz, and seismic isolation systems considered in the VS have dominant response in the low-frequency range < 2 Hz).

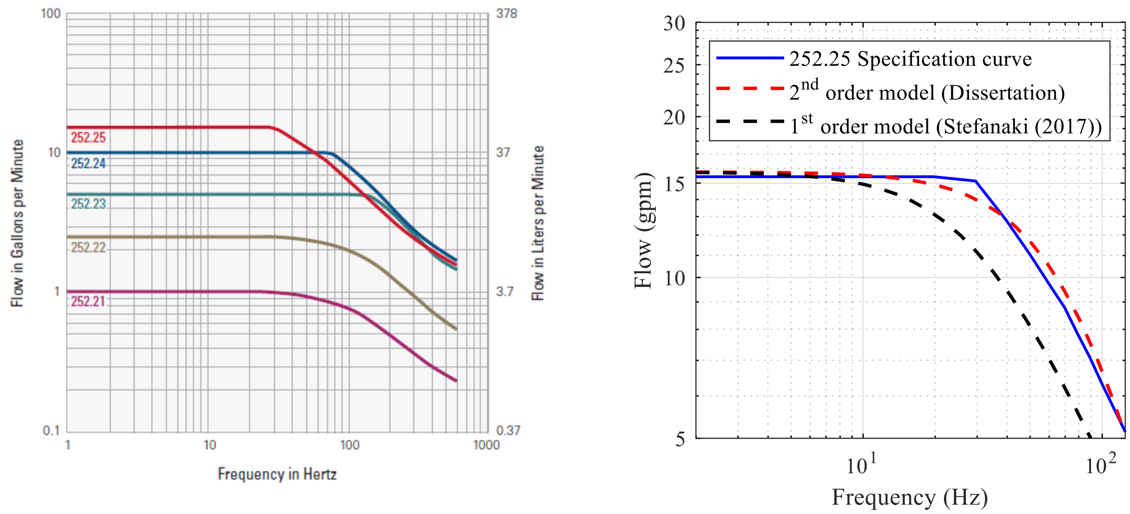

a) specification curve

b) empirical fitting

Figure 4.3. Modeling of servovalve dynamics using MTS specification curve (MTS, 2003)

For the same shake table, Stefanaki (2017) approximated servovalve dynamics using a first-order transfer function with a cutoff frequency at $2\pi 30$ rad/s (see the dashed black line in Figure 4.3b). The first-order model under predicts the valve response after frequencies greater than 10 Hz. In the MIL experiments presented in this report, the need for an accurate servovalve model over a broader frequency range relative to Stefanaki (2017) is noteworthy and necessitated by the greater relative degree of H_{zu}^{st} in motion-controlled MIL as opposed to the force-controlled MIL in Stefanaki (2017). The control flow to the actuator ports, Q, and the spool displacement are linearly related as $Q = K_{\mathrm{s}} u_{\mathrm{s}}$, where K_{s} is the spool flow gain (in^3/in). The valve transfer function is therefore written as:

$$\frac{Q(s)}{u_{\mathrm{i}}(s)} = \frac{K_{\mathrm{r}}}{K_{\mathrm{s}}} \frac{1}{(s+\alpha_1)(s+\alpha_2)} \tag{4-2}$$

Equation 4-3 presents state-space model of the servovalve with the valve current, u_{i}, as the input variable and the spool displacement, u_{s}, as one of the state variables:

$$\begin{pmatrix} \dot{u}_{\mathrm{s}} \\ \dot{v}_{\mathrm{s}} \end{pmatrix} = \begin{bmatrix} 0 & 1 \\ -\alpha_1\alpha_2 & -(\alpha_1+\alpha_2) \end{bmatrix} \begin{pmatrix} u_{\mathrm{s}} \\ v_{\mathrm{s}} \end{pmatrix} + \begin{pmatrix} 0 \\ K_{\mathrm{r}}\alpha_1\alpha_2 / K_{\mathrm{s}} \end{pmatrix} u_{\mathrm{i}} \tag{4-3}$$

where v_s is the spool velocity, α_1 and α_2 are the poles of the rational transfer function obtained by curve-fitting, and K_r is the servovalve static flow gain (i.e., ratio of the rated flow, Q_{max}, to the rated current, $u_{i,\,max}$). For the MOOG 760F264A servovalve, $K_r = Q_{max}/u_{i,\,max} = 57/25 \approx 2.3$ in^3/sec/mA (MTS, 2003).

4.3.3 Phase II: Modeling of actuator-table dynamics

The hydraulic flow through an actuator port depends on the pressure difference across the port and the area of the port opening. Merritt (1967) derived the following flow function using Bernoulli's principle:

$$Q = C_d A_o \sqrt{\frac{2\Delta P}{\rho}} \tag{4-4}$$

where C_d is the discharge coefficient of the port, ρ is the density of the hydraulic fluid, A_o is the area of the port opening, and ΔP is the differential pressure across the port. If the spool is perfectly aligned with the port dimensions, the port area, A_o, assumes an ideal profile as shown in Figure 4.4a (i.e., $A_o = 0$ when $u_s = 0$) with no leakage of flow when the spool is centered. However, manufacturing tolerances involve mechanical deadband (i.e., clearance between the spool landings and port ends), which results in a finite flow when the spool is centered, referred to as the null flow. A realistic profile for the port area is shown in Figure 4.4b with nonlinear transition near the null region and a gradual transition to saturation at the full port opening. Thus, A_o can be mathematically expressed as $A_o = G u_s$, where the area gradient (i.e., flow area/spool displacement), G, is a function of the spool displacement.

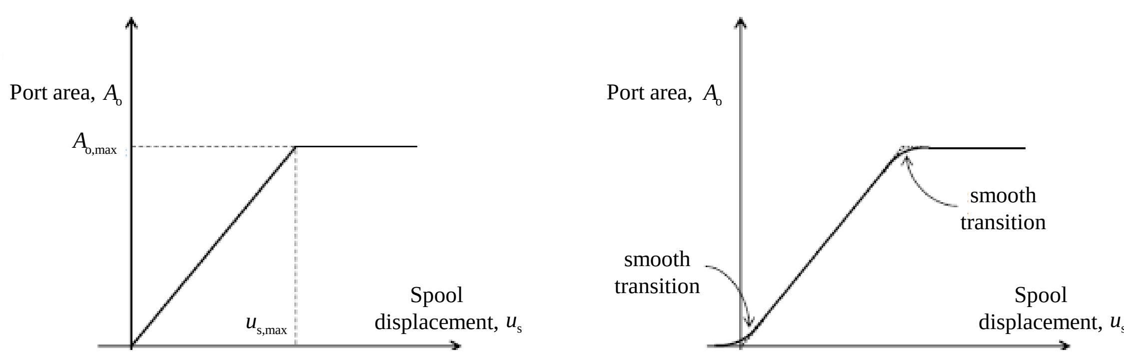

a) ideal orifice with abrupt opening and saturation

b) real orifice with null flow and gradual saturation

Figure 4.4. Qualitative description of the area of port opening (Stefanaki, 2017)

For the displaced spool position, u_s, flow through the actuator ports are given by:

$$Q_1 = C_{d1} G u_s \sqrt{\frac{2(P_S - P_1)}{\rho}} \tag{4-5a}$$

$$Q_2 = C_{d2} G u_s \sqrt{\frac{2(P_2 - P_R)}{\rho}} \tag{4-5b}$$

where P_S is the supply pressure (= 3000 psi herein), P_R is the return pressure (≈ 0 psi), P_1 and P_2 are the pressures in the two actuator chambers, and C_{d1} and C_{d2} are the discharge coefficients of the actuator ports. The uniaxial shake table utilizes a double-acting actuator with a symmetrical servovalve. The discharge coefficients, C_{d1} and C_{d2}, are equal, and denoted by C_d. The rate of fluid flow through the ports must compensate for (i) the change in the volume of the hydraulic fluid in each actuator chamber resulting from the piston displacement and (ii) compressibility of the oil. The flow continuity equations are therefore written as (Merritt, 1967):

$$\dot{P}_1 = \frac{\kappa}{V_{a1}} \left(C_d G u_s \sqrt{\frac{2(P_S - P_1)}{\rho}} - A_p v_a \right) \tag{4-6a}$$

$$\dot{P}_2 = \frac{\kappa}{V_{a2}} \left(A_p v_a - G u_s \sqrt{\frac{2(P_2 - P_R)}{\rho}} \right) \tag{4-6b}$$

where V_{a1} and V_{a2} are the volumes of hydraulic fluid in the actuator chambers, A_p is the area of actuator piston, κ is the bulk modulus of the hydraulic fluid, v_a is the velocity of the actuator piston, and other terms were defined previously. If the displacement of the piston from its mid-stroke position, x_m, is denoted by x_a, the chamber volumes can be calculated as $V_{a1} = A_p(x_m + x_a)$ and $V_{a2} = A_p(x_m - x_a)$. Manufacturing imperfections result in the leakage of flow between the actuator chambers across the piston. The leakage flow is modeled as $Q_L = K_l(P_1 - P_2)$, where K_l is the leakage coefficient, also known as, flow-pressure coefficient (Blondet and Esparza, 1988). In the presence of a test article, force equilibrium for the shake table results in the following equations of motion:

$$\dot{x}_{st} = v_{st} \tag{4-7a}$$

$$m_{st} z_{st} - w = \underbrace{A_p(P_1 - P_2)}_{\text{actuator force}} \tag{4-7b}$$

where m_{st} is the moving mass of the shake table that is assumed to be rigid. Hence, $x_{\mathrm{a}} = x_{\mathrm{st}}$, and $v_{\mathrm{a}} = v_{\mathrm{st}}$. Friction forces near the rail guides and within the actuator seals are assumed to be negligible compared to the actuator force, and hence are ignored in the modeling. The implications of ignoring friction are discussed in Sections 8 and 9. Combining Equations 4-6 and 4-7, the system of equations for the combined actuator and table system can be written as:

$$\dot{x}_{\mathrm{st}} = v_{\mathrm{st}} \tag{4-8a}$$

$$\dot{v}_{\mathrm{st}} = \frac{A_{\mathrm{p}}\left(P_1 - P_2\right)}{m_{\mathrm{st}}} + \frac{w}{m_{\mathrm{st}}} \tag{4-8b}$$

$$\dot{P}_1 = \frac{\kappa}{A_{\mathrm{p}}\left(x_{\mathrm{m}} + x_{\mathrm{st}}\right)}\left(C_{\mathrm{d}} G u_{\mathrm{s}} \sqrt{\frac{2\left(P_{\mathrm{S}} - P_1\right)}{\rho}} - A_{\mathrm{p}} v_{\mathrm{st}} - K_l\left(P_1 - P_2\right)\right) \tag{4-8c}$$

$$\dot{P}_2 = \frac{\kappa}{A_{\mathrm{p}}\left(x_{\mathrm{m}} - x_{\mathrm{st}}\right)}\left(-C_{\mathrm{d}} G u_{\mathrm{s}} \sqrt{\frac{2\left(P_2 - P_{\mathrm{R}}\right)}{\rho}} + A_{\mathrm{p}} v_{\mathrm{st}} + K_l\left(P_1 - P_2\right)\right) \tag{4-8d}$$

where x_{st}, v_{st}, P_1, and P_2 are the state variables, and u_{s} and w are the inputs to the system. From above, the state equations 4-8c and 4-8d are nonlinear. These equations are linearized with respect to an equilibrium state derived for the input conditions: $u_{\mathrm{s}} = 0$ and $w = 0$. At equilibrium, the position and velocity of the shake table are zero and the sum of the pressures in the actuator chambers is $P_1 + P_2 = P_{\mathrm{S}} + P_{\mathrm{R}}$. The equilibrium states are therefore calculated as $x_{\mathrm{st,e}} = 0$, $v_{\mathrm{st,e}} = 0$, and $P_{\mathrm{a1,e}} = P_{\mathrm{a2,e}} = 0.5P_{\mathrm{S}}$. The linearized state-space system is then reduced[11] to three states by representing the differential pressure in the actuator chambers ($\Delta P = P_1 - P_2$) as a single state variable. The reduced state equations of the linear shake-table model are:

$$\begin{pmatrix} \dot{x}_{\mathrm{st}} \\ \dot{v}_{\mathrm{st}} \\ \Delta\dot{P} \end{pmatrix} = \begin{bmatrix} 0 & 1 & 0 \\ 0 & 0 & A_{\mathrm{p}}/m_{\mathrm{st}} \\ 0 & -2\kappa/x_{\mathrm{m}} & -2\kappa K_l/A_{\mathrm{p}} x_{\mathrm{m}} \end{bmatrix} \begin{pmatrix} x_{\mathrm{a}} \\ v_{\mathrm{a}} \\ \Delta P \end{pmatrix} + \begin{pmatrix} 0 \\ 0 \\ 2\kappa C_{\mathrm{d}} G_{u_{\mathrm{s}}=0}\sqrt{P_{\mathrm{S}}} \big/ A_{\mathrm{p}} x_{\mathrm{m}} \sqrt{\rho} \end{pmatrix} u_{\mathrm{s}} + \begin{pmatrix} 0 \\ 1/m_{\mathrm{st}} \\ 0 \end{pmatrix} w \tag{4-9}$$

The eigenvalues of the above state matrix are calculated as $\lambda_1 = 0$, and $\lambda_{2,3} = -\zeta_{\mathrm{oil}}\omega_{\mathrm{oil}} \pm \omega_{\mathrm{oil}}\sqrt{1-\zeta_{\mathrm{oil}}^2}$. The complex conjugate pair of the eigenvalues, $\lambda_{2,3}$, corresponds to what is commonly referred to as *oil-column*

[11] Transitioning from a four-state model in Equation 4-8 to three-state model in Equation 4-9 is based on some observability/controllability arguments (see Chapter 3 of Stefanaki (2017) for details).

resonance in the literature. The oil-column frequency, ω_{oil}, is representative of the shake-table mass m_{st} connected to two linear springs (oil in the actuator chambers) of stiffness $\kappa A_{\mathrm{p}}/x_{\mathrm{m}}$, and is given by Equation 4-10a, and ζ_{oil} corresponds to the damping in the oil-column and is given by Equation 4-10b. (Other flexibilities and damping related to spool, piston, actuator body, and platform are ignored in the modeling.)

$$\omega_{\mathrm{oil}} = \sqrt{\frac{2A_{\mathrm{p}}\kappa}{m_{\mathrm{st}}x_{\mathrm{m}}}} \tag{4-10a}$$

$$\zeta_{\mathrm{oil}} = K_l\sqrt{\frac{\mathrm{m}_{\mathrm{st}}\kappa}{2A_{\mathrm{p}}^3 x_{\mathrm{m}}}} \tag{4-10b}$$

Combining Equations 4-3, 4-9, and 4-10, the linear state-space model of the combined servovalve-actuator-table system can be written as:

$$\begin{pmatrix}\dot{x}_1\\ \dot{x}_2\\ \dot{x}_3\\ \dot{x}_4\\ \dot{x}_5\end{pmatrix} = \begin{bmatrix} 0 & 1 & 0 & 0 & 0\\ 0 & 0 & A_{\mathrm{p}}/m_{\mathrm{st}} & 0 & 0\\ 0 & -\omega_{\mathrm{oil}}^2 m_{\mathrm{st}}/A_{\mathrm{p}} & -2\zeta_{\mathrm{oil}}\omega_{\mathrm{oil}} & d & 0\\ 0 & 0 & 0 & 0 & 1\\ 0 & 0 & 0 & -\alpha_1\alpha_2 & -(\alpha_1+\alpha_2)\end{bmatrix}\begin{pmatrix}x_1\\ x_2\\ x_3\\ x_4\\ x_5\end{pmatrix} + \begin{pmatrix}0\\ 0\\ 0\\ 0\\ \alpha_1\alpha_2\end{pmatrix}u_{\mathrm{i}} + \begin{pmatrix}0\\ 1/m_{\mathrm{st}}\\ 0\\ 0\\ 0\end{pmatrix}w \tag{4-11}$$

where x_1, x_2, and x_3 are the actuator states, x_4 and x_5 are the servovalve states, and d is a model constant given by

$$d = \frac{2\kappa}{A_{\mathrm{p}}x_{\mathrm{m}}}C_{\mathrm{d}}G_{u_{\mathrm{s}}=0}\sqrt{\frac{P_{\mathrm{S}}}{\rho}\frac{K_{\mathrm{r}}}{K_{\mathrm{s}}}} \tag{4-12}$$

4.3.4 Phase III. Hydraulic control of shake table

In Equation 4-11, the inputs to the system are the valve current, u_{i}, and the feedback force, w. However, in the MIL experiments, the valve current is not commanded directly. Rather, the shake table is operated in a closed-loop control mode wherein the control input, u, is a reference position command issued by the user, and the valve command, u_{v}, is computed by implementing the hydraulic control loop with position and differential pressure feedback: $u_{\mathrm{v}} = K_{\mathrm{e}}e - K_{\mathrm{p}}\Delta P$, where $e = u - x_{\mathrm{st}}$ is the error between the commanded and the measured displacement of the table, K_{e} is the proportional error gain, and K_{p} is the ΔP gain. (The integral error and derivative error gains are set to zero.) Note that the AA1 axis module of the RMC75E implements this hydraulic loop, outputs the calculated u_{v} to the VC2124 unit which then drives a proportional valve current of magnitude $u_{\text{i}} = K_{\text{v}} u_{\text{v}}$.

The hydraulic control equation above assumes that the valve command is generated in continuous-time. However, a digital controller, like the RMC75E, implements this equation and issues valve command at discrete time intervals equal to the sampling time, τ_{s} (or frequency, f_{s}) of the controller. Such digital control utilizes the feedback measurements saved from the previous loop time, $x_1(t-\tau_{\text{s}})$ and $x_3(t-\tau_{\text{s}})$, for computations: $u_{\text{v}}(t) = K_{\text{e}}\left(u(t) - x_1(t-\tau_{\text{s}})\right) - K_{\text{p}} x_3(t-\tau_{\text{s}})$, indicating that the feedback is delayed by one loop time[12]. The longer the loop time, the greater the delay, and more apparent are the consequences (see Section 4.4.4) of using a digital controller. The Laplace-domain representation of the hydraulic control equation is: $u_{\text{v}}(s) = K_{\text{e}}\left(u(s) - e^{-s\tau_{\text{s}}} x_1(s)\right) - K_{\text{p}} e^{-s\tau_{\text{s}}} x_3$. Considering a first-order Taylor series approximation for the delay term, $e^{-s\tau_{\text{s}}} \approx 1 - s\tau_{\text{s}}$ for $|s\tau_{\text{s}}| << 1$, $u_{\text{v}}(s)$ can be rewritten as $u_{\text{v}}(s) = K_{\text{e}} u(s) - K_{\text{e}}(1-s\tau_{\text{s}}) x_1(s) - K_{\text{p}}(1-s\tau_{\text{s}}) x_3(s)$, whose time-domain representation is:

$$u_{\text{v}} = K_{\text{e}} u - K_{\text{e}} x_1 + \tau_{\text{s}}\left(K_{\text{e}} - K_{\text{p}} \omega_{\text{oil}}^2 m^{\text{st}} \big/ A_{\text{p}}\right) x_2 - K_{\text{p}}\left(1 + \tau_{\text{s}} \varepsilon\right) x_3 + \tau_{\text{s}} K_{\text{p}} d x_4. \tag{4-13}$$

Combining Equations 4-11 and 4-13, the linear state-space model of the shake table is given by Equation 4-14a (for a digital controller with a finite loop time, τ_{s}) and 4-14b (for an analog controller, $\tau_{\text{s}} = 0$). The analytical transfer functions of the shake table are derived from the linear model and are presented in Equations 4-15a through 4-15f.

> Another key difference between the current model and that described in Stefanaki (2017) is the explicit modeling of delay in hydraulic feedback to account for the effect of controller sampling (τ_{s} or f_{s}). The experiments in Stefanaki (2017) utilized an analog controller and hence there was no sampling ($\tau_{\text{s}} = 0$). It will be shown in Section 4.5.3 that the frequency response of the table is significantly affected by τ_{s}, particularly when large values of K_{p} are used.

[12] Loop time is the pre-selected time interval at which the digital controller reads inputs, runs user programs, processes motion commands, performs hydraulic control action, and updates outputs. When the controller completes its calculations for a particular loop time, it waits until the next loop time (the control action is zero in this period) to repeat its calculations. On the other hand, the sampling time of an analog controller is the interval at which the outputs are written to a data acquisition system, but the control action is continuous-time.

$$\begin{pmatrix}\dot{x}_1\\ \dot{x}_2\\ \dot{x}_3\\ \dot{x}_4\\ \dot{x}_5\end{pmatrix}=\begin{bmatrix}0 & 1 & 0 & 0 & 0\\ 0 & 0 & A_{\mathrm{p}}/m_{\mathrm{st}} & 0 & 0\\ 0 & -\omega_{\mathrm{oil}}^2 m_{\mathrm{st}}/A_{\mathrm{p}} & -\varepsilon & d & 0\\ 0 & 0 & 0 & 0 & 1\\ -K_{\mathrm{v}}K_{\mathrm{e}}\gamma & K_{\mathrm{v}}\gamma\tau_{\mathrm{s}}\left(K_{\mathrm{e}}-K_{\mathrm{p}}\omega_{\mathrm{oil}}^2 m_{\mathrm{st}}/A_{\mathrm{p}}\right) & -K_{\mathrm{v}}K_{\mathrm{p}}\gamma\left(1+\tau_{\mathrm{s}}\varepsilon\right) & \gamma\left(dK_{\mathrm{p}}\tau_{\mathrm{s}}-1\right) & -\left(\alpha_1+\alpha_2\right)\end{bmatrix}\begin{pmatrix}x_1\\ x_2\\ x_3\\ x_4\\ x_5\end{pmatrix}+\begin{pmatrix}0\\ 0\\ 0\\ 0\\ K_{\mathrm{v}}K_{\mathrm{e}}\gamma\end{pmatrix}u+\begin{pmatrix}0\\ 1/m_{\mathrm{st}}\\ 0\\ 0\\ 0\end{pmatrix}w \tag{4-14a}$$

$$\begin{pmatrix}\dot{x}_1\\ \dot{x}_2\\ \dot{x}_3\\ \dot{x}_4\\ \dot{x}_5\end{pmatrix}=\begin{bmatrix}0 & 1 & 0 & 0 & 0\\ 0 & 0 & A_{\mathrm{p}}/m_{\mathrm{st}} & 0 & 0\\ 0 & -\omega_{\mathrm{oil}}^2 m_{\mathrm{st}}/A_{\mathrm{p}} & -2\zeta_{\mathrm{oil}}\omega_{\mathrm{oil}} & d & 0\\ 0 & 0 & 0 & 0 & 1\\ -K_{\mathrm{v}}K_{\mathrm{e}}\alpha_1\alpha_2 & 0 & -K_{\mathrm{v}}K_{\mathrm{p}}\alpha_1\alpha_2 & -\alpha_1\alpha_2 & -\left(\alpha_1+\alpha_2\right)\end{bmatrix}\begin{pmatrix}x_1\\ x_2\\ x_3\\ x_4\\ x_5\end{pmatrix}+\begin{pmatrix}0\\ 0\\ 0\\ 0\\ K_{\mathrm{v}}K_{\mathrm{e}}\alpha_1\alpha_2\end{pmatrix}u+\begin{pmatrix}0\\ 1/m_{\mathrm{st}}\\ 0\\ 0\\ 0\end{pmatrix}w \tag{4-14b}$$

where $\delta=\alpha_1+\alpha_2,\ \gamma=\alpha_1\alpha_2,\ \varepsilon=2\zeta_{\mathrm{oil}}\omega_{\mathrm{oil}}$.

$$H_{zu}^{\mathrm{st}} = \frac{\left(\gamma d A_{\mathrm{p}} K_{\mathrm{v}} K_{\mathrm{e}} / m_{\mathrm{st}}\right) s^2}{s^5 + \left(\delta + \varepsilon\right) s^4 + \left(\omega_{\mathrm{oil}}^2 + \delta\varepsilon + \gamma - \gamma d K_{\mathrm{v}} K_{\mathrm{p}} \tau_{\mathrm{s}}\right) s^3 + \left(\delta\omega_{\mathrm{oil}}^2 + \gamma\varepsilon + \gamma d K_{\mathrm{v}} K_{\mathrm{p}}\right) s^2 + \left(\gamma\omega_{\mathrm{oil}}^2 - \gamma d A_{\mathrm{p}} K_{\mathrm{v}} K_{\mathrm{e}} \tau_{\mathrm{s}} / m_{\mathrm{st}}\right) s + \left(\gamma d A_{\mathrm{p}} K_{\mathrm{v}} K_{\mathrm{e}} / m_{\mathrm{st}}\right)} \tag{4-15a}$$

$$H_{xu}^{\mathrm{st}} = \frac{\gamma d A_{\mathrm{p}} K_{\mathrm{v}} K_{\mathrm{e}} / m_{\mathrm{st}}}{s^5 + \left(\delta + \varepsilon\right) s^4 + \left(\omega_{\mathrm{oil}}^2 + \delta\varepsilon + \gamma - \gamma d K_{\mathrm{v}} K_{\mathrm{p}} \tau_{\mathrm{s}}\right) s^3 + \left(\delta\omega_{\mathrm{oil}}^2 + \gamma\varepsilon + \gamma d K_{\mathrm{v}} K_{\mathrm{p}}\right) s^2 + \left(\gamma\omega_{\mathrm{oil}}^2 - \gamma d A_{\mathrm{p}} K_{\mathrm{v}} K_{\mathrm{e}} \tau_{\mathrm{s}} / m_{\mathrm{st}}\right) s + \left(\gamma d A_{\mathrm{p}} K_{\mathrm{v}} K_{\mathrm{e}} / m_{\mathrm{st}}\right)} \tag{4-15b}$$

$$H_{\Delta Pu}^{\mathrm{st}} = \frac{\left(\gamma d K_{\mathrm{v}} K_{\mathrm{e}}\right) s^2}{s^5 + \left(\delta + \varepsilon\right) s^4 + \left(\omega_{\mathrm{oil}}^2 + \delta\varepsilon + \gamma - \gamma d K_{\mathrm{v}} K_{\mathrm{p}} \tau_{\mathrm{s}}\right) s^3 + \left(\delta\omega_{\mathrm{oil}}^2 + \gamma\varepsilon + \gamma d K_{\mathrm{v}} K_{\mathrm{p}}\right) s^2 + \left(\gamma\omega_{\mathrm{oil}}^2 - \gamma d A_{\mathrm{p}} K_{\mathrm{v}} K_{\mathrm{e}} \tau_{\mathrm{s}} / m_{\mathrm{st}}\right) s + \left(\gamma d A_{\mathrm{p}} K_{\mathrm{v}} K_{\mathrm{e}} / m_{\mathrm{st}}\right)} \tag{4-15c}$$

$$H_{zw}^{\mathrm{st}} = \frac{\left(1/m_{\mathrm{st}}\right)\left(s^5 + \left(\delta + \varepsilon\right) s^4 + \left(\delta\varepsilon + \gamma - \gamma d K_{\mathrm{v}} K_{\mathrm{p}} \tau_{\mathrm{s}}\right) s^3 + \left(\gamma\varepsilon + \gamma d K_{\mathrm{v}} K_{\mathrm{p}}\right) s^2\right)}{s^5 + \left(\delta + \varepsilon\right) s^4 + \left(\omega_{\mathrm{oil}}^2 + \delta\varepsilon + \gamma - \gamma d K_{\mathrm{v}} K_{\mathrm{p}} \tau_{\mathrm{s}}\right) s^3 + \left(\delta\omega_{\mathrm{oil}}^2 + \gamma\varepsilon + \gamma d K_{\mathrm{v}} K_{\mathrm{p}}\right) s^2 + \left(\gamma\omega_{\mathrm{oil}}^2 - \gamma d A_{\mathrm{p}} K_{\mathrm{v}} K_{\mathrm{e}} \tau_{\mathrm{s}} / m_{\mathrm{st}}\right) s + \left(\gamma d A_{\mathrm{p}} K_{\mathrm{v}} K_{\mathrm{e}} / m_{\mathrm{st}}\right)} \tag{4-15d}$$

$$H_{xw}^{\mathrm{st}} = \frac{\left(1/m_{\mathrm{st}}\right)\left(s^3 + \left(\delta + \varepsilon\right) s^2 + \left(\delta\varepsilon + \gamma - \gamma d K_{\mathrm{v}} K_{\mathrm{p}} \tau_{\mathrm{s}}\right) s^1 + \left(\gamma\varepsilon + \gamma d K_{\mathrm{v}} K_{\mathrm{p}}\right)\right)}{s^5 + \left(\delta + \varepsilon\right) s^4 + \left(\omega_{\mathrm{oil}}^2 + \delta\varepsilon + \gamma - \gamma d K_{\mathrm{v}} K_{\mathrm{p}} \tau_{\mathrm{s}}\right) s^3 + \left(\delta\omega_{\mathrm{oil}}^2 + \gamma\varepsilon + \gamma d K_{\mathrm{v}} K_{\mathrm{p}}\right) s^2 + \left(\gamma\omega_{\mathrm{oil}}^2 - \gamma d A_{\mathrm{p}} K_{\mathrm{v}} K_{\mathrm{e}} \tau_{\mathrm{s}} / m_{\mathrm{st}}\right) s + \left(\gamma d A_{\mathrm{p}} K_{\mathrm{v}} K_{\mathrm{e}} / m_{\mathrm{st}}\right)} \tag{4-15e}$$

$$H_{\Delta Pw}^{\mathrm{st}} = \frac{-\left(\omega_{\mathrm{oil}}^2 / A_{\mathrm{p}}\right) s^3 - \left(\delta\omega_{\mathrm{oil}}^2 / A_{\mathrm{p}}\right) s^2 - \left(\gamma\omega_{\mathrm{oil}}^2 / A_{\mathrm{p}} - \gamma d K_{\mathrm{v}} K_{\mathrm{e}} \tau_{\mathrm{s}} / m_{\mathrm{st}}\right) s - \left(\gamma d K_{\mathrm{v}} K_{\mathrm{e}} / m_{\mathrm{st}}\right)}{s^5 + \left(\delta + \varepsilon\right) s^4 + \left(\omega_{\mathrm{oil}}^2 + \delta\varepsilon + \gamma - \gamma d K_{\mathrm{v}} K_{\mathrm{p}} \tau_{\mathrm{s}}\right) s^3 + \left(\delta\omega_{\mathrm{oil}}^2 + \gamma\varepsilon + \gamma d K_{\mathrm{v}} K_{\mathrm{p}}\right) s^2 + \left(\gamma\omega_{\mathrm{oil}}^2 - \gamma d A_{\mathrm{p}} K_{\mathrm{v}} K_{\mathrm{e}} \tau_{\mathrm{s}} / m_{\mathrm{st}}\right) s + \left(\gamma d A_{\mathrm{p}} K_{\mathrm{v}} K_{\mathrm{e}} / m_{\mathrm{st}}\right)} \tag{4-15f}$$

* K_{e}, K_{p}, K_{v}, and τ_{s} are control parameters of the shake table, and are highlighted in red to distinguish from other parameters. These parameters can be carefully tuned to alter the frequency response of the shake table. In Section 4.4, the above analytical transfer functions are used to assess the dynamic characteristics of the shake table for different combinations of control parameters to identify their optimal values for MIL experiments.

4.3.5 Model parameters

The analytical shake-table transfer functions presented in Equation 4-15 are derived as a function of: (i) four control parameters: K_e, K_p, K_v, and τ_s, which are to be defined by the user, (ii) three specification parameters: x_m, A_p, and m_{st}, which are determined from the manufacturer's specifications, and (iii) five system parameters: d, α_1, α_2, ζ_{oil}, and ω_{oil}, which are determined from the frequency-response measurements of the shake table. Table 4.1 reports the values of these parameters used in the MIL experiments.

Table 4.1. Model parameters used for the MIL experiments

Parameter	Symbol	Value	Unit	Comment
Proportional gain	K_e	5	V/in	Tuned for a robust and accurate mathematical model (see Section 4.4)
ΔP gain	K_p	0.001	V/psi	
Controller loop time	τ_s	500	μs	
Voltage-to-current gain	K_v	3	mA/V	
Piston area	A_p	2.1	in^2	Specification manual
Mid-stroke position	x_m	3.2	in	
Table mass	m_{st}	4.14	lb-s/in^2	
Model constant	d	3×10^5	lb-mA/in^5/V	Determined empirically
Servovalve poles	α_1, α_2	2π70, 2π110	rad/sec	
Oil-column damping	ζ_{oil}	0.09	-	
Oil-column frequency	ω_{oil}	2π27	rad/sec	

***Control gains K_e and K_p*:** In the traditional approaches to MIL reviewed in Section 2.1, the control gains are typically tuned for accurate tracking of the reference command (i.e., minimize the difference between the commanded and the actual displacement), hence such controllers are referred to as 'tracking controllers'. In the MIL experiments of this report, although the shake table is operated in closed-loop position control mode, the goal is not to track the reference position command. Rather, the control gains are tuned so that analytical H_{zu}^{st} and H_{zw}^{st} closely matches the measured frequency response of the table (see Figures 4-16 and 4-18), thus enabling the use of these transfer functions for design and implementation of the MIL controller. The gain values that enabled this outcome are $K_e = 5$ V/in and $K_p = 0.001$ V/psi (see

Sections 4.4.2 and 4.4.3). As noted previously in Section 2.1, the key feature of the impedance-matching approach is that the reference command (i.e., control input) need not be the desired boundary condition that needs to be controlled at the actuator-test article interface. Herein, the control input, u, is the reference position command but the boundary condition controlled at the interface is the table acceleration

Controller loop time, τ_s : The feedback terms x_{st} and ΔP in the hydraulic control loop are delayed by the controller loop time. For an analog controller, $\tau_s \to 0$. Digital controllers with smaller loop times are preferred for the reasons to be discussed in Section 4.4.4. A controller loop time of 500 μs (sampling frequency of 2000 Hz) is used in the MIL experiments.

Voltage-to-current gain, K_v : This VC2124 setting determines the amount of current driven through the servovalve for the calculated valve command, u_v. Ideally, when u_v assumes its maximum value of 10 V, the valve must be operated at full-flow condition (i.e., actuator port area is fully open, $A_{o,max}$ and the control flow is Q_{max}). In the MIL experiments, the dial on VC2124 is set to 30 mA, close to the rated full-flow current of the MOOG servovalve ($u_{i,max} = 25$ mA). Thus, K_v is computed to be 30 mA/10 V = 3 mA/V.

Mid-stroke position, x_m : This information is provided by the manufacturer. The end-to-end dynamic stroke of the MTS 244.12 actuator is 6.4 inches (MTS, 2017). Therefore, x_m is 3.2 inches.

Piston area, A_p : This information is provided by the manufacturer. For the MTS 244.12 actuator, A_p = 2.1 in^2 (MTS, 2017).

Table mass, m_{st} : This corresponds to the total moving mass of the shake table including the platform, posts, connecting blocks, and stiffeners. It is measured directly using a scale as 4.14 lb-s/in^2 (1600 lb).

Model constant, d : The model constant (see Equation 4-12) depends on other system parameters. It is difficult to accurately quantify some of these parameters (e.g., C_d, $G_{u_s=0}$, K_s), hence d is determined empirically from the frequency response measurements of the shake-table as 10^5 lb-mA/in^5/V.

Servovalve poles, α_1, α_2 : The servovalve poles are determined are deduced from the valve specification curve by curve-fitting (see Figure 4.3b): α_1 = 2π70 rad/s and α_2 = 2π110 rad/s.

Oil-column frequency, ω_{oil} : For A_p = 2.1 in^2, x_m = 3.2 in, m_{st} = 4.14 lb-s^2/in, and assuming $\kappa = 10^5$ lb/in^2 (Merritt, 1967), the oil-column frequency of the uniaxial shake table is calculated using Equation 4-10a as 178 rad/s or 28.3 Hz. However, the bulk modulus, κ, is a function of fluid type and temperature.

The frequency-response experiments of Section 4.5 revealed the oil-column frequency to be 27 Hz, within 5% of the value calculated theoretically for $\kappa = 10^5$ lb/in^2.

Oil-column damping ratio, ζ_{oil} : Equation 4-10b indicates that oil-column damping is associated with the leakage coefficient, K_1, which is difficult to quantify theoretically. The value for $\zeta_{\text{oil}} = 0.09$ is determined by comparing the frequency responses of the model and the table measurements (see Section 4.5.3).

4.4 Tuning the shake-table control parameters

4.4.1 Overview

This subsection describes a rational procedure for tuning the shake-table control parameters (K_e, K_p, τ_s, and K_v) to meet the dual objectives of: (i) acceptable responsiveness of the system to the control input at low frequencies; this is a qualitative measure and is essential for negating the effects of friction[13], and is achieved by tuning the proportional error gain, K_e and (ii) damping the table response near the oil-column resonance frequencies to the extent possible; this is to curtail the effects of nonlinearities in the servovalve-actuator system, which are largely associated with the oil column resonance, and is achieved by carefully tuning the ΔP gain.

The analytical transfer functions of Equation 4-15 are used to investigate the effect of these control parameters on the dynamics response of the shake table by: (i) gradually increasing the value of K_e when $K_p = 0$ and $\tau_s = 0$, (ii) by setting K_e to the acceptable value determined in step (i) and gradually increasing the value of K_p, and (iii) by setting K_e and K_p to the values determined in steps (i) and (ii), respectively, and varying τ_s per the loop times available in the RMC75E controller. The fourth control parameter K_v, namely, the voltage-to-current conversion gain of VC2124, is set constant at 3 mA/V for all the cases. Bode diagrams[14] and root locus[15] plots (Ogata, 2010) are used to assess the dynamic characteristics and shake table for different combinations of the control parameters.

---

[13] In the MIL experiments, the shake table is predominantly operated in the low-frequency range (< 2 Hz) corresponding to the seismic isolation systems. Therefore, a sufficiently large proportional gain is needed to reduce the effects of friction, which are significant at low frequencies, for accurate MIL control.

[14] Bode diagrams present the frequency response of a dynamic system, $H(s)$. The magnitude plot is the locus of the absolute values of the transfer function, evaluated as $|H(j\omega)|$, frequency by frequency, and j is the imaginary unit. Phase charts are plotted as $\tan^{-1}\left(\text{Im}(H(j\omega))/\text{Re}(H(j\omega))\right)$ versus frequency.

[15] Root locus is a powerful tool for investigating the stability of a closed-loop control system. It is a graphical representation of the poles of the system as the feedback gain (or any system parameter) is varied from 0 to ∞.

4.4.2 Tuning the proportional gain, K_e

Figure 4.5 presents Bode plots of the shake-table transfer functions, H_{zu}^{st}, H_{xu}^{st}, H_{zw}^{st}, and H_{xw}^{st}, for the cases where $K_p = 0$, $\tau_s = 0$ (i.e., analog controller), and K_e is increased from 1 to 5 V/in, in increments of 1 V/in. Other model parameters are taken per Table 4.1. The following key observations are made from the Bode plots, which are well recognized in the literature (e.g., Conte and Trombetti, 2000).)

- In the magnitude charts of Figure 4.5a and Figure 4.5c, the sharp peaks observed near 27 Hz correspond to the oil-column resonance in the shake-table. As the gain K_e is increased, the system becomes more responsive, and therefore the magnitude of this peak increases with no appreciable change in the associated frequency.

- For smaller values of K_e (< 2 V/in), the shake table exhibits a sluggish (i.e., poor tracking of the reference u) response in the low frequency range (< 3 Hz), as indicated by the blue and orange lines for H_{xu}^{st} in Figure 4.5b. The performance of sluggish system is more prone to the effects of friction and is not desirable because the linear model does not account for such effects.

- Increasing the proportional gain sufficiently increases system's responsiveness, and consequently, improves tracking performance at low frequencies (see the blue and green lines in Figure 4.5b), but the trade-off is seen in terms of significant amplification of the response near the oil-column frequencies, that is, in the range of 20 to 40 Hz.

- The traditional approaches to MIL reviewed in Section 2.1 focus on tuning the control gains for accurate tracking of the reference displacement command u, that is, $\left|H_{xu}^{st}\right|$ should ideally be ≈ 1 and $\varphi(H_{xu}^{st})$ $\approx 0^{o}$, over a broad frequency range. However, like any other dynamic system, the shake table cannot track the reference command accurately across all frequencies.

The dynamic characteristics of the shake table are assessed by plotting the root locus of H_{zu}^{st} (i.e., loci of the roots of its denominator: $s^5 + (\delta + \varepsilon)s^4 + (\omega_{oil}^2 + \delta\varepsilon + \gamma)s^3 + (\delta\omega_{oil}^2 + \gamma\varepsilon)s^2 + (\gamma\omega_{oil}^2)s + (\gamma d K_e A_p / m_{st}) = 0.$) for increasing values of K_e. A pole in the left half of the complex s-plane is associated with a frequency and damping ratio (see Figure 4.6). For $K_e = 0$ V/in, $K_p = 0$ V/psi, and $\tau_s = 0\ \mu s$, H_{zu}^{st} has three real poles and one pair of complex-conjugate poles: pole $p_1 = 0$, is associated with the table mass moving as a rigid body, the poles $p_{2,3} = -2\pi 70, -2\pi 110$, are associated with the servovalve dynamics, and the complex-conjugate pair of poles, $p_{4,5} = -15.3 \pm i169$, are associated with the oil-column resonance.

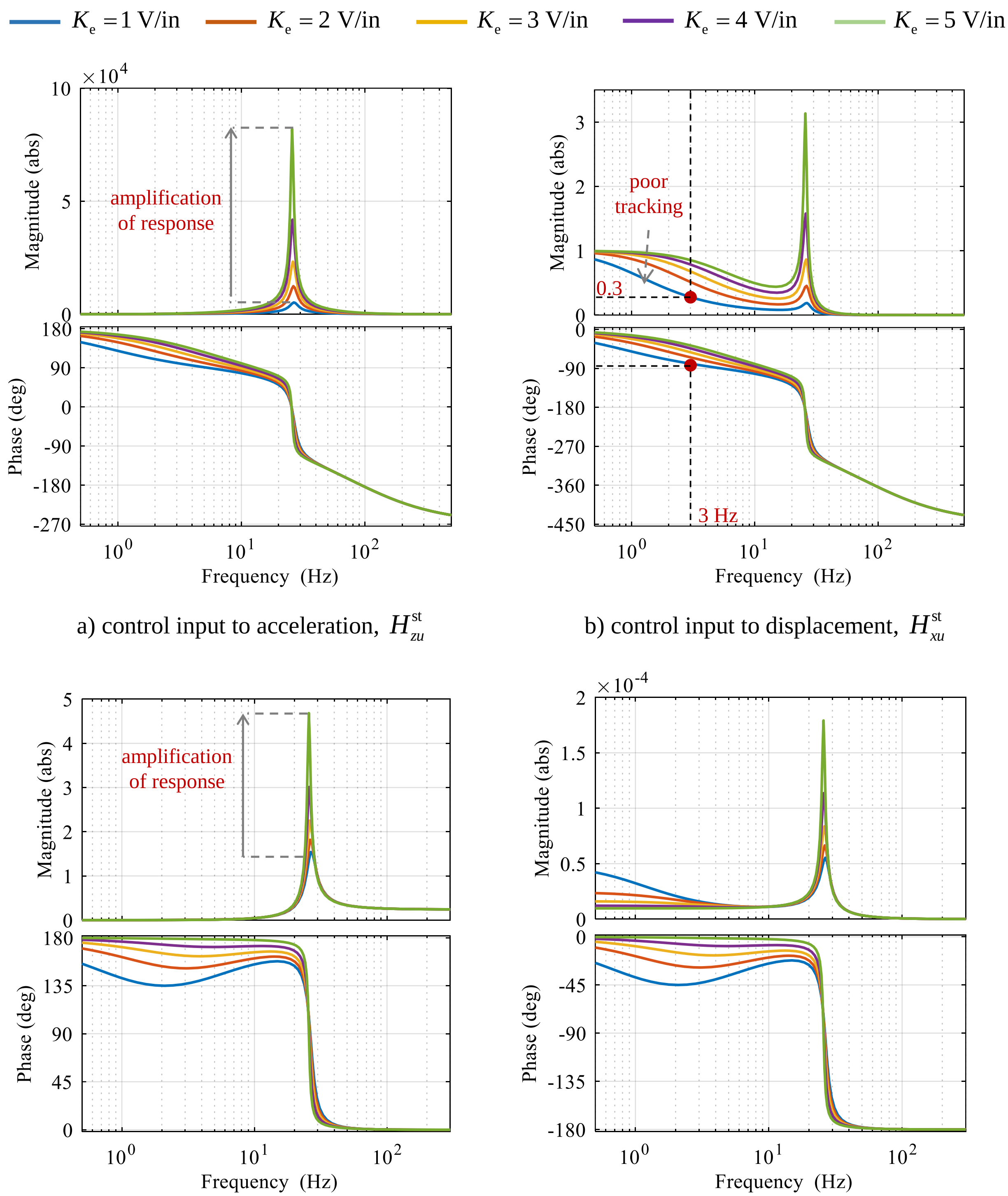

a) control input to acceleration, H_{zu}^{st}

b) control input to displacement, H_{xu}^{st}

c) force input to acceleration, H_{zw}^{st}

d) force input to displacement, H_{xw}^{st}

Figure 4.5. Sensitivity of the analytical transfer functions of the shake table to proportional gain; $K_p = 0$ V/psi and $\tau_s = 0$ μs

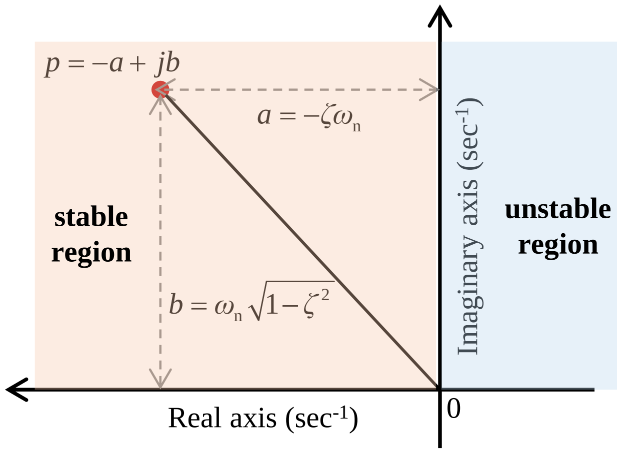

A pole in the left-half of the complex s-plane can be written in the form $p = -\zeta\omega \pm i\omega\sqrt{1-\zeta^2}$. The magnitude of the pole $|p| = \omega = 2\pi f$ informs the contributing frequency. The angle made with the negative real axis is a measure of the associated damping ratio, $\varphi(p) = \cos^{-1}(\zeta)$. A pole on the negative real-axis implies $\zeta = 1$ (i.e., critically damped), and a pole on the imaginary axis implies a marginally stable pole (i.e., $\zeta = 0$). For stability, all poles of a system must lie in the left-half of the complex s-plane.

Figure 4.6. Dynamic characteristics of a pole in the complex *s*-plane

Figure 4.7 plots loci of the poles of H_{zu}^{st} as K_e is varied from zero to infinity. The corresponding pole data (ω and ζ) is reported in Table 4.2. As K_e is increased from 0 to 5 V/in, the damping ratio of the oil-column poles, $p_{4,5}$, is reduced from 9% to 3%, explaining the amplification of the shake-table response near oil-column frequencies in Figure 4.5. For $K_e > 6.7$ V/in, the poles $p_{4,5}$ cross the imaginary axis (negative damping) indicating an unstable system. From the above results, the tracking performance of H_{xu}^{st} is considered acceptable for K_e in the range of 4 to 6 V/in; a value of 5 V/in is used in the experiments. The amplification of the oil-column peak caused by increasing the proportional gain is compensated by tuning the ΔP gain, as discussed next.

Table 4.2. Dynamic characteristics of the roots of for different values of K_e; K_p = 0 V/psi and τ_s = 0 µs

Pole:	K_e = 0 V/in	K_e = 2 V/in	K_e = 5 V/in	K_e = 6.7 V/in	K_e = 39.3 V/in
$p_1\,[f,\ \zeta]$	-	[2 Hz; 1]	[5 Hz; 1]	[6.5 Hz; 1]	[45 Hz; 0.99↓]
$p_2\,[f,\ \zeta]$	[70 Hz; 1]	[69 Hz; 1]	[68 Hz; 1]	[67 Hz; 0]	[45 Hz; 0.99↓]
$p_3\,[f,\ \zeta]$	[110 Hz; 1]	[110 Hz; 1]	[110 Hz; 1]	[111 Hz; 1]	[112 Hz; 1]
$p_4\,[f,\ \zeta]$	[27 Hz; 0.09]	[26 Hz; 0.07↓]	[26 Hz; 0.03↓]	marginally stable	unstable
$p_5\,[f,\ \zeta]$	[27 Hz; 0.09]	[26 Hz; 0.07↓]	[26 Hz; 0.03↓]		

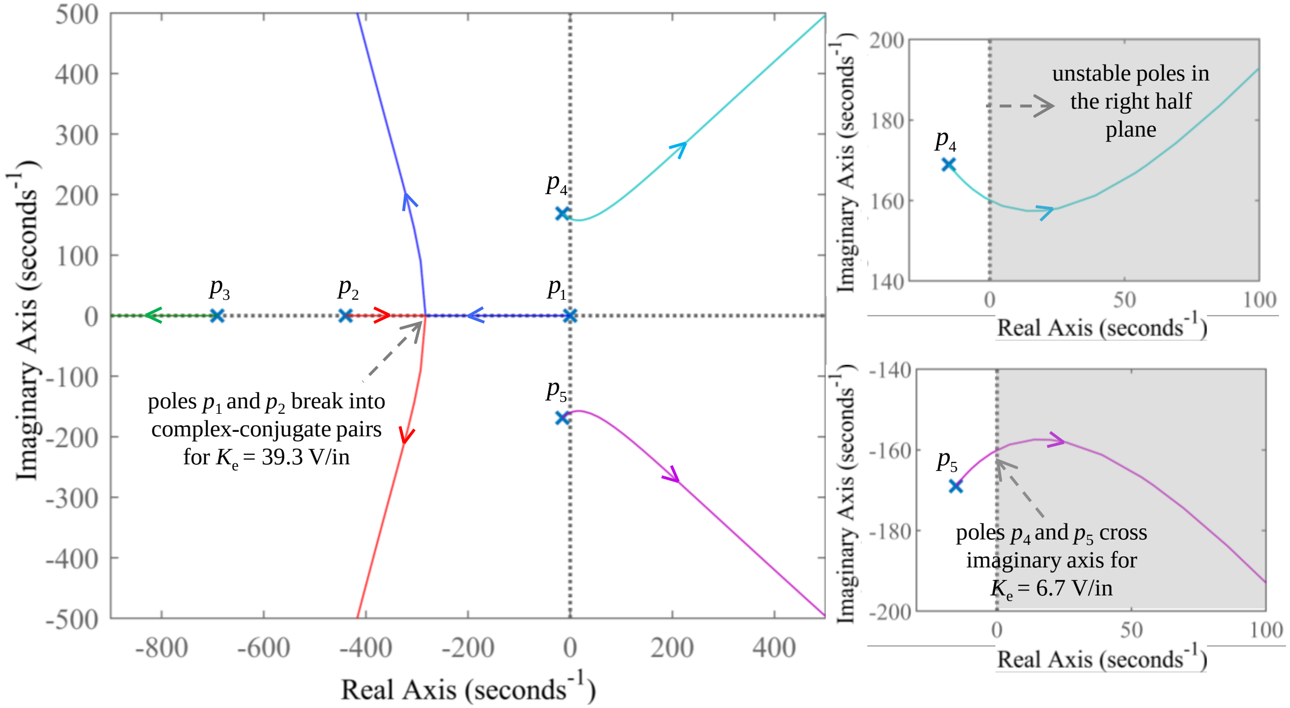

Figure 4.7. Root locus of the shake-table poles for increasing values of K_e; $K_p = 0$ V/psi and $\tau_s = 0$ μs

As K_e is increased from zero to infinity: (i) poles p_1 and p_2 remain as real poles and move towards each other up to $K_e = 39.3$ V/in, referred to as the breakaway point. Beyond this value, the real poles break into a pair of complex conjugate poles as indicated by the paths of the red and the blue lines, (ii) pole p_3 moves along the negative real-axis and converges to $-\infty$ as $K_e \to \infty$ (see the path of the green line), and (iii) poles p_4 and p_5, which initially lie in the left half of the complex *s*-plane for $K_e = 0$, cross the imaginary axis for $K_e > 6.7$ V/in, indicating an unstable system. See the paths of the cyan and magenta lines.

4.4.3 Tuning of the differential pressure gain, K_p

Figure 4.8 presents Bode plots of the analytical transfer functions for the cases where $K_e = 5$ V/in, $\tau_s = 0$, and K_p is gradually increased: 0.0001, 0.0005, 0.001, 0.002, 0.003 V/psi. As K_p is increased from 0.0001 to 0.001 V/psi, the magnitude of the oil-column peak decreases and the frequency associated with the peak increases (see Figure 4.8a and 4-8c), consistent with the observations of Conte and Trombetti (2000).

- For $K_p = 0.001$, the damping ratio of the oil-column poles, $p_{4,5}$, is increased to 0.26 (see Table 4.3), which is approximately nine times greater than that achieved without the ΔP feedback; $\zeta = 0.03$ for $K_p = 0$. The ΔP feedback is thus viewed as a stabilizing measure in hydraulic control because it has the effect of increasing (digitally) damping of the oil-column resonance.
- However, beyond a threshold value of K_p (herein > 0.001 V/psi, when $K_e = 5$ V/in and $\tau_s = 0$ μs), the ΔP feedback starts to act negatively on the system and amplifies the table response near the oil-column frequencies, as indicated by the solid green line in Figure 4.8a. The threshold value of K_p up to which the ΔP feedback is beneficial depends on the values of K_e and τ_s. Using extremely large values of K_p (> 0.0035 V/psi) results in an unstable system.

Table 4.3. Dynamic characteristics of the roots of for different values of K_p; $K_e = 5$ V/in and $\tau_s = 0$ μs

Pole:	K_p = 0	K_p = 0.0001	K_p = 0.0002	K_p = 0.001	K_p = 0.003
$p_1 [f, \zeta]$	[5 Hz; 1]	[5 Hz; 1]	[5 Hz; 1]	[7.3 Hz; 0.8↓]	[4.4 Hz; 0.5↓]
$p_2 [f, \zeta]$	[68 Hz; 1]	[57 Hz; 1]	[47 Hz; 1]	[7.3 Hz; 0.8↓]	[4.4 Hz; 0.5↓]
$p_3 [f, \zeta]$	[110 Hz; 1]	[117 Hz; 1]	[122 Hz; 1]	[144 Hz; 1]	[113 Hz; 1]
$p_4 [f, \zeta]$	[25 Hz; 0.03]	[27 Hz; 0.11↑]	[28 Hz; 0.20↑]	[55 Hz; 0.26↑]	[85 Hz; 0.05↓]
$p_5 [f, \zeta]$	[25 Hz; 0.03]	[27 Hz; 0.11↑]	[28 Hz; 0.20↑]	[55 Hz; 0.26↑]	[85 Hz; 0.05↓]

The root locus plots presented in Figure 4.9 show that for $K_p > 0.001$: (i) the magnitude (i.e., ω) of the complex oscillatory poles (see the cyan and the red lines) increases, explaining the shift in the peak frequency, and (ii) the angle made with the negative real-axis (i.e., $\varphi = \cos^{-1}(\zeta)$) increases, implying a decreased ζ, explaining the amplification of the shifted peak. Therefore, for $K_p = 0.001$ V/psi, the oil-column damping is maximum (approximately), and is considered optimal for the MIL experiments. Note that the optimal K_p maximizing the oil-column damping changes if a different value of K_e used.

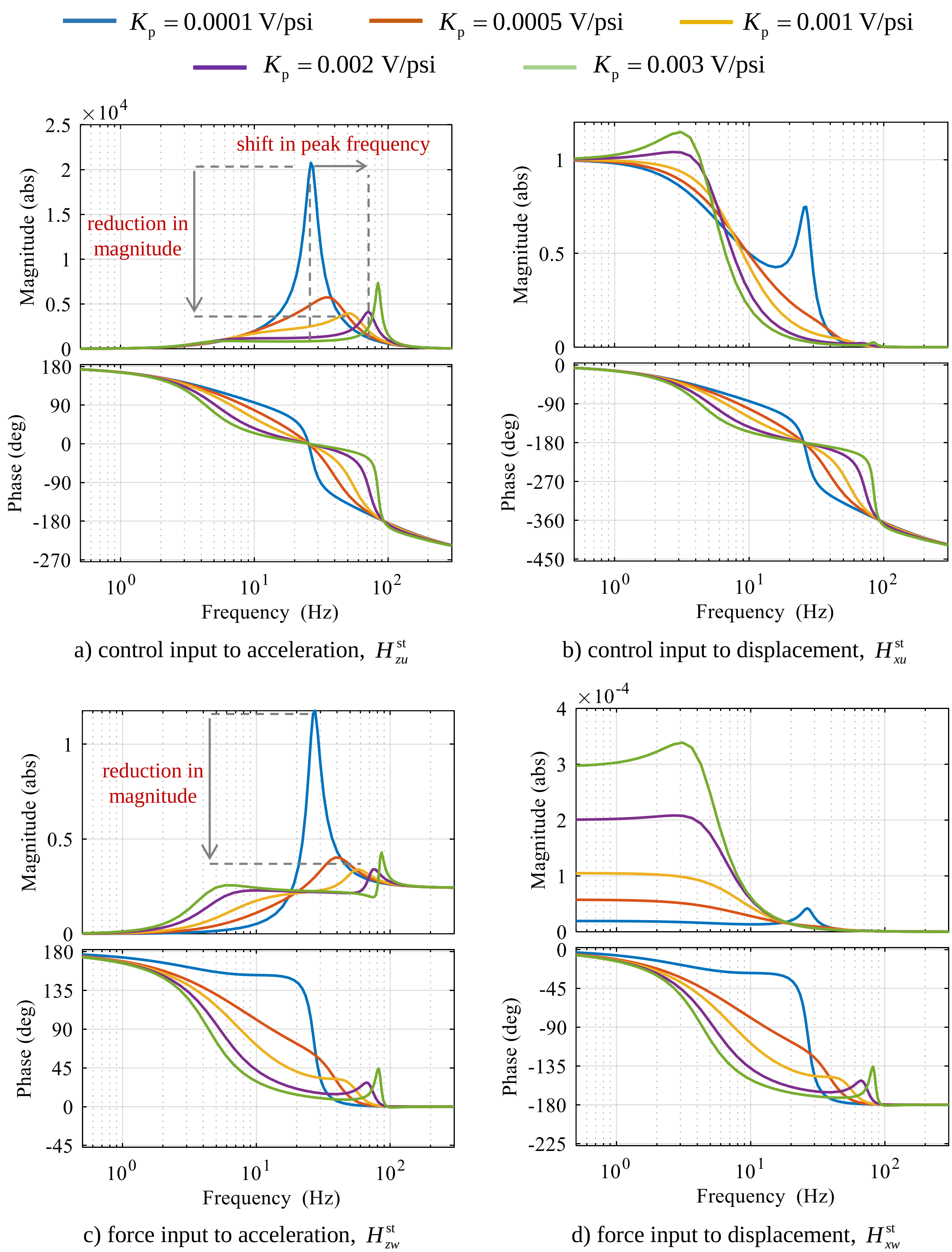

Figure 4.8. Sensitivity of the analytical transfer functions of the shake table to differential pressure gain; K_e = 5 V/in, τ_s = 0 μs

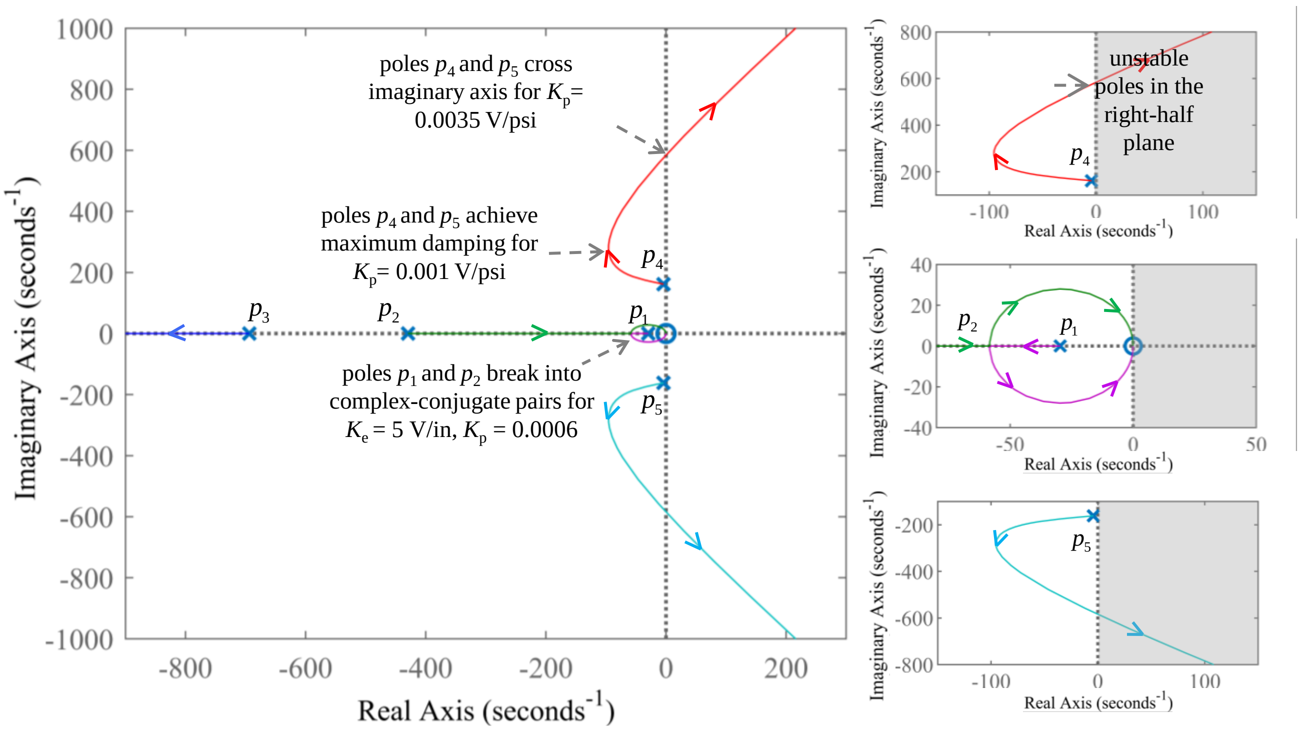

Figure 4.9. Root locus of shake-table poles for increasing values of K_p; K_e = 5 V/in and τ_s = 0 μs

For $K_e = 5$ V/in, and as K_p is increased from zero to infinity: (i) poles p_1 and p_2 break into a pair of complex-conjugate poles for $K_p = 0.0006$ V/psi, as indicated by the paths of the magenta and the green lines, which eventually converge at the origin, (ii) pole p_3 moves along the negative real-axis and converges to $-\infty$ as $K_p \to \infty$ (see the path of the blue line), and (iii) the damping in the poles p_4 and p_5 increases up to $K_p = 0.001$ V/psi and decreases thereafter (as indicated by the path of the red and the cyan lines), and the poles eventually cross the imaginary axis for $K_p > 0.0035$ V/psi, indicating instability.

4.4.4 Effect of the controller sampling (loop) time

Figure 4.10 evaluates the effect of the controller loop time, τ_s, on the shake-table response. Bode plots are presented for two values of $K_p = 0.0003$ V/psi and 0.001 V/psi, as τ_s is varied from 0 μs (analog controller) per the increment of loop times available in the RMC75E: 250 μs (4000 Hz), 500 μs (2000 Hz) and 1000 μs (1000 Hz).

The plots show that: (i) larger loop times result in amplification of the shake-table response near the oil-column frequencies, thereby counteracting the benefits achieved by the ΔP stabilization, and (ii) the influence of τ_s is more pronounced for larger values of K_p (see the difference between the peaks in Figure 4.10a and Figure 4.10b). This influence of τ_s is counterintuitive because the loop frequencies (inverse of τ_s) considered herein are at least 30 times greater than the oil-column frequency and are generally thought of not to affect the table response in this frequency range.

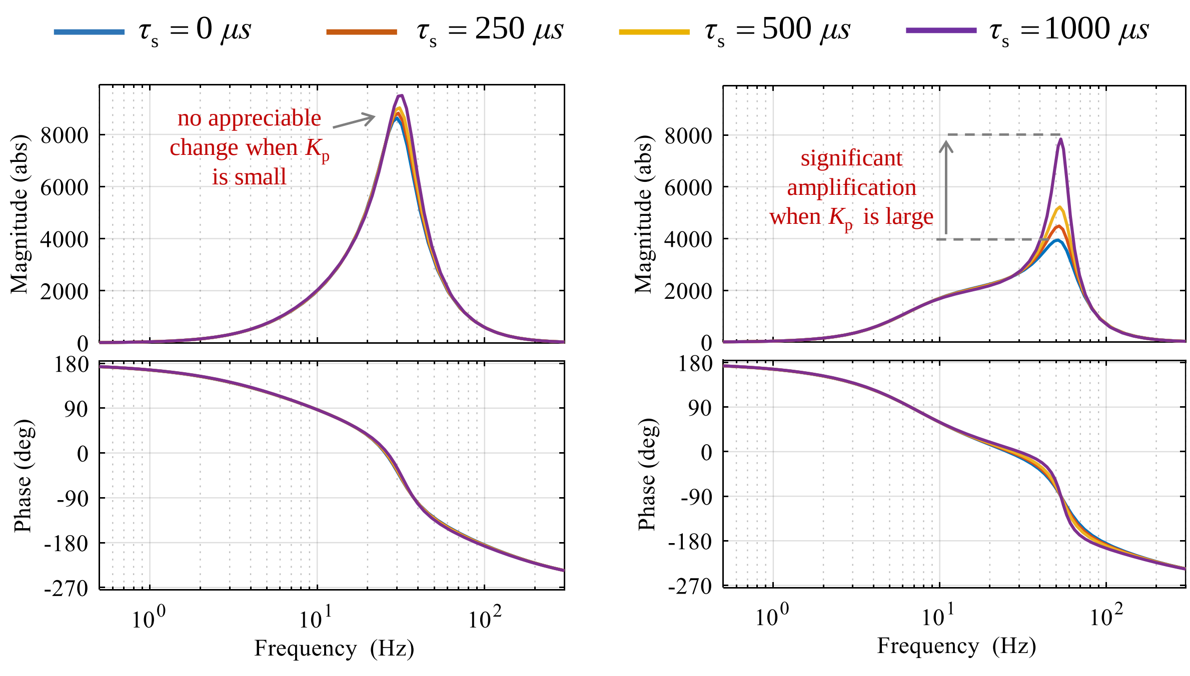

a) H_{zu}^{st}, $K_p = 0.0003$ V/psi

b) H_{zu}^{st}, $K_p = 0.001$ V/psi

Figure 4.10. Sensitivity of the analytical transfer functions of the shake table to controller loop time; K_e = 5 V/psi

Figure 4.11 plots the loci of one of the oil-column poles, p_4, for different loop times. For the same value of $K_p = 0.001$ V/psi, the damping ratio of the oil column pole is: 26% when $\tau_s = 0$; 23% when $\tau_s = 250$

μs; 19% when $\tau_s = 500$ μs; and 12% when $\tau_s = 1000$ μs. The larger the loop time, the smaller the damping, and the less beneficial is the ΔP feedback. Therefore, analog controllers, or digital controllers with smaller loop times are needed to best utilize the benefits of ΔP feedback in terms of maximizing oil-column damping. The minimum loop time available in the RMC75E controller is 250 μs (i.e., a maximum sampling rate of 4000 Hz). However, this loop time does not support time-critical applications involving large computations[16]. The next smallest loop time of 500 μs is used in the MIL experiments.

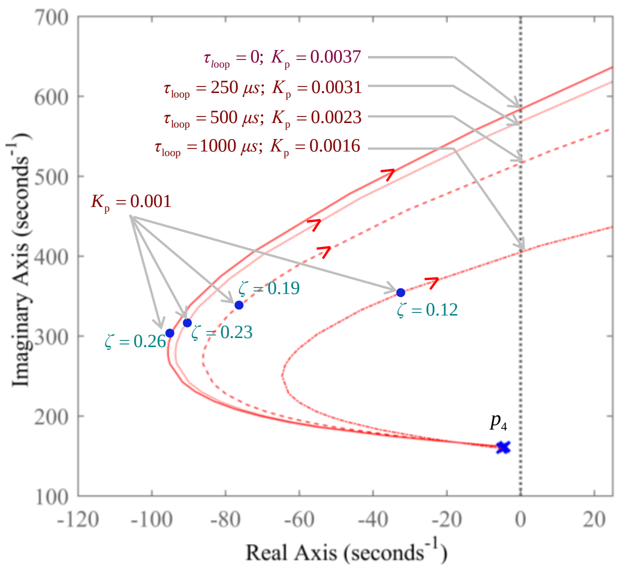

Plotted in this figure are the root loci of one of the oil-column oscillatory poles as a function of K_p for different loop times. As seen in the figure, for the same value of $K_p = 0.001$ V/psi, the amount of damping in the oil-column poles is severely limited by the controller loop time. Larger loop times result in smaller damping values, explaining the amplification of response near the oil-column frequencies in Figure 4-10b. As τ_s increases, the oscillatory pole gets closer to the imaginary axis, thereby decreasing the stability margin.

Figure 4.11. Root locus of one of the oil-column poles for increasing values of K_p; K_e = 5 V/in and different loop times

4.5 Experimental evaluation of the analytical transfer functions

4.5.1 Overview

This subsection presents results of the frequency-response experiments performed to evaluate the accuracy of the shake-table transfer functions. Experiments are performed on (i) bare shake table (without the vessel) and (ii) shake table mounted with the vessel. In both configurations, the control input, u, is the broadband multisine time series described in Section 4.5.2. Test results for the bare shake table are used to evaluate the analytical transfer functions corresponding to the control input (see Section 4.5.3) and test results for

[16] The MIL code is implemented in the RMC as user programs (see Section 7). The RMC CPU allocates a fixed amount of memory and time for processing these user programs. The time required for processing the MIL user programs exceeds the allocated their time when τ_s is set to 250 μs, and hence cannot be used.

the combined table-vessel configuration are used to evaluate (indirectly) the transfer functions corresponding to the reaction force input (see Section 4.5.4).

4.5.2 Multisine timeseries

The multisine time series used in the frequency-response experiments is a periodic broadband signal obtained by summing sinusoidal signals of constant amplitude and different frequencies. The phases of the sinusoids are selected so that the ‘crest factor’ is minimal, that is, the ratio of maximum peak to minimum peak in the signal is close to one (Schoukens *et al.*, 2012). This maximizes the signal-noise ratio in the output at all frequencies. Figure 4.12a presents the multisine series sampled at 2000 Hz. The signal is periodic in three windows. Each window is 4.096-sec long and composed of 8192 sample points. The Fast Fourier Transform (FFT) of the signal, presented in Figure 4.12b, show that a total of 512 distinct frequencies of equal amplitude are excited in the frequency range of 0.25 to 125 Hz. The frequency resolution of the signal, calculated as the ratio of the sampling frequency (2000 Hz) to the number of FFT points in each window (8192), is approximately 0.25 Hz.

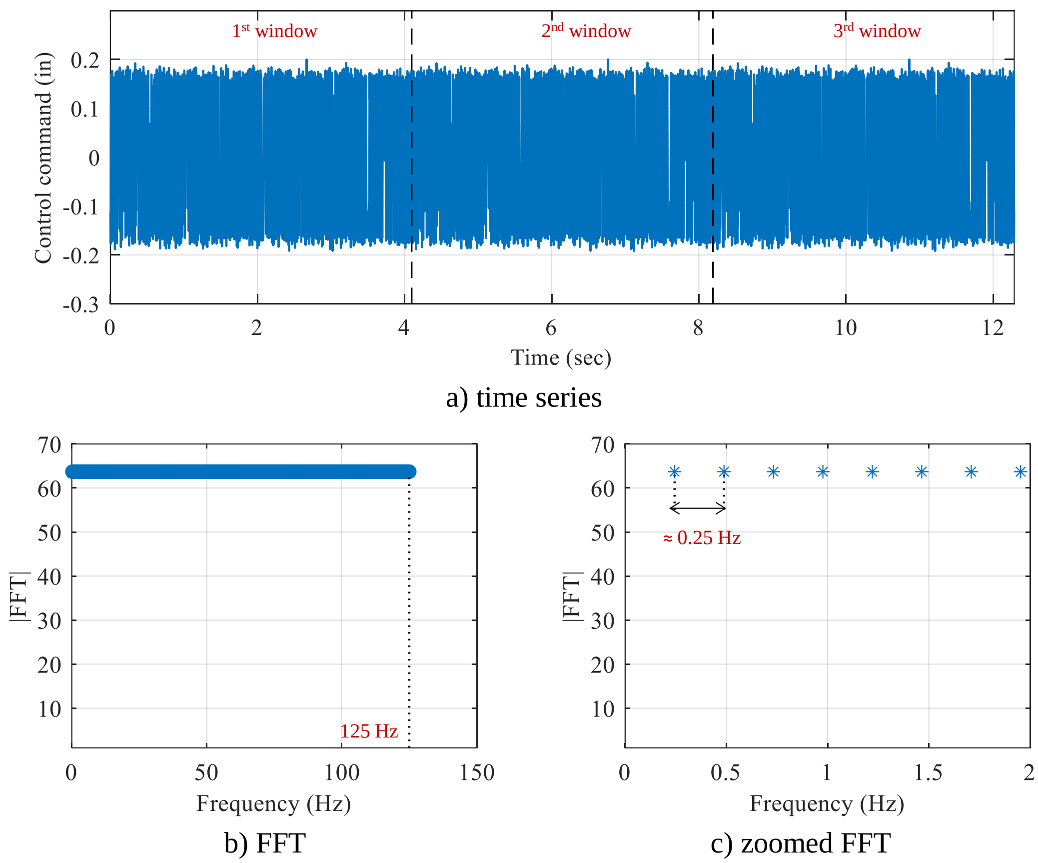

Figure 4.12. Multisine input for the frequency-response experiments

4.5.3 Experimental evaluation of the bare shake table

The analytical transfer functions corresponding to the control input, H_{zu}^{st}, H_{xu}^{st}, and $H_{\Delta Pu}^{\mathrm{st}}$, are directly evaluated using the acceleration, displacement, and ΔP measurements of the shake table, respectively. Frequency response functions (FRFs) are generated from the multisine control input to the measured z_{st}, x_{st}, and ΔP, and are compared with the responses of the analytical transfer functions. Herein, experiments are performed for different combinations of K_{e}, K_{p}, and τ_{s} to evaluate the accuracy and robustness of the analytical transfer functions over a broad range of system parameters, and identify optimal values resulting in a high-fidelity shake-table model. Only H_{zu}^{st} is evaluated herein.

4.5.3.1 Evaluation of the bare table for different values of K_{p}

Figure 4.13a through 4-13f present the test results for constant $K_{\mathrm{e}} = 5$ V/in and $\tau_{\mathrm{s}} = 500\ \mu s$, and for increasing values of K_{p}: 0 V/psi, 0.0001 V/psi, 0.0003 V/psi, 0.0006 V/psi, 0.0009 V/psi, and 0.0012 V/psi. The solid blue lines are the measured frequency responses of the table, the dashed red lines are the Bode diagrams of the analytical H_{zu}^{st} (Equation 4-15a), and the dotted green lines are the model responses assuming an analog controller (i.e., Equation 4-15a substituted with $\tau_{\mathrm{s}} = 0$). The key takeaways from the figures are:

- As seen in Figures 4-13a and 4-13b, the measured and the model responses are in poor agreement for smaller values of $K_{\mathrm{p}} \leq 0.0001$ V/psi. In the absence of the ΔP feedback, the shake table is highly sensitive to (or affected by) modeling uncertainties[17] and other nonlinear effects and therefore the difference between the response of the linear model and the table measurement is quite significant, particularly near the oil-column frequencies .
- The accuracy of the linear model is improved as K_{p} is increased (see Figures 4-13c through 4-13e), supporting the hypothesis of Section 1 that a sufficiently large value of the gain K_{p} is forgiving of modeling errors, uncertainties, and other approximations, and enables a linear model to predict table response with high fidelity. This is further clarified in Figure 4-16.

[17] Some of these uncertainties include: (i) consequences of modeling assumptions, such as ignoring friction, ignoring structural damping associated with the spool, actuator, and table mass, and (ii) uncertainty in the estimation of the empirically-determined model parameters; for example, the oil-column properties, ζ_{oil} and ω_{oil}, are functions of the oil-column compressibility and are sensitive to the fluctuations in the oil temperature and type of the hydraulic fluid.

- The accuracy of the linear model without feedback delay (dotted green line) deteriorates for $K_p >$ 0.0003 V/psi. This is attributed to the influence of the controller sampling time, τ_s, when large values of the ΔP gain are used, resulting in increased deviation between the dotted green and the solid blue lines. The first-order approximation of the feedback delay of Section 4.3.4 is shown to capture the effects of τ_s sufficiently well, as indicated by the excellent agreement between the red and the blue lines for $0.0003 < K_p < 0.0012$.
- As K_p is increased beyond a threshold value (> 0.0012 V/psi), the ΔP feedback acts negatively on the system by amplifying the table response near the oil-column frequencies (see Figure 4.13f). For these large values of K_p neither of the two models (with and without sampling delay) are accurate.
- The linear model with sampling delay is shown to accurately predict the shake-table response in the frequency range of 0.25 Hz to 80 Hz for K_p between 0.0006 V/psi and 0.0012 V/psi. The small peak around 100 Hz observed in the measured response is not captured by the model and is attributed to the unmodeled dynamics of the actuator system.

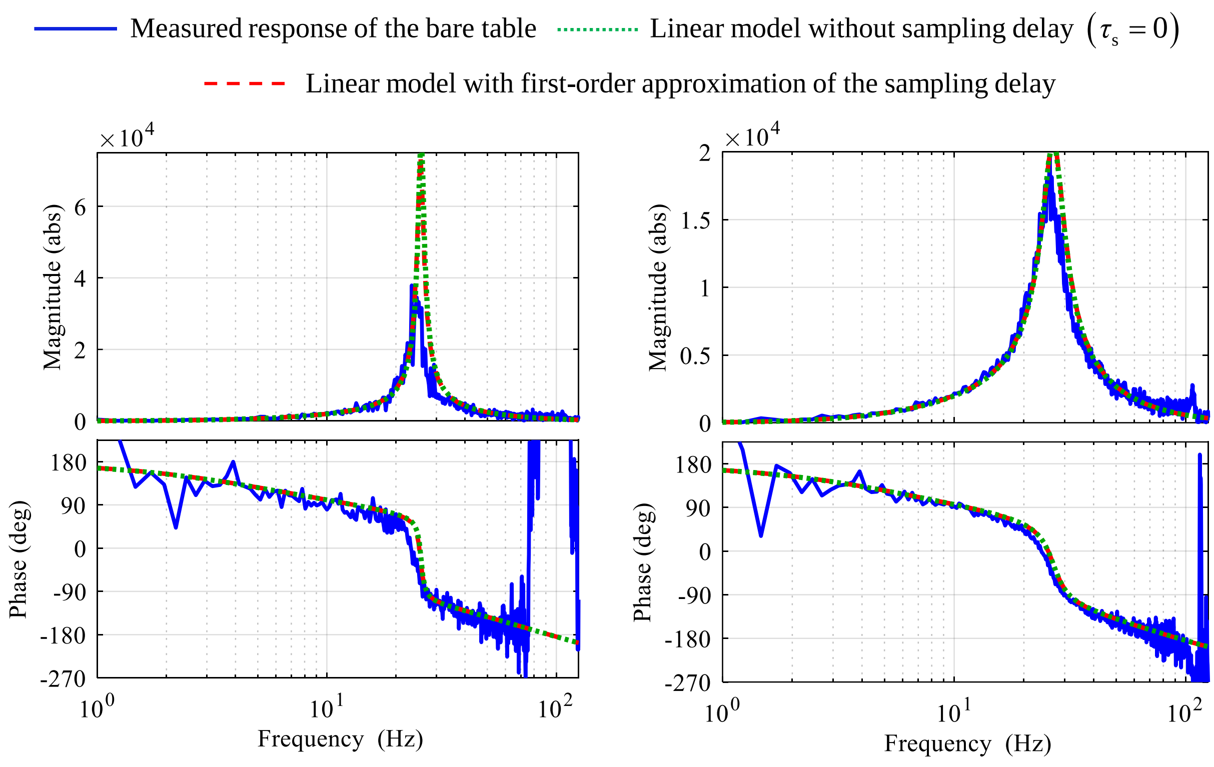

a) K_p = 0 V/psi

b) K_p = 0.0001 V/psi

Figure 4.13. Experimental evaluation of the bare shake table for different values of K_p; K_e = 5 V/in and τ_s = 500 μs [2000 Hz]

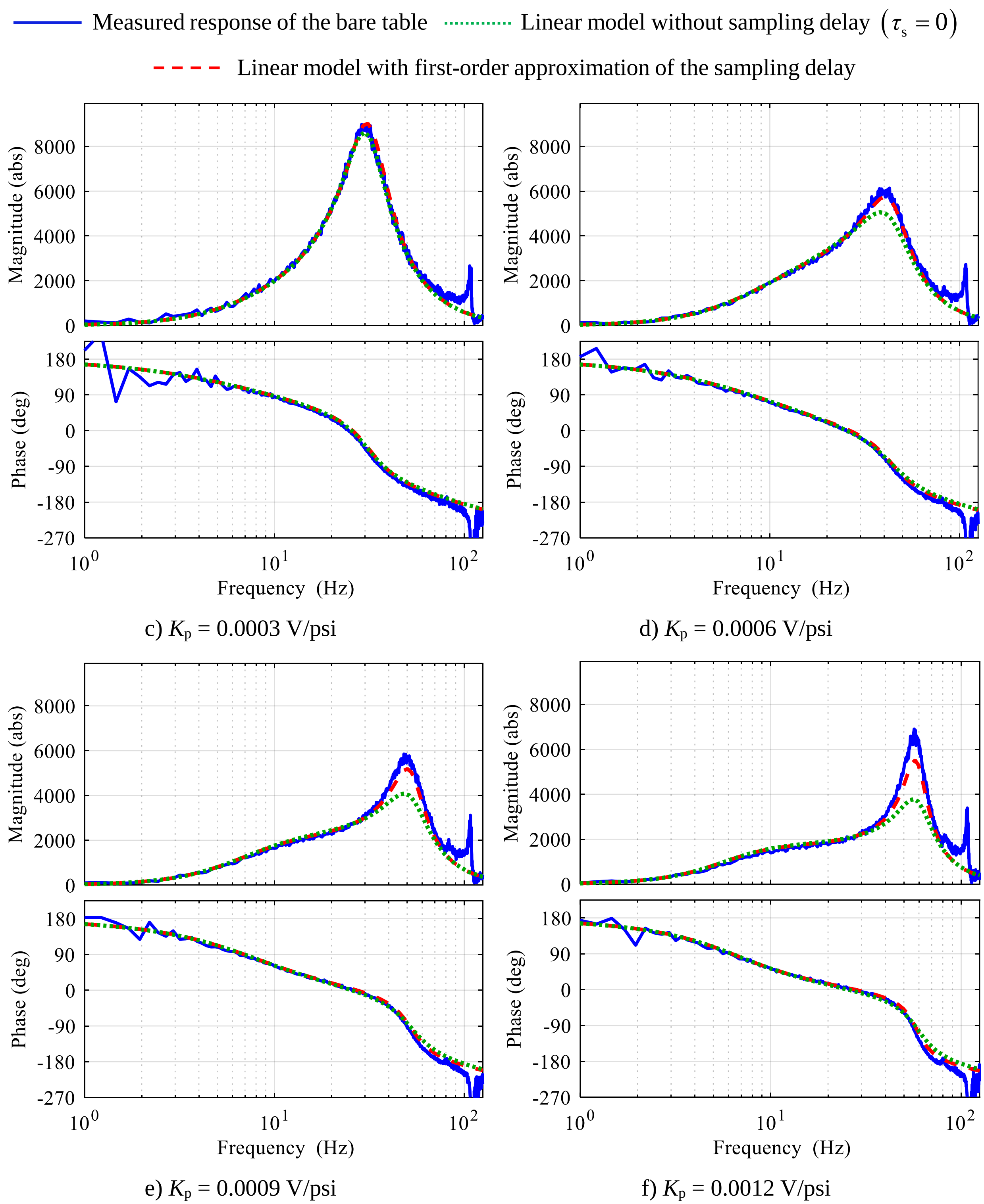

Figure 4-13. Experimental evaluation of the bare shake table for different values of K_p; K_e = 5 V/in and τ_s = 500 μs [2000 Hz] (cont'd)

4.5.3.2 Evaluation of the bare shake table for different values of K_e

Figure 4.14a through 4-14d enable comparison of the measured and the model responses for increasing values of K_{e} and for constant K_{p} and τ_{s}. Herein, K_{e} is increased from 3.75 V/in to 7.5 V/in in the increments of 1.25 V/in. The values of K_{p} and τ_{s} are set constant to 0.0009 V/psi and 500 μs, respectively. The results show that the linear model without feedback delay (green lines) under predicts the shake-table response near the oil-column frequencies, whereas the first-order approximation of the feedback delay is seen to capture the effect of τ_{s} sufficiently accurately for the range of K_{e} values considered herein.

4.5.3.3 Evaluation of the bare shake table for different controller loop times

Figure 4.15 presents test results for constant values of $K_{\mathrm{e}} = 5$ V/in and $K_{\mathrm{p}} = 0.0009$ V/psi, and varying controller loop times (frequencies): 250 μs (4000 Hz), 500 μs (2000 Hz), and 1000 μs (1000 Hz). For $\tau_{\mathrm{s}} = 250\ \mu s$, the responses of the green and the red lines are similar, and close to the measured response (see Figure 4.15a). The effectiveness of the linear model with feedback delay, in terms of improved accuracy, is evident for $\tau_{\mathrm{s}} = 500\ \mu s$, where the model (red line) and measured (blue) responses are in excellent agreement. However, for $\tau_{\mathrm{s}} > 1000\ \mu s$, the analytical transfer functions are not reliable because the first-order Taylor series approximation of the sampling delay, $e^{-s\tau_{\mathrm{s}}} = 1 - s\tau_{\mathrm{s}}$, as considered in Section 4.3.4, becomes inaccurate.

From the above results, the analytical transfer function, $H_{\mathrm{zu}}^{\mathrm{st}}$, predicts the shake-table response with sufficient accuracy for the envelope combinations of K_{e} in the range of 3 V/in to 7 V/in, K_{p} in the range 0.0006 V/psi to 0.0012 V/psi, and controller loop times less than or equal to 500 μs. Values $K_{\mathrm{e}} = 5$ V/in, $K_{\mathrm{p}} = 0.001$ V/psi, and $\tau_{\mathrm{s}} = 500$ μs [2000 Hz] are used in the MIL experiments.

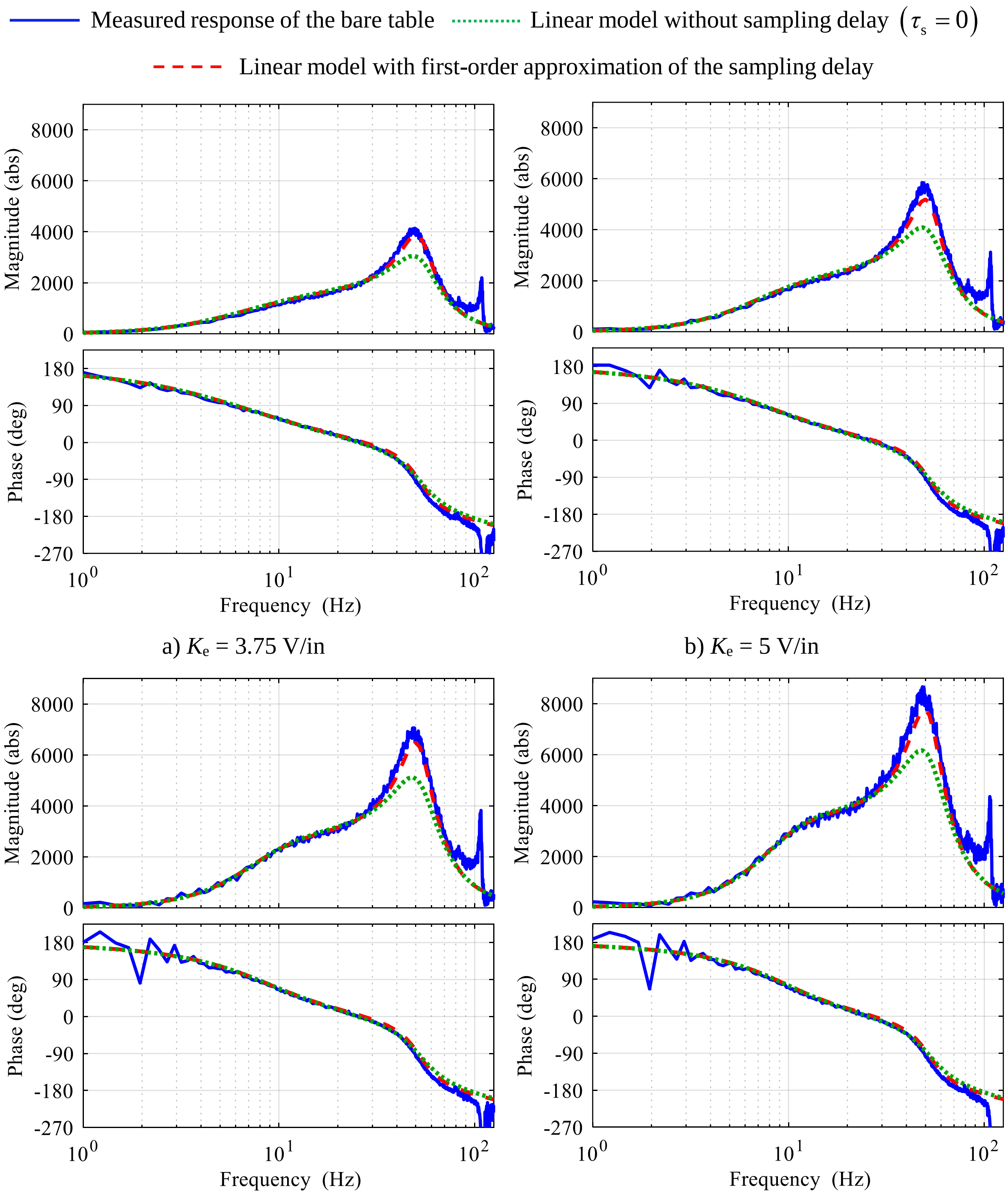

Figure 4.14. Experimental evaluation of the bare shake table for different values of K_e; K_p = 0.0009 V/psi and τ_s = 500 μs.

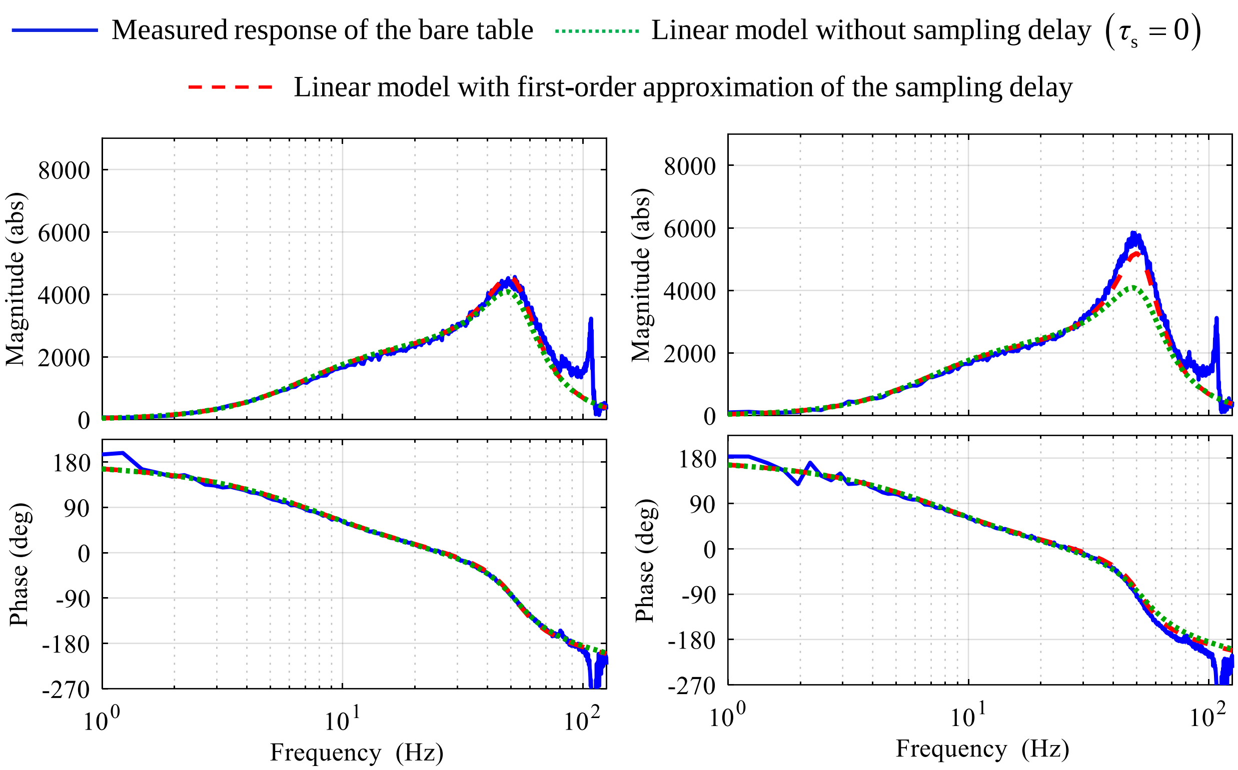

a) $\tau_{\text{loop}} = 250\ \mu s$

b) $\tau_{\text{loop}} = 500\ \mu s$

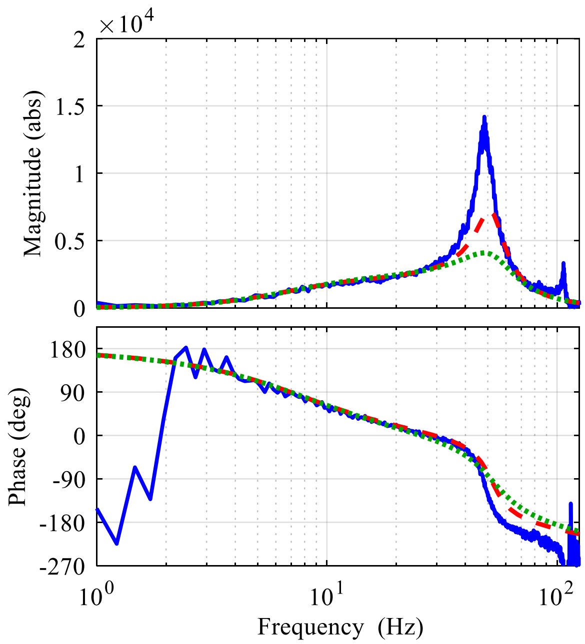

c) $\tau_{\text{loop}} = 1000\ \mu s$

Figure 4.15. Experimental evaluation of the bare shake table for different values of τ_s; K_e = 5 V/in and K_p = 0.0009 V/psi.

4.5.4 Experimental evaluation of the combined table and vessel system

The transfer functions corresponding to the reaction force input are not commonly reported/utilized in the literature because the feedback force is often rejected as external disturbance in control design. By contrast, the impedance-matching approach embraces this physical feedback by viewing it as an external input to the MIL controller. Therefore, accurate characterization of H_{zw}^{st} and measurement of w is key to the successful implementation of the impedance-matching approach. Experimental measurement of $H_{\mathrm{zw}}^{\mathrm{st}}$, $H_{\mathrm{xw}}^{\mathrm{st}}$, and $H_{\Delta\mathrm{Pw}}^{\mathrm{st}}$ requires driving the shake table with another much larger actuator, which is often challenging in a laboratory setting. Therefore, these transfer functions are evaluated indirectly using the measured frequency response of the combined table-vessel system for different gain combinations, as described below.

- The control input, u, is set to multisine time series; the table responses (z_{exp}, x_{exp}, and ΔP_{exp}), and the feedback force, w, at the interface are measured.
- For the known control input, u, and the measured feedback force, w, the model predictions are calculated as: $z_{\mathrm{model}} = H_{zu}^{\mathrm{st}}u + H_{zw}^{\mathrm{st}}w$, $x_{\mathrm{model}} = H_{xu}^{\mathrm{st}}u + H_{xw}^{\mathrm{st}}w$, and $\Delta P_{\mathrm{model}} = H_{\Delta Pu}^{\mathrm{st}}u + H_{\Delta Pw}^{\mathrm{st}}w.$
- The frequency response functions (FRFs) of the model predictions and the measured outputs are compared to evaluate (indirectly)[18] the accuracy of H_{zw}^{st}, H_{xw}^{st}, and $H_{\Delta Pw}^{\mathrm{st}}$.

Figure 4.16 enables comparison of the model (including sampling delay) and the measured table responses for $K_{\mathrm{e}} = 5$ V/in, $\tau_{\mathrm{s}} =$ 500 μs, and for increasing values of K_{p}. Figures 4-17 and 4-18 present results for the table displacement and the differential pressure, ΔP, respectively, for the same control gains. For $K_{\mathrm{p}} = 0.0002$ V/psi, the model fidelity is poor in the frequency range of 10 Hz to 50 Hz (see Figure 4.16a). Similar to the observations in Section 4.5.3, the accuracy (magnitude and phase response) of the linear model is marginally improved for K_{p} = 0.0006 V/psi, is substantially better for $K_{\mathrm{p}} = 0.001$ V/psi, and deteriorates for $K_{\mathrm{p}} > 0.0014$ V/psi.

From the results presented herein and from those in Section 4.5.3, the linear shake-table model predicts the table response with high fidelity for the control parameters $K_{\mathrm{e}} = 5$ V/in, $K_{\mathrm{p}} = 0.001$ V/psi, and $\tau_{\mathrm{s}} = 500$ μs, and these values are used in the MIL experiments.

---

[18] It is noteworthy to mention that an inherent problem with this evaluation approach is that the inputs, u and w to the table are not uncorrelated because of vessel-table interaction. However, the approach, at the least, gives a sense for the accuracy/validity of the analytical transfer functions corresponding to the reaction force input.

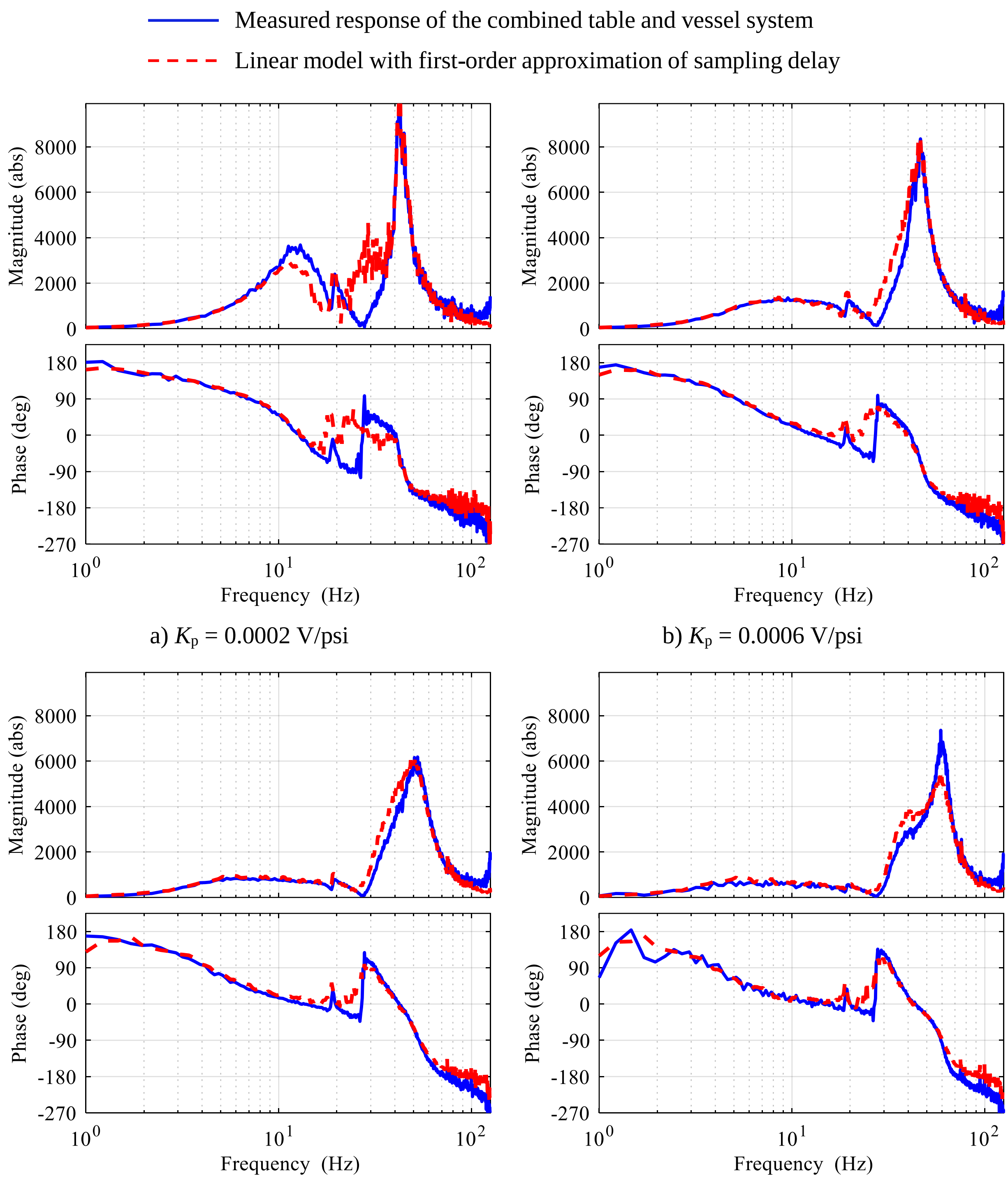

a) K_p = 0.0002 V/psi

b) K_p = 0.0006 V/psi

c) K_p = 0.001 V/psi

d) K_p = 0.0014 V/psi

Figure 4.16. Experimental evaluation of the combined table and vessel system, acceleration responses, different values of K_p, water depth of 36 inches, K_e = 5 V/in, and τ_s = 500 μs

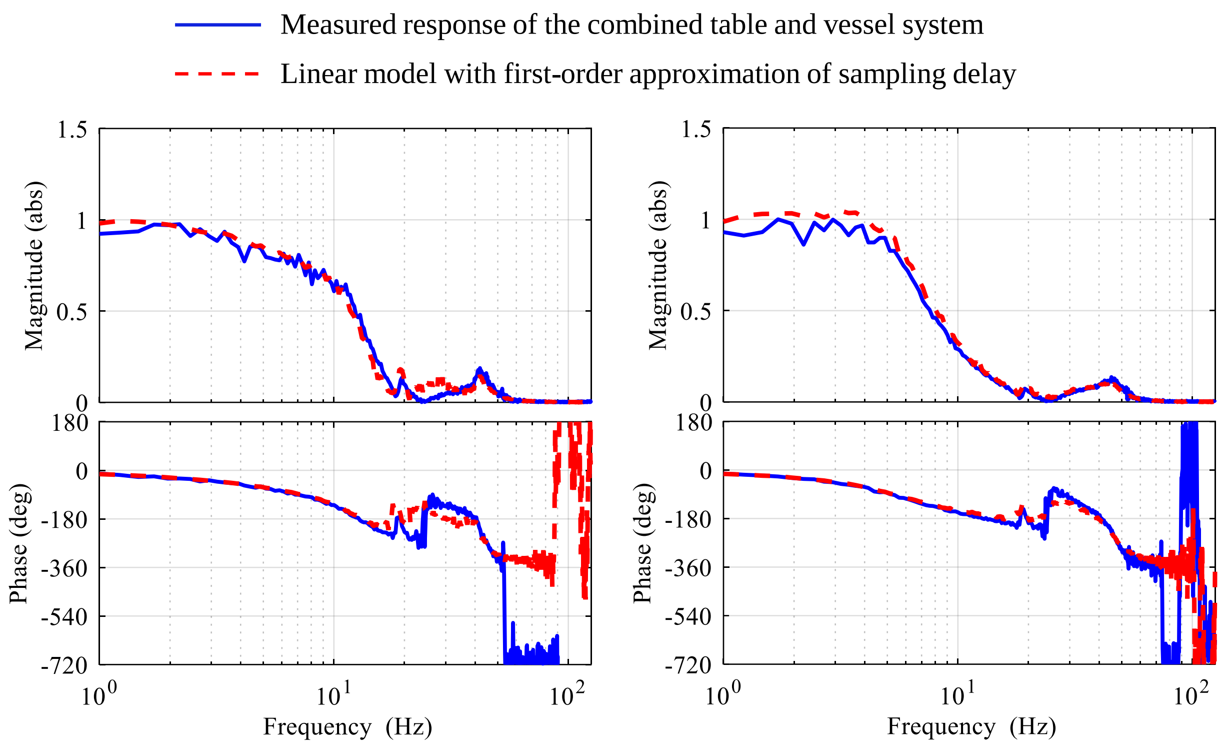

a) K_p = 0.0002 V/psi

b) K_p = 0.0006 V/psi

c) K_p = 0.001 V/psi

d) K_p = 0.0014 V/psi

Figure 4.17. Experimental evaluation of the combined table and vessel system, displacement responses, different values of K_p, water depth of 36 inches, K_e = 5 V/in, and τ_s = 500 μs

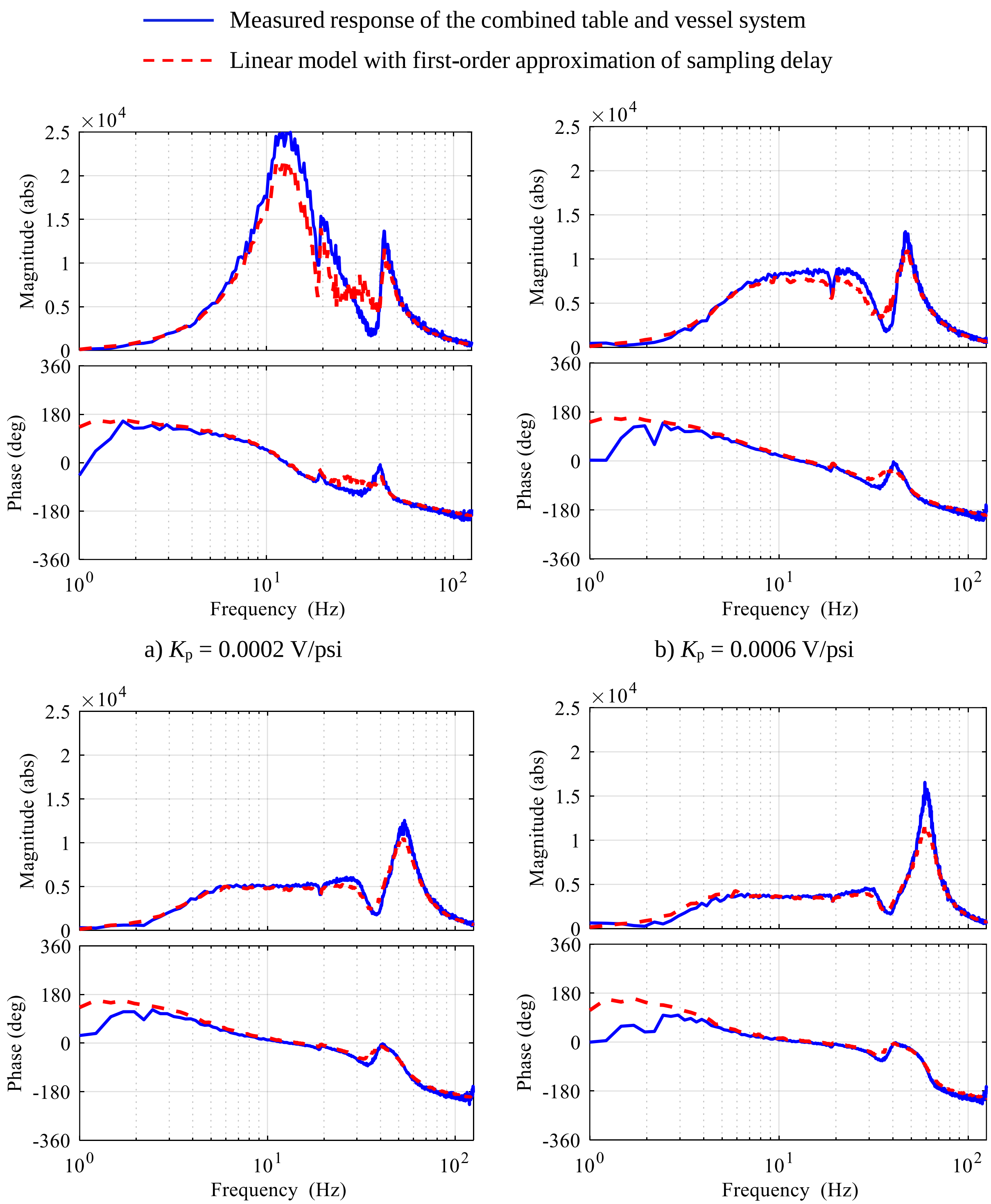

a) K_p = 0.0002 V/psi

b) K_p = 0.0006 V/psi

c) K_p = 0.001 V/psi

d) K_p = 0.0014 V/psi

Figure 4.18. Experimental evaluation of the combined table and vessel system, differential pressure res ponses, different values of K_p, water depth of 36 inches, K_e = 5 V/in, and τ_s = 500 μs

SECTION 5
MATHEMATICAL MODELING OF THE VIRTUAL SYSTEMS

5.1 Section prologue

This section discusses mathematical models for the three types of virtual systems, introduced previously in Section 3.3: linear spring-damper (SD), and nonlinear lead-rubber (LR) and Friction Pendulum (FP) isolation systems. These mathematical models enable calculation of the target VS acceleration history, z_{vs}, that needs to be imitated by the shake table at the base of the test article. The impedance-matching MIL procedure, as outlined in Section 1, is directly applicable for the linear SD systems because z_{vs} can be expressed as $z_{\text{vs}} = H_{za_{\text{g}}}^{\text{vs}} a_{\text{g}} + H_{zw}^{\text{vs}} w$. The LR and FP isolation systems exhibit nonlinear hysteretic behavior, rendering the above linear representation of z_{vs} inapplicable. This section presents an alternate strategy to implement MIL for such nonlinear systems. Section 5.2 lists some general assumptions considered in the VS modeling. Sections 5.3, 5.4, and 5.5 present the mathematical models (and derivation of the VS transfer functions) for the SD, LR, and FP systems, respectively.

5.2 Modeling assumptions

It is well documented that LR and FP isolators exhibit coupled nonlinear response between the two horizontal and between the horizontal and the vertical directions (e.g., Koh and Kelly (1987); Warn and Whittaker (2006); Constantinou *et al.* (2007); Kalpakidis and Constantinou (2008)). Because the scope of the current MIL setup is limited to 1D (uniaxial shake table), only unidirectional horizontal shear behavior of these isolators is considered in the VS modeling. The limitation of the test setup to 1D does not affect the outcomes of this research, because the focus herein is to advance the impedance-matching MIL theory and validate the approach by physical testing, and not to test the fluid-filled vessel for the effects of seismic isolation. Hence, similitude and scaling requirements are neither addressed for the test article (including fluid) nor for the seismic isolators modeled in the VS.

If the current MIL framework is to be extended for studying the dynamic response of the test article, such as characterizing the effects of seismic isolation on sloshing response of the fluid similar to Mir *et al.* (2020) and Yu *et al.* (2021) studies: (i) the VS should be represented using advanced mathematical models (Kumar *et al*., (2019a; 2019b)) for the LR and FP isolators that can capture the horizontal coupling, horizontal-and-vertical coupling, and other important effects such as heating in the isolators, (ii) the impedance-matching framework outlined in Section 1 will have to be extended to 3D so that a multi-axis shake table can be used to simulate the VS impedance in all three directions, and (iii) the isolators, the test article, and the fluid inside should comply with similitude and scaling requirements, which is beyond the scope of this report.

5.3 Mathematical modeling of the linear spring-damper virtual system

The linear spring-damper virtual system includes a basemat of mass, m_{vs}. Assuming the basemat to be rigid, the shear force in (and stiffness of) the isolation system can be calculated as the sum of the shear force in (and stiffness of) the individual bearings. (The assumption is valid for the LR and FP systems too.) The horizontal shear response of the SD system is idealized as a linear spring of stiffness, k_{s}, and a linear viscous dashpot with a damping coefficient, c, as illustrated in Figure 5.1a. The corresponding idealized horizontal shear force-displacement loop is presented in Figure 5.1b. For this uniaxial configuration, the virtual system has two inputs: (i) ground acceleration, a_{g}, and (ii) feedback force from the test article, w. The output acceleration of the basemat, z_{vs}, is the target boundary condition of the VS that needs to be simulated at the base of the test article. From force equilibrium, the governing differential equation of the VS is written as: $m_{\mathrm{vs}}\ddot{x} + c\dot{x} + k_{\mathrm{s}}x = w - m_{\mathrm{vs}}a_{\mathrm{g}}$, where x is the displacement of the basemat relative to the ground.

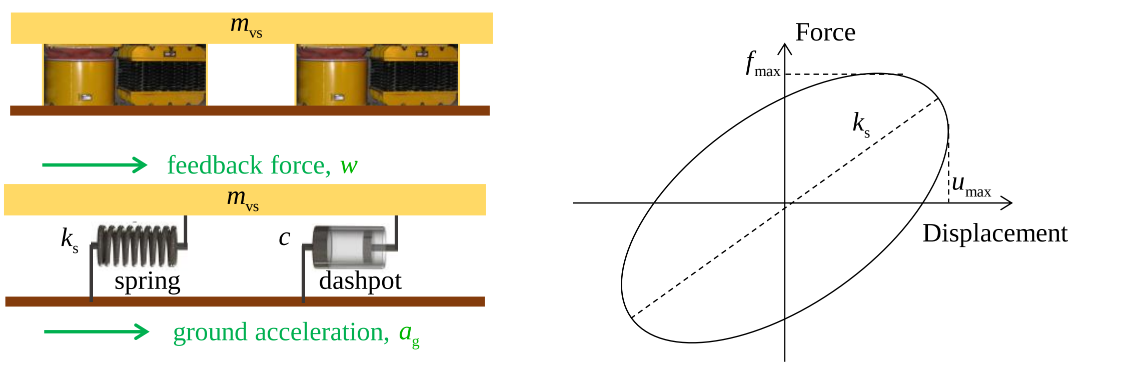

a) mathematical idealization b) idealized horizontal shear-force displacement loop

Figure 5.1. Linear spring-damper virtual system

The state-space representation of the linear SD system is:

$$\begin{pmatrix} \dot{x}_1 \\ \dot{x}_2 \end{pmatrix} = \begin{bmatrix} 0 & 1 \\ -c/m_{\mathrm{vs}} & -k_{\mathrm{s}}/m_{\mathrm{vs}} \end{bmatrix} \begin{pmatrix} x_1 \\ x_2 \end{pmatrix} + \begin{pmatrix} 0 \\ -1 \end{pmatrix} a_{\mathrm{g}} + \begin{pmatrix} 0 \\ 1/m_{\mathrm{vs}} \end{pmatrix} w \qquad \begin{matrix} \text{(5-1a)} \\ \text{(5-1b)} \end{matrix}$$

where the state variables x_1 and x_2 are the displacement and velocity of the basemat relative to the ground, respectively. The properties c and k_{s} in the above equations correspond to the isolation system, calculated as the sum of the individual bearing properties. The transfer functions for the linear SD system, $H_{za_g}^{sd}$ and H_{zw}^{sd}, are derived from the above state-space model and presented in Equations 5-2a and 5-2b, respectively. The superscript ‘sd’ denotes spring-damper system.

$$H_{za_g}^{sd} = \frac{cs + k_s}{m_{vs}s^2 + cs + k_s} \tag{5-2a}$$

$$H_{zw}^{sd} = \frac{s^2}{m_{vs}s^2 + cs + k_s} \tag{5-2b}$$

5.4 Mathematical modeling of the nonlinear lead-rubber virtual system

Similar to the linear SD system, the lead-rubber (LR) virtual system also includes a rigid basemat of mass m_{vs}. An LR isolator constitute vertically stacked, alternating layers of bonded rubber and steel shims with top and bottom end plates, and a cylindrical, central lead core (see Figure 3.3b). The 1D horizontal shear response of LR isolator is modeled as a combination of viscoelastic behavior of the rubber (idealized using linear spring and linear dashpot) and hysteretic behavior of the lead core, as shown in Figure 5.2a. The hysteretic element is based on the Bouc-Wen model (Bouc (1967); Wen (1976)), which was extended by Park *et al.* (1986) and Nagarajaiah *et al.* (1989) for the analysis of seismic isolation systems.

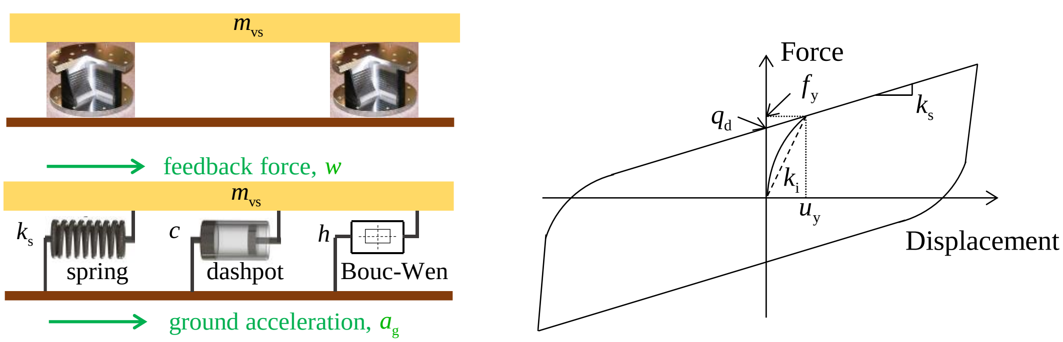

a) mathematical idealization b) idealized horizontal shear force-displacement loop

Figure 5.2. Nonlinear lead-rubber virtual system

Figure 5.2b is an idealized shear force-horizontal displacement loop for the LR bearing, where q_d is the characteristic strength (calculated as the product of the effective yield stress of the lead core, σ_L, and its cross-sectional area, A_L), f_y is the yield strength, k_i and k_s are the initial and the post-yield stiffnesses, and u_y is the yield displacement. (Note: k_i herein corresponds to the initial stiffness of the isolator calculated as the sum of the initial stiffness of the hysteretic component, k_o, and rubber stiffness, k_s).

The shear force in the LR isolation system is given by:

$$F = \underbrace{\alpha k_{\mathrm{i}} x + c\dot{x}}_{\text{viscoelastic}} + \underbrace{q_{\mathrm{d}} h}_{\text{hysteretic}} \tag{5-3}$$

where α is the ratio of the post-yield stiffness to the initial stiffness, c is the damping coefficient of the viscoelastic rubber layers, x is the relative horizontal displacement of the isolation system, $\dot{x}$ is the relative horizontal velocity, and h is the Bouc-Wen hysteretic evolution parameter given by:

$$\dot{h} = 1/u_{\mathrm{y}} \times \left(1 - 0.5(h)^{n}\left(1 + \mathrm{sign}(\dot{x}h)\right)\right)\dot{x} \tag{5-4}$$

where n is a smoothing parameter, u_{y} is the yield displacement given by $u_{\mathrm{y}} = q_{\mathrm{d}}/(1-\alpha)k_{\mathrm{i}} = f_{\mathrm{y}}/k_{\mathrm{i}}$, and 'sign' represents the signum function. From above, the governing differential equations for the LR virtual system are written as:

$$\dot{x}_1 = x_2 \tag{5-5a}$$

$$\dot{x}_2 = \left(w - \alpha k_{\mathrm{i}} x_1 - c x_2 - q_{\mathrm{d}} x_3\right)/m_{\mathrm{vs}} - a_{\mathrm{g}} \tag{5-5b}$$

$$\dot{x}_3 = q_{\mathrm{d}}/(1-\alpha)k_{\mathrm{i}} \times \left(1 - 0.5(x_3)^{\mathrm{n}}\left(1 + sign(x_2 x_3)\right)\right)x_2 \tag{5-5c}$$

where the state variables x_1, x_2, and x_3 are given by x, . $\dot{x}$, . and h, respectively. (The strength and stiffness properties in the above equations correspond to the isolation system, calculated as the sum of the individual isolator properties.) The LR system of Equation 5-5 is nonlinear. However, the nonlinearity is confined only to the third state equation, $\dot{x}_3$ (i.e., Equation 5-5c), for which the linear and nonlinear terms can be separated as:

$$\dot{x}_3 = \underbrace{\left(q_{\mathrm{d}}/(1-\alpha)k_{\mathrm{i}}\right)x_2}_{\text{linear}} - \underbrace{0.5(x_3)^{\mathrm{n}}\left(1 + sign(x_2 x_3)\right)x_2}_{\text{nonlinear}} \tag{5-6}$$

This structured nonlinearity (i.e., clear separation of linear and nonlinear terms) of the LR system is exploited and an alternate strategy for implementing MIL is proposed. If the nonlinear component in Equation 5-6, $f_{\mathrm{h}} = 0.5(x_3)^{\mathrm{n}}\left(1 + sign(x_2 x_3)\right)x_2$, is viewed as an external input to the VS, the system of equations for the LR virtual system can be rewritten in the state-space form as:

$$\begin{pmatrix} \dot{x}_1 \\ \dot{x}_2 \\ \dot{x}_3 \end{pmatrix} = \begin{bmatrix} 0 & 1 & 0 \\ -\alpha k_{\mathrm{i}}/m_{\mathrm{vs}} & -c/m_{\mathrm{vs}} & -q_{\mathrm{d}}/m^{\mathrm{vs}} \\ 0 & (1-\alpha)k_{\mathrm{i}}/q_{\mathrm{d}} & 0 \end{bmatrix} \begin{pmatrix} x_1 \\ x_2 \\ x_3 \end{pmatrix} + \begin{bmatrix} 0 \\ 1/m_{\mathrm{vs}} \\ 0 \end{bmatrix} w + \begin{bmatrix} 0 \\ -1 \\ 0 \end{bmatrix} a_g + \begin{bmatrix} 0 \\ 0 \\ -1 \end{bmatrix} f_{\mathrm{h}} \qquad \begin{matrix} (5\text{-}7a) \\ (5\text{-}7b) \\ (5\text{-}7c) \end{matrix}$$

The above linear system has three state variables and three input variables. The first input a_{g} is known a prior, the second input w is measured by the reaction load cells in real time. The third input, f_{h}, is calculated in real time by solving the VS differential equations (i.e., the state variables, x_2 and x_3, obtained at each time step are used to compute $f_{\mathrm{h}} = 0.5(x_3)^{\mathrm{n}}(1+sign(x_2x_3))x_2$). This alternate strategy is illustrated using the block diagram of Figure 5.3a. In simple terms, the nonlinear system is represented as a linear system with the nonlinear component/s considered as an external input/s to (and in constant feedback with) the linear parts of the system. Similar approach has been adopted by Verma *et al.* (2019).

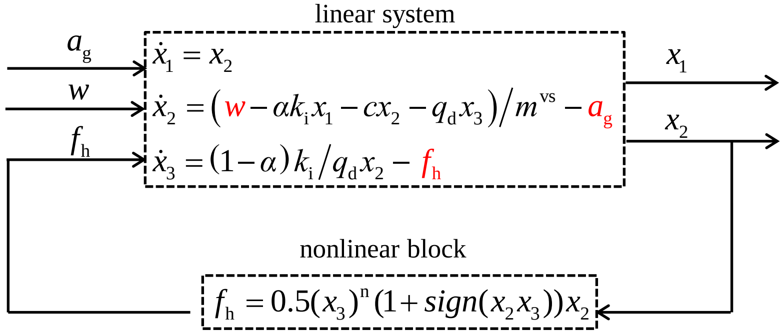

a) without heating effects (used in this report)

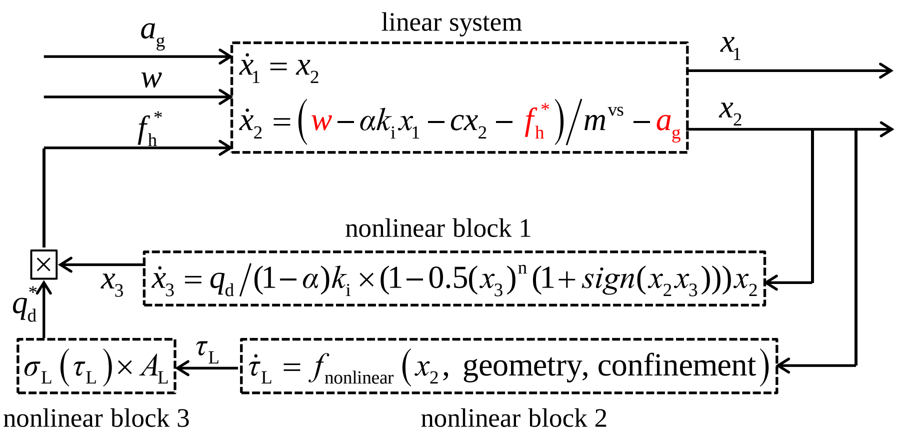

b) with heating effects

Figure 5.3. Modeling strategy for the LR system: linear system representation with nonlinear compone nts viewed as external inputs in feedback

The strategy of Figure 5.3 also accommodates VS complexities, for example, heating effects of the lead core. Kalpakidis and Constantinou (2009) characterized the nonlinear dependency of the effective yield stress of lead (and by extension of q_{d}) on the instantaneous temperature of the lead core, τ_{L}, which is further expressed as a nonlinear state variable evolving as a nonlinear function of geometric properties of the lead core, speed of motion, loading time, and confinement provided by the rubber and the steel shims. If such heating effects were to be included in the VS modeling, both Equation 5-5b and 5-5c will be nonlinear. The block diagram of Figure 5.3a transitions to Figure 5.3b, wherein the linear system then constitute two state variables and three input variables. The third input, f_{h}^{*}, is calculated by evaluating multiple nonlinear blocks, which are in feedback with the linear system.

From the linear system representation of Figure 5.3a, the target basemat acceleration for the LR system can be written as $z_{\mathrm{vs}}^{\mathrm{lr}} = H_{\mathrm{za_g}}^{\mathrm{lr}} a_{\mathrm{g}} + H_{\mathrm{zw}}^{\mathrm{lr}} w + H_{\mathrm{zf_h}}^{\mathrm{lr}} f_{\mathrm{h}}$, where the transfer functions $H_{za_{\mathrm{g}}}^{\mathrm{lr}}$, H_{zw}^{vs}, and $H_{zf_{\mathrm{h}}}^{\mathrm{lr}}$ are given by Equations 5-8a through 5-8c. The MIL controller can then be designed per the procedure outlined in Section 1 by equating the VS and the shake-table accelerations: $H_{\mathrm{zu}}^{\mathrm{st}} u + H_{\mathrm{zw}}^{\mathrm{st}} = H_{\mathrm{za_g}}^{\mathrm{lr}} a_{\mathrm{g}} + H_{\mathrm{zw}}^{\mathrm{lr}} w + H_{\mathrm{zf_h}}^{\mathrm{lr}} f_{\mathrm{h}}$. The controller equation then includes three terms: $u = \left(H_{\mathrm{zu}}^{\mathrm{st}}\right)^{-1} H_{\mathrm{za_g}}^{\mathrm{lr}} a_{\mathrm{g}} + \left(H_{\mathrm{zu}}^{\mathrm{st}}\right)^{-1} \left(H_{\mathrm{zw}}^{\mathrm{lr}} - H_{\mathrm{zw}}^{\mathrm{st}}\right) w + \left(H_{\mathrm{zu}}^{\mathrm{st}}\right)^{-1} H_{\mathrm{zf_h}}^{\mathrm{lr}} f_{\mathrm{h}}$.

$$H_{za_{\mathrm{g}}}^{\mathrm{lr}} = \frac{cs + k_{\mathrm{i}}}{m_{\mathrm{vs}} s^2 + cs + k_{\mathrm{i}}} \tag{5-8a}$$

$$H_{zw}^{\mathrm{lr}} = \frac{s^2}{m_{\mathrm{vs}} s^2 + cs + k_{\mathrm{i}}} \tag{5-8b}$$

$$H_{zf_{\mathrm{h}}}^{\mathrm{lr}} = \frac{s}{m_{\mathrm{vs}} s^2 + cs + k_{\mathrm{i}}} \tag{5-8c}$$

5.5 Mathematical modeling of the nonlinear Friction Pendulum virtual system

A single concave FP bearing (see Figure 3.3c) consists of a spherical sliding surface made of stainless steel, a housing plate, and a slider coated with low-friction, high-load composite, typically a polytetrafluorethylene (PTFE) type composite. The pendulum action of the slider along the spherical surface provides horizontal flexibility to the isolator, and the coefficient of friction at the PTFE-stainless steel interface governs its strength. Similar to LR isolator, the shear force in an FP isolator can be decomposed into linear elastic and nonlinear hysteretic components, as illustrated in Figure 5.4a. Figure 5.4b is an idealized shear force-horizontal displacement loop for the FP bearing.

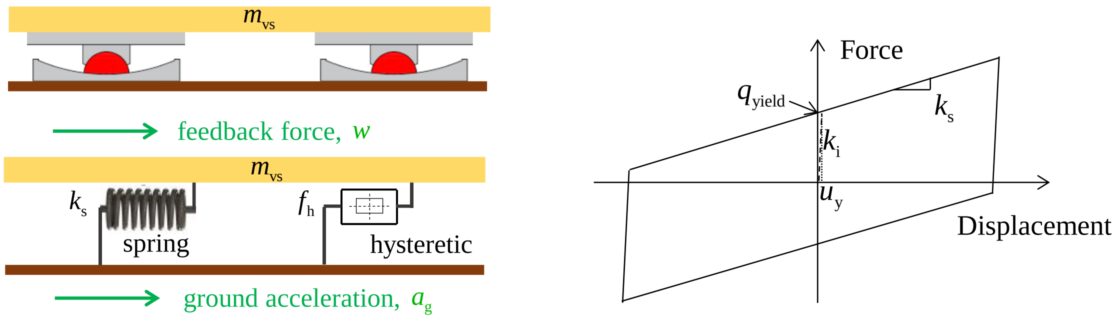

a) mathematical idealization b) idealized horizontal shear force-displacement loop

Figure 5.4. Nonlinear single concave Friction Pendulum VS

The yield strength, q_{yield}, and the sliding stiffness, k_s, of the isolation system are given by:

$$q_{yield} = \mu W \tag{5-9a}$$

$$k_s = W / R_{eff} \tag{5-9b}$$

where W is the instantaneous axial load, μ is the coefficient of sliding friction, R_{eff} is the effective radius of curvature of the sliding surface, k_i is the initial stiffness, and u_y is the yield displacement (typically < 1 mm). At a given instant of time, the coefficient of sliding friction, μ, depends on the instantaneous sliding velocity, instantaneous axial pressure, and the instantaneous temperature at the sliding interface (Kumar *et al.*, 2019b). In the MIL experiments of this report: (i) the axial pressure is constant because vertical excitation of the test article is not considered, (ii) the heating effects in the isolator are small at the scale the experiments are performed, hence not considered, and (iii) the dependency of μ on the sliding velocity is modeled using the following expression proposed by Mokha *et al.* (1988):

$$\mu(v) = \mu_{max}\left[1 - \left(1 - \mu_{min}/\mu_{max}\right)e^{-a|v|}\right] \tag{5-10}$$

where v is the instantaneous sliding velocity, a is a rate parameter, and μ_{max} and μ_{min} are the coefficients of friction at fast and slow velocities, respectively. The system of equations for the FP system are:

$$\dot{x}_1 = x_2 \tag{5-11a}$$

$$\dot{x}_2 = \left(w - k_s x_1 - \mu(x_2) W x_3\right) / m^{vs} - a_g \tag{5-11b}$$

$$\dot{x}_3 = 1/u_y \times \left(1 - 0.5\left(x_3\right)^{n}\left(1 + sign\left(x_2 x_3\right)\right)\right) x_2 \tag{5-11c}$$

In the above equations, μ is a nonlinear function of the state variable x_2, which makes both Equations 5-11b and 5-11c nonlinear. The alternate strategy of Figure 5.3 is extended for the FP system with two nonlinear blocks in feedback: one to calculate the hysteretic evolution parameter and the other to evaluate the dependency of friction on the instantaneous sliding velocity, as illustrated in Figure 5.5. The linear FP system has two state variables and three external inputs. The third input, $f_\mathrm{h} = \mu(x_2)Wx_3$ is computed by evaluating the two nonlinear blocks in real time.

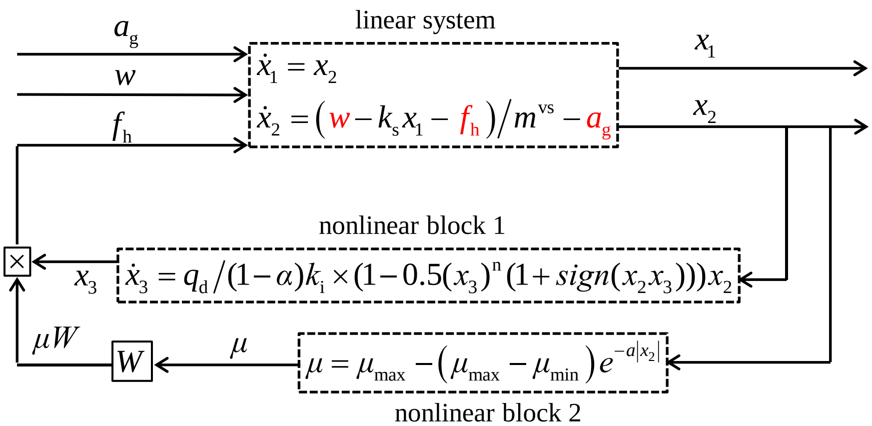

Figure 5.5. Modeling strategy for the FP system: linear system representation with nonlinear components viewed as external inputs in feedback

The linear state-space representation of the FP virtual system model is:

$$\begin{pmatrix} \dot{x}_1 \\ \dot{x}_2 \end{pmatrix} = \begin{bmatrix} 0 & 1 \\ -k_\mathrm{s}/m_\mathrm{vs} & 0 \end{bmatrix} \begin{pmatrix} x_1 \\ x_2 \end{pmatrix} + \begin{pmatrix} 0 \\ -1 \end{pmatrix} a_\mathrm{g} + \begin{pmatrix} 0 \\ 1/m_\mathrm{vs} \end{pmatrix} w + \begin{pmatrix} 0 \\ -1 \end{pmatrix} f_\mathrm{h} \qquad \begin{matrix} (5\text{-}12a) \\ (5\text{-}12b) \end{matrix}$$

The VS basemat acceleration can be expressed as: $z_\mathrm{vs} = H^\mathrm{fp}_{za_\mathrm{g}} a_\mathrm{g} + H^\mathrm{fp}_{zw} w + H^\mathrm{fp}_{zf_\mathrm{h}} f_\mathrm{h}$, where the transfer functions $H^\mathrm{fp}_{za_\mathrm{g}}$, H^fp_{zw}, and $H^\mathrm{fp}_{zf_\mathrm{h}}$ are given by:

$$H^\mathrm{fp}_{za_\mathrm{g}} = \frac{k_\mathrm{s}}{m_\mathrm{vs}s^2 + k_\mathrm{s}} \tag{5-13a}$$

$$H^\mathrm{fp}_{zw} = \frac{s^2}{m_\mathrm{vs}s^2 + k_\mathrm{s}} \tag{5-13b}$$

$$H^\mathrm{fp}_{zf_\mathrm{h}} = \frac{-s^2}{m_\mathrm{vs}s^2 + k_\mathrm{s}} \tag{5-13c}$$

SECTION 6
DESIGN OF THE MIL CONTROLLER

6.1 Section prologue

As discussed in Section 1.3.4, the MIL controller, namely, $u = \left(H_{zu}^{\mathrm{st}}\right)^{-1} H_{za_g}^{\mathrm{vs}} \alpha + \left(H_{zu}^{\mathrm{st}}\right)^{-1} \left(H_{zw}^{\mathrm{vs}} - H_{zw}^{\mathrm{st}}\right) w,$ cannot be implemented directly in real time (as a state-space system) because the inverse transfer function term $\left(H_{zu}^{\mathrm{st}}\right)^{-1}$ often results in improper (non-causal) controller terms, making their state-space implementation impractical. Additionally, noise in the measurement of the feedback force and low fidelity of the shake-table model (H_{zu}^{st} and H_{zw}^{st}) at high frequencies make it necessary to limit the controller response at high frequencies. These constrains requires approximations to the controller equation prior to its state-space implementation.

A particular form of controller approximation is considered in this report, namely using lowpass filters, $H_{a_{\mathrm{g}}}^{\mathrm{filter}}$ and H_{w}^{filter}, which are implemented as: $u = H_{\alpha}^{\mathrm{filter}} \left(H_{\mathrm{zu}}^{\mathrm{as}}\right)^{-1} H_{z\alpha}^{\mathrm{vs}} \alpha + H_{w}^{\mathrm{filter}} \left(H_{\mathrm{zu}}^{\mathrm{as}}\right)^{-1} \left(H_{\mathrm{zw}}^{\mathrm{vs}} - H_{\mathrm{zw}}^{\mathrm{as}}\right) w,$ However, limiting the controller response at higher frequencies penalizes MIL performance at lower frequencies, which can sometimes lead to instability. Therefore, understanding the tradeoffs associated with the filters is central to the successful implementation of the impedance-matching approach to MIL and is the focus of this section.

The fundamental basis for the MIL controller is derived in Section 6.2. Section 6.3 discusses challenges associated with the implementation of MIL controller and demonstrates the need for approximations. Section 6.4 describes a rational procedure to design the lowpass filters. The process makes explicit that the filter design is a tradeoff between performance (how closely the controlled shake table mimics the VS impedance), desired control effort (to minimize the controller response at high frequencies to curtail the effects of measurement noise), and stability (assessed herein using the notion of passivity). The approximated MIL controller is then discretized in time and a state-space realization of this discretization is implemented as a mathematical code, as described in Section 6.5.

6.2 Fundamental basis for the MIL controller

As discussed in Section 4.5**,** for carefully tuned control parameters, K_{e}, K_{p}, and τ_{loop}, the shake table response is linear (approximately), which can be predicted with high fidelity using the analytical transfer functions, H_{zu}^{st} and H_{zw}^{st}. This outcome enables writing the shake-table acceleration, z_{st}, in the linear form:

$$z_{\mathrm{st}} = H_{zu}^{\mathrm{st}} u + H_{zw}^{\mathrm{st}} w \tag{6-1}$$

where H_{zu}^{st} and H_{zw}^{st} are given by Equations 4-15a and 4-15d, respectively. For the cases where the shake table is to represent a linear system (e.g., spring-damper isolation system), the target basemat acceleration of the VS, z_{vs}, can be written as:

$$z_{\mathrm{vs}} = H_{za_{\mathrm{g}}}^{\mathrm{vs}} a_{\mathrm{g}} + H_{zw}^{\mathrm{vs}} w. \tag{6-2}$$

where a_{g} is the ground acceleration (external input to the VS). The transfer functions $H_{za_{\mathrm{g}}}^{\mathrm{vs}}$ and H_{zw}^{vs} for the linear SD system are given by Equations 5-2a and 5-2b. For simulating a linear SD system, the MIL controller is designed by posing the question:

> What should the control input, u, to the actuator be so that for the measured feedback force, w, from the test article, the acceleration applied by the shake table, z_{st}, at the base of the test article is equal to the z_{vs} computed by the isolation-system model?

The problem statement naturally presents a solution by equating the shake-table and VS accelerations, $z_{\mathrm{st}} = z_{\mathrm{vs}}$, that is, $H_{zu}^{\mathrm{st}} u + H_{zw}^{\mathrm{st}} w = H_{za_{\mathrm{g}}}^{\mathrm{vs}} a_{\mathrm{g}} + H_{zw}^{\mathrm{vs}} w.$ The control input, u, to the actuator is calculated as:

$$u = \left(H_{zu}^{\mathrm{st}}\right)^{-1} H_{za_{\mathrm{g}}}^{\mathrm{vs}} a_{\mathrm{g}} + \left(H_{zu}^{\mathrm{st}}\right)^{-1} \left(H_{zw}^{\mathrm{vs}} - H_{zw}^{\mathrm{st}}\right) w \tag{6-3}$$

The MIL controller of Equation 6-3 is identical to Equation 1-4, conceptualized in Section 1 for a generic setting. In the absence of a_{g}, the force-motion behavior of the VS is given by:

$$z_{\mathrm{vs}} = H_{zw}^{\mathrm{vs}} w \tag{6-4}$$

where H_{zw}^{vs} is a measure of the VS impedance/admittance/resistance. Similarly, from Equations 6-1 and 6-3, the force-motion relationship of the controlled shake table can be written as:

$$z_{\mathrm{st}} = \left(H_{zu}^{\mathrm{st}} H_{uw} + H_{zw}^{\mathrm{st}}\right) w \tag{6-5}$$

where $H_{uw} = \left(H_{zu}^{\mathrm{st}}\right)^{-1} \left(H_{zw}^{\mathrm{vs}} - H_{zw}^{\mathrm{st}}\right)$. Equations 6-4 and 6-5 imply matching the impedance of the shake table with that of the VS using suitable controls, hence the approach is termed as ‘impedance matching’.

The above formulation, however, is valid for only those virtual systems for which z_{vs} can be expressed in the linear form: $z_{\mathrm{vs}} = H_{za_{\mathrm{g}}}^{\mathrm{vs}} a_{\mathrm{g}} + H_{zw}^{\mathrm{vs}} w.$ An alternate strategy[19] to implement MIL for the nonlinear VS such as the LR and FP isolation systems was presented in Section 5.3. This alternate strategy enables writing the basemat acceleration in the linear form, but with three inputs: $z_{\mathrm{vs}} = H_{za_{\mathrm{g}}}^{\mathrm{vs}} a_{\mathrm{g}} + H_{zw}^{\mathrm{vs}} w + H_{zf_{\mathrm{h}}}^{\mathrm{vs}} f_{\mathrm{h}},$ where the third input f_{h} accounts for the nonlinear component of the VS. The MIL controller then takes the form:

$$u = \left(H_{zu}^{\mathrm{st}}\right)^{-1} H_{za_{\mathrm{g}}}^{\mathrm{vs}} a_{\mathrm{g}} + \left(H_{zu}^{\mathrm{st}}\right)^{-1}\left(H_{zw}^{\mathrm{vs}} - H_{zw}^{\mathrm{st}}\right) w + \left(H_{zu}^{\mathrm{st}}\right)^{-1} H_{zf_{\mathrm{h}}}^{\mathrm{vs}} f_{\mathrm{h}} \tag{6-6}$$

The MIL controllers of Equations 6-3 and 6-6 includes the VS transfer function terms, $H_{za_{\mathrm{g}}}^{\mathrm{vs}}$, H_{zw}^{vs}, and $H_{zf_{\mathrm{h}}}^{\mathrm{vs}}$, meaning that the controller terms, $H_{ua_{\mathrm{g}}} = \left(H_{zu}^{\mathrm{st}}\right)^{-1} H_{za_{\mathrm{g}}}^{\mathrm{vs}}$, $H_{uw} = \left(H_{zu}^{\mathrm{st}}\right)^{-1}\left(H_{zw}^{\mathrm{vs}} - H_{zw}^{\mathrm{st}}\right)$, and $H_{uf_{\mathrm{h}}} = \left(H_{zu}^{\mathrm{st}}\right)^{-1} H_{zf_{\mathrm{h}}}^{\mathrm{vs}}$, will be unique to each VS based on its type and properties. As an example, the external input f_{h} and its corresponding transfer function, $H_{zf_{\mathrm{h}}}^{\mathrm{vs}}$, for the LR system (Equation 5-8c) is different from that of the FP system (Equation 5-13c). Moreover, the controller form shown in Equations 6-3 and 6-6, although promising, may not work in all cases particularly if the VS exhibits complex nonlinear behavior making the alternate strategy of Figure 5.3 inapplicable. For such cases, an alternate form of the MIL controller can be considered by directly equating $z_{\mathrm{vs}} = z_{\mathrm{st}} = H_{zu}^{\mathrm{st}} u + H_{zw}^{\mathrm{st}} w$:

$$u = \left(H_{zu}^{\mathrm{st}}\right)^{-1} z_{\mathrm{vs}} - \left(H_{zu}^{\mathrm{st}}\right)^{-1} H_{zw}^{\mathrm{st}} w \tag{6-7}$$

The fundamental assumption of the above form of MIL controller is that no compromises (in terms of performance) need to be made in representing the VS. The controller has two inputs: (i) the feedback force, w, measured by the reaction load cells, and (ii) the target VS acceleration, z_{vs}, which is computed in real time by solving the VS differential equations (e.g., Equations 5-11a through 5-11c for the FP system) for known a_{g} and measured w.

A key feature of Equation 6-7 is that the controller terms $H_{uz} = \left(H_{zu}^{\mathrm{st}}\right)^{-1}$ and $H_{uw} = \left(H_{zu}^{\mathrm{st}}\right)^{-1} H_{zw}^{\mathrm{st}}$, depend only on the shake-table parameters. This representation enables the use of a standardized MIL controller to represent different linear and nonlinear virtual systems, without (or with only few) modifications.

[19] The Bouc-Wen hysteresis model enabled separation of the linear and nonlinear terms in the differential equations, where the nonlinear terms are viewed as external inputs to (and acting in feedback) with the linear system, as illustrated by the block diagrams of Figures 5-3 and 5-5).

Table 6.1contrasts some of the key differences between Equations 6-6 (6-3) and 6-7. The goal of this table is to inform the experimentalist of the advantages and limitations of each approach, but not identifying a preference. The choice of the MIL controller should be made based on the test system configuration and the goals of the experiment. Equation 6-7 is adopted in this rpeort because it enables the use of a standardized controller equation that can be implemented to represent all three virtual systems (SD, LR, and FP), independent of their dynamic behavior.

Table 6.1. Impedance-matching MIL controller

Equation 6-6 (6-3)	*Equation 6-7*
Controller transfer functions depend on both the VS and the shake-table dynamics	Controller transfer functions depend only on the shake-table dynamics
Can represent linear and only some nonlinear virtual systems	Can represent all linear and nonlinear virtual systems
Virtual system dynamics must be explicitly characterized in the form of transfer functions	Explicit VS transfer functions are not required
Time-integration schemes are required to evaluate the nonlinear blocks of Figures 5-3 and 5-5 and compute f_{h}	Time-integration schemes are required to solve VS differential equations enabling calculation of z_{vs}
Implementation is simpler when the VS is linear	Implementation is computationally challenging when the VS includes several degrees of freedom; finite element software may need to be employed
Controller equation is VS dependent (function of the VS dynamics, nonlinearity, and properties)	Controller equation is largely standardized; depends only on the shake-table transfer functions
Allows for making direct compromises on the VS representation, that is, the VS transfer functions can be approximated to tradeoff performance in the frequency range where the VS dynamics need not be represented accurately	Compromises on the VS behavior are possible but may have to be indirect, for example, the basemat acceleration needs to be calculated using approximate models for the VS

6.3 Need for approximations to the MIL controller

The MIL controller presented in Equation 6-7 (and those in Equations 6-6 and 6-3) cannot be implemented directly in real time as state-space system because of the following constraints:

1. Causality of H_{uz} and H_{uw}: In Section 4, the transfer function $H_{\text{zu}}^{\text{st}}$ is derived as the ratio of a second-order polynomial to a fifth-order polynomial (see Equation 4-15a), and H_{zw}^{st} includes fifth-order polynomials both in the numerator and the denominator (see Equation 4-15d). For the shake-table parameters of Table 4.1, the controller terms, $H_{\text{uz}} = \left(H_{\text{zu}}^{\text{st}}\right)^{-1}$ and $H_{\text{uw}} = \left(H_{\text{zu}}^{\text{st}}\right)^{-1} H_{\text{zw}}^{\text{st}}$, are given by:

$$H_{uz} = \frac{4.32\times10^{-12}s^5 + 5.02\times10^{-9}s^4 + 1.39\times10^{-6}s^3 + 5.75\times10^{-4}s^2 + 3.73\times10^{-2}s + 1}{s^2} \quad \text{(6-8a)}$$

$$H_{uw} = 1.04\times10^{-12}s^3 + 1.21\times10^{-9}s^2 + 3.06\times10^{-7}s + 1.04\times10^{4} \quad \text{(6-8b)}$$

The above transfer functions are non-causal (i.e., order of the numerator polynomial greater than the order of its denominator polynomial) by a relative degree of 3. State-space implementation of such systems is physically not realizable and necessitates suitable approximations to modify H_{uz} and H_{uw} for causality, that is, to make the order of the denominator equal (or greater) than the order of the numerator[20].

2. Noise in the measurement of w: Figure 6.1 presents Bode plots of H_{uz} and H_{uw} (Equations 6-8a and 6-8b), respectively. It can be seen from the magnitude charts that these transfer functions exhibit infinitely growing response at high frequencies, due to the number of zeros being greater than the number of poles. Such response is not desirable, particularly for H_{uw}, because the controller then becomes sensitive to (and amplifies) noise in the measurement of w, which then propagates through the entire feedback system: noise in the measurement of w $\xrightarrow{\text{input to the } H_{uw} \text{ controller}}$ control input $\xrightarrow{\text{command to the shake table}}$ table acceleration $\xrightarrow{\text{physically applied to the test article}}$ measurement of w with amplified high-frequency content[21] $\xrightarrow{\text{input to the } H_{uw} \text{ controller}}$ …. and the cycle repeats. The result is large-amplitude high-frequency oscillations of the table, which eventually makes the feedback system unstable. For stability, $\left|H_{uz}z\right|$ and $\left|H_{uw}w\right|$ must be kept small at high frequencies where there is greater noise. Another reason for limiting the controller response is because of the poor fidelity of the shake-table model at high frequencies. It is for this reason an accurate shake-table model is sought across a frequency range as broad as possible. The broader the frequency range of accuracy, the less the need to make controller approximations.

---

[20] If Equation 6-6 is to be used, approximations for fixing causality will be specific to the VS type and its nonlinearity, unlike the case with Equation 6-7.

[21] The dominant horizontal frequencies of the fluid-filled vessel considered herein are greater than 60 Hz. It will be seen in Sections 8 and 9 that if the controller response is not sufficiently curtailed at high frequencies, the test article responds to (and further amplifies) the propagated noise in the system, making the feedback system unstable.

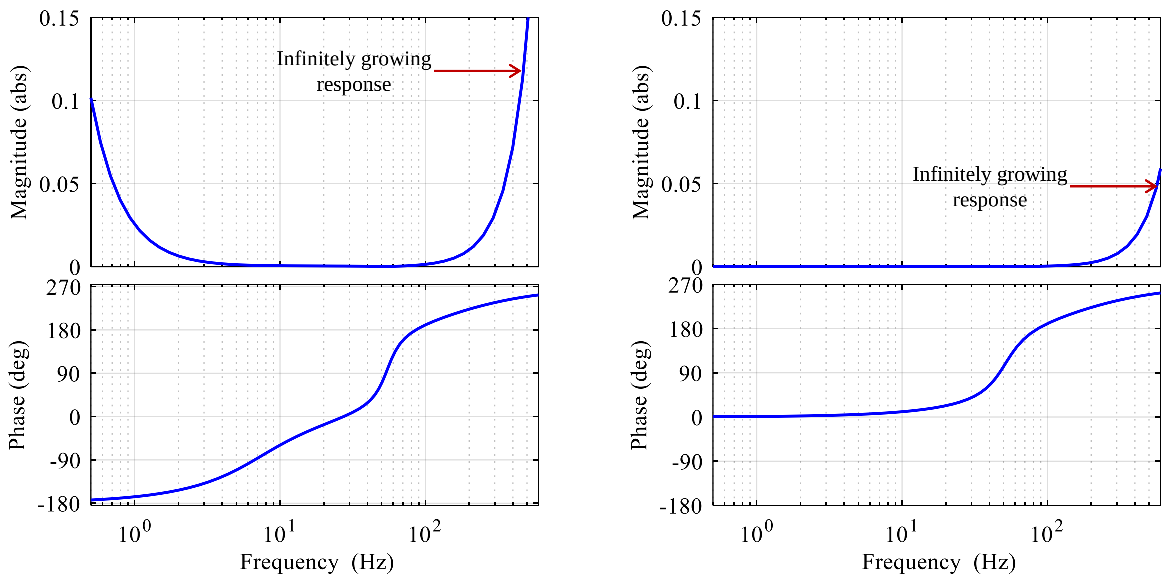

a) H_{uz} b) H_{uw}

Figure 6.1. Bode plots of the controller transfer functions; properties per Table 4-1

6.4 Controller approximation using lowpass filters and consequent tradeoffs

The above constraints to the implementation of the MIL controller are addressed in this report by approximating the controller using lowpass filters H_z^{filter} and H_w^{filter}, respectively. The MIL controller of Equation 6-7, after including the filter terms, can be rewritten as:

$$u = H_z^{\text{filter}} H_{uz} z_{\text{vs}} - H_w^{\text{filter}} H_{uw} w \tag{6-9}$$

Because H_{uz} and H_{uw} are non-causal by a relative degree of 3, a third-order (or higher order) filter is required, leaving the cut-off frequency, f_{c}, as the only design parameter. Design criteria for f_{c} are determined based on: (i) *performance*: the magnitude and phase response of the approximated controller is minimally affected in the frequency range of interest for the MIL experiments, (ii) *desired control effort*: $\left|H_z^{\text{filter}} H_{uz}\right|$ and $\left|H_w^{\text{filter}} H_{uw}\right|$ are sufficiently curtailed at high frequencies, and (iii) *stability:* ensured herein using notion of passivity, which comes to light in Section 9.3. Criterion (i) is made possible by using lowpass filters with an order as small as possible and a cut-off frequency, f_{c}, as large as possible. Figure 6.2 presents Bode plots of the controller transfer functions approximated using third-order Butterworth lowpass filters with cut-off frequencies: 40 Hz, 80 Hz, 120 Hz, 160 Hz, and 200 Hz. These third-order filters, although ensures causality of $H_z^{\text{filter}} H_{uz}$ and $H_w^{\text{filter}} H_{uw}$, significantly penalize the controller response at lower frequencies, as indicated by the blue and the orange lines in Figures 6-2b and 6-2c.

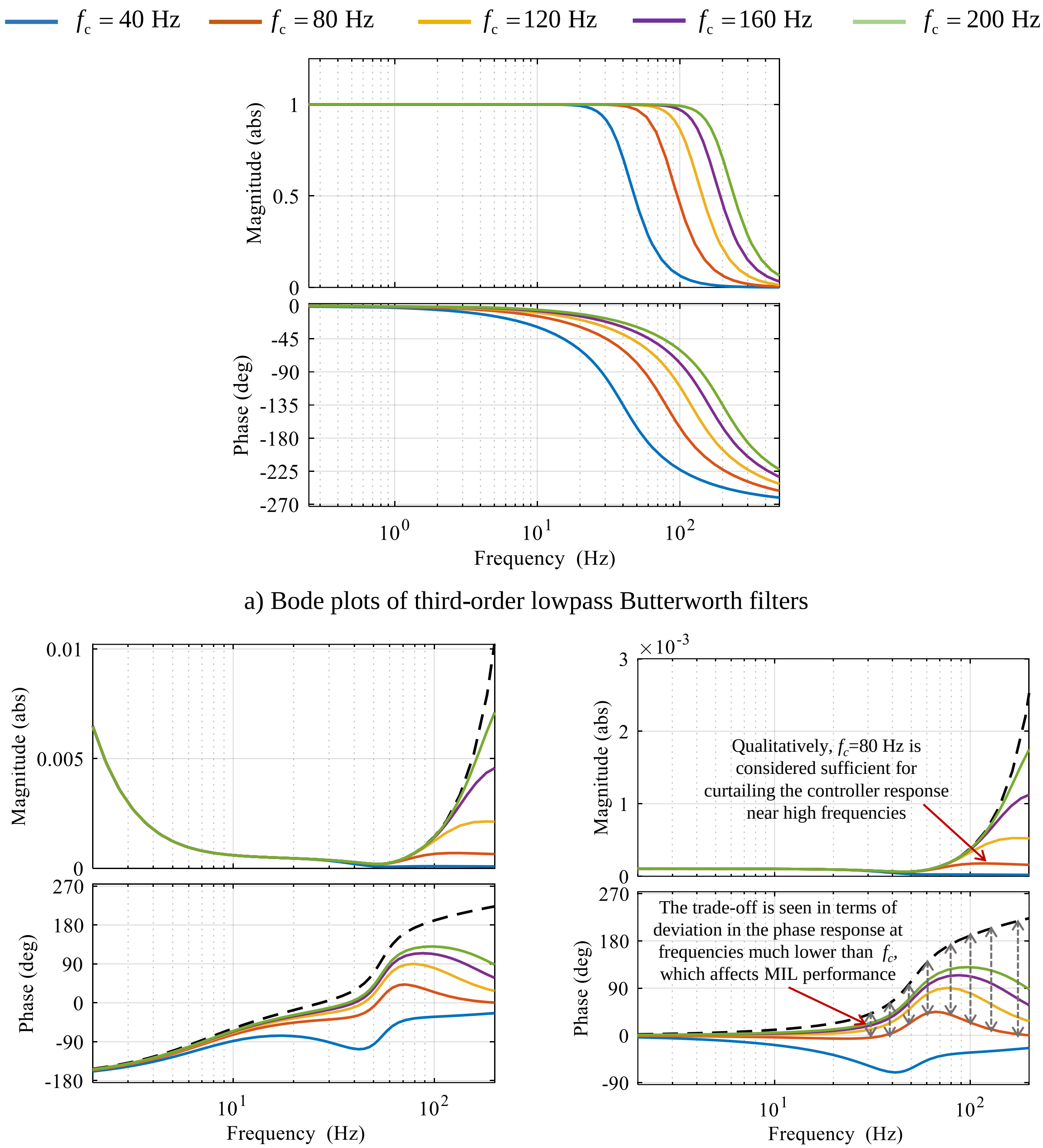

a) Bode plots of third-order lowpass Butterworth filters

b) $H_z^{\text{filter}} H_{uz}$

c) $H_w^{\text{filter}} H_{uw}$

Figure 6.2. Bode plots of the approximated controller transfer functions; different cut-off frequencies; shake-table properties per Table 4-1;

The smaller the cut-off frequency, f_c, of the filter, the more the controller performance is penalized at low frequencies, as seen in the phase charts of Figures 6-2b and 6-2c. Conversely, if the cut-off frequency is high, say $f_c > 120$ Hz, the controller response is not sufficiently curtailed at high frequencies making it sensitive (responsive) to the effects of measurement noise in w and model inaccuracies: the constraints determining stability. The cut-off frequency of the filters is therefore determined as a tradeoff between performance and stability. For the MIL experiments of Section 9, both H_z^{filter} and H_w^{filter} are represented using third-order Butterworth lowpass filters with a cut-off frequency of 80 Hz[22]. The continuous-time representation of this filter is:

$$H^{\text{filter}} = \frac{1.27\times10^{8}}{s^{3}+1.01\times10^{3}s^{2}+5.05\times10^{5}s+1.27\times10^{8}} \tag{6-10}$$

The approximated controller transfer functions are:

$$H_z^{\text{filter}}H_{uz} = \frac{5.5\times10^{-4}s^{5}+6.4\times10^{-1}s^{4}+1.8\times10^{2}s^{3}+7.3\times10^{4}s^{2}+4.7\times10^{6}s+1.3\times10^{8}}{s^{5}+1\times10^{3}s^{4}+5.1\times10^{5}s^{3}+1.3\times10^{8}s^{2}} \tag{6-11a}$$

$$H_w^{\text{filter}}H_{uw} = \frac{1.33\times10^{-4}s^{3}+1.54\times10^{-1}s^{2}+3.9\times10^{1}s+1.3\times10^{4}}{s^{3}+1.01\times10^{3}s^{2}+5.05\times10^{5}s+1.27\times10^{8}} \tag{6-11b}$$

6.5 Time-discretization and state-space implementation of the MIL controller

The approximated controller transfer functions, $H_z^{\text{filter}}H_{uz}$ and $H_w^{\text{filter}}H_{uw}$, derived above are in continuous-time. These transfer functions are time-discretized (sampled), and a state-space realization of this discretization is implemented as code in the RMCTools (controller software; see Section 3.6.2.2). Presented next is a series of MATLAB (Mathworks, 2020) commands that are used to obtain the discrete state-space form of the MIL controller.

---

[22]It is demonstrated in Section 9 that for the test cases where the shake table is controlled to imitate different seismic isolation systems, the controller performance is not affected significantly when f_c is varied in the range of 60 Hz to 200 Hz. This is because the table response in these test cases is largely dominated by low-frequency ($f < 3$ Hz) motion of the isolation system, which is at least twenty times smaller than the considered cut-off frequencies. However, for the test cases where the shake table is used to imitate an input ground motion trajectory, as-is, at the base of the test article (i.e., $z_{\text{vs}} = a_{\text{g}}$), $f_c > 100$ Hz resulted in a highly oscillatory table response indicating instability. The value $f_c = 80$ Hz is identified as trade-off between stability and performance for more than 100 test cases (combinations of physical systems (different water depths), virtual systems (different isolation system type and properties), and input ground motions (acceleration histories with different amplitude and spectral content)). Note that for the proposed impedance-matching approach, once the control gains are tuned to obtain an accurate shake-table model, the cut-off frequency of the filters is the only design parameter that needs to be identified/tuned/controlled by the experimentalist.

Step 1: Obtain controller transfer functions H_{uz} and H_{uw}

```
H_uz = minreal(1/H_zu_st);
H_uw = minreal(H_zw_st/H_zu_st);
```

The transfer functions `H_zu_st` and `H_zw_st` are obtained from the linear state-space model of the shake table (Equation 4-14). The function `mineral` is used to cancel pole-zero pairs when dividing two transfer functions in MATLAB.

Step 2: Obtain controller filters

```
[b,a] = butter(3, 2*pi*80, 'low', 's');
H_z_filter = tf(b,a);
H_w_filter = tf(b,a);
```

The function `butter` has four input arguments and returns transfer function coefficients of a Butterworth filter. The first argument is order of the filter (specified as 3), the second is the cut-off frequency of the filter to be expressed in rad/s (`2*pi*80`), the third determines the type of the filter (`'low'` indicates lowpass filter), and the fourth argument `'s'` specifies that the filter output is analog (i.e., continuous time).

Step 3: Obtain approximated controller transfer functions

```
H_uz_approx = minreal(H_uz*H_z_filter);
H_uw_approx = minreal(H_uw*H_w_filter);
```

Step 4: Convert the approximated transfer functions to discrete state-space form

```
H_uz_discrete = c2d(prescale(ss(H_uz_approx))), dt, 'tustin');
H_uw_discrete = c2d(prescale(ss(H_uz_approx))), dt, 'tustin');
```

The approximated controller transfer functions are converted to state-space form using the functions `ss(H_uz_approx)` and `ss(H_uw_approx)`. The function `c2d` is a MATLAB function used for discretizing a continuous-time system, `dt` is the sampling interval for discretization (i.e., loop time of the RMC75E, τ_s), and `'tustin'` is one of the continuous-discrete conversion methods available in the MATLAB's Control System ToolboxTM.

The RMC75E controller processes all variables using single-precision arithmetic. Discretizing the continuous-time system using single precision arithmetic resulted in a poorly conditioned state matrix. The command `prescale` is used to scale the entries of the state-space matrices to preserve their accuracy and numerical conditioning after discretization. Note that prescaling is not a requirement of the impedance-matching approach but of the hardware environment (RMC75E herein) in which it is implemented (e.g., MTS controllers with double-precision arithmetic may not require prescaling).

Step 5: Obtain entries of the discrete state-space MIL controller

```
% State-space matrices of the H_uz_discrete controller
 A = single(H_uz_discrete.A); % State matrix
 B = single(H_uz_discrete.B); % Input matrix
 C = single(H_uz_discrete.C); % Output matrix
 D = single(H_uz_discrete.D); % Feedforward matrix

% State-space matrices of the H_uw_discrete controller
 E = single(H_uw_discrete.A); % State matrix
 F = single(H_uw_discrete.B); % Input matrix
 G = single(H_uw_discrete.C); % Output matrix
 H = single(H_uw_discrete.D); % Feedforward matrix
```

The command `single` converts the entries of the state-space matrices from double-precision (default output of MATLAB) to single-precision arithmetic.

Step 6: Implementation of the MIL controller as a discrete state-space system

```
% Calculate control input
u_z(i,1) = C*x(:,i) + D*z_vs(i,1); % control input from z_vs
u_w(i,1) = G*x(:,i) + H*z_vs(i,1); % control input from w
u(i,1) = u_z(i,1) - u_w(i,1);      % control input to the table

% Update controller states for the next time step
x(:,i+1) = A*x(:,i) + B*z_vs(i,1);
y(:,i+1) = E*y(:,i) + F*w(i,1);
```

where `x` and `y` are states of the discrete controller terms, `H_uz_discrete` and `H_uw_discrete`, respectively, and `i` is the time-step number. In the above code, `A` and `E` are matrices of order 5×5, `B` and `F` are vectors of order 5×1, `C` and `G` are vectors of order 1×5, and states `x` and `y` are vectors of order 5×1.

SECTION 7
IMPLEMENTATION OF MIL CONTROLLER IN THE RMC75E

7.1 Section Prologue

The discrete state-space MIL controller of Section 6.5 is implemented in the RMC75E as user programs. These programs are structured to: (i) acquire sensor signals, (ii) solve the VS differential equations of Section 5, (iii) implement the discrete MIL controller in real time as a state-space system, (iv) issue reference position command (i.e., control input, u) to the actuator, (v) calculate the valve command, u_{v}, by implementing closed loop hydraulic control (see Section 4.3.4), and (vi) update the states of the MIL controller and of the VS for computations in the next loop time.

Section 7.2 presents details of the shake-table instrumentation, wiring of various sensors with the controller hardware, and important control definitions in the RMCTools. Section 7.3 presents details of the MIL user programs. A step-by-step procedure for configuring the RMC75E hardware and software with the MIL test system is presented in Appendix B.

7.2 Configuring the RMC75E controller hardware with the MIL test system

7.2.1 Instrumentation of the shake table

The shake-table is instrumented with various sensors for the MIL experiments (see Figure 7.1) consisting of:

- A unidirectional accelerometer mounted on the side of the platform to measure table acceleration.
- A linear string potentiometer, with its body attached to base plate and magnet connected to one of the table posts, to measure table displacement.
- A ΔP cell to measure differential pressure in the actuator chambers.
- Two unidirectional load cells, denoted ALC1 and ALC2, installed at the ends of the actuator piston to measure force in the actuator.
- Four reaction load cells installed above the platform to measure reaction force feedback from the test article.

The calibration factors for the shake-table sensors are reported in Table 7.1. Some of these sensors are conditioned using external signal conditioners, as indicated in the table.

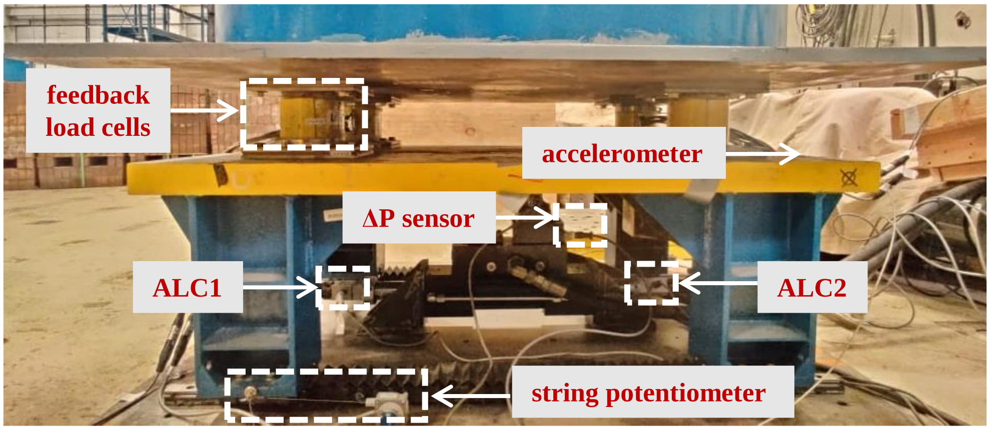

Figure 7.1. Instrumentation of the uniaxial shake table

Table 7.1. Calibration factors of the shake-table sensors

Sensor	Calibration		Signal Conditioner
	Scale	Offset	
Table accelerometer	0.6711 g/V	0.067 g	-
Linear string potentiometer	-1.25 in/V	+6 in	-
ΔP cell	-400 psi/V	0 psi	MTS 407
Actuator load cells (ALC1, ALC2)	-1000 lb/V	0 lb	MTS 407
Feedback reaction load cells	200 lb/V	0 lb	VC2124

7.2.2 Configuring RMC75E hardware modules

As described in Section 3.6.2, the RMC75E controller[23] is configured with a CPU module, an AA1 axis[24] module, four expansion modules (one of type AP2 and three of type A2), and a VC2124[25] unit. The

[23] The CPU module, the axis module, and the VC2124 constitute a complete motion controller setup referred to as the base module. Expansion modules are optional modules and are added to the right of the base module if the actuator control requires interfacing with more than one transducer input. The expansion modules are input-only modules, meaning they cannot control actuators.

[24] The AA1 axis module has a ±10 V output slot for closed-loop servo-control (i.e., issue valve command, u_v, by implementing hydraulic feedback loop) and an input slot for receiving the transducer feedback (herein string potentiometer measuring table displacement).

[25] The VC2124 inputs the valve command generated by the AA1 module and drives an appropriate current, u_i, through the servovalve coils.

controller hardware interfaces with the valve command, u_v, on the AA1 axis module and nine transducer inputs: one on the AA1 module, two on the AP2 module, and six on the three A2 modules combined, as shown in Figure 7.2. All input/outputs are ±10 V analog with 16-bit resolution (i.e., single precision arithmetic).

The analog output from the AA1 module is connected to the 'input' slot on the VC2124, whose 'output' is connected to the servovalve (see the solid green line in Figure 7.2). The table displacement, as measured by the string potentiometer, is connected to the 'input' slot on the AA1 module because the shake table is operated in closed-loop control with position feedback. The AP2 module is configured to interface with the actuator load cells, ALC1 and ALC2. The table accelerometer and the ΔP cell are connected to the input slots on the first A2 expansion module. The shear channels of the four reaction load cells are connected to the inputs slots on the last two A2 modules.

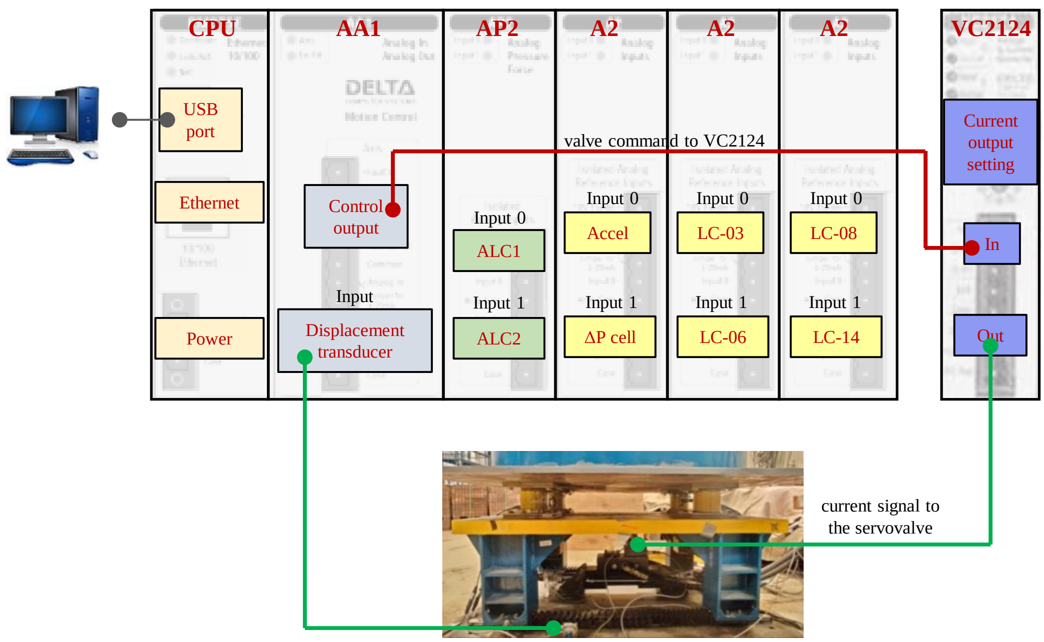

Figure 7.2. Configuring the RMC75E hardware with the uniaxial shake table

7.2.3 Creating axis definitions in the RMCTools

The RMCTools software is developed as an Integrated Development Environment (IDE) to provide an immediate overview of (and easy access to) all features of the RMC controllers. It allows the user to interact with the controller hardware, issue commands to the RMC, create user programs to perform complex arithmetic, troubleshoot errors, and visualize plots in real-time. The RMCTools is installed on a host computer, which communicates with the physical hardware via a USB cable connected between the CPU module (see Figure 7.2) and the host computer.

In the RMC framework, motion commands to the controller are issued by creating Axis definitions. An axis can be defined as either a *control axis*[26] or a *reference axis*[27]. The control axis includes information on the type of control loop (e.g., closed-loop/open-loop), feedback quantities used in hydraulic control (e.g., position/force/pressure), and the physical inputs/outputs on the controller hardware (e.g., AA1, A2) that are utilized by the axis. Figure 7.3 is snippet of the axis definition dialog for the current MIL setup in which one control axis (denoted Axis0) and three reference axes (denoted Axis1, Axis2, and Axis3) are defined. Individual axis definitions are presented in Figure 7.4.

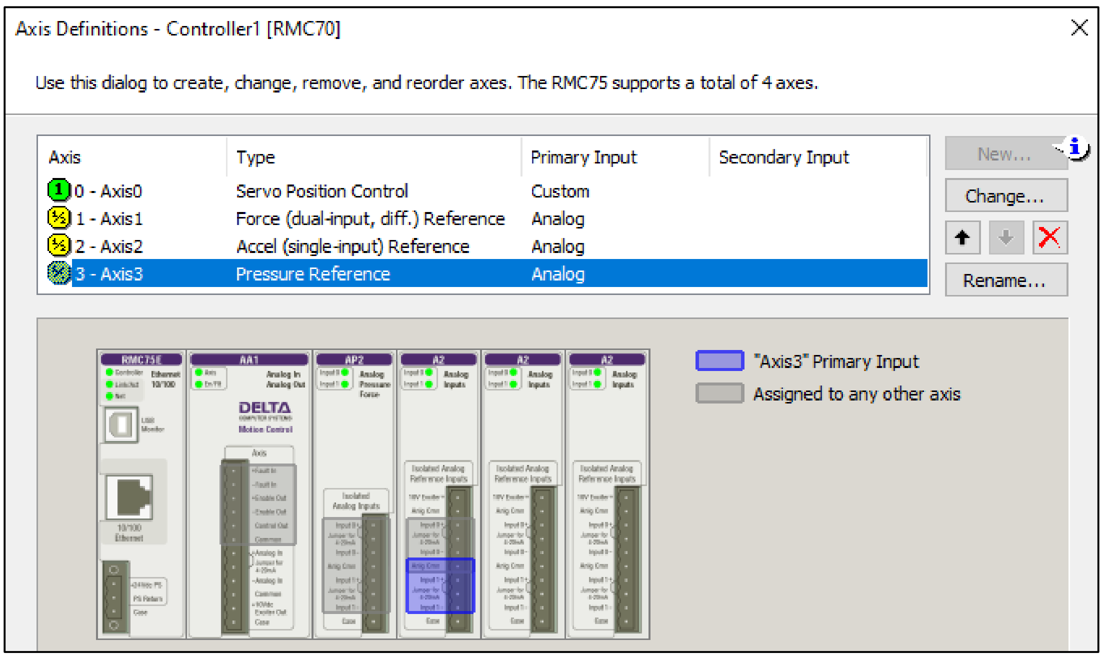

Figure 7.3. Axis definition dialog window in the RMCTools

---

[26] A control axis controls the servo-actuator system. It has one control output and can have zero, one, or two feedback inputs assigned to it, based on the control mode (e.g., zero indicates open-loop control, position control requires one feedback input, position-pressure control requires two feedback inputs). All control outputs and the corresponding feedback inputs used in the actuator hydraulic control must be assigned to the control axis. Motion commands can be issued only to control axes.

[27] Defining reference axis/axes is optional. A reference axis is assigned only a transducer input and has no control output, meaning it cannot control an actuator. The RMCTools enables advanced processing features (e.g., filtering, create halts, output scaling, and offset) on only those analog inputs which are assigned to either a control or a reference axis.

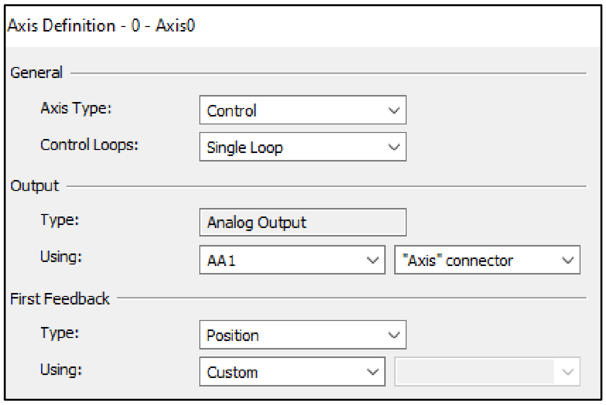

a) Axis0

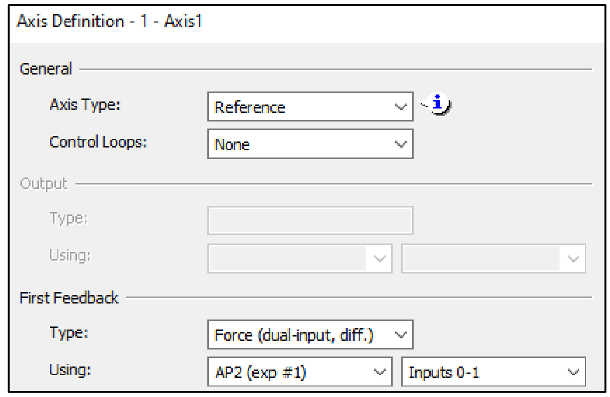

b) Axis1

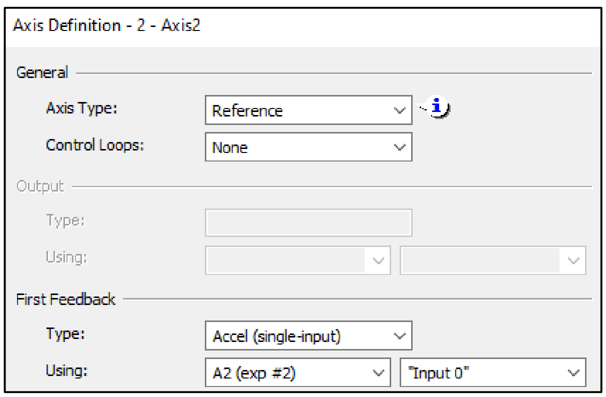

c) Axis2

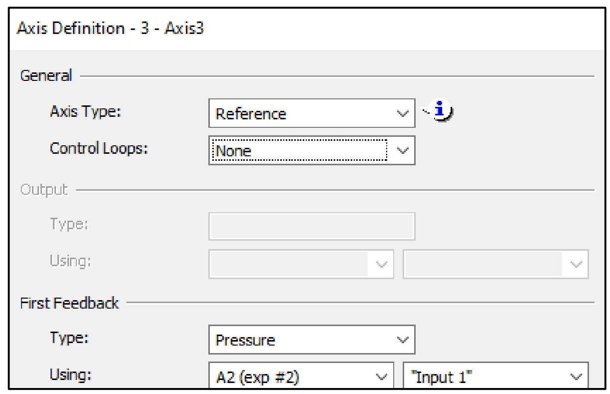

d) Axis3

Figure 7.4. Axis definitions in the RMCTools

The control axis definition informs the RMC on implementing the hydraulic control equation, namely, $u_v = K_e(u - x_{st}) - K_p(\Delta P)$. In Figure 7.4a, the control loop type is 'single', and the feedback type is selected 'position', consistent with the closed-loop position control of the shake table. The RMC controllers are structured to perform hydraulic control computations using only PID (proportional, derivative, and integral) terms. The ΔP feedback is incorporated indirectly by rewriting the hydraulic control equation as:

$$u_v = K_e\left(u - \underbrace{\left(x_{st} + K_p \Delta P / K_e\right)}_{custom\ feedback}\right)$$

The above equation appears as only proportional control with the term indicated as the *custom feedback* taken as the modified displacement feedback. This value is custom computed and written to the feedback register of the control axis. The above representation enables perform hydraulic control using the default PID settings of the RMC, whereas the effect of the ΔP feedback is indirectly accounted via the custom feedback option. Hence, the feedback input to Axis0 is defined as 'custom' in Figure 7.4b.

Axis1 through Axis3 are reference axes with no control output, meaning they cannot drive the servovalve. The feedback type for Axis1 is set to 'Force (dual-input)' and utilizes the physical inputs connected to the AP2 module. Axis2 and Axis3 are assigned a feedback type 'Accel (single input)' and 'Pressure (single input)', respectively, and read inputs connected to the first A2 expansion module. The analog inputs from the reaction load cells are not assigned any axis because the limit on the number of axes supported by RMC75E (=4) is exceeded.

7.3 User programs in the RMC75E

7.3.1 Introduction to user-programming

The RMCTools allows to create user programs and user functions for executing a sequence of commands and performing complex arithmetic. A typical user program constitutes *action* and *link* elements. The *actions* broadly include: (i) issuing *motion commands*, (ii) declaring *local variables*, and (iii) defining *expressions* for performing arithmetic. The *link* element informs the processor when to jump to a next step and which step to jump to. Each step in a user program must be executed within one loop time. A user program may contain many steps; each step can perform mathematical operations, issue motion commands, and is linked to another step or the program terminated. Figure 7.5 is a snippet of an example user program taken from the RMCTools manual (Delta, 2021b), which includes three steps, numbered as 0, 1, and 2.

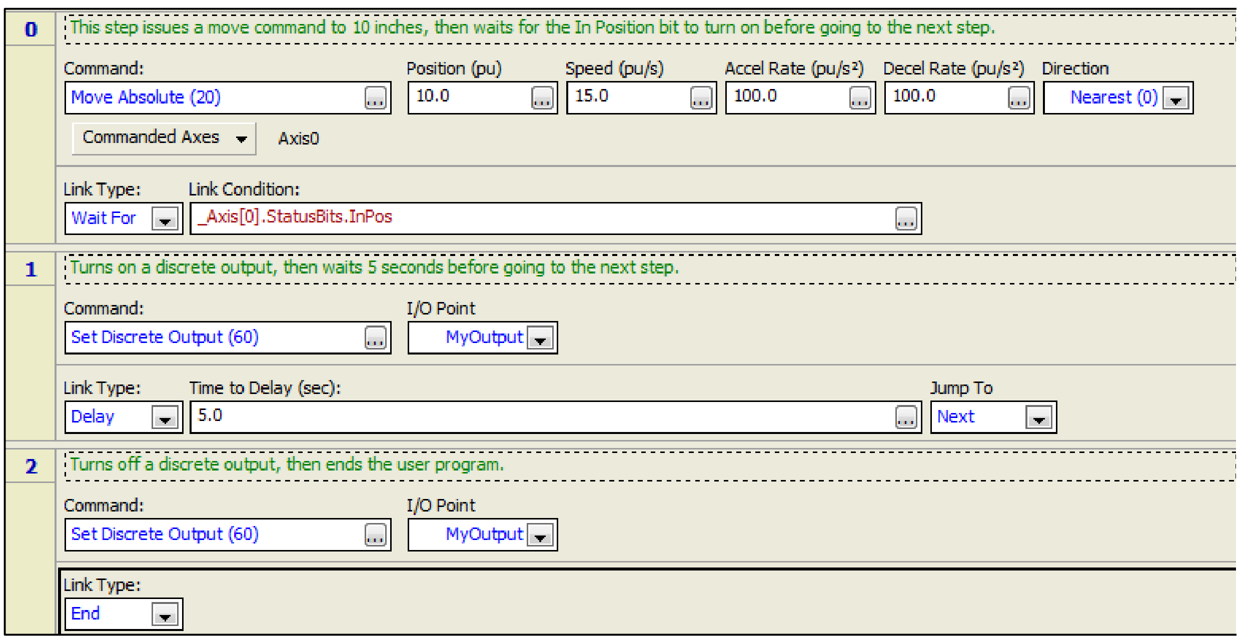

Figure 7.5. Example user program reproduced from the RMC manual (Delta, 2021b)

In Step 0, a motion command *Move Absolute (20)*' is issued to the control axis (i.e., Axis0) to move the actuator from its current position to 10 pu (position units), at the specified speed and the acceleration rate. The program waits for the actuator to move to the target position, as specified by the link condition, and then jumps to Step 1. This step turns on a discrete output, and then waits for five seconds before jumping to the next step. In Step 2, the discrete output is turned off and the program is terminated. This way, a user program efficiently executes a series of commands/operations/calculations in a sequential order.

The following subsections describes the user programs and user functions that were created to: (i) implement hydraulic control equation with custom feedback, (ii) execute the multisine experiments discussed in Section 4.5, (iii) execute the input-acceleration tracking experiments (i.e., $z_{vs} = a_g$, a special case of MIL), and (iv) execute the MIL experiments imitating different seismic isolation systems: spring-damper, lead-rubber, and Friction Pendulum.

7.3.2 User program implementing hydraulic control with custom feedback

Figure 7.6 is a snippet of the user program[28] that implements hydraulic control with position feedback manually computed as $x_{st} + K_p \Delta P / K_e$ (refer to the discussion below Figure 7.4). *Expression (113)* command in the RMCTools is used for calculating this custom position and the computed value is written to the feedback register of the control axis (Axis0), namely to, '_Axis[0].CustomCounts'. The user program includes only one step whose link type is set to repeat, implying that the program repeats through its code after every loop time.

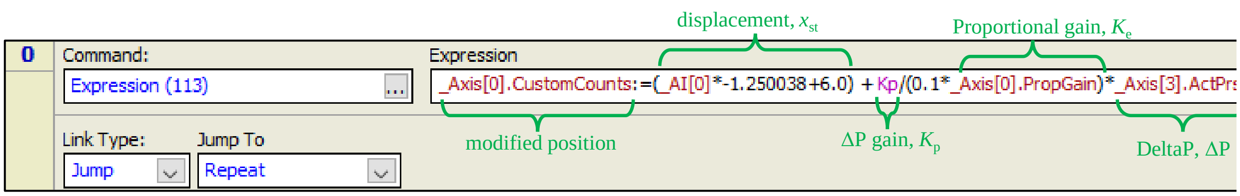

Figure 7.6. User program for implementing the hydraulic control loop in the RMCTools

In the above program:

- The ΔP measurement is accessed using the tag '_Axis[3].ActPrs' because the analog input from the ΔP cell is assigned to Axis3 (see Figure 7.4d). The ΔP gain, K_p, is defined as a variable.
- The table displacement, x_{st}, is accessed as '_AI[0]', which corresponds to the analog input connected to the AA1 axis module. Here, -1.250038 and 6 are the scale and offset factors, respectively, converting the displacement measurement of the potentiometer from volts to inches.
- The proportional gain, K_e, is accessed as '_Axis[0].PropGain'. The gain value in the controller tuning wizard is specified as a % of the maximum value of the valve command (10V). Hence, a factor of 0.1 is used to convert the % gain value to engineering units (V/in).

[28] Note that this user program must run continuously, which necessitates additional settings as defined here.

7.3.3 User program for the multisine experiments

Figure 7.7 is a snippet of the user program created for executing the frequency-response experiments described in Section 4.5. The control input, u, in these experiments is set to the multisine time series of Figure 4.12a, which is uploaded as a data curve (ID 1) in the RMCTools. The user program has two steps. In Step 0, the actuator is moved to its mid-stroke position and the program executor jumps to the next step. In Step 1, the motion command 'Curve Start Advanced (88)', is issued to the control axis (Axis 0) commanding the actuator to track the curve-time profile (multisine time series) per the curve ID I.

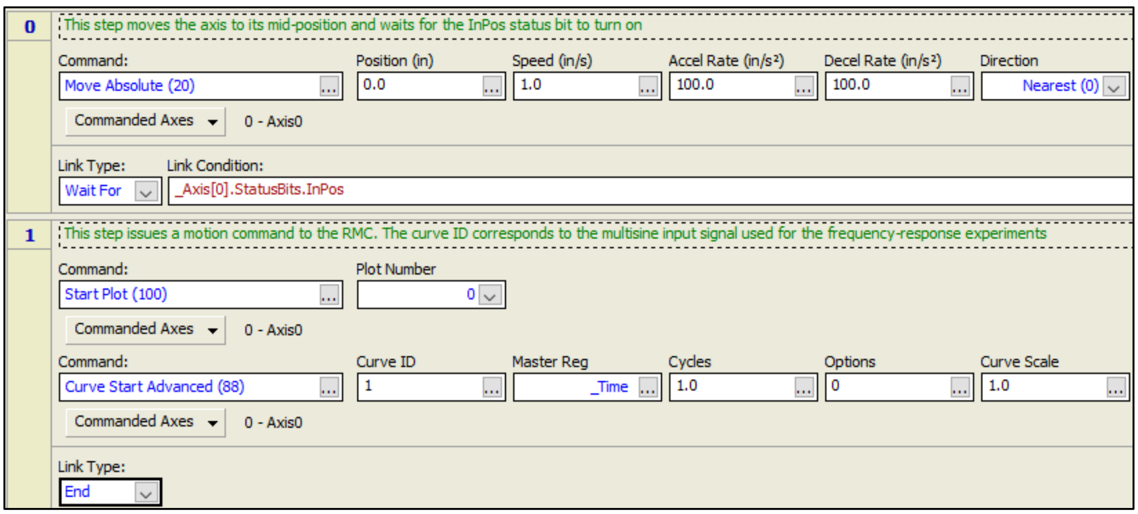

Figure 7.7. User program executing the frequency-response experiments of Section 4.5

7.3.4 User program for the acceleration-tracking experiments

Figure 7.8 is a snippet of the user program created for executing the input acceleration-tracking experiments. These experiments are special cases of MIL for which $z_{vs} = a_g$, that is, the shake table is controlled to track a prescribed acceleration history, a_g, as-is, at the base of the test article. The user program includes two steps. The program variables are initialized in Step 0, hence it is executed only once and jumps to the next step. Step 1, the core of the user program, is parsed into three blocks.

The first block of the code, enclosed within the dashed brown rectangle, reads the inputs a_g and w. Here, the acceleration time series, a_g, sampled at τ_s, is uploaded to the RMC curve tool and assigned a curve ID = 2. At each time step, the code reads the corresponding value of a_g from this curve ID. The reaction force, w, is calculated as the sum of the load cell measurements, accessed herein using the tags '_AI[5] through _AI[8]'. A conversion factor of '200' is used to convert the force measurement from volts to lbs.

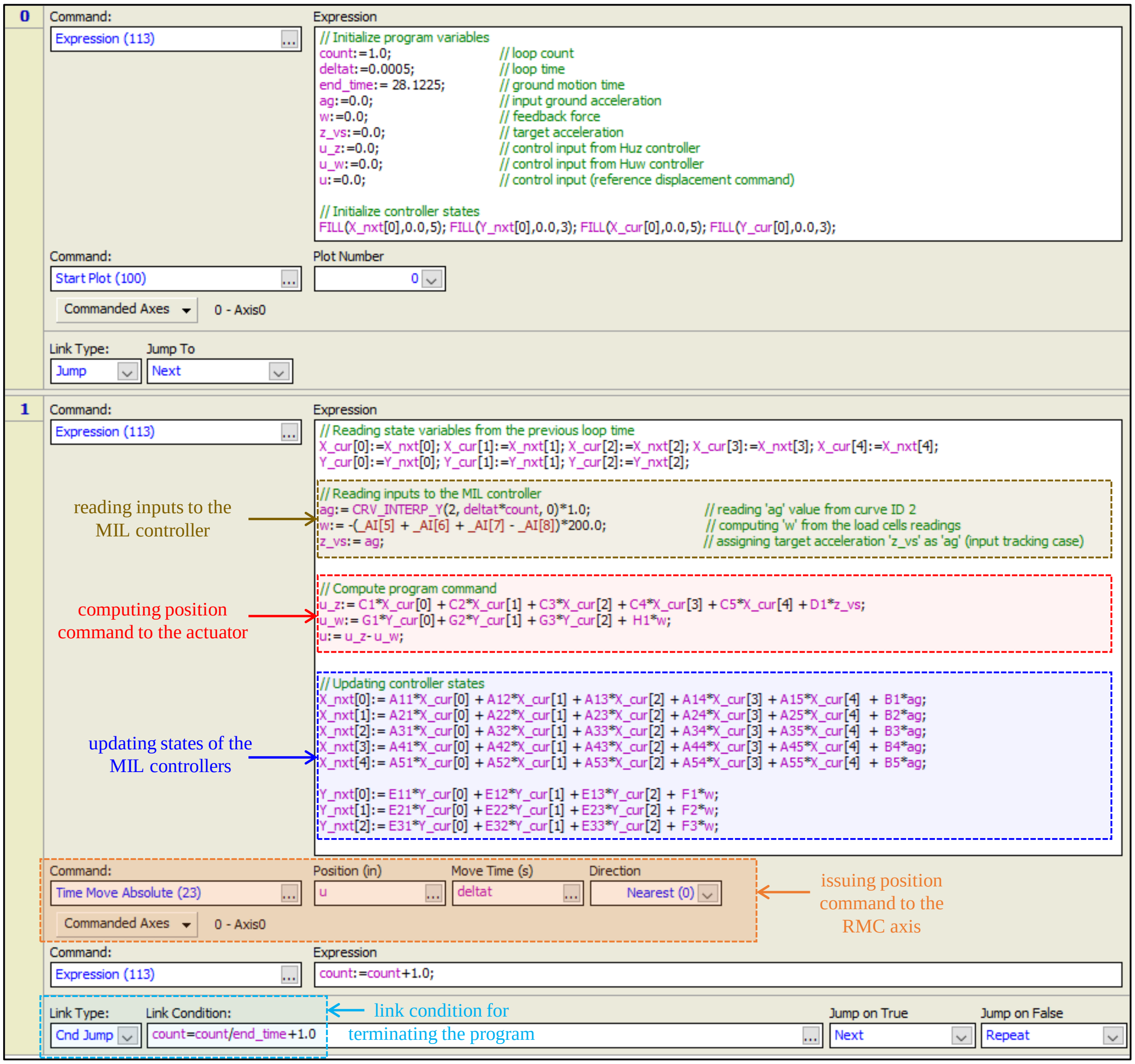

Figure 7.8. User program for executing the input-acceleration tracking experiments

- The second block of the code, enclosed within the dashed red rectangle, computes the position command to the actuator, $u = u_z - u_w$, from the state-space implementation of the MIL controllers. The variables 'X_cur' and 'Y_cur' denotes states of the approximated MIL controllers, 'H_uz' and 'H_uw', respectively, for the current loop time. The alpha-numeric coefficients, A11 through E33, are the entries of the state-space matrices of the MIL controller, obtained as described in Section 6.5.

- The third block of the code, enclosed within the dashed blue rectangle, updates the state variables of the MIL controller ('H_uz' and 'H_uw' has five and three states, respectively). The updated states are saved to the variables 'X_nxt' and 'Y_nxt' for computations in the next loop time.

After executing the three blocks in Step 1, a pre-programmed RMC motion command '*Time Move Absolute*' is issued to the control axis with the target position specified as u (computed in the red block) and a move time equal to the controller loop time, herein 0.0005 sec. The link type for this step is specified as *Cnd Jump*, meaning the program jumps to the next step only if the link condition is satisfied. In summary, the RMC performs the following operations in one loop time:

1. The user program implementing the hydraulic control (Figure 7.6) computes the custom position feedback based on the x_{st} and ΔP measurements.
2. Step 1 of the user program of Figure 7.8 computes the target position, u, and issues a motion command to the control axis.
3. The control axis (Axis 0) calculates the required valve command, u_{v}, based on u and modified position feedback, and the value is passed to the analog output of the AA1 module.
4. The VC2124 inputs u_{v}, and drives an equivalent current, $u_{\mathrm{i}} = K_{\mathrm{v}} u_{\mathrm{v}}$, through the servovalve coils.
5. The servovalve responds to the input current signal, the resulting hydraulic flow to the actuator chambers drives the shake table platform.
6. The table responses, x_{st} and ΔP, are measured by the respective sensors, input to the controller hardware, and saved in the RMCTools for computations in the next loop time.

7.3.5 User programs for the MIL experiments imitating seismic isolation systems

Figure 7.9 presents the MIL user program for imitating spring-damper virtual systems. The structure of this user program is similar to that of Figure 7.8 with additional blocks of code added to Steps 0 and 1.

The added block of code to Step 0, enclosed within the dashed sea-blue rectangle, defines the properties (mass, stiffness, and damping coefficient) of the spring-damper system to be imitated in the MIL experiments.

The added block of code to Step 1, enclosed within the dashed green rectangle, calculates the target basemat acceleration, z_{vs}, by numerically integrating the VS differential equations. An explicit time-integration scheme based on the third-order Runge-Kutta method is employed herein to obtain the VS states, 's1' and 's2', and subsequently to calculate 'z_vs'. Figures 7-10 and 7-11 present the MIL user programs for simulating LR and FP virtual systems. The Runge-Kutta blocks (dashed green rectangles) in Figures 7-9, 7-10, and 7-11 calls for various user functions, whose definitions are declared in Figure 7-12.

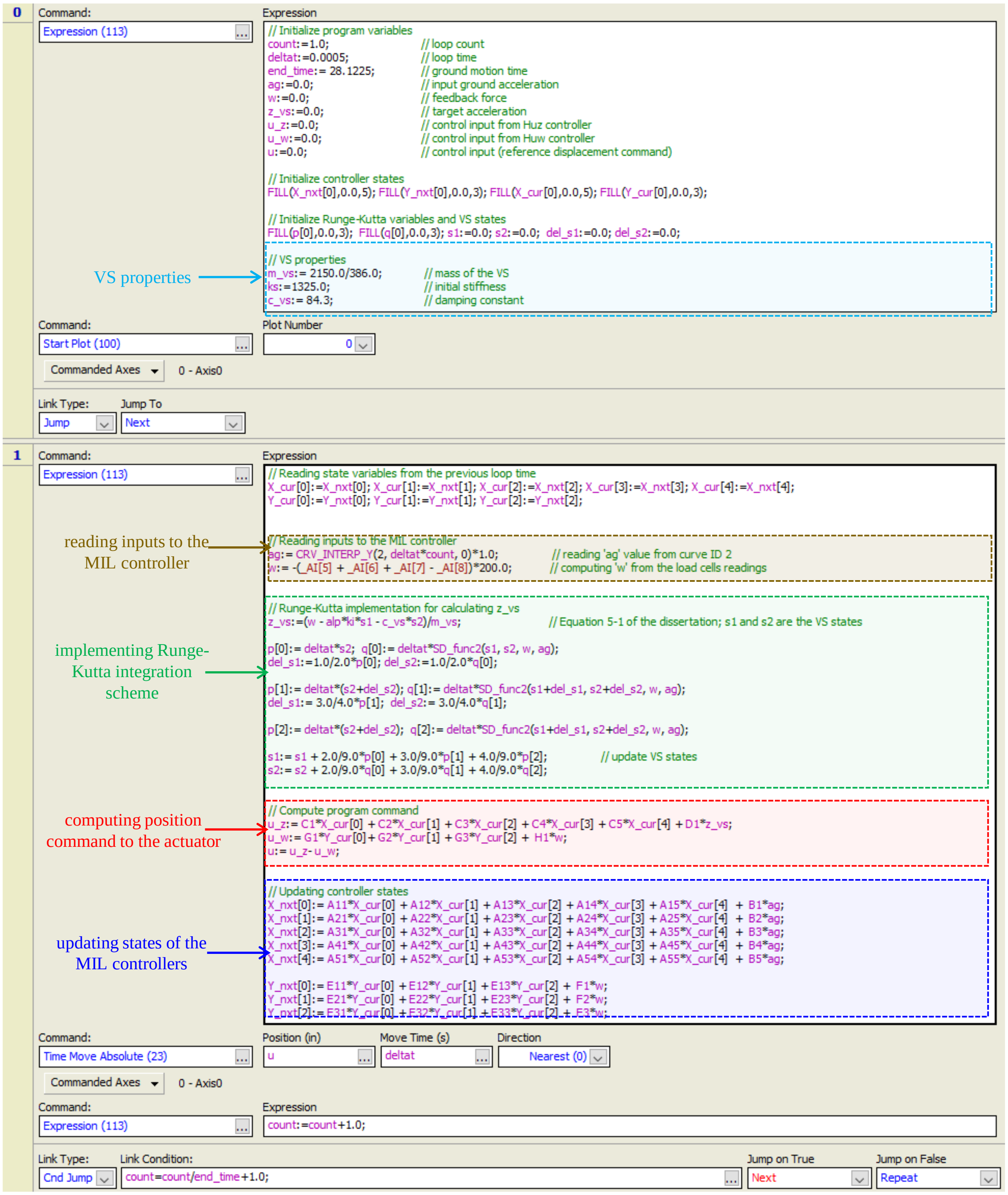

Figure 7.9. User program for executing the MIL experiments for the spring-damper virtual system

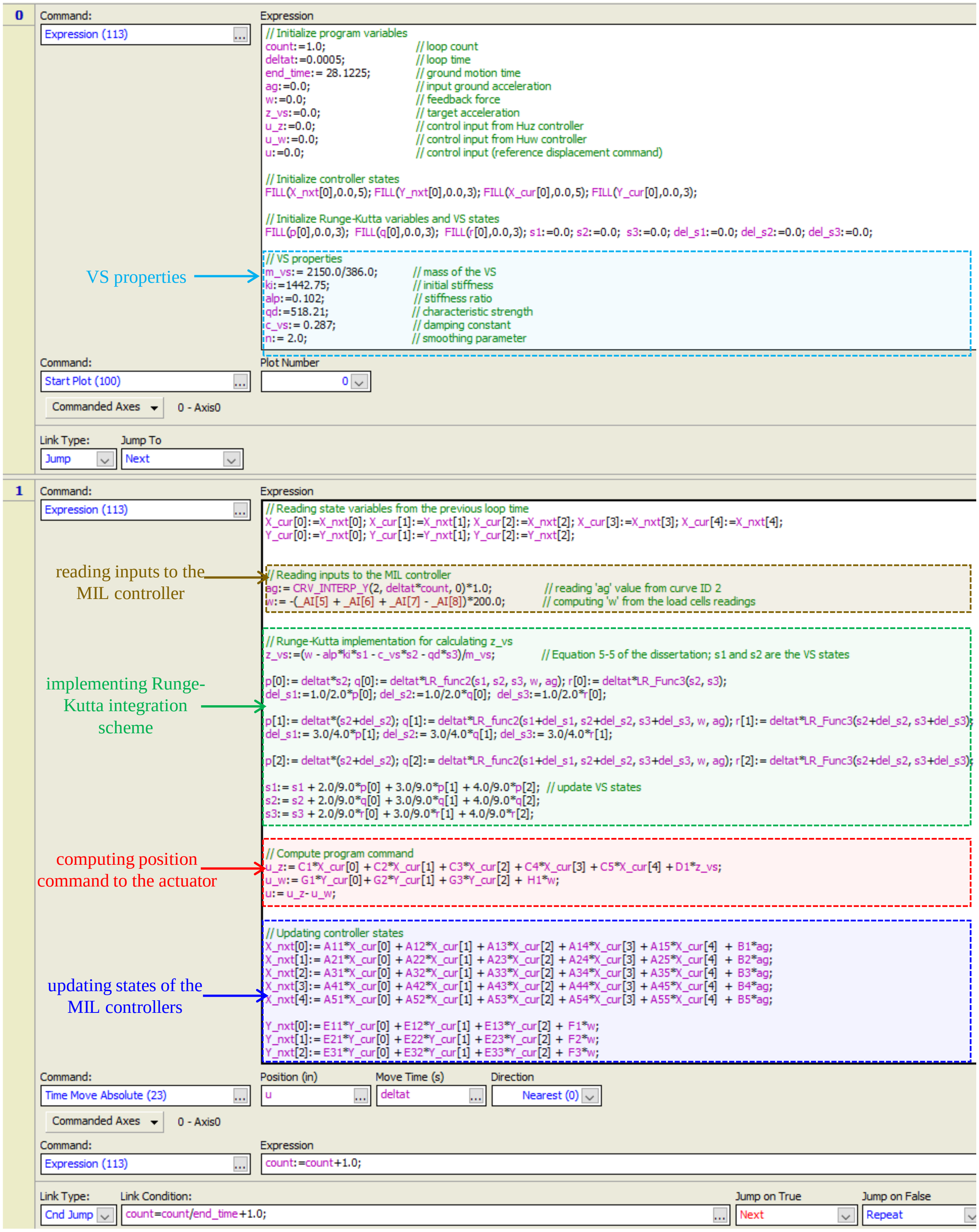

Figure 7.10. User program for executing the MIL experiments for the lead-rubber virtual system

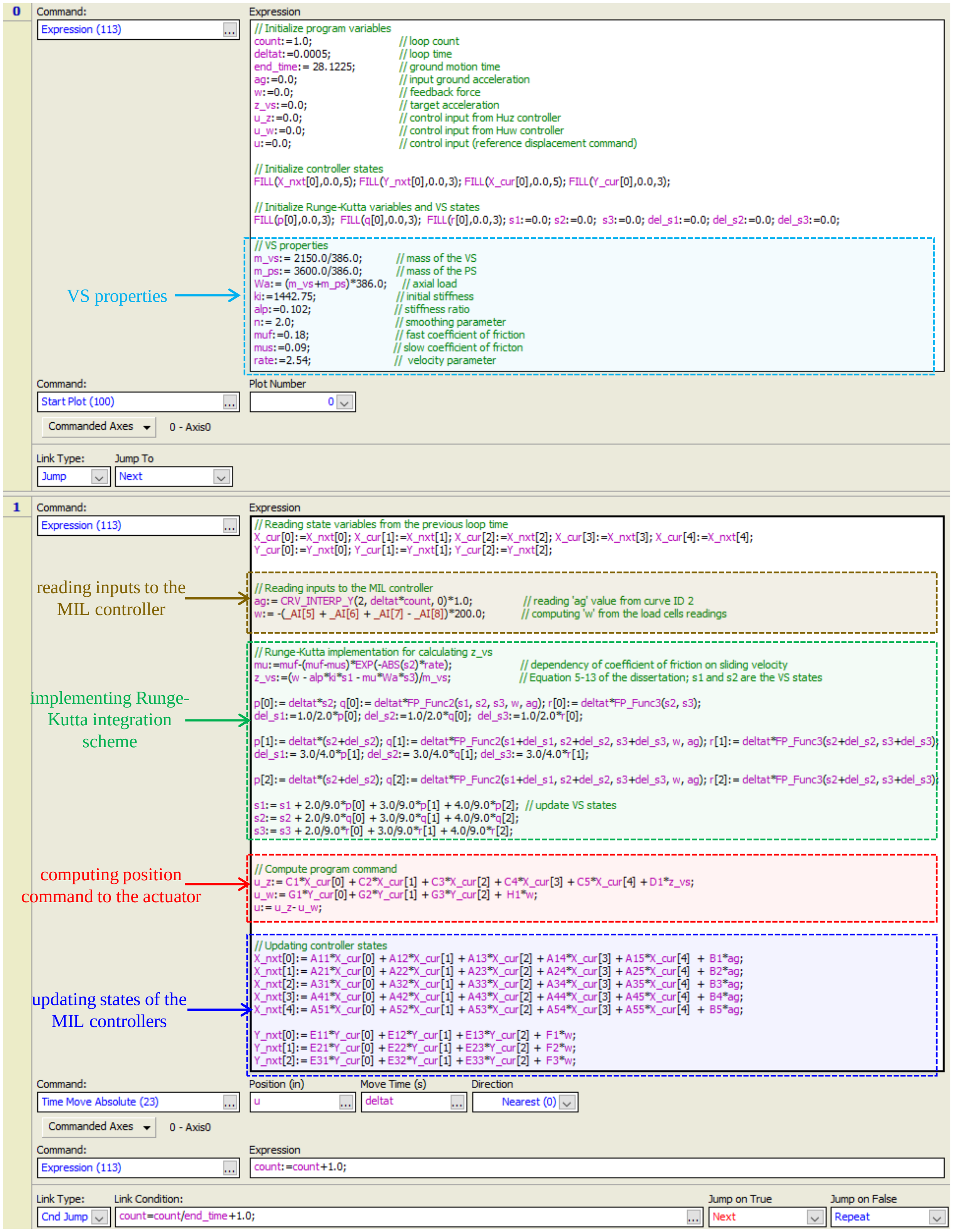

Figure 7.11. User program for executing the MIL experiments for the Friction Pendulum virtual system

The main differences between the user programs of Figures 7-9, 7-10, 7-11, and 7-12 are the VS property definition block in Step 0, and the Runge-Kutta implementation block in Step 1, which are specific to the type and dynamics of the virtual system that needs to be imitated. The blocks of code that implement the MIL controllers (dashed blue, brown, and red rectangles) are identical in all four user programs because the state-space coefficients of the MIL controller depend only on the shake-table dynamics (see Equation 6-7), thereby largely standardizing the process of implementing MIL, and addressing Contribution #8 listed in Section 1.5. These user programs enable performing MIL experiments for a diverse family of virtual systems by simply changing the parameters of the two VS-specific blocks

```
FUNCTION SD_func2 : REAL

  VAR_INPUT
    s1 : REAL;
    s2 : REAL;
    w: REAL;
    ag: REAL;
  END_VAR

  SD_func2 := (w - alp*ki*s1 - c_vs*s2)/m_vs - ag;

END_FUNCTION
```

a) function ‘SD_Func2’

```
FUNCTION LR_Func2 : REAL

  VAR_INPUT
    s1 : REAL;
    s2 : REAL;
    s3 : REAL;
    w: REAL;
    ag: REAL;
  END_VAR

  LR_Func2 := (w - alp*ki*s1 - c_vs*s2 - qd*s3)/m_vs - ag;

END_FUNCTION
```

b) function ‘LR_func2’

```
FUNCTION LR_Func3 : REAL

  VAR_INPUT
    s2 : REAL;
    s3 : REAL;
  END_VAR

  LR_Func3 := ki*(1.0-alp)/qd*(1.0-(s3**2.0)*0.5*(1.0+SIGNUM(s2*s3)))*s2;

END_FUNCTION
```

c) function ‘LR_func3’

```
FUNCTION FP_Func2 : REAL

  VAR_INPUT
    s1 : REAL;
    s2 : REAL;
    s3 : REAL;
    w: REAL;
    ag: REAL;
  END_VAR

  FP_Func2 := (w - alp*ki*s1 - mu*Wa*s3)/m_vs - ag;

END_FUNCTION
```

d) function ‘FP_func2’

```
FUNCTION FP_Func3 : REAL

  VAR_INPUT
    s2 : REAL;
    s3 : REAL;
  END_VAR

  FP_Func3 := ki*(1.0-alp)/qd*(1.0-(s3**2.0)*0.5*(1.0+SIGNUM(s2*s3)))*s2;

END_FUNCTION
```

e) function ‘FP_Func3’

Figure 7.12. User functions used in the MIL programs

SECTION 8
VALIDATION OF THE MIL CONTROLLER FOR INPUT ACCELERATION-TRACKING EXPERIMENTS

8.1 Section prologue

In the input acceleration-tracking experiments, the shake table is controlled to impose a prescribed acceleration history, a_g, at the base of the test article. This can be viewed as a special case of MIL with a zero-impedance (or infinite stiffness) virtual system, represented as $H_{za_g}^{vs} = 1$ and $H_{zw}^{vs} = 0$. The shake-table controller assumes the form: $u = H_{a_g}^{filter}\left(H_{zu}^{st}\right)^{-1} a_g - H_w^{filter} H_{zw}^{st}\left(H_{zu}^{st}\right)^{-1} w$, where $u_{a_g} = H_{a_g}^{filter}\left(H_{zu}^{st}\right)^{-1} a_g$ is the control input required to drive the bare shake table (without the test article) with an acceleration a_g, and $u_w = H_w^{filter} H_{zw}^{st}\left(H_{zu}^{st}\right)^{-1} w$ compensates for the table-structure interaction and ensures tracking a_g. The heavier the test article relative to the shake-table mass, the greater the interaction, and the greater the required compensation u_w. This way, the techniques of the impedance-matching approach can be applied for controlling shake tables for testing structural systems for the effects of earthquake shaking.

Section 8.2 presents the ground motions used in the experiments. Section 8.3 presents tests results for a diverse combination of water depths in the vessel, input ground motions, and control parameters of the table (e.g., ΔP gain, filter cutoff frequency) to support the hypotheses: (i) a sufficiently large value of ΔP gain is effective for shake-table control, and by extension for input acceleration-tracking, and (ii) the choice of filter cutoff frequency is a tradeoff between performance and stability.

8.2 Input acceleration motions

Table 8.1 presents information on the acceleration motions used in the experiments. Three earthquake records with Record Sequence Numbers (RSN) 6, 864, and 2632 are selected from the PEER strong ground motion (NGA-West) database with peak ground acceleration (PGA) in the range of 0.15 g and 0.3 g. The seed motions are time-scaled by a factor of 2, and are amplitude-scaled per Table 8.1 to represent input motions with different peak amplitudes and with spectral content distributed over a broad frequency range. (Time-scaling is performed to prevent the shake-table displacement from exceeding its maximum stroke of ±3 inches when applying acceleration histories with PGAs > 0.4 g). Figure 8.1 presents 5% damped acceleration response spectra of the time- and amplitude-scaled motions. The peak accelerations (i.e., zero-period spectral accelerations) of the scaled motions are: 0.8 g for GM_1, 0.6 g for GM_2, and 0.4 g for GM_3.

Table 8.1. Input acceleration motions for the experiments

Motion	Earthquake	PGA	
		Original	Scaled
GM_1	Imperial Valley – 02, 1940, NS component (RSN 6)	0.28 g	0.8 g
GM_2	Chalfant Valley -06, 1986, NS component (RSN 864)	0.27 g	0.6 g
GM_3	Chi-Chi, 1999, NS component (RSN 2632)	0.14 g	0.4 g

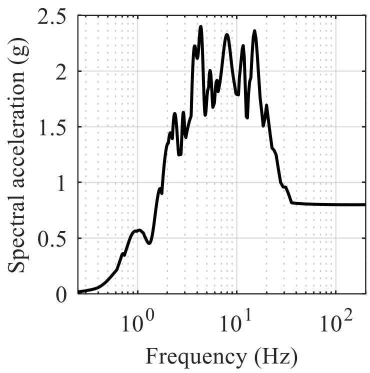

a) GM_1

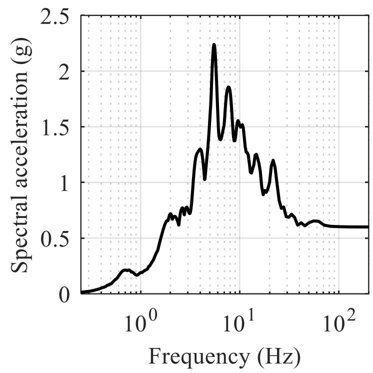

b) GM_2

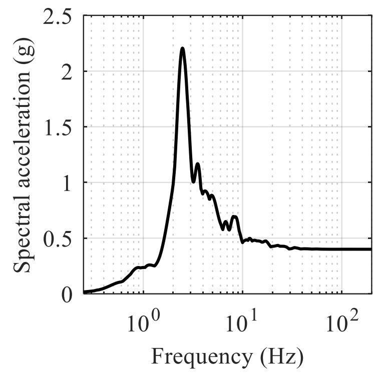

c) GM_3

Figure 8.1. 5%-damped acceleration response spectra of the input ground motions

Experiments are performed for different water depths, d_w, in the vessel: 0 (empty tank), 18, 30, and 42 inches. The mass of the empty vessel including the tank, base plate, flange, and head is approximately 1200 lb. For different water depths, [the weight of the test article; corresponding mass ratio, m_{ratio}, (i.e., ratio of mass of the test article to the mass of the shake table)] are: 0 inches [1200 lb; 0.75]; 18 inches [2370 lb; 1.5]; 30 inches [3200 lb; 2]; and 42 inches [3980 lb; 2.5].

8.3 Results of input acceleration-tracking experiments

8.3.1 Test results for different water depths

Figures 8-2 through 8-4 present acceleration-tracking results for the empty vessel ($d_w = 0$; mass ratio of 0.75) for GM_1, GM_2, and GM_3, respectively. Experiments are performed for the control parameters: $K_e = 5$ V/in, $K_p = 0.001$ V/psi, $\tau_s = 500$ μs [2000 Hz], and $f_c = 80$ Hz. Panels a), b), and c) of the figures present the displacement, velocity, and acceleration histories, respectively, and panel d) presents the 5%-damped acceleration response spectra. The solid blue lines are the measured shake-table responses and the dashed red lines are the target histories of the input motion. Results show that the shake table is able to track the input motions accurately across all frequencies, barring the small deviation above 20 Hz in Figure 8.4d.

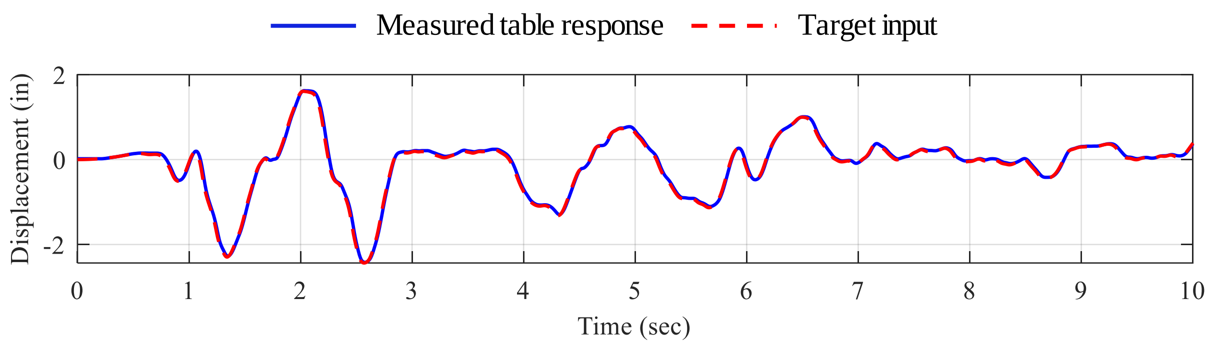

a) displacement history

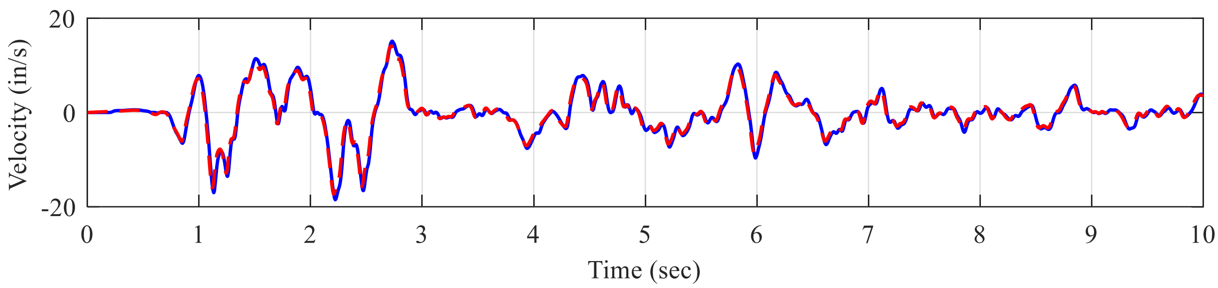

b) velocity history

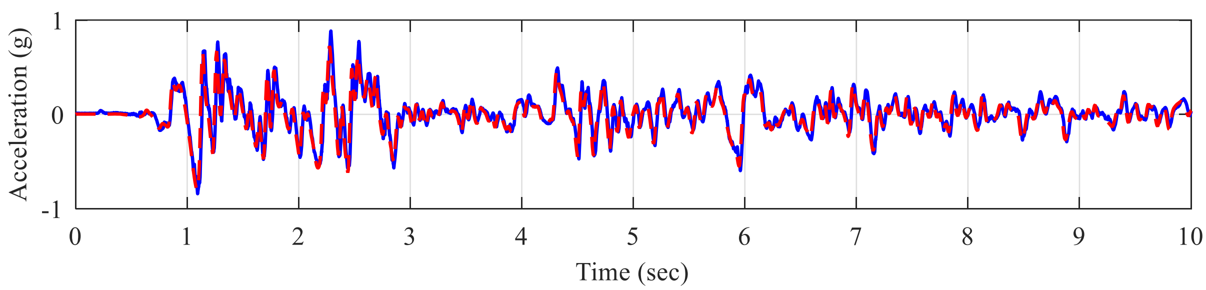

c) acceleration history

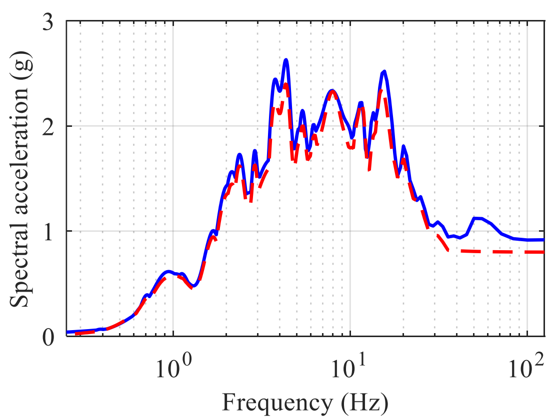

d) acceleration response spectra

Figure 8.2. Results of acceleration-tracking experiments, GM_1, empty vessel ($m_{ratio} = 0.75$), $K_e = 5$ V/in, $K_p = 0.001$ V/psi, $f_c = 80$ Hz, $\tau_s = 500$ μs [2000 Hz]

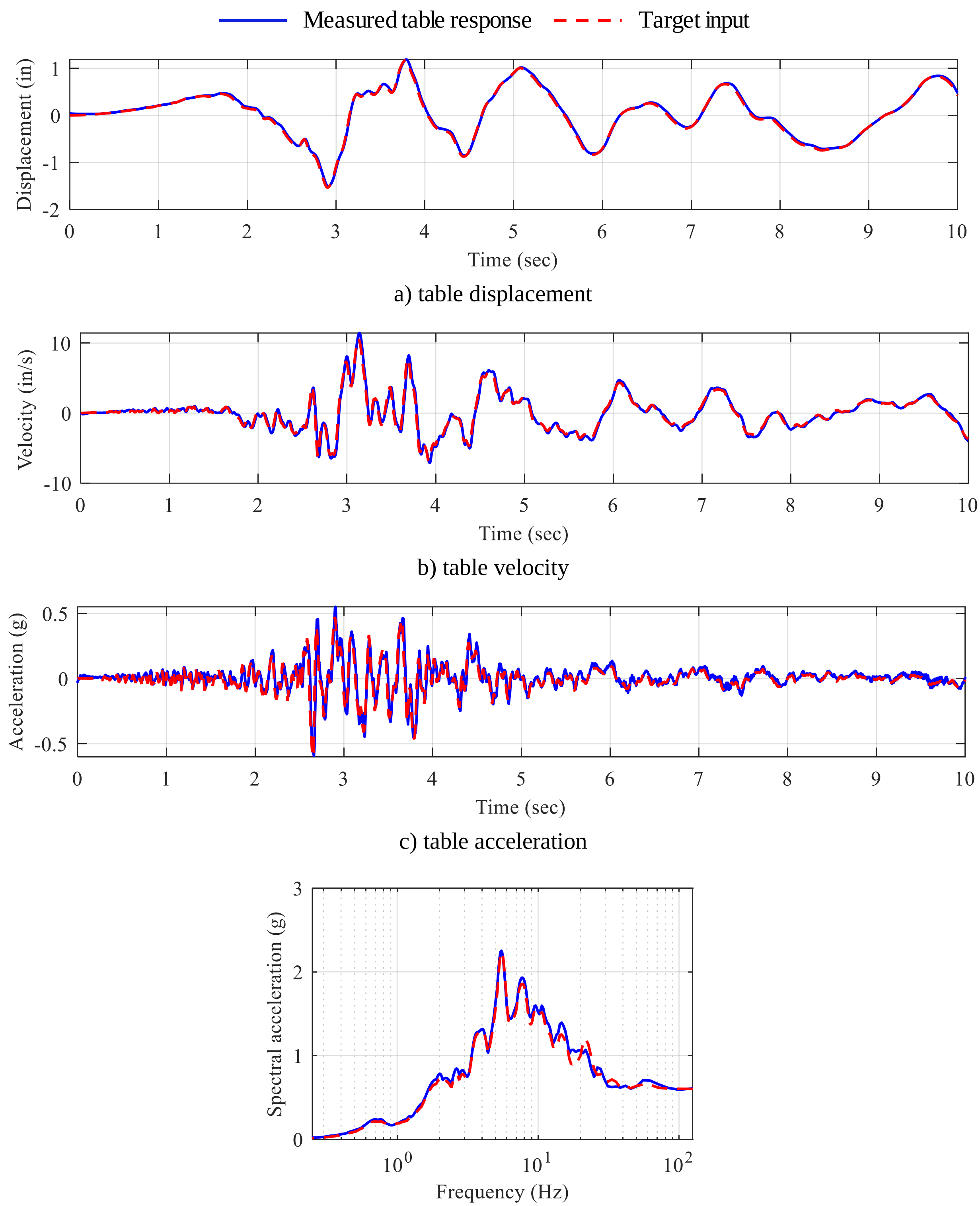

a) table displacement

b) table velocity

c) table acceleration

d) table acceleration response spectra

Figure 8.3. Results of acceleration-tracking experiments, GM_2, empty vessel (m_{ratio} = 0.75), K_e = 5 V/in, K_p = 0.001 V/psi, f_c = 80 Hz, τ_s = 500 μs [2000 Hz]

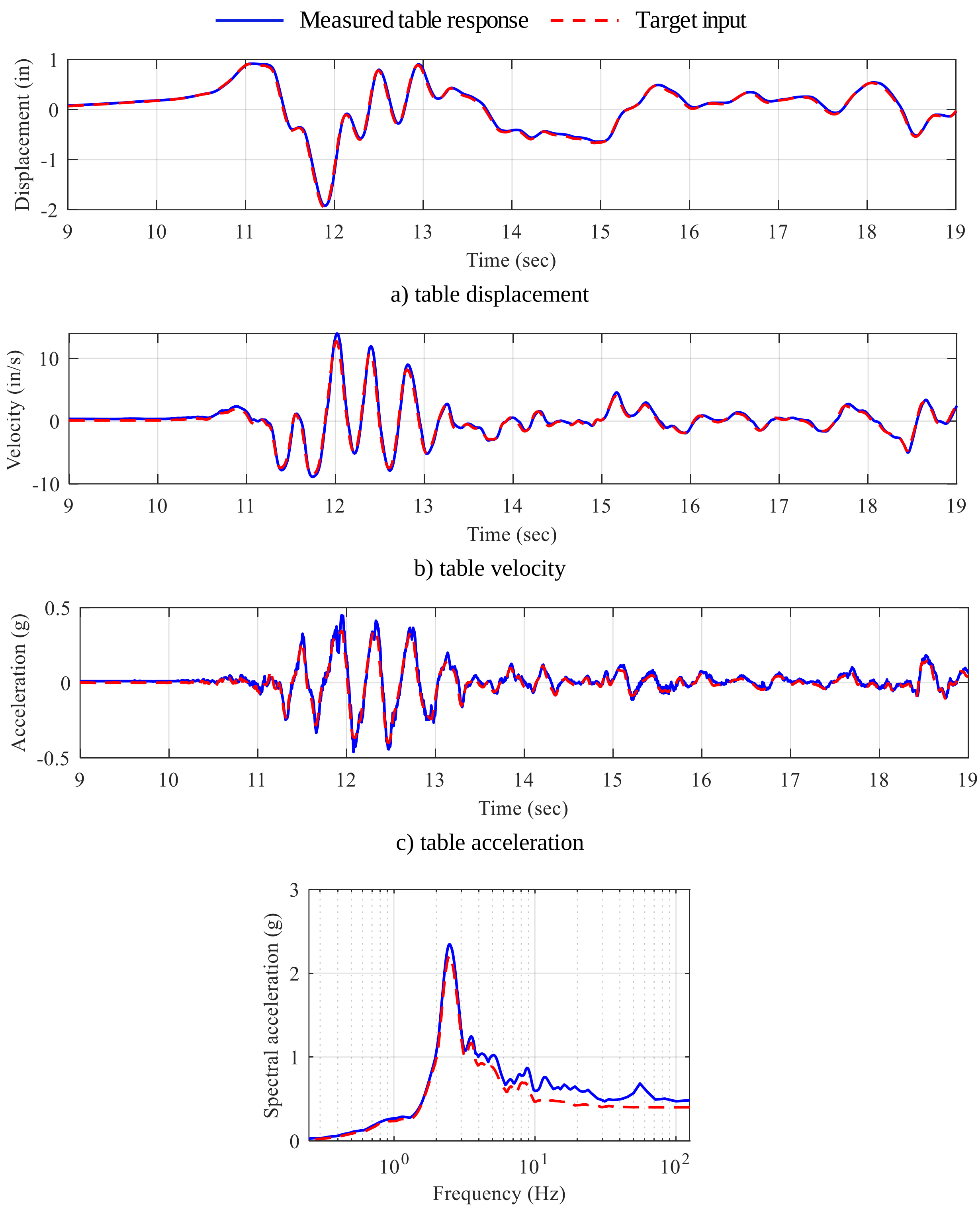

Figure 8.4. Results of acceleration-tracking experiments, GM_3, empty vessel (m_{ratio} = 0.75), K_e = 5 V/in, K_p = 0.001 V/psi, f_c = 80 Hz, τ_s = 500 μs [2000 Hz]

Figure 8.5 presents test results (acceleration response spectra only) for increasing water depths in the vessel: 18, 30, and 42 inches (i.e., mass ratios of 1.5, 2, and 2.5). As seen in the figures, the measured (blue) and the target (red) acceleration spectra are in close agreement for mass ratios up to 2 with slightly reduced accuracy for higher mass ratios (> 2.5). This is because as the water depth in the vessel increases, the feedback force from the test article, w, is larger, and the compensation term, $u_{\mathrm{w},}$ becomes comparable with u_{a_g}, indicating significant table-structure interaction (see the time series plots presented in Figure 8.6). For smaller mass ratios (= 0.75), the term u_{w} is small and hence the effect of model inaccuracies (H_{zw}^{st}), controller approximations (H_{w}^{filter}), and fidelity of the feedback-measuring load cells on the tracking performance is minimal. However, as the feedback force increases, the effects of these discrepancies become dominant, resulting in inaccurate (or less accurate) computation of u_w, and consequently reducing the tracking performance for test cases with large mass ratio (see panels c), f), and i) of Figure 8.5). Therefore, high-fidelity load cells for measuring w and accurate characterization of H_{zw}^{st} is critical to the shake-table controller, and this is even more so if the mass of the test article is comparable to (or higher than) the shake-table mass[29].

> The results presented in Figures 8-2 through 8-6 show that the shake-table controller (modified form of the impedance-matching MIL controller) is effective for acceleration-tracking even for test articles that are thrice heavier than the shake table: an outcome difficult to achieve using the way most commercial shake tables are controlled, addressing Contribution #7 listed in Section 1.3.6. The key features of the current approach are: (i) the shake-table is controlled independent of knowledge of dynamics of the test article, (ii) the controller is standardized meaning that there is no need for motion-specific or test article-specific tuning of the shake table, and (ii) table-structure interaction is explicitly compensated by measuring the feedback force and accordingly compensating the control input though the term u_w, thus eliminating the need for adaptive compensation techniques, which are time-consuming and laborious.

[29] Experiments for mass ratios greater than 2.5 were not performed due to the limitations of the test system (e.g., the actuator force capacity, water depth in the vessel). However, a mass ratio of 2+ is not common in shake-table testing.

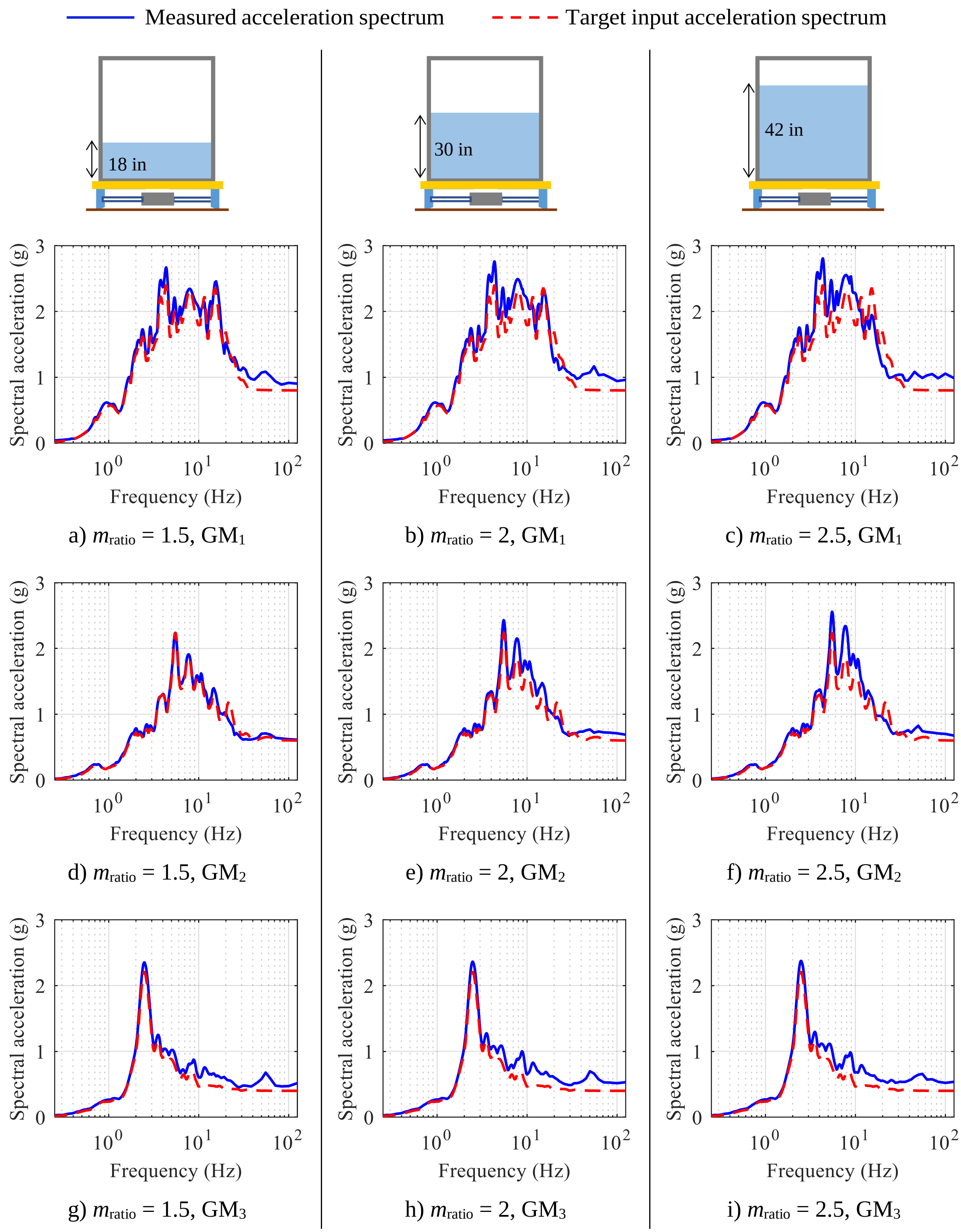

Figure 8.5. Results of acceleration-tracking experiments, different water depths and input motions, K_e = 5 V/in, K_p = 0.001 V/psi, f_c = 80 Hz, τ_s = 500 μs [2000 Hz]

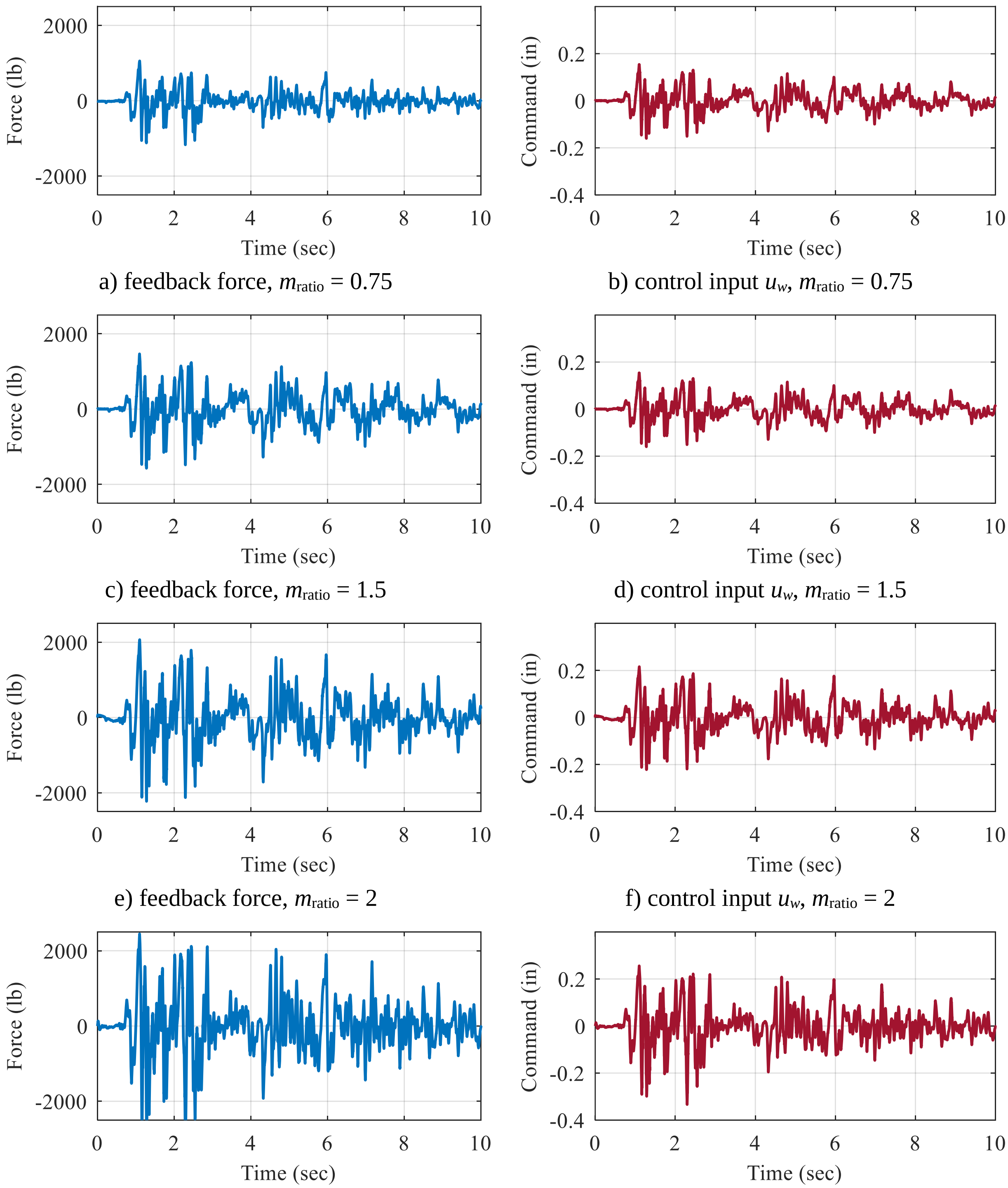

a) feedback force, m_{ratio} = 0.75 b) control input u_w, m_{ratio} = 0.75

c) feedback force, m_{ratio} = 1.5 d) control input u_w, m_{ratio} = 1.5

e) feedback force, m_{ratio} = 2 f) control input u_w, m_{ratio} = 2

g) feedback force, m_{ratio} = 2.5 h) control input u_w, m_{ratio} = 2.5

Figure 8.6. Measured feedback force and the corresponding control input different water depths, GM_1, K_e = 5 V/in, K_p = 0.001 V/psi, f_c = 80 Hz, τ_s = 500 μs [2000 Hz]

8.3.2 Effect of different sources of feedback measurement

In the experiments thus far, the shake-table controller utilized the feedback force measurement from the reaction load cells, $w_{\mathrm{LC},}$ for computing u_{w}. Alternately, it can be calculated from force equilibrium of the shake table as the table inertia minus the actuator force: $w_{\mathrm{FE}} = m_{\mathrm{st}} z_{\mathrm{st}} - A_{\mathrm{p}} \Delta P,$ which is valid if the frictional forces in the shake table are negligible compared to the actuator force. This alternate way of computing w is attractive because it eliminates the need for the reaction load cells for shake-table control. The fidelity of w_{FE} is first examined using the measured frequency response of the combined table and the vessel system subjected to a multisine control input. Figure 8.7 presents the measured frequency response functions (FRFs) of the feedback force computed from the force equilibrium, w_{FE}, represented by the solid blue line, and of that directly measured by the reaction load cells, w_{LC}, represented by the dashed red line. The magnitudes of the two FRFs deviate in the frequency range between 5 and 20 Hz (see the dashed green rectangle in Figure 8.7).

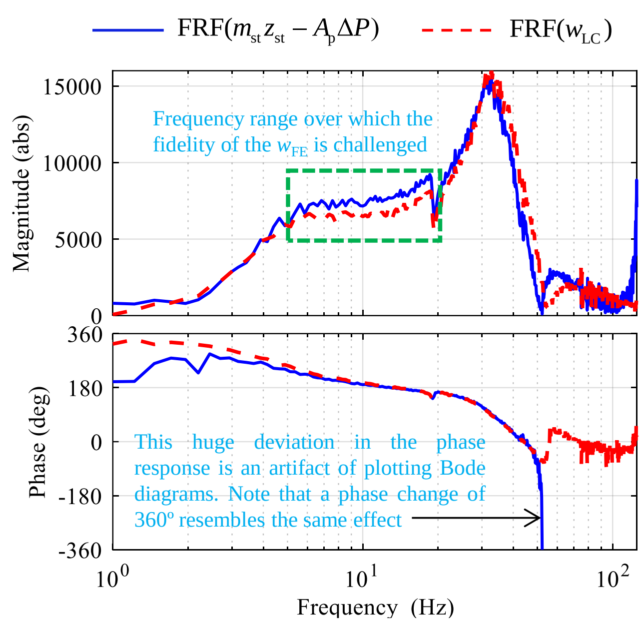

Figure 8.7. Frequency response measurements of the combined table and the vessel system, d_{w} = 36 inches, K_{e} = 5 V/in, K_{p} = 0.001 V/psi, and τ_{s} = 500 μs [2000 Hz]

Figure 8.8 illustrate the effect of different feedback measurement considerations on the tracking performance for the empty vessel configuration. Each figure consists of nine panels. The panels in the first and second columns utilized w_{LC} and w_{FE} for calculations, respectively. Test cases in the third column includes only $u_{a_{\mathrm{g}}}$ and the control term compensating for the table-structure interaction is ignored ($u_w = 0$). Figure 8.9 presents similar set of results for test cases with a water depth of 42 inches (m_{ratio} = 2.5).

It is seen that the use of both w_{LC} and w_{FE} resulted in acceptable tracking performance for smaller mass ratios, thus eliminating the need for installation of the reaction load cells for measuring w. However, as the test article becomes heavier (e.g., $m_{\mathrm{ratio}} = 2.5$), the use of w_{FE} resulted in inaccurate tracking of the input in the frequency range of 5 to 20 Hz, consistent with the deviations between the measured FRFs of w_{LC} and w_{FE} in this frequency range (see Figure 8.7). The poor tracking performance in the figures presented in the third column (i.e., Figures 8-9c, 8-9f, and 8-9i) illustrate the importance of u_{w}, the term addressing the table-structure interaction, for accurate shake-table control

8.3.3 Effect of the differential pressure gain

Figures 8-10 through 8-13 illustrate the effect of the ΔP gain on the tracking performance. Each figure consists of four panels. Panels a), b), and c) present test results for GM_1, GM_2, and GM_3, respectively. Results presented in Figure 8.10, for $K_{\mathrm{p}} = 0.0002$ V/psi, show that the measured and the target acceleration spectra are in poor agreement for frequencies greater than 5 Hz. The poor tracking of input is attributed to the low fidelity of the analytical model (H_{zu}^{st} and H_{zw}^{st}) in this frequency range, for $K_{\mathrm{p}} = 0.0002$ V/psi, as illustrated in Figure 8.10d (reproduced from Section 4.5). The model prediction (dashed orange line) significantly deviates from the table measurement (solid blue line) in the frequency range between 10 and 40 Hz. The tracking performance is poor in this frequency range because the MIL controller is designed based on a low-fidelity linear model of the shake table.

Figures 8-11 and 8-12 present test results for $K_{\mathrm{p}} = 0.0006$ V/psi and 0.001 V/psi, respectively. As observed in panel d) of these figures, the fidelity of the linear model is significantly improved as K_{p} is increased. Consequently, the accuracy of the tracking performance increases. As K_{p} is increased to 0.0014 V/psi (see Figure 8.13), the fidelity of the linear model deteriorates after 30 Hz. Because neither of the three input motions have dominant spectral content after 30 Hz, the tracking performance for $K_{\mathrm{p}} = 0.0014$ is similar to that observed for $K_{\mathrm{p}} = 0.001$ V/psi.

The results of Figures 8-10 through 8-13 illustrate that a sufficiently large value of the ΔP gain, K_{p}, improves the fidelity of the linear model significantly, and by extension, is highly effective for designing shake-table controls to track a prescribed acceleration history at the base of the test article – one of the key hypotheses of Section 1.

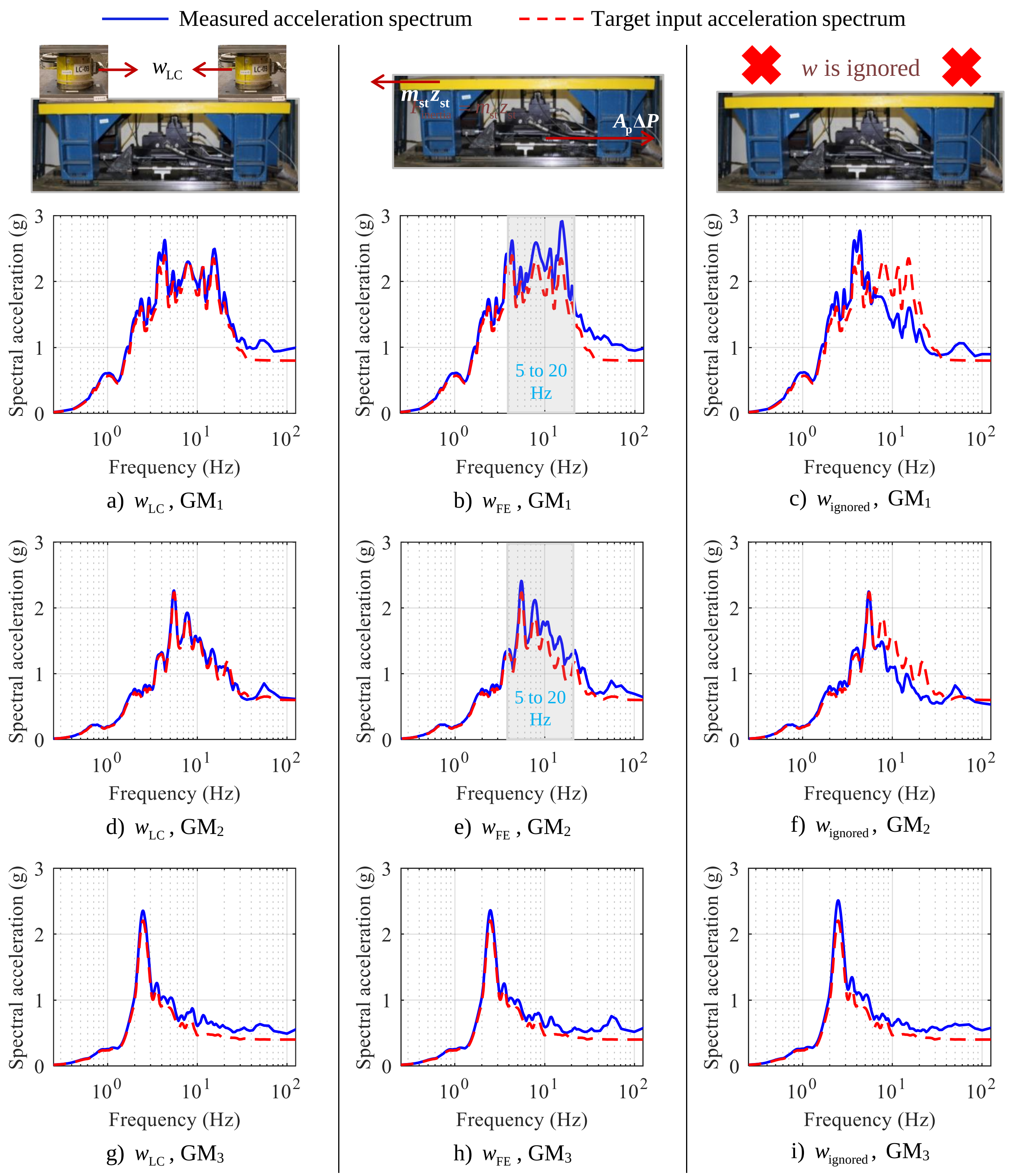

Figure 8.8. Results of acceleration-tracking experiments, different feedback measurements, empty vessel, K_e = 5 V/in, K_p = 0.001 V/psi, f_c = 80 Hz, τ_s = 500 μs [2000 Hz]

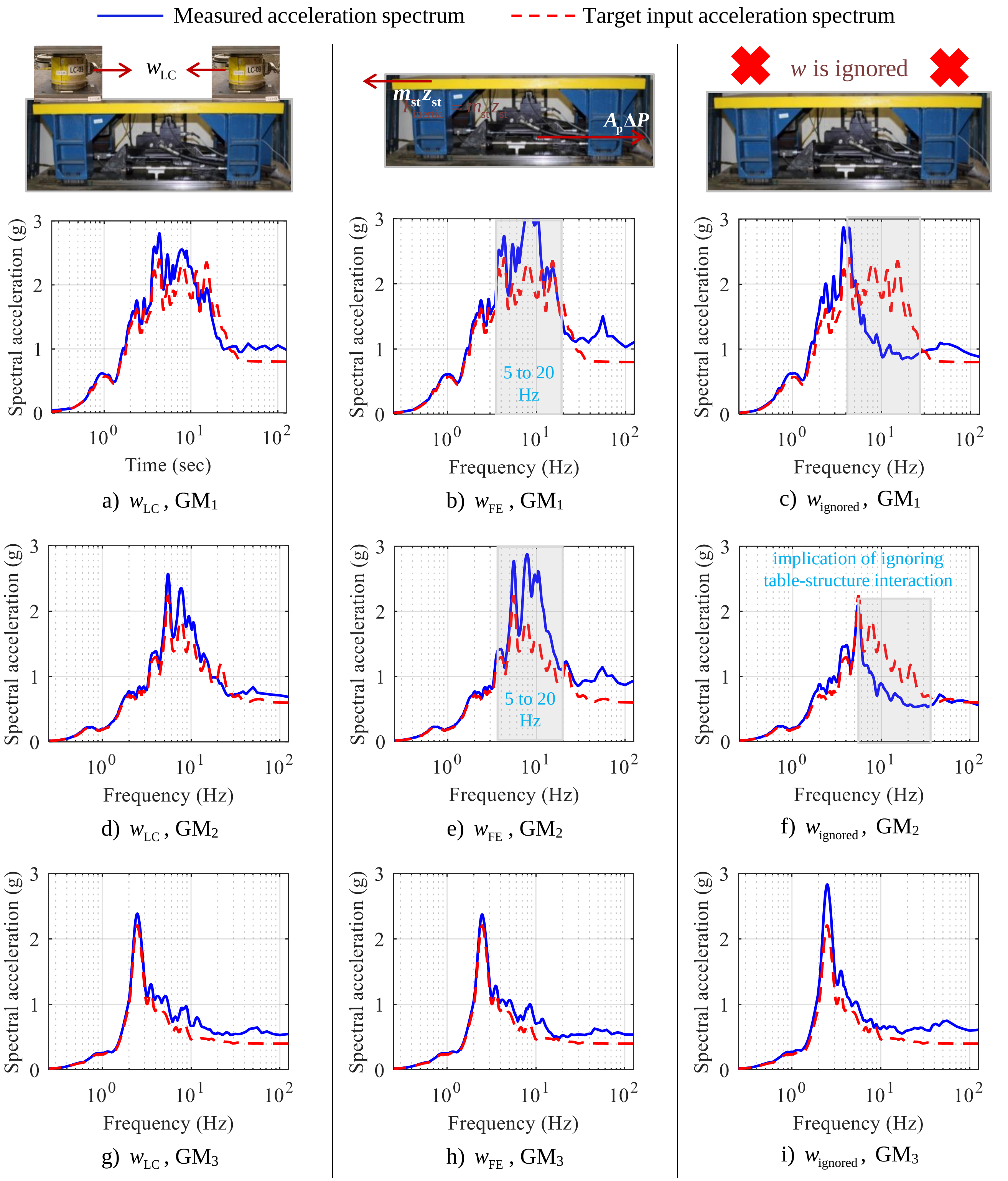

Figure 8.9. Results of acceleration-tracking experiments, different feedback measurements, d_w = 42 inches, K_e = 5 V/in, K_p = 0.001 V/psi, f_c = 80 Hz, τ_s = 500 μs [2000 Hz]

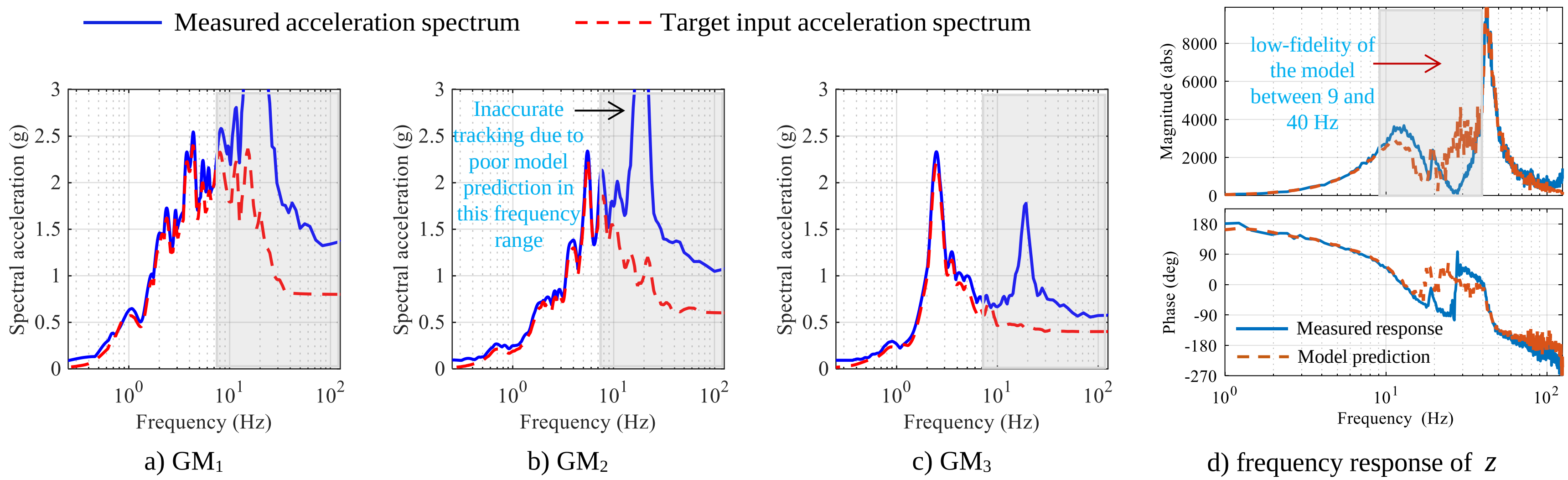

Figure 8.10. Results of acceleration-tracking experiments, K_e = 5 V/in, K_p = 0.0002 V/psi, f_c = 80 Hz, τ_s = 500 μs [2000 Hz]

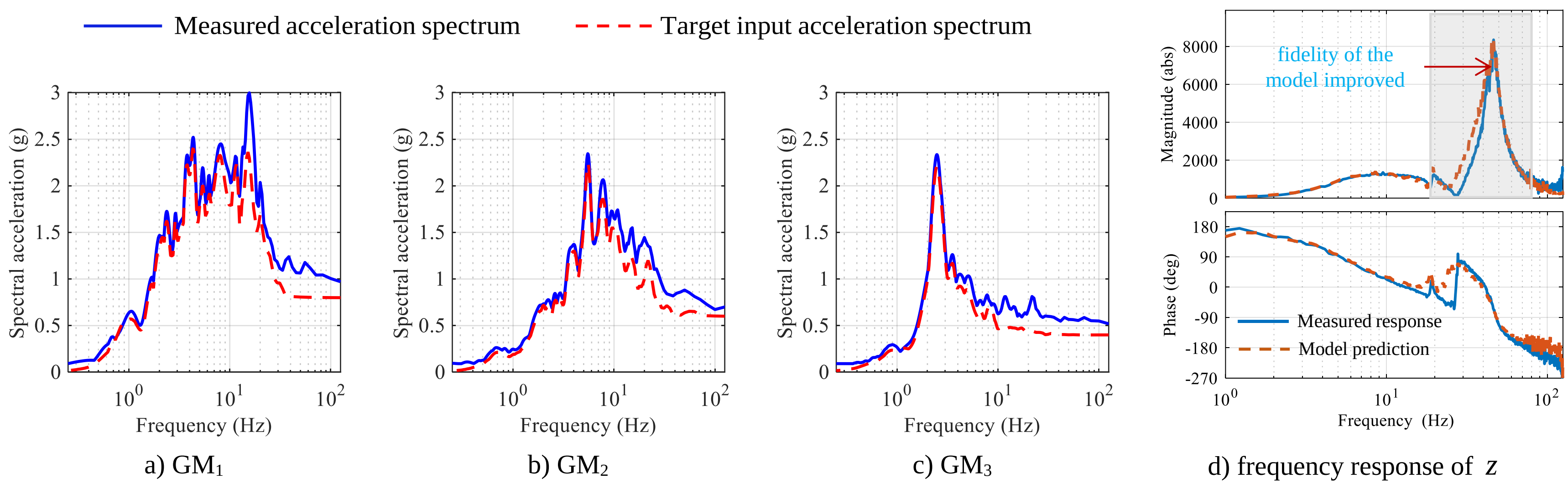

Figure 8.11. Results of acceleration-tracking experiments, K_e = 5 V/in, K_p = 0.0006 V/psi, f_c = 80 Hz, τ_s = 500 μs [2000 Hz]

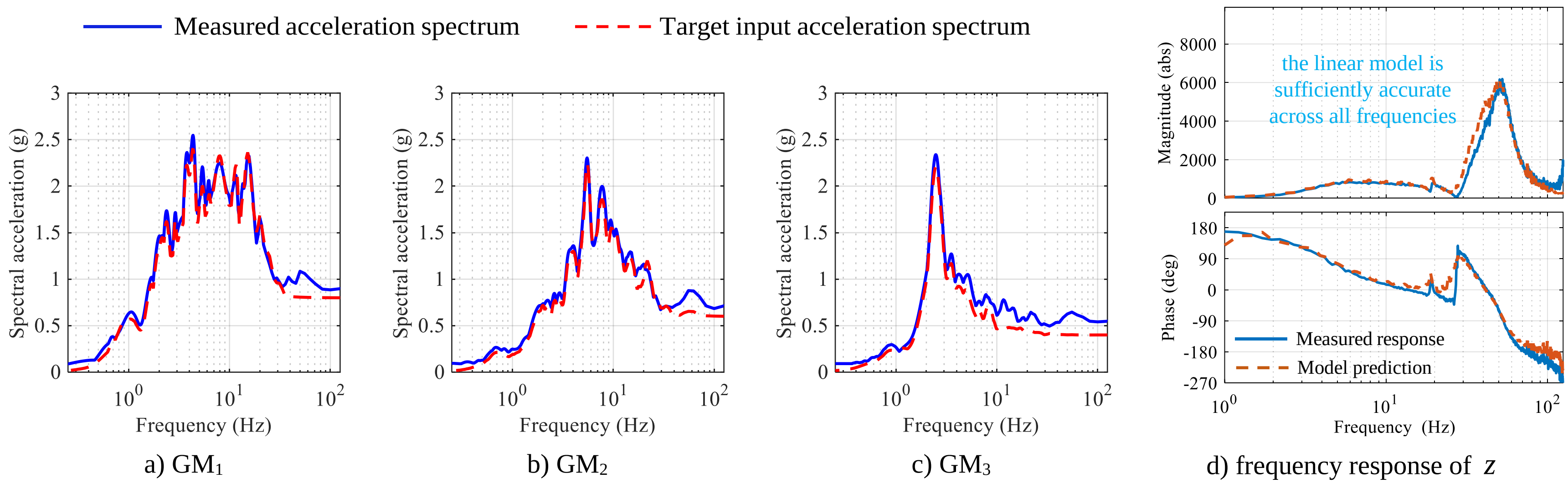

Figure 8.12. Results of acceleration-tracking experiments, K_e = 5 V/in, K_p = 0.001 V/psi, f_c = 80 Hz, τ_s = 500 μs [2000 Hz]

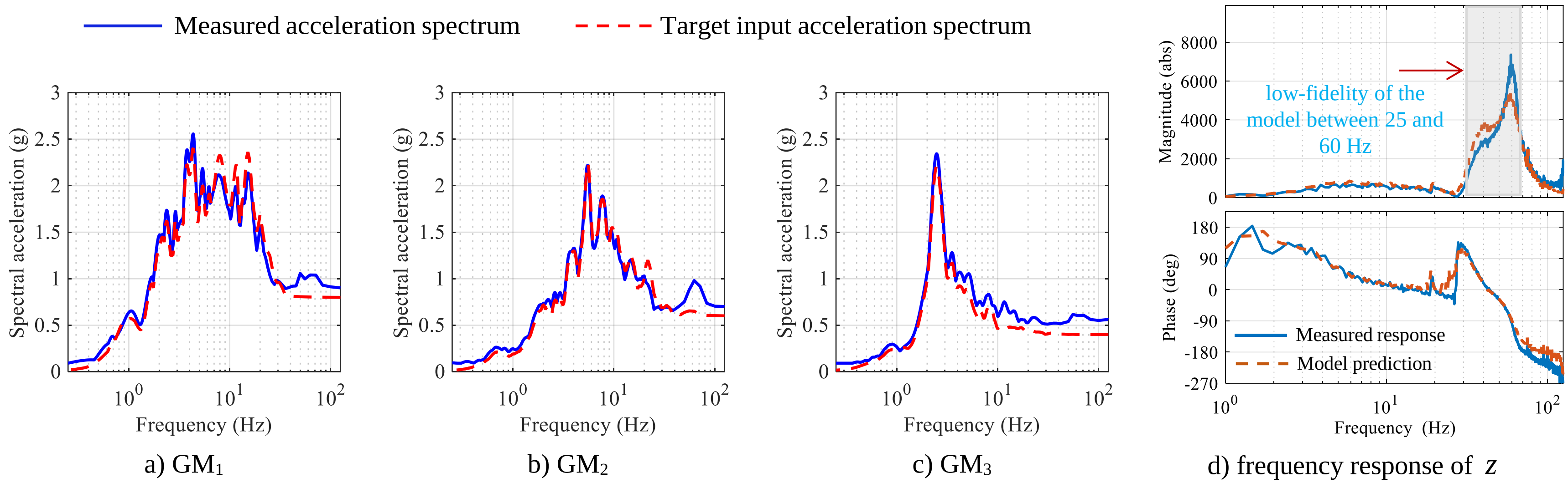

Figure 8.13. Results of acceleration-tracking experiments, K_e = 5 V/in, K_p = 0.0014 V/psi, f_c = 80 Hz, τ_s = 500 μs [2000 Hz]

8.3.4 Effect of the cutoff frequency of the filter

Figures 8-14 and 8-15 illustrate the effect of the filter cutoff frequency of the filter, f_c, on the tracking performance. Each figure consists of six panels. The panels in the top row present the frequency response of the H_{uw} controller, original (solid blue line) and approximated with the third-order Butterworth lowpass filter (dashed orange line), for increasing values of cutoff frequencies, f_c. The resulting performance tradeoff in the controller response is identified by the grey hatching. The higher the filter cutoff frequency, the smaller the performance tradeoff. The lower three panels in the figures present tracking results corresponding to the $\left|H_w^{\text{filter}} H_{uw}\right|$ presented above it. The key takeaways from the figures are:

- For the empty vessel case (see Figure 8.14), the tracking performance is shown less sensitive to (or affected by) the filter cutoff frequency. Herein, f_c is varied as: 40 Hz in panel a); 60 Hz in panel b); and 80 Hz in panel c). For a mass ratio of 0.75, the feedback force is small, and consequently, the contribution of the table-structure interaction term u_w is negligible in comparison with u_{a_g}. In such cases, the effect of model inaccuracy and controller filters on tracking performance is minimal.
- If the test article is considerably heavier (twice or more) than the shake table (see the responses of Figure 8.15 plotted for a mass ratio of 2.5), the tradeoffs of using lower cutoff frequencies are clearly seen in terms of reduced tracking performance. The tracking performance is improved if the filter cutoff frequency is in increased from 40 Hz in Figure 8.15d to 80 Hz in Figure 8.15f.
- If f_c is increased to 100 Hz, $\left|H_w^{\text{filter}} H_{uw}\right|$ is not sufficiently curtailed at high frequencies, as shown in Figure 8.16a. The controller then responds to (and amplifies) the noise in the measurement of w, which propagates through the feedback system: noise in the measurement of w $\xrightarrow{\text{input to the } H_{uw} \text{ controller}}$ control input $\xrightarrow{\text{command to the shake table}}$ table acceleration $\xrightarrow{\text{applied on the test article}}$ measurement of w with amplified high-frequency content…. and the cycle repeats. This cascading effect makes the feedback system impractical with large high-frequency oscillations, as shown in Figure 8.16b.

For the test case with water depth of 42 inches, a smaller value of $f_c = 40$ Hz results in poor tracking of the input because of the significant tradeoff in the approximated controller $\left|H_w^{\text{filter}} H_{uw}\right|$. On contrary, a higher value of $f_c = 100$ Hz results in impractical shake-table response (instability) because the controller response is not sufficiently curtailed at high frequencies where the shake-table model is inaccurate and measurement noise is greater. The cutoff frequency of the filter is therefore determined as a tradeoff between performance and stability, making clear Contribution #5 listed in Section 1.3.4.

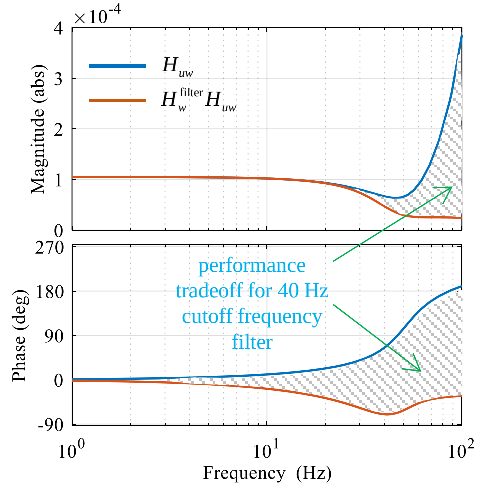

a) controller response, $f_c = 40$ Hz

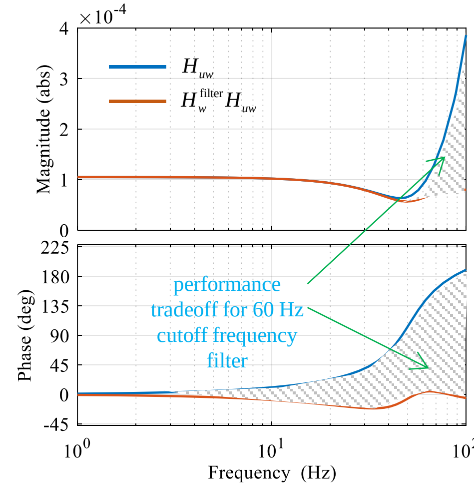

b) controller response, $f_c = 60$ Hz

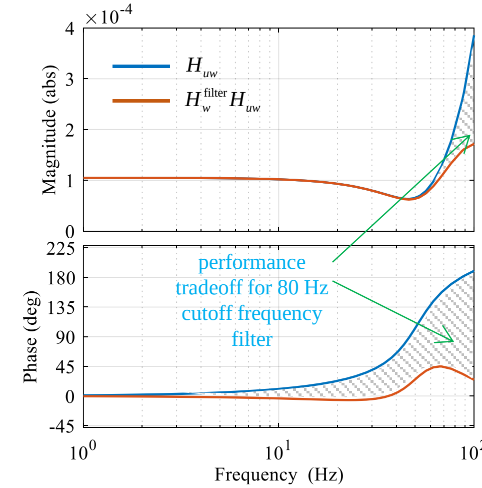

c) controller response, $f_c = 80$ Hz

Measured acceleration spectrum   Target input acceleration spectrum

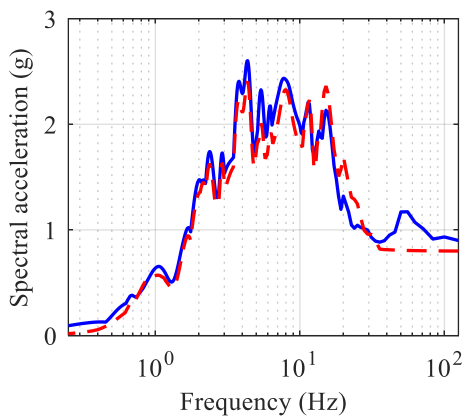

d) tracking response, $f_c = 40$ Hz

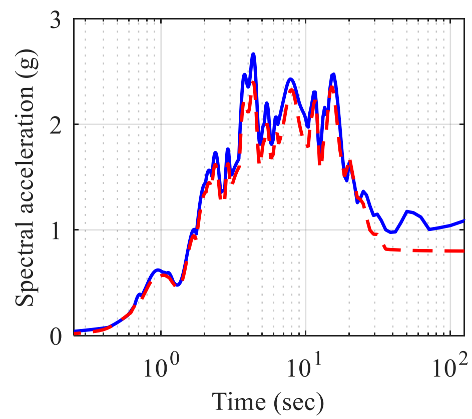

e) tracking response, $f_c = 60$ Hz

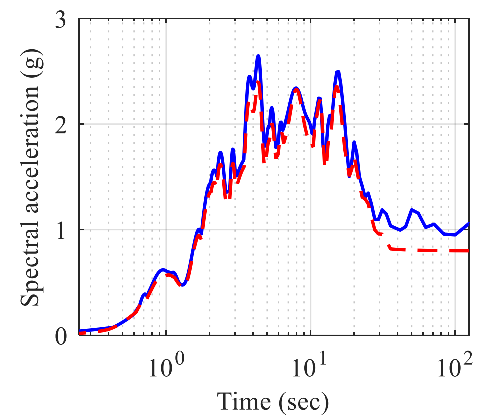

f) tracking response, $f_c = 80$ Hz

Figure 8.14. Results of acceleration-tracking experiments, different cutoff frequencies of the filters, empty vessel, GM$_1$, K_e = 5 V/in, K_p = 0.001 V/psi, τ_s = 500 μs [2000 Hz]

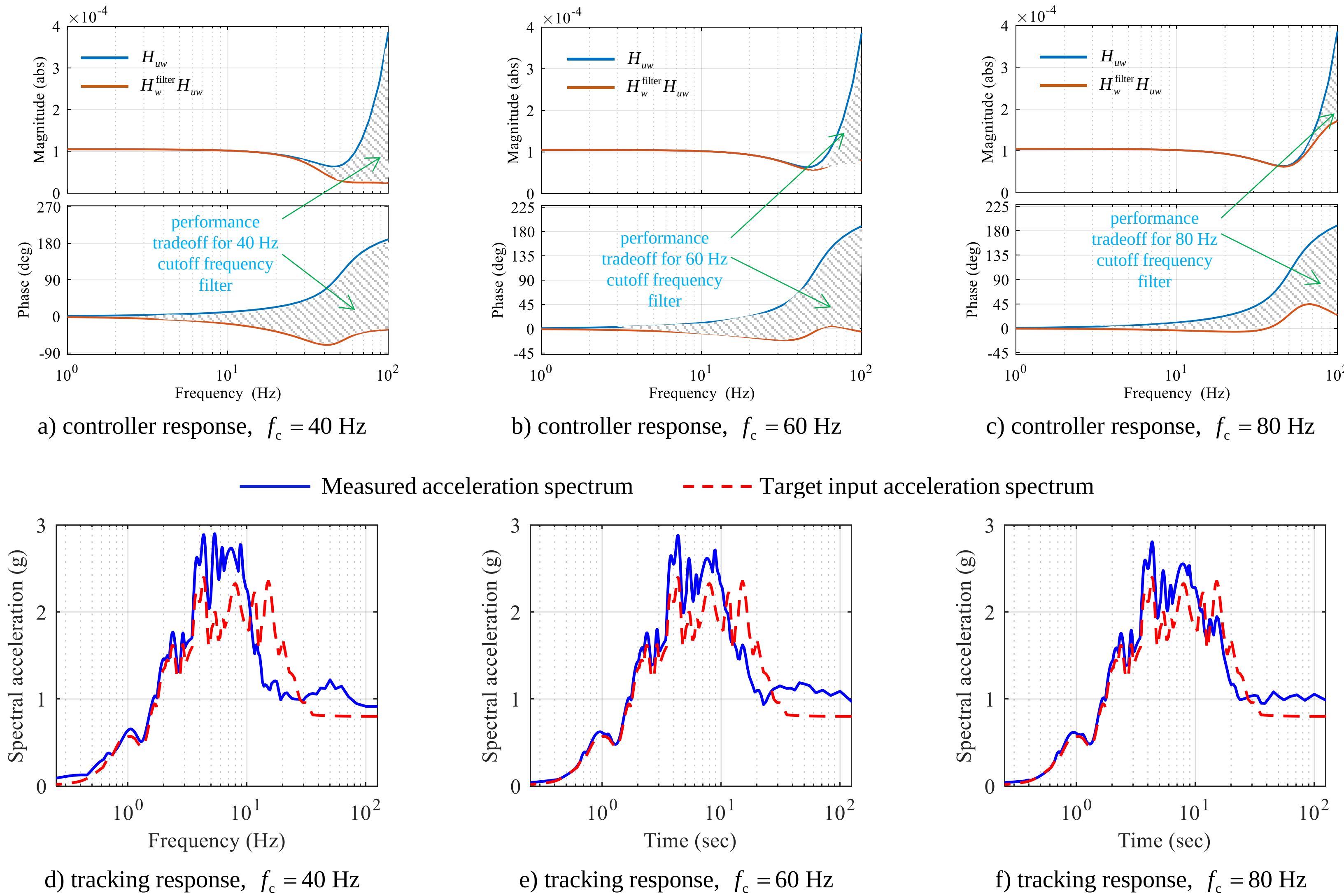

Figure 8.15. Results of acceleration-tracking experiments, different cutoff frequencies of the filters, d_w = 42 inches, GM$_1$, K_e = 5 V/in, K_p = 0.001 V/psi, τ_s = 500 μs [2000 Hz]

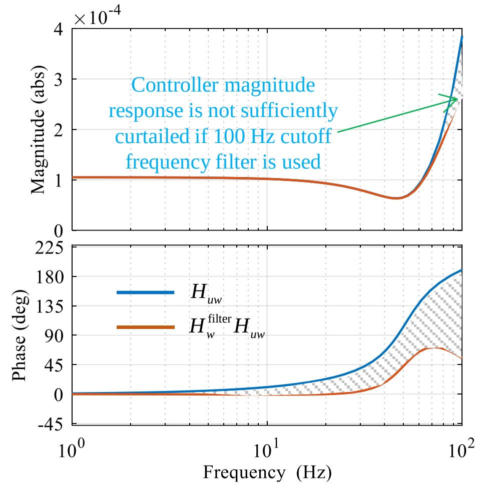

a) controller frequency response, $f_c = 100$ Hz

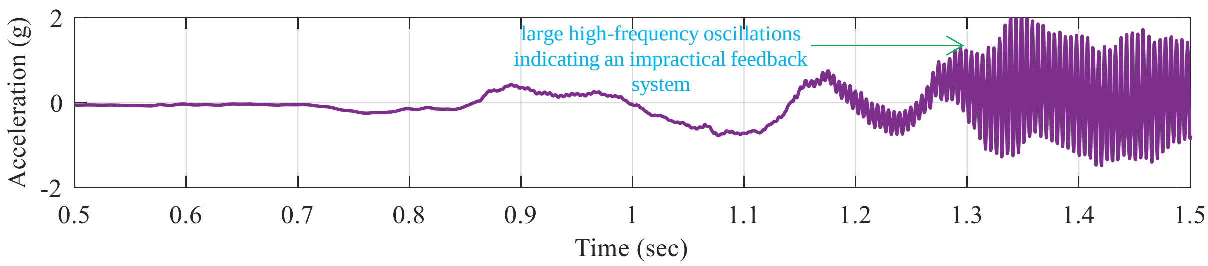

b) measured acceleration timeseries

Figure 8.16. Results of acceleration-tracking experiments, d_w = 42 inches, GM$_1$, K_e = 5 V/in, K_p = 0.001 V/psi, f_c = 100 Hz, τ_s = 500 µs [2000 Hz]

SECTION 9
VALIDATION OF THE MIL CONTROLLER FOR SIMULATING VIRTUAL SEISMIC ISOLATION SYSTEMS

9.1 Section prologue

This section presents results of the model-in-the-loop (MIL) experiments that imitated different seismic isolation systems at the base of the test article, and completes the discussion on the impedance-matching approach to MIL – the central theme of this report. In the MIL experiments, the target acceleration history of the VS basemat, z_{vs}, which needs to be imitated by the shake table, is computed by solving the VS differential equations for the inputs: (i) ground acceleration, a_{g}, which is known a priori, and (ii) feedback force from the test article, w, which is measured in real time. The computed z_{vs} and the measured w are then used to calculate the control input to the shake table, $u = H_z^{\text{filter}} \left(H_{zu}^{\text{st}}\right)^{-1} z_{\text{vs}} - H_w^{\text{filter}} H_{zw}^{\text{st}} \left(H_{zu}^{\text{st}}\right)^{-1} w$, required to imitate the VS acceleration. Herein, MIL experiments are performed for a diverse combination of virtual systems (seismic isolation systems of different types and properties) and input ground motions (acceleration histories with different peak intensities and spectral content) to evaluate the performance of the designed MIL controls over a broad range of system parameters.

Section 9.2 reports the virtual system properties considered in the experiments. Section 9.3 presents results of the MIL experimental. Of the many cases evaluated, results are presented for twenty-seven cases – combinations of nine virtual systems (three for each of the spring-damper, lead-rubber, and Friction Pendulum systems) and the three input ground motions described in Section 8.2. Results show that the shake table with the designed MIL controls is able to imitate different isolation systems sufficiently accurately in the frequency range of 0.25 Hz to 15 Hz, and with reduced accuracy at higher frequencies.

The poorer MIL performance after 15 Hz emphasizes the fact that it is not practically possible to control one dynamic system to imitate the impedance (i.e., force-motion behavior) of another accurately across all frequencies because the two systems will often have different dynamic characteristics. For example, herein, the dominant response of the isolation systems is in the low-frequency range (< 2 Hz) whereas the oil-column resonance frequency of the shake table is close to 30 Hz. Additionally, there are some fundamental limitations to what can be achieved with controls. Section 9.4 discusses these limitations to MIL testing, framed herein as tradeoffs between performance (i.e., how closely the controlled shake-table system imitates the impedance of the desired VS) and stability (which is assessed herein using passivity controlled shake table). The presentation emphasizes the two parameters: (i) ratio of the VS basemat mass, m_{vs}, relative to the shake-table mass, m_{st}, and (ii) cutoff frequency, f_{c}, of the controller filter, H_{w}^{filter}, which are shown critical in determining these tradeoffs.

9.2 Properties of the virtual systems for the MIL experiments

As discussed in Section 5, the dynamic response of a spring-damper (SD) system (see Section 5.3) depends on three parameters: m_{vs}, k_{s}, and c; of a lead-rubber (LR) system (see Section 5.4) on seven parameters: m_{vs}, q_{d}, k_{i}, k_{s}, u_{y}, n, and c; and of a single concave Friction Pendulum (FP) system (see Section 5.5) on six parameters: m_{vs}, $\mu_{\max}$, $\mu_{\min}$, k_{s}, u_{y}, and a. In the MIL experiments, these parameters are varied to represent a family of isolation systems with strength and stiffnesses distributed over a broad range.

The properties of the SD systems are selected to achieve target horizontal periods of the isolated vessel, T_{s}, in the range of 0.57 sec (1.75 Hz) and 1.33 sec (0.75 Hz), and damping ratios, ζ, in the range 0.2 to 0.3. The [T_{s}, ζ] pairs for the three spring-damper systems are selected as: [1.33 sec and 0.3] for SD_1; [0.8 sec and 0.25] for SD_2; and [0.57 sec and 0.2] for SD_3, to represent isolation systems with behavior ranging from low-stiffness, high-damping (SD_1) to high-stiffness, low-damping (SD_3).

In the MIL experiments, the sum of the masses of the vessel (physically tested with a water depth of 36 inches), m_{ps}, and of the virtual-system basemat (virtually represented), m_{vs}, is the total axial load on the isolation system. The stiffness, k_{s}, and damping coefficient, c, of the SD systems are therefore calculated as $k_{\mathrm{s}} = (2\pi f)^2 \times (m_{\mathrm{vs}} + m_{\mathrm{ps}})$ and $c = 2\zeta\sqrt{k_{\mathrm{s}}(m_{\mathrm{vs}} + m_{\mathrm{ps}})}$, and reported in Table 9.1. Figure 9.1a presents the idealized shear force-horizontal displacement loops for the three SD systems. The shear force normalized by the axial load is the ordinate and the horizontal displacement is the abscissa.

Table 9.1. Properties of the SD isolation systems

Property	Symbol	SD_1	SD_2	SD_3
Target frequency (Hz)	f	0.75	1.25	1.75
Target damping (%)	ζ	30	25	20
Mass of the basemat (lb)	m_{vs}	2000	2000	2000
Mass of the test article (lb), d_{w} =36 in	m_{ps}	3600	3600	3600
Horizontal stiffness (lb/in)	k_{s}	322	894	1753
Viscous damping coefficient (lb-s/in)	c	41	57	64

For the LR and FP systems, the two parameters: (i) ratio of the characteristic strength of the isolation system to the total axial load, $q_{\text{ratio}} = q_{\text{d}} / \left(m_{\text{vs}} + m_{\text{ps}} \right)$, and (ii) post-elastic period of the isolated vessel, T_{s}, are varied over a broad range, $0.06 \le q_{\text{ratio}} \le 0.21$ and $1 \text{ sec} \le T_{\text{s}} \le 2.25 \text{ sec}$, to represent a family of isolation systems with behavior ranging from low-strength, high-flexibility to high-strength, low-flexibility: [0.06, 2.25 sec] for FP_1; [0.09, 2 sec] for LR_1; [0.12, 1.75 sec] for FP_2; [0.15, 1.5 sec] for LR_2; [0.18, 1.25 sec] for FP_3; and [0.21, 1 sec] for LR_3. Figure 9.1b presents the idealized shear force-horizontal displacement loops for the LR and FP systems. The strength and stiffness properties are reported in Tables 9-2 and 9-3.

Table 9.2. Properties of the LR isolation systems

Property	Symbol	LR_1	LR_2	LR_3
Target characteristic strength ratio	q_{ratio}	0.09	0.15	0.21
Target post-elastic period (sec)	T_{s}	2	1.5	1
Mass of the basemat (lb)	m_{vs}	2000	2000	2000
Mass of the test article (lb), d_{w} =36 in	m_{ps}	3600	3600	3600
Yield displacement (in)	u_{y}	0.4	0.4	0.4
Characteristic strength (lb)	q_{d}	504	839	1175
Initial (post-elastic) stiffness (lb/in)	k_{i} (k_{s})	1402 (143)	2353 (254)	3510 (572)
Stiffness ratio	α	0.10	0.11	0.16
Smoothing parameter	n	2	2	2
Damping coefficient (lb-s/in)	c	0.11	0.15	0.22

Table 9.3. Properties of the FP isolation systems

Property	Symbol	FP_1	FP_2	FP_3
Target characteristic strength ratio	q_{ratio}	0.06	0.12	0.18
Target post-elastic period (sec)	T_{s}	2.25	1.75	1.25
Mass of the basemat (lb)	m_{vs}	2150	2150	2150
Fast (slow) coefficient of friction	$\mu_{\max}$ ($\mu_{\min}$)	0.06 (0.03)	0.12 (0.06)	0.18 (0.09)
Rate parameter (sec/in)	a	2.54	2.54	2.54
Initial stiffness (lb/in)	k_{i}	8395	16789	25183
Sliding stiffness (lb/in)	k_{s}	113	187	366

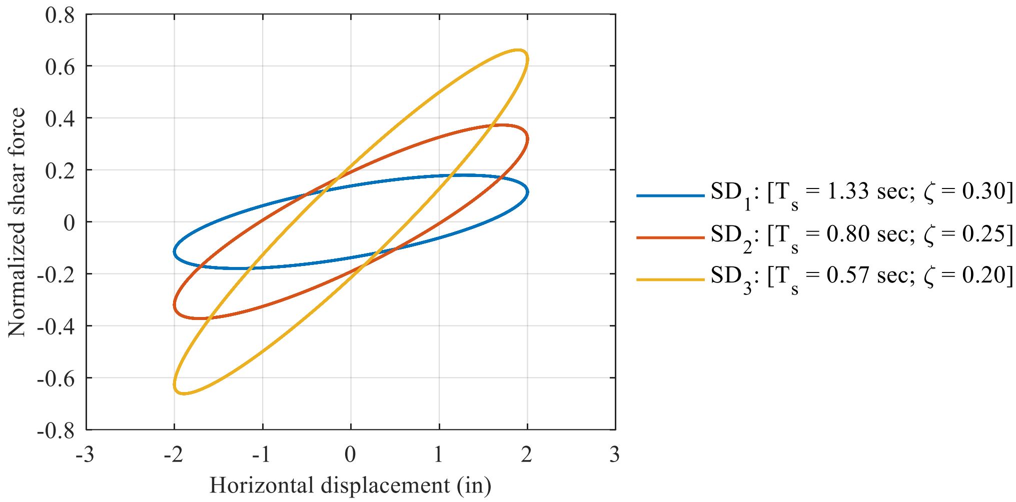

a) SD isolation systems

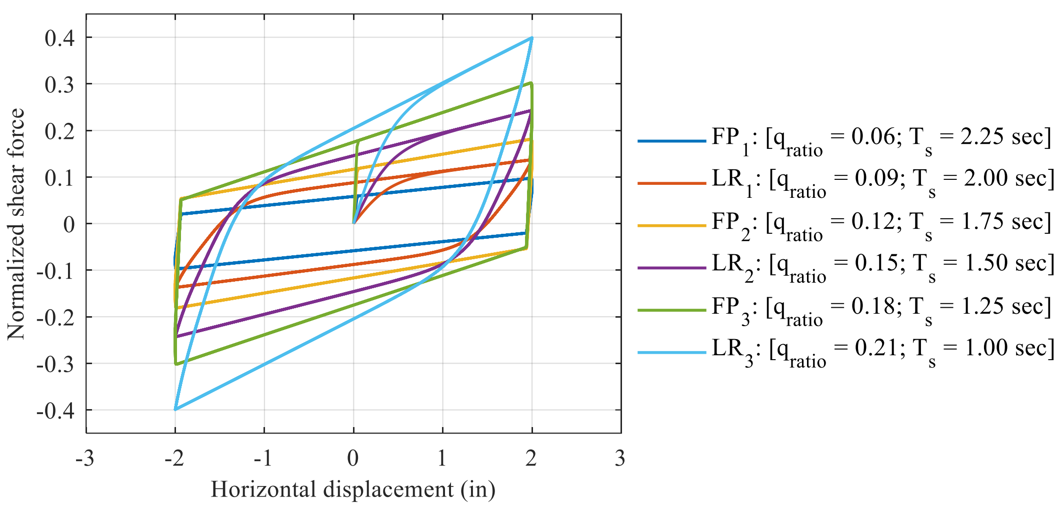

b) LR and FP isolation systems

Figure 9.1. Normalized shear force-horizontal displacement loops

9.3 Results of MIL experiments imitating different seismic isolation systems

Figures 9-2 through 9-28 present MIL experimental results for the twenty-seven test cases: combinations of nine isolation systems (SD_1, SD_2, SD_3, LR_1, LR_2, LR_3, FP_1, FP_2, and FP_3,) and three input ground motions (GM_1, GM_2, and GM_3). These test cases utilized the feedback force measurement from the reaction load cells for MIL-related computations. The effects of using alternate sources of feedback measurement on MIL accuracy is investigated in Appendix C. All experiments are performed for the control parameters: $K_e = 5$ V/in, $K_p = 0.001$ V/psi, and $\tau_s = 500$ μs [2000 Hz], and the cutoff frequency of the filters is set to 80 Hz. Figures 9-2 through 9-10 present results for the three SD isolation systems, 9-11 through 9-19 for the three

LR isolation systems, and 9-20 through 9-28 for the three FP isolation systems. Table 9.4 maps each test case to the corresponding figure that presents results.

Table 9.4. Mapping between the MIL test cases and presentation of results

	GM_1	GM_2	GM_3
SD_1	Figure 9-2	Figure 9-3	Figure 9-4
SD_2	Figure 9-5	Figure 9-6	Figure 9-7
SD_3	Figure 9-8	Figure 9-9	Figure 9-10
LR_1	Figure 9-11	Figure 9-12	Figure 9-13
LR_2	Figure 9-14	Figure 9-15	Figure 9-16
LR_3	Figure 9-17	Figure 9-18	Figure 9-19
FP_1	Figure 9-20	Figure 9-21	Figure 9-22
FP_2	Figure 9-23	Figure 9-24	Figure 9-25
FP_3	Figure 9-26	Figure 9-27	Figure 9-28

Each figure consists of three panels. Panel a) presents acceleration histories. The solid blue line is the acceleration of the shake table measured in the experiments and the dashed red line is the target basemat acceleration history, $\ddot{z}_{\mathrm{vs}}$, that is computed in real time by numerical integration of the VS differential equations based on known a_{g} and real-time measurement of *w*. Panel b) presents 5% damped response spectra of the measured table and the target VS acceleration histories. The solid black line in the figure is the response spectrum of the input ground motion, a_{g}.

Panel c) of the figure presents isolation system's force-displacement (FD) response to the input ground motion. The displacement response in blue is the difference between the measured displacement of the shake table and the displacement history of the input motion: $D_{\mathrm{exp}} = x_{\mathrm{exp}} - x_{\mathrm{g}}$. This is because the shake table is controlled to imitate the total (absolute) motion of the VS basemat. The experimental force history, F_{exp}, is computed as the measured feedback force minus the basemat inertia[30]: $F_{\mathrm{exp}} = w - m_{\mathrm{vs}} \ddot{z}_{\mathrm{exp}}$. The force and displacement histories from the VS model are obtained from its state variables[31].

[30] The force resisted by the isolation system, F_{exp}, equals the actuator force, $F_{\mathrm{a}} = w - m_{\mathrm{st}} \ddot{z}_{\mathrm{exp}}$, when $m_{\mathrm{vs}} = m_{\mathrm{st}}$.

[31] For example, the total force resisted by the SD isolation system is computed as the sum of the contributions from the spring and the dashpot units: $F_{\mathrm{model}} = k_{\mathrm{s}} x_1 + c x_2$, wherein the state variables x_1 and x_2 are the displacement and velocity of the VS basemat relative to the ground. Therefore, $D_{\mathrm{model}} = x_1$.

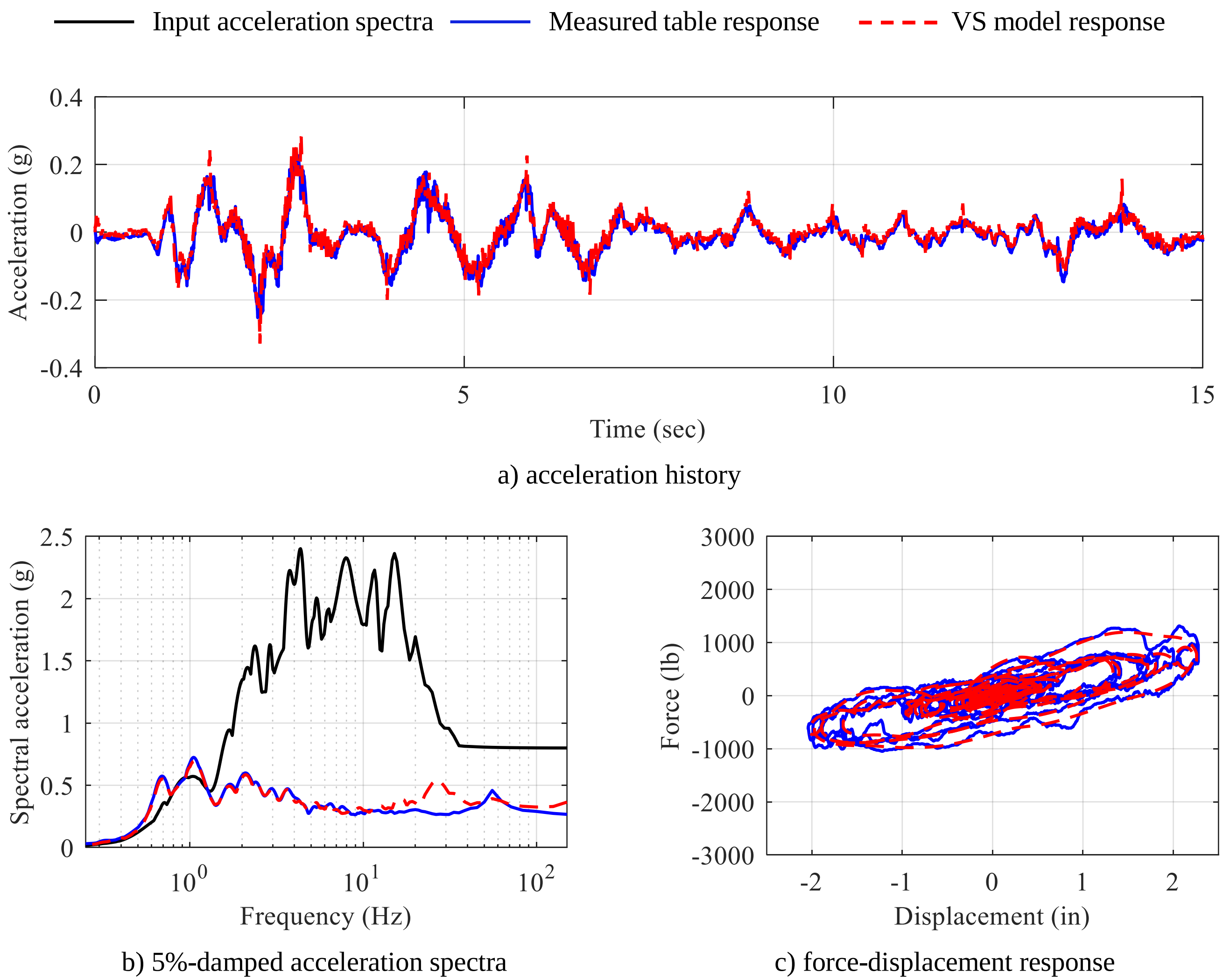

Figure 9.2. Results of MIL experiments imitating SD_1 isolation system subjected to input motion GM_1, K_e = 5 V/in, K_p = 0.001 V/psi, f_c = 80 Hz, and τ_s = 500 µs (2000 Hz)

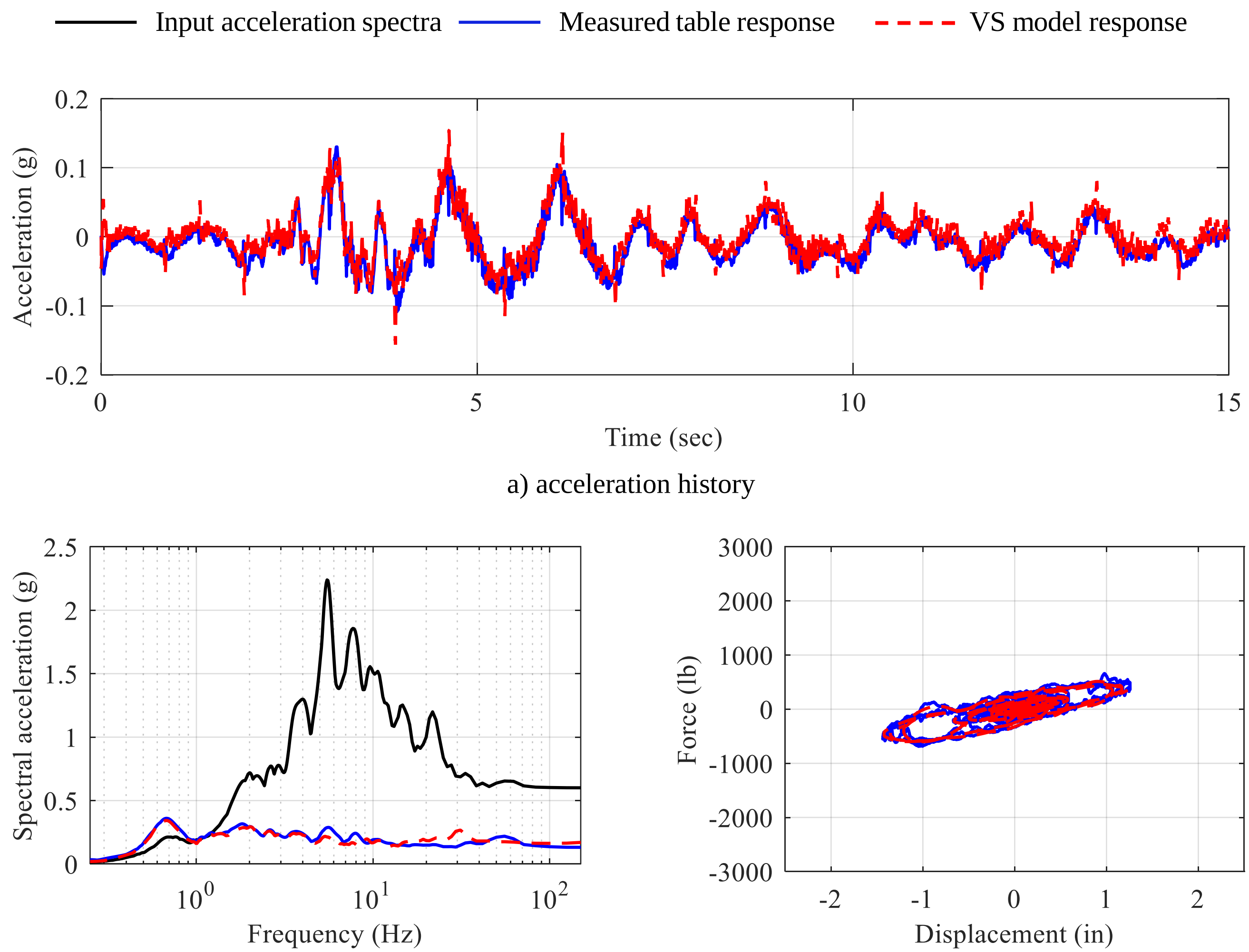

a) acceleration history

b) 5%-damped acceleration spectra

c) force-displacement response

Figure 9.3. Results of MIL experiments imitating SD_1 isolation system subjected to input motion GM_2, K_e = 5 V/in, K_p = 0.001 V/psi, f_c = 80 Hz, and τ_s = 500 µs (2000 Hz)

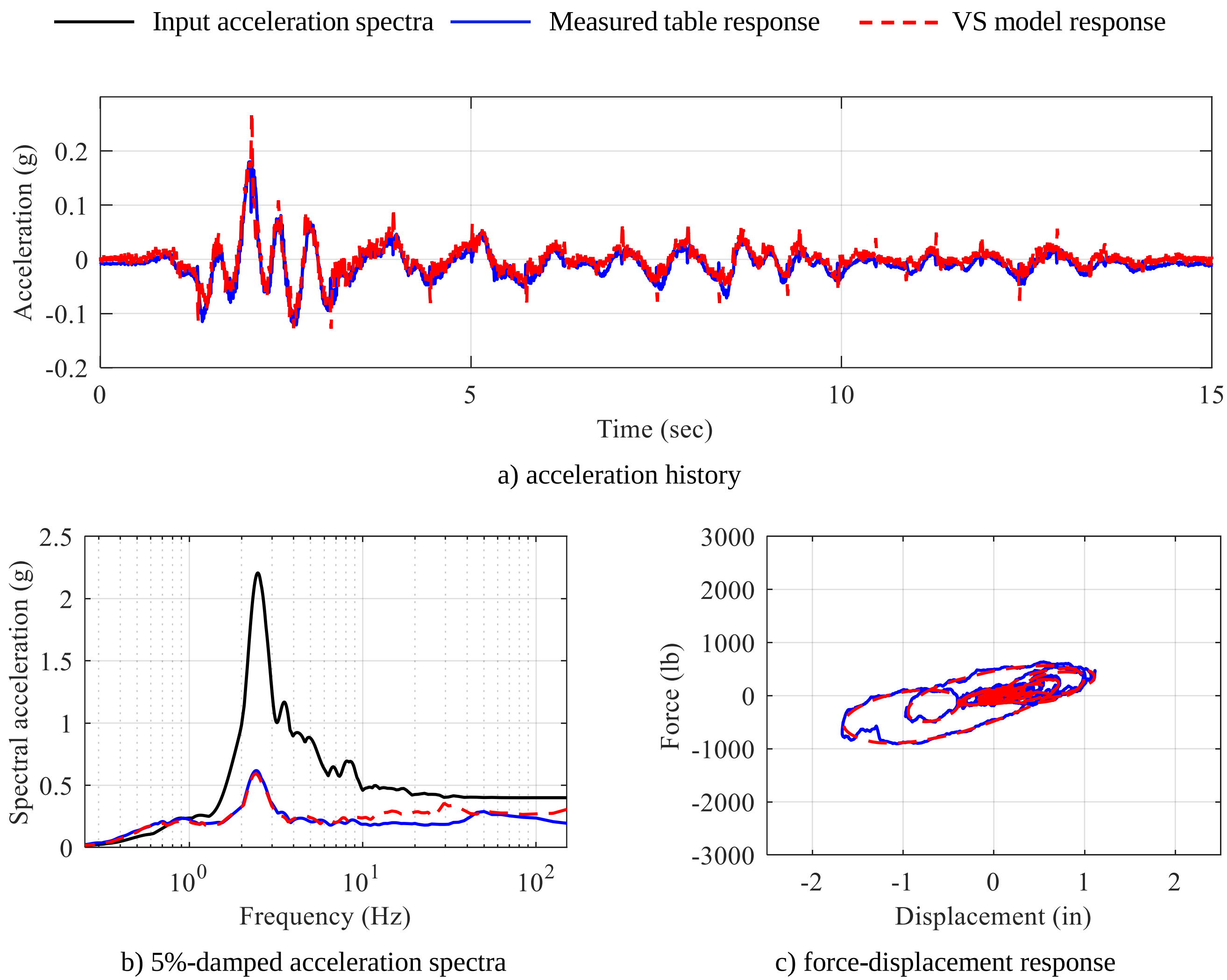

Figure 9.4. Results of MIL experiments imitating SD_1 isolation system subjected to input motion GM_3, K_e = 5 V/in, K_p = 0.001 V/psi, f_c = 80 Hz, and τ_s = 500 µs (2000 Hz)

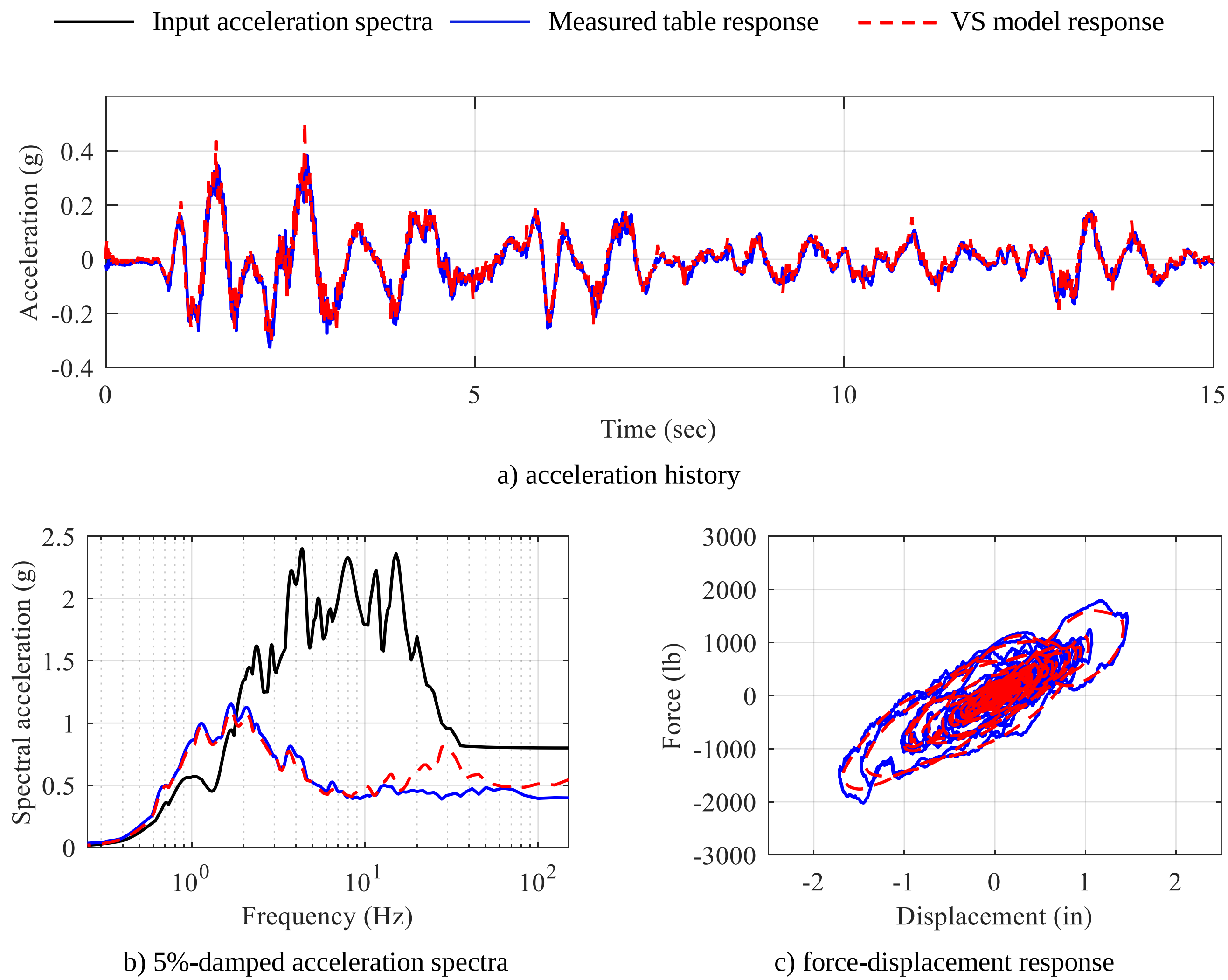

Figure 9.5. Results of MIL experiments imitating SD_2 isolation system subjected to input motion GM_1, K_e = 5 V/in, K_p = 0.001 V/psi, f_c = 80 Hz, and τ_s = 500 μs (2000 Hz)

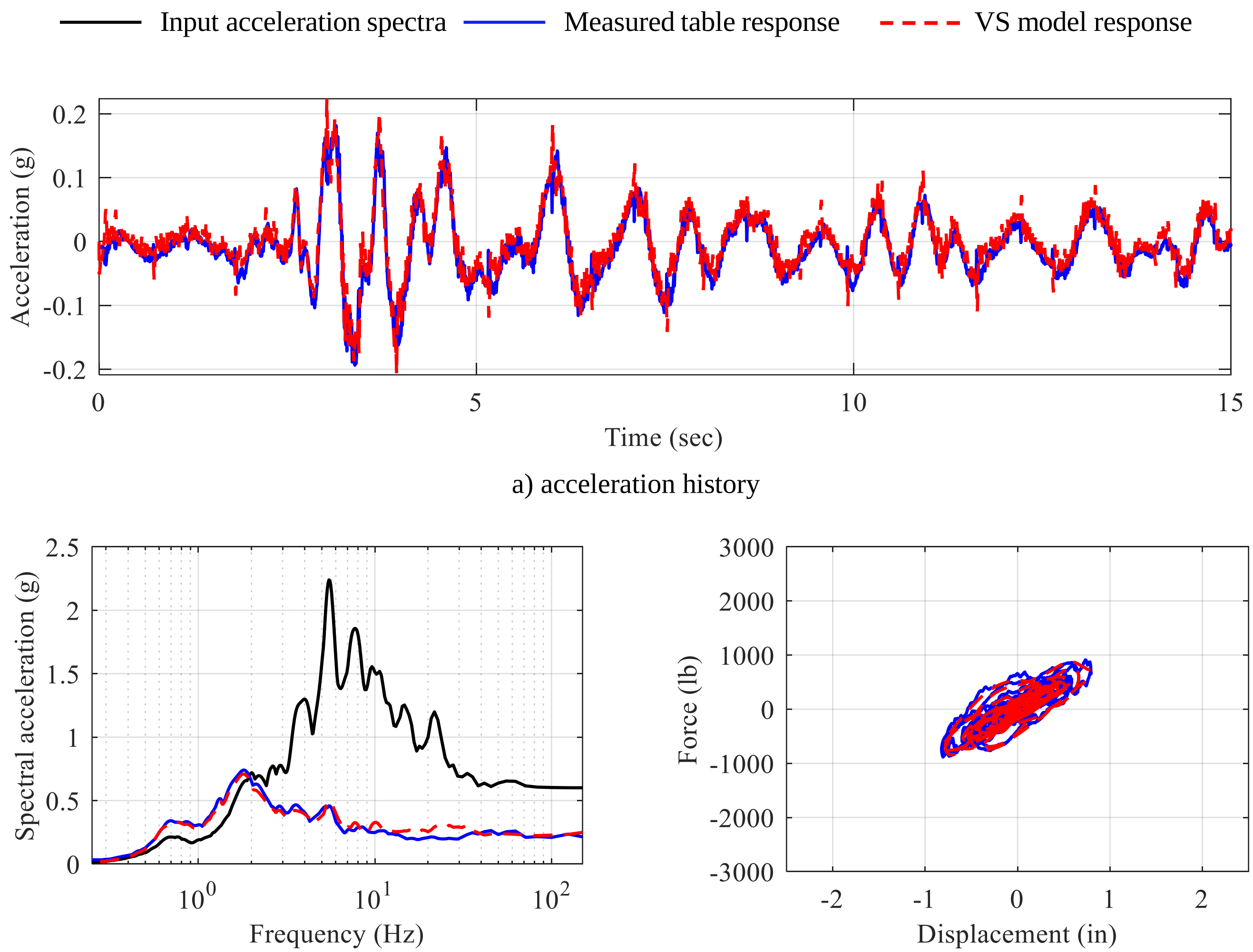

b) 5%-damped acceleration spectra

c) force-displacement response

Figure 9.6. Results of MIL experiments imitating SD_2 isolation system subjected to input motion GM_2, K_e = 5 V/in, K_p = 0.001 V/psi, f_c = 80 Hz, and τ_s = 500 μs (2000 Hz)

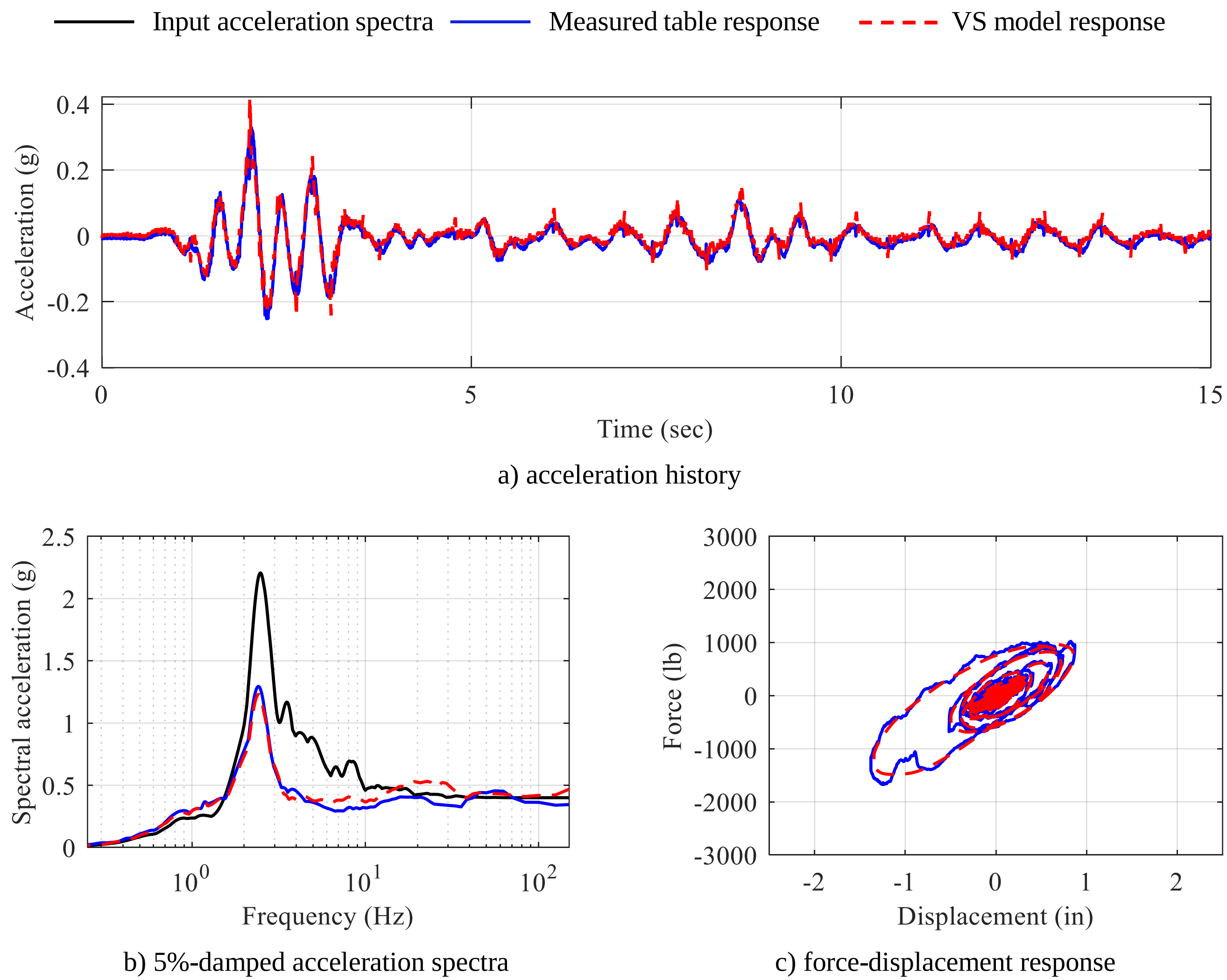

Figure 9.7. Results of MIL experiments imitating SD_2 isolation system subjected to input motion GM_3, K_e = 5 V/in, K_p = 0.001 V/psi, f_c = 80 Hz, and τ_s = 500 μs (2000 Hz)

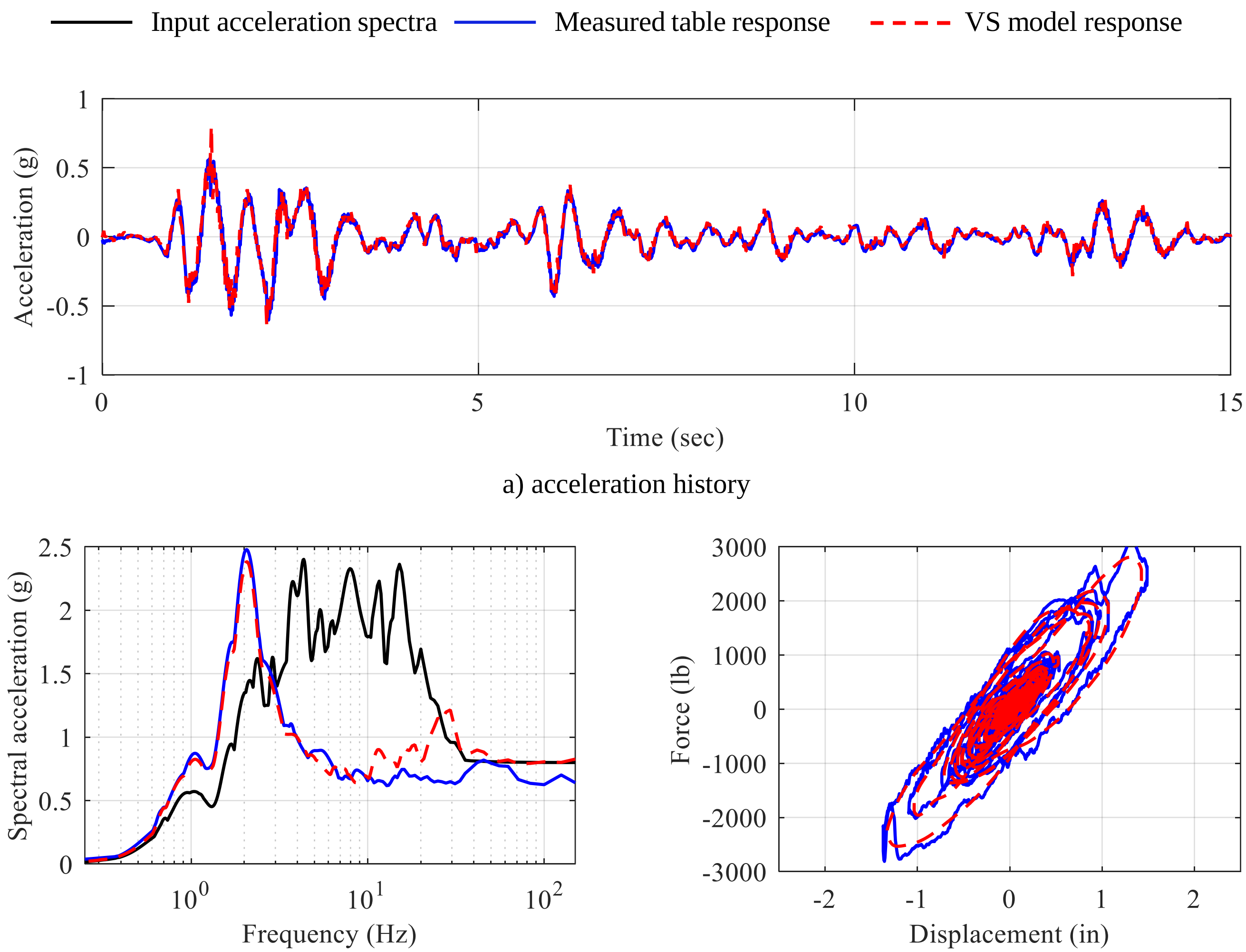

a) acceleration history

b) 5%-damped acceleration spectra

c) force-displacement response

Figure 9.8. Results of MIL experiments imitating SD_3 isolation system subjected to input motion GM_1, K_e = 5 V/in, K_p = 0.001 V/psi, f_c = 80 Hz, and τ_s = 500 µs (2000 Hz)

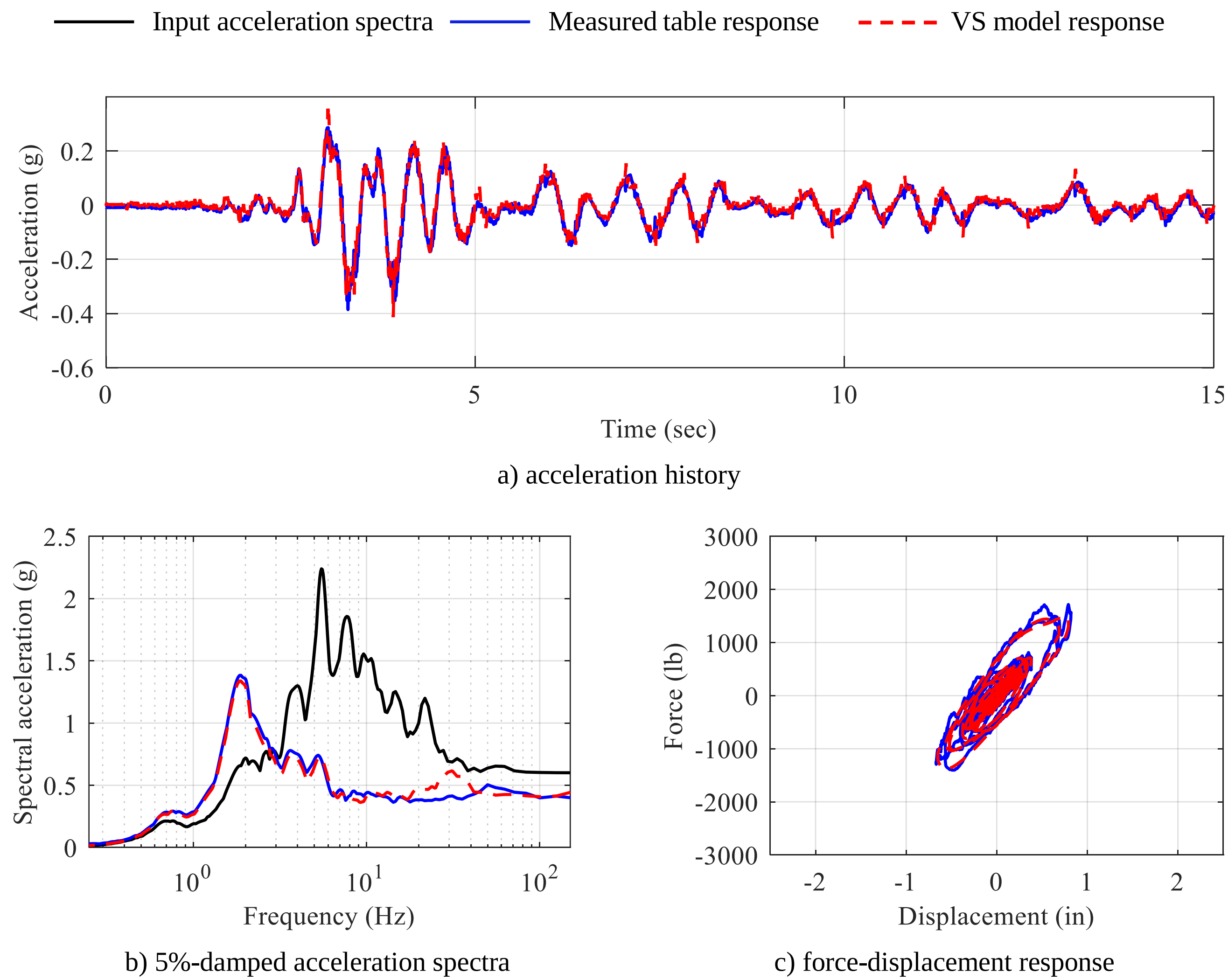

Figure 9.9. Results of MIL experiments imitating SD_3 isolation system subjected to input motion, K_e = 5 V/in, K_p = 0.001 V/psi, f_c = 80 Hz, and τ_s = 500 μs (2000 Hz)

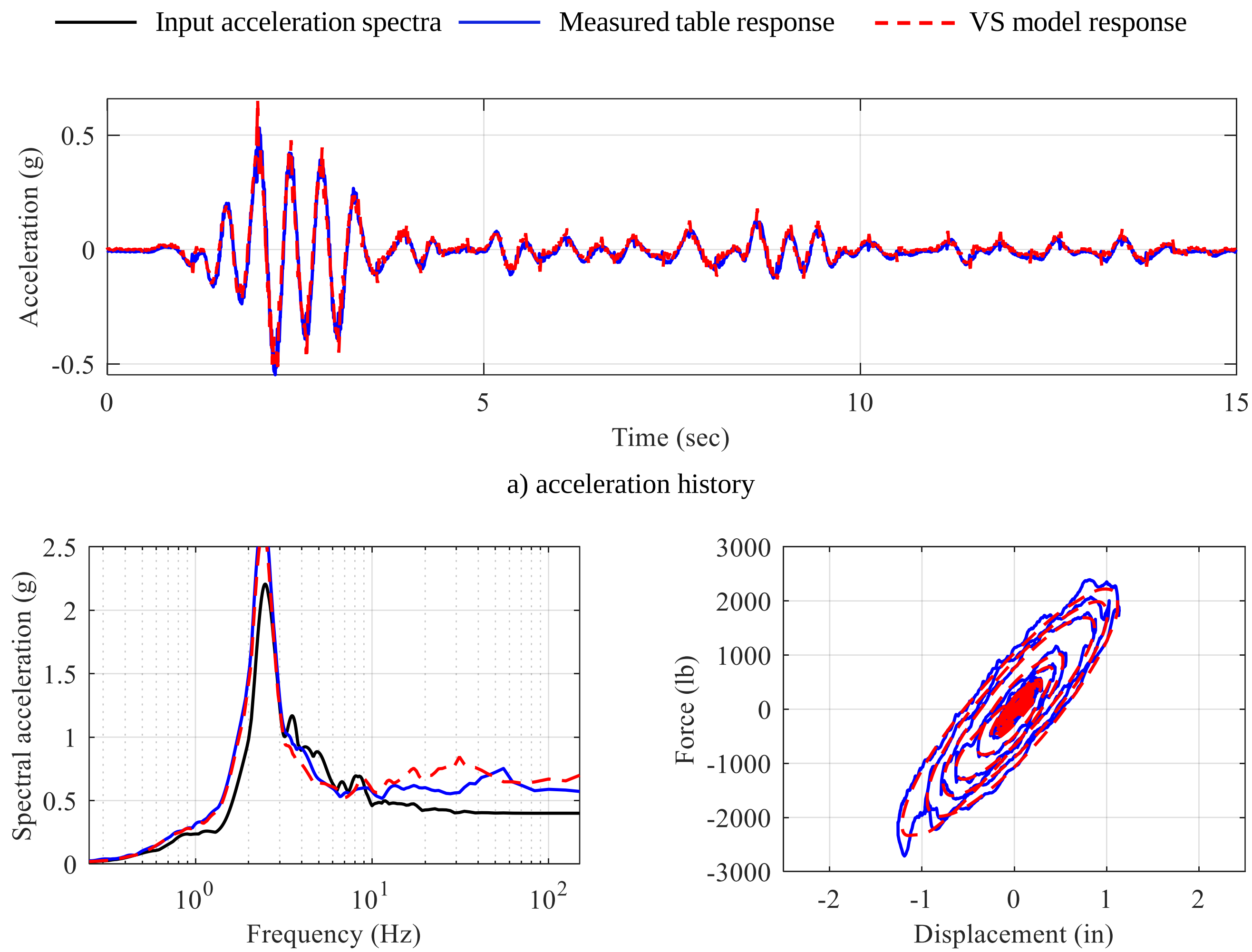

a) acceleration history

b) 5%-damped acceleration spectra

c) force-displacement response

Figure 9.10. Results of MIL experiments imitating SD_3 isolation system subjected to input motion GM_3, K_e = 5 V/in, K_p = 0.001 V/psi, f_c = 80 Hz, and τ_s = 500 μs (2000 Hz)

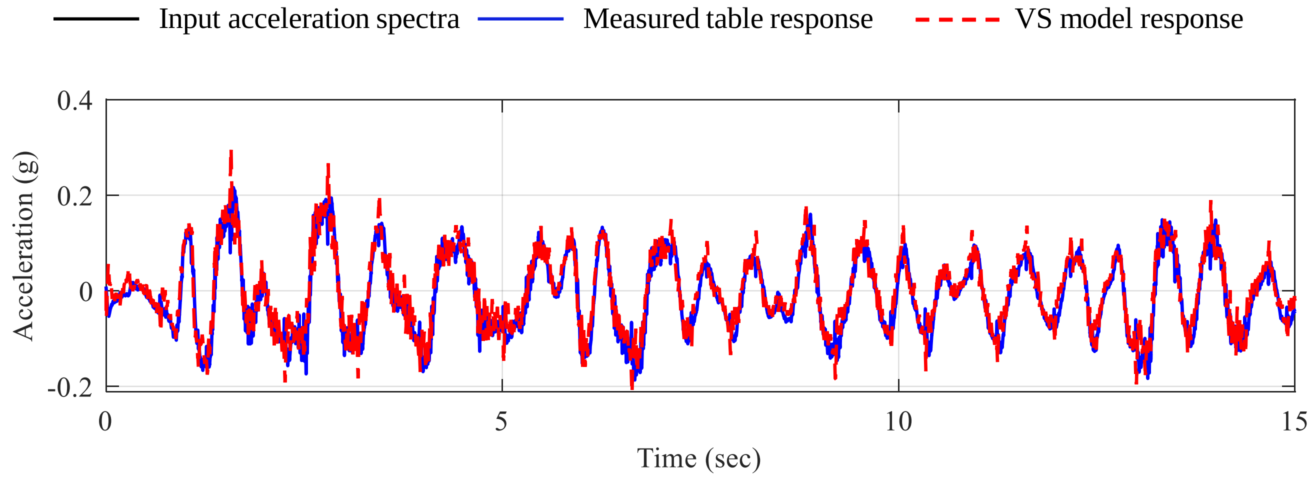

a) acceleration history

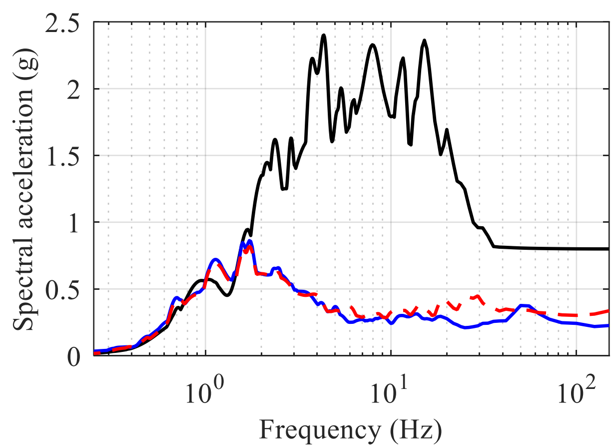

sb) 5%-damped acceleration spectra

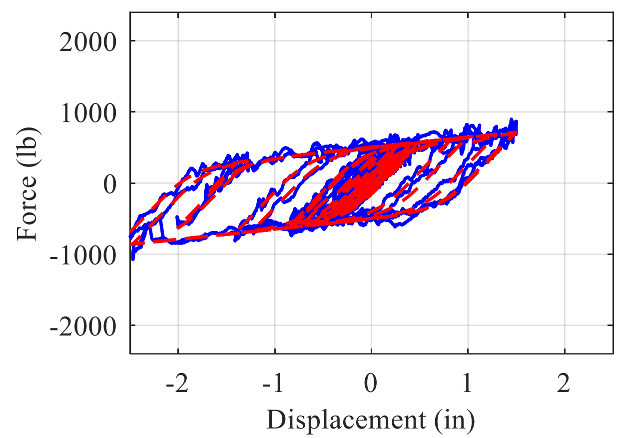

c) force-displacement response

Figure 9.11. Results of MIL experiments imitating LR_1 isolation system subjected to input motion GM_1, K_e = 5 V/in, K_p = 0.001 V/psi, f_c = 80 Hz, and τ_s = 500 μs (2000 Hz)

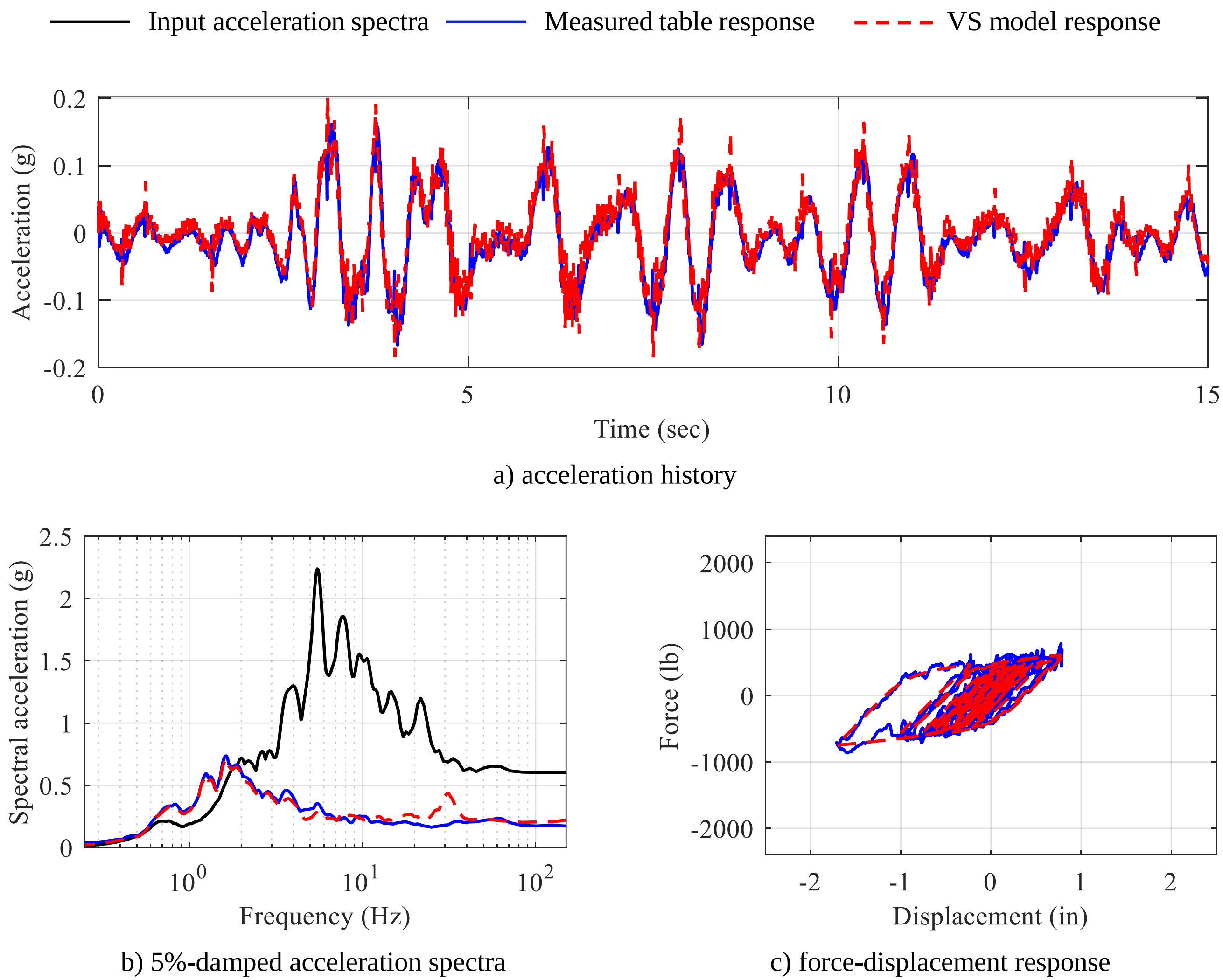

Figure 9.12. Results of MIL experiments imitating LR_1 isolation system subjected to input motion GM_2, K_e = 5 V/in, K_p = 0.001 V/psi, f_c = 80 Hz, and τ_s = 500 μs (2000 Hz)

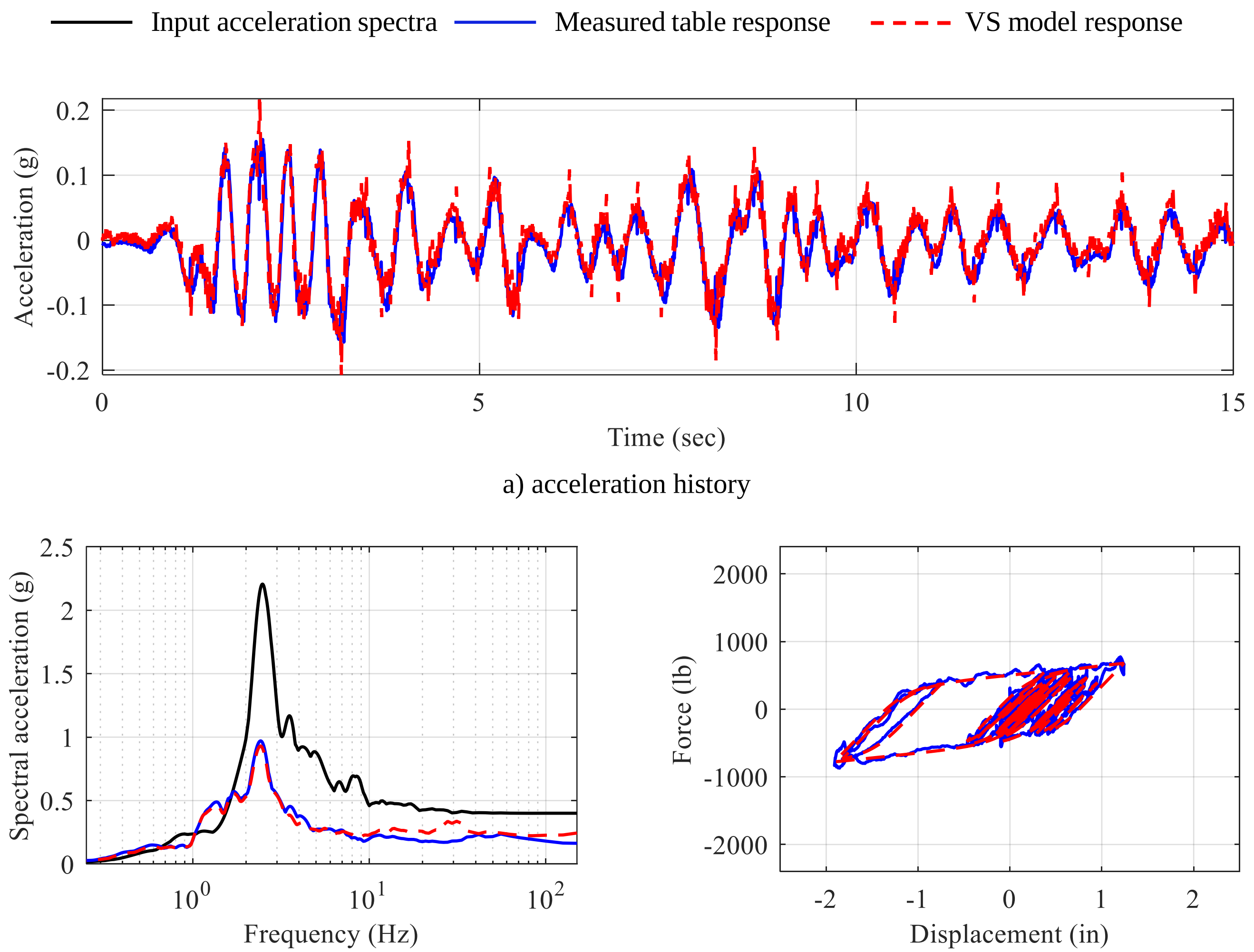

a) acceleration history

b) 5%-damped acceleration spectra

c) force-displacement response

Figure 9.13. Results of MIL experiments imitating LR_1 isolation system subjected to input motion GM_3, K_e = 5 V/in, K_p = 0.001 V/psi, f_c = 80 Hz, and τ_s = 500 μs (2000 Hz)

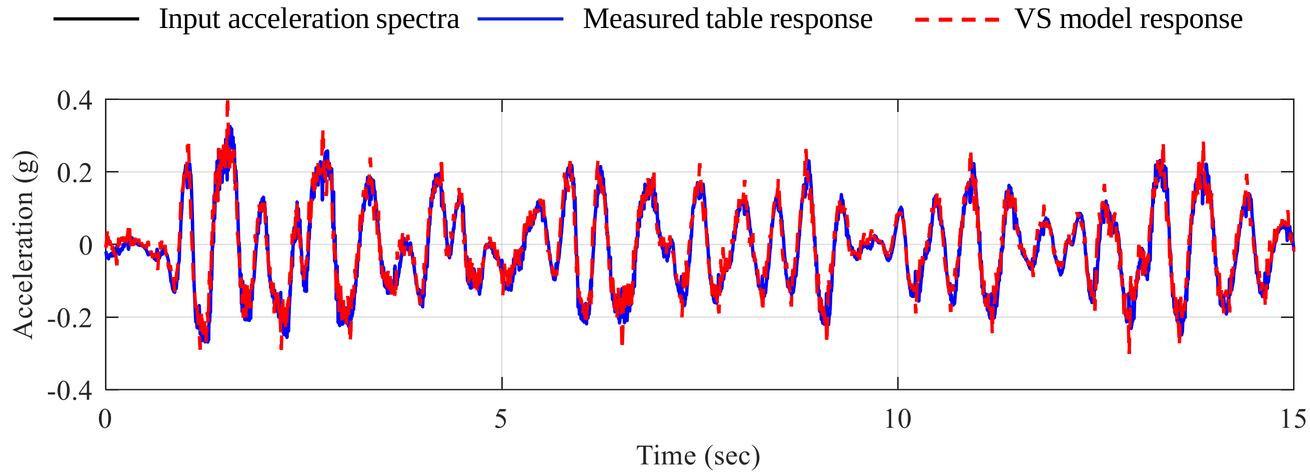

a) acceleration history

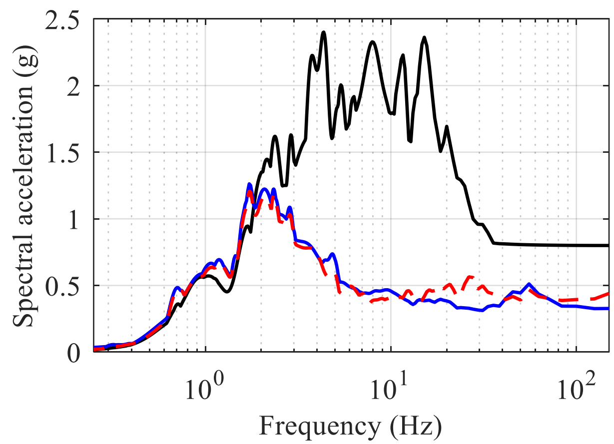

b) 5%-damped acceleration spectra

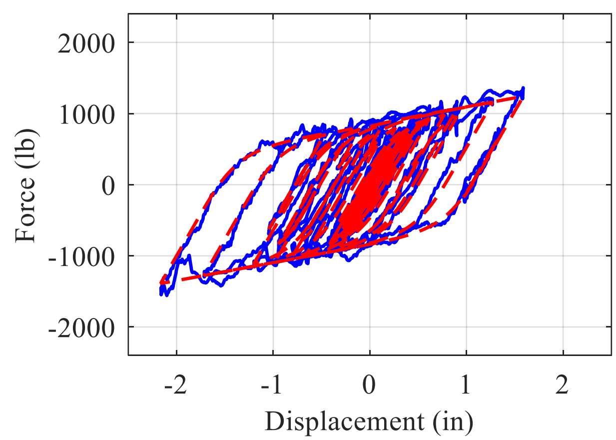

c) force-displacement response

Figure 9.14. Results of MIL experiments imitating LR_2 isolation system subjected to input motion GM_1, K_e = 5 V/in, K_p = 0.001 V/psi, f_c = 80 Hz, and τ_s = 500 μs (2000 Hz)

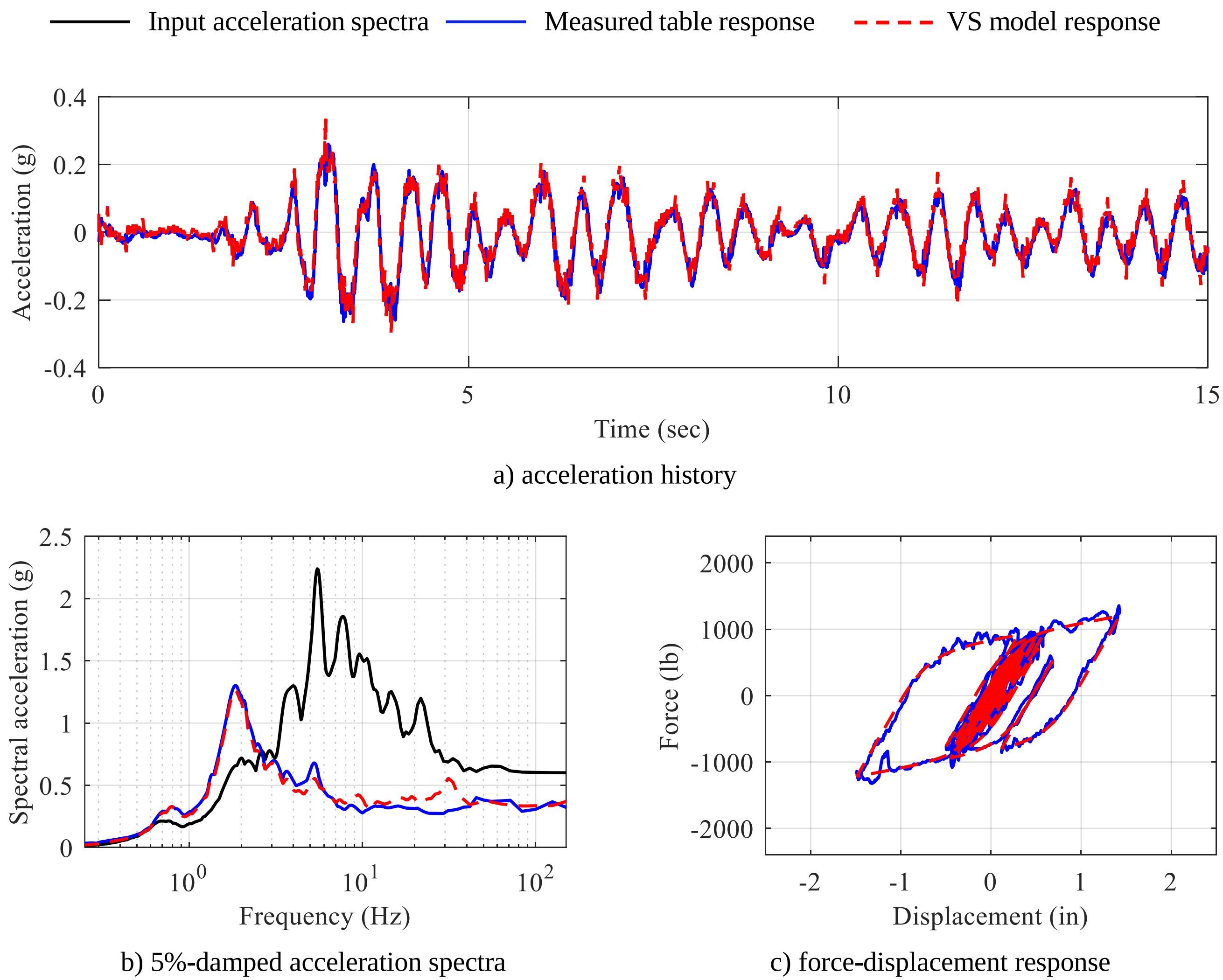

Figure 9.15. Results of MIL experiments imitating LR_2 isolation system subjected to input motion GM_2, K_e = 5 V/in, K_p = 0.001 V/psi, f_c = 80 Hz, and τ_s = 500 μs (2000 Hz)

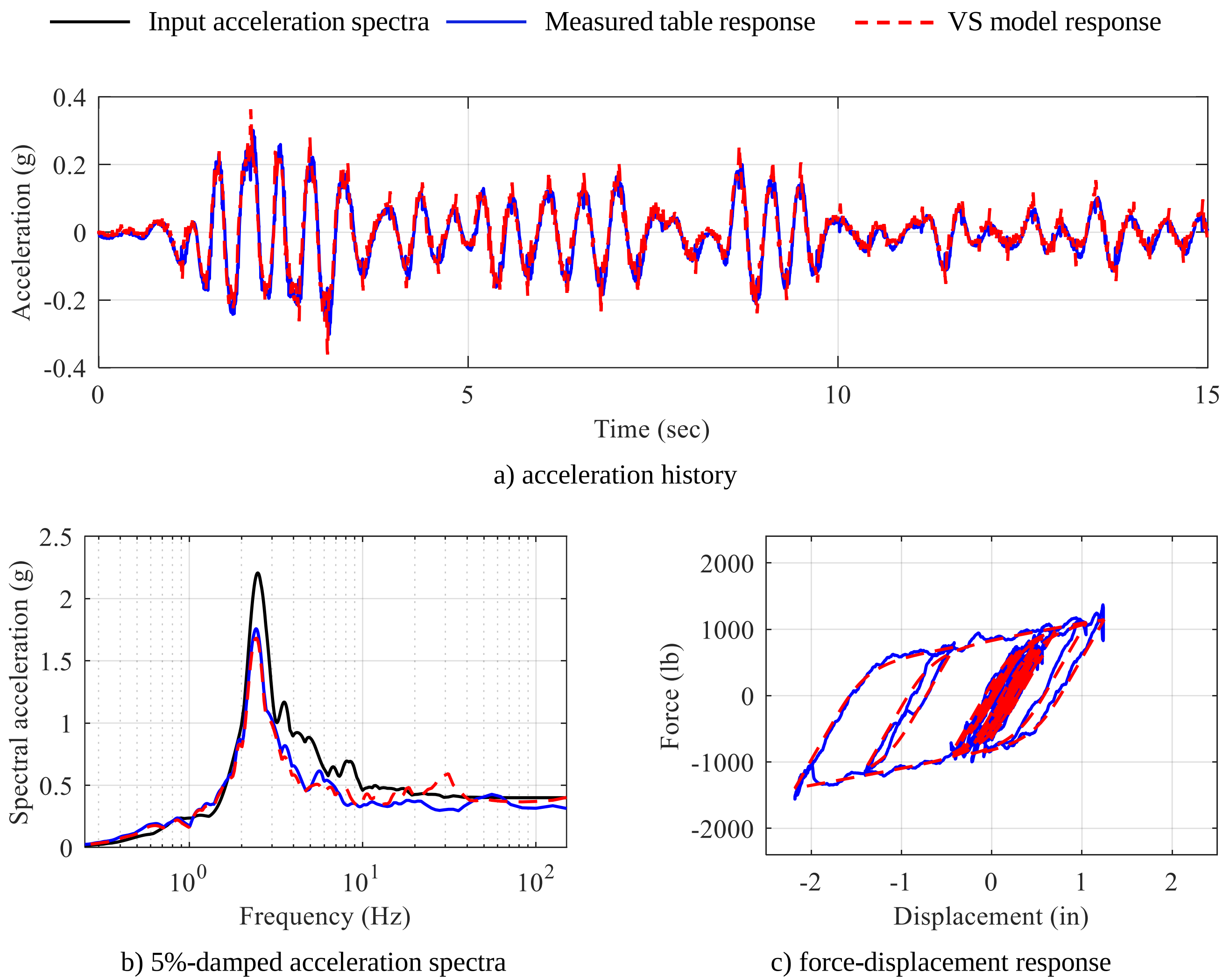

Figure 9.16. Results of MIL experiments imitating LR_2 isolation system subjected to input motion GM_3, K_e = 5 V/in, K_p = 0.001 V/psi, f_c = 80 Hz, and τ_s = 500 μs (2000 Hz)

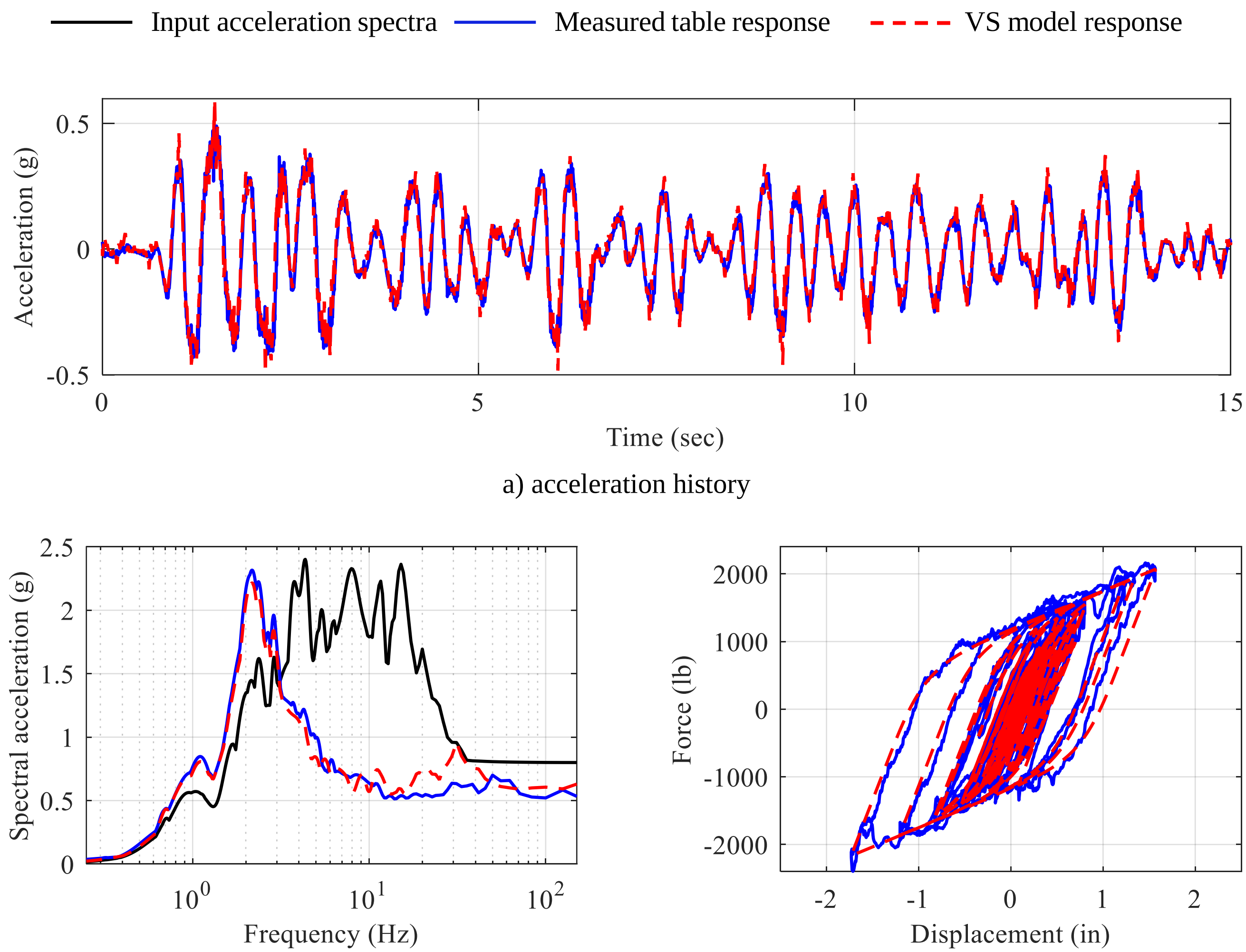

a) acceleration history

b) 5%-damped acceleration spectra

c) force-displacement response

Figure 9.17. Results of MIL experiments imitating LR_3 isolation system subjected to input motion GM_1, K_e = 5 V/in, K_p = 0.001 V/psi, f_c = 80 Hz, and τ_s = 500 μs (2000 Hz)

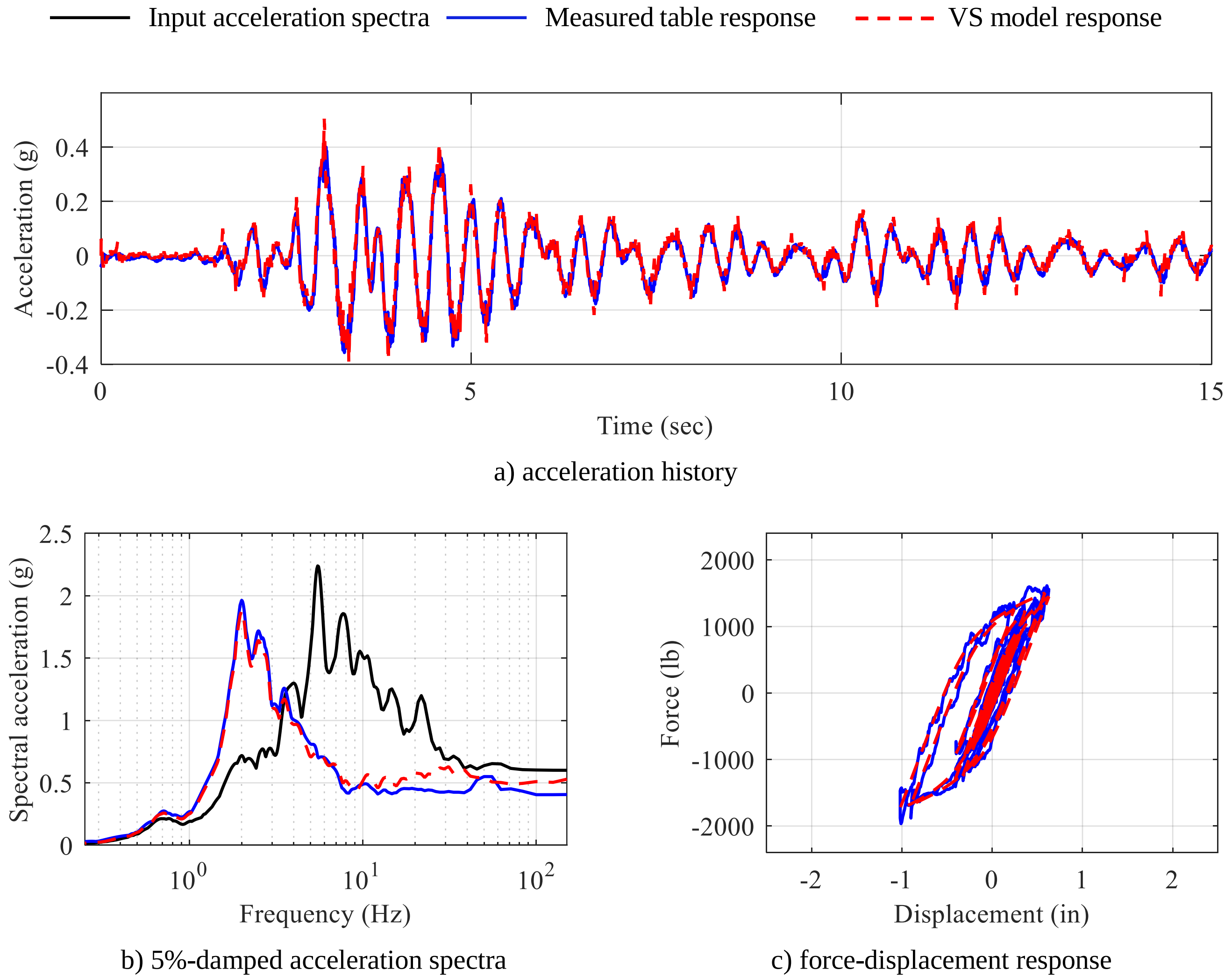

Figure 9.18. Results of MIL experiments imitating LR_3 isolation system subjected to input motion GM_2, K_e = 5 V/in, K_p = 0.001 V/psi, f_c = 80 Hz, and τ_s = 500 μs (2000 Hz)

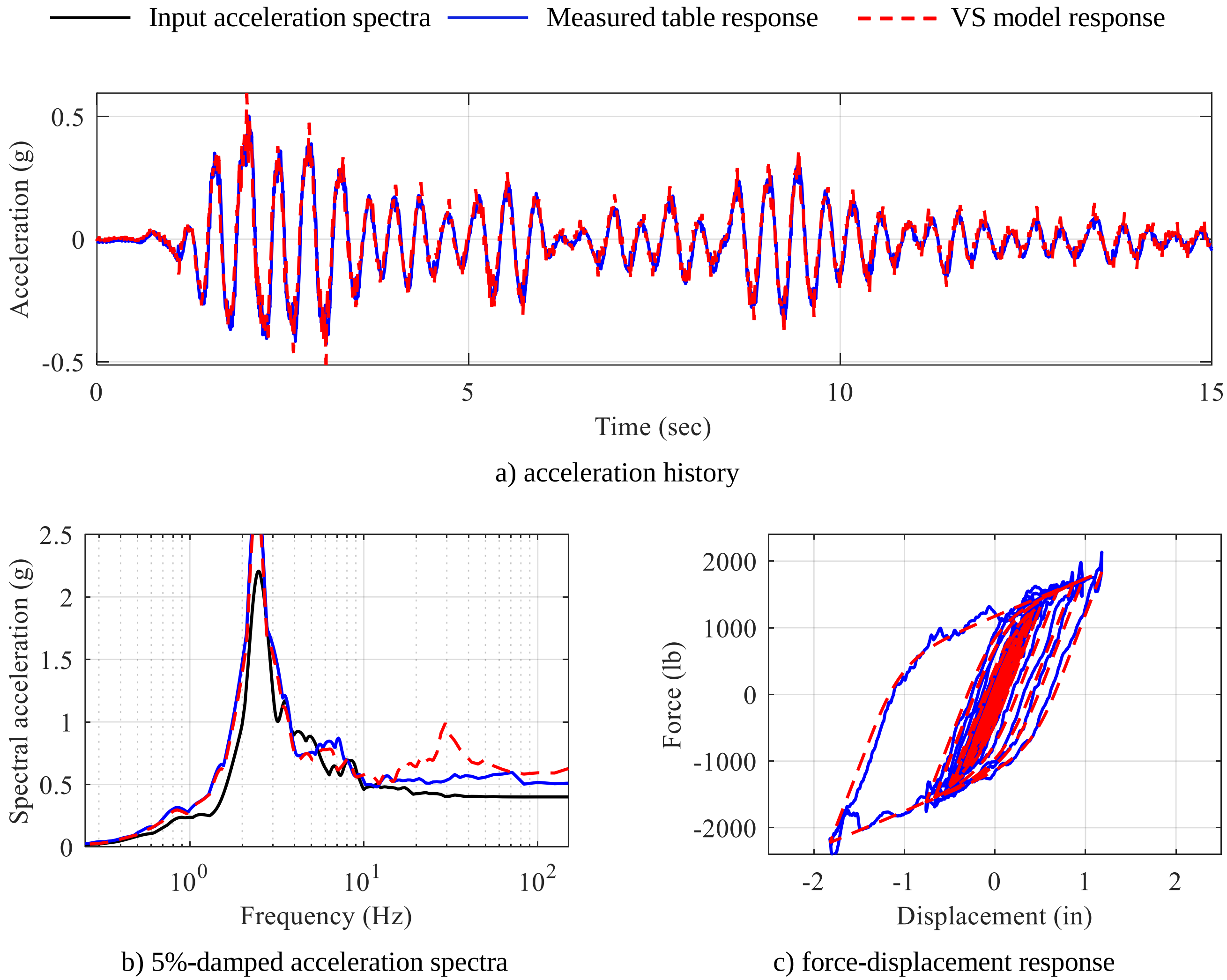

Figure 9.19. Results of MIL experiments imitating LR_3 isolation system subjected to input motion GM_3, K_e = 5 V/in, K_p = 0.001 V/psi, f_c = 80 Hz, and τ_s = 500 μs (2000 Hz)

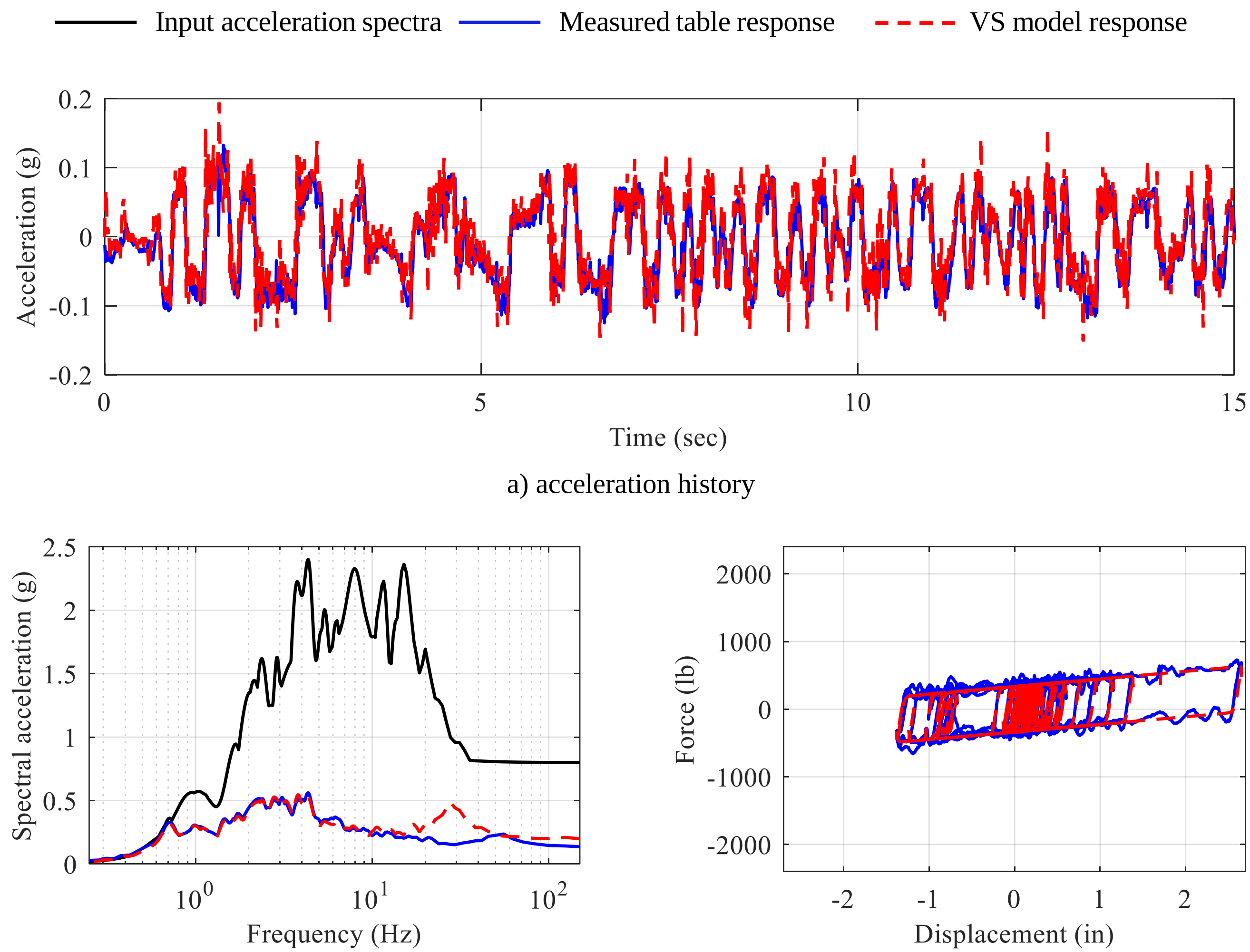

a) acceleration history

b) 5%-damped acceleration spectra

c) force-displacement response

Figure 9.20. Results of MIL experiments imitating FP_1 isolation system subjected to input motion GM_1, K_e = 5 V/in, K_p = 0.001 V/psi, f_c = 80 Hz, and τ_s = 500 µs (2000 Hz)

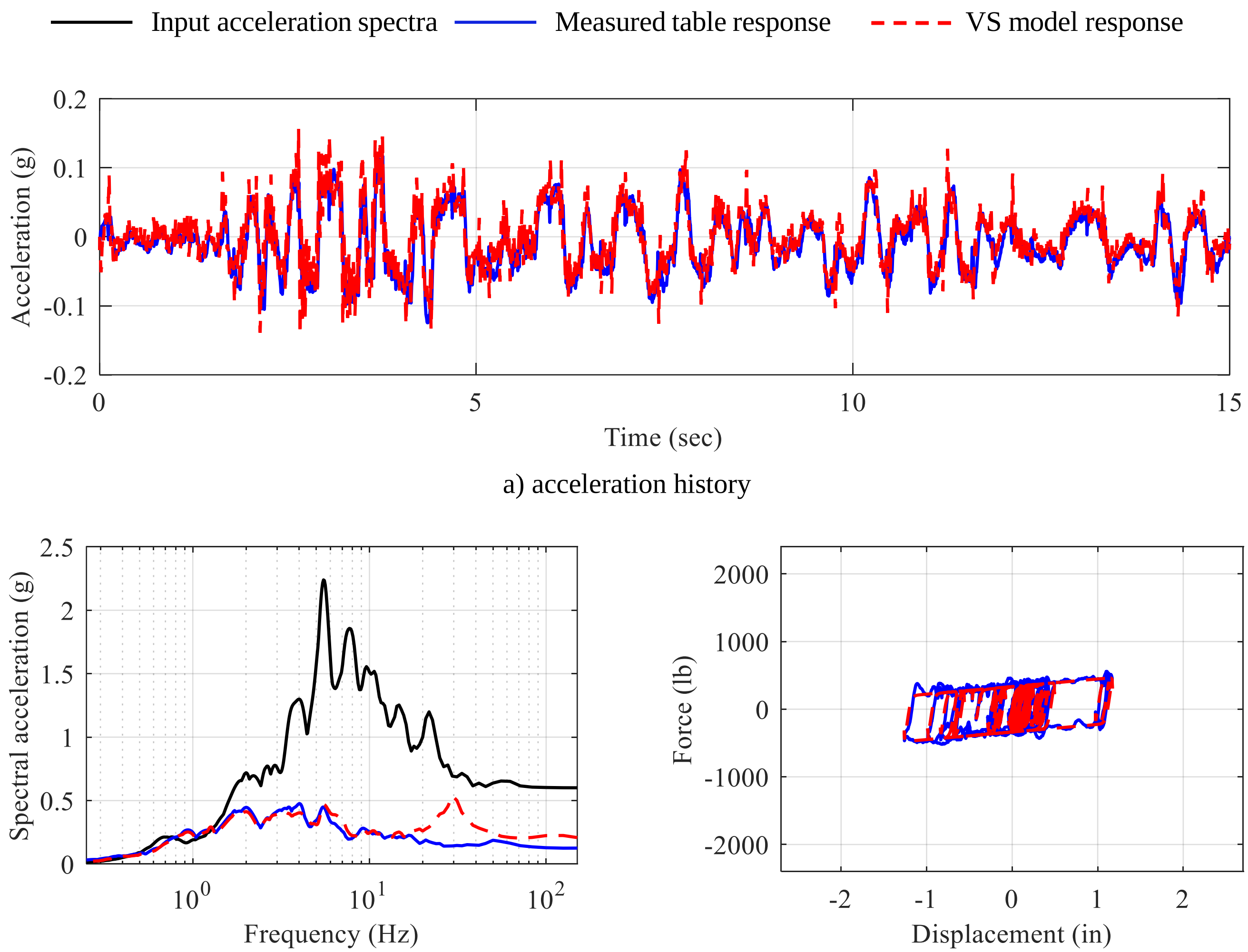

a) acceleration history

b) 5%-damped acceleration spectra

c) force-displacement response

Figure 9.21. Results of MIL experiments imitating FP_1 isolation system subjected to input motion GM_2, K_e = 5 V/in, K_p = 0.001 V/psi, f_c = 80 Hz, and τ_s = 500 μs (2000 Hz)

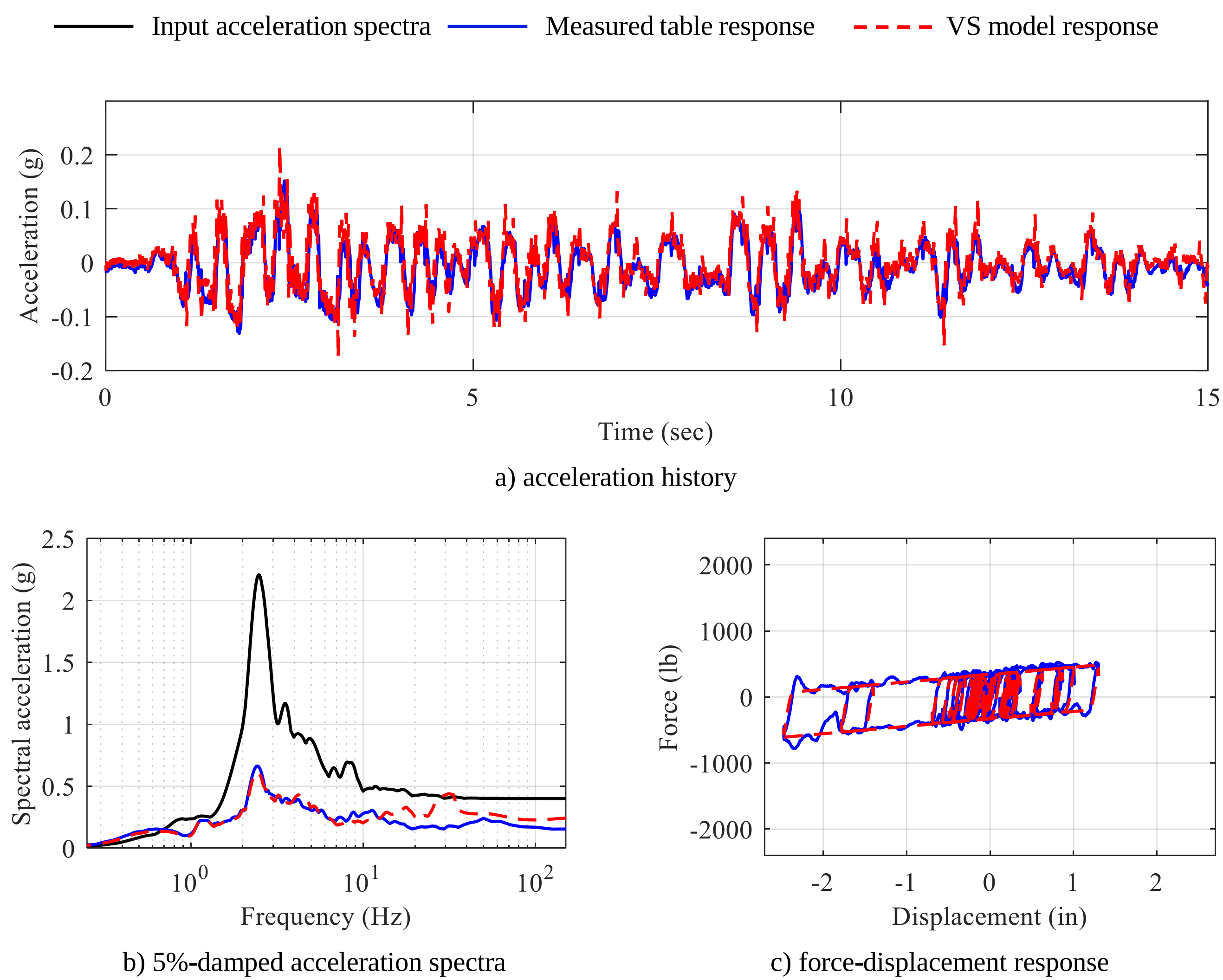

Figure 9.22. Results of MIL experiments imitating FP_1 isolation system subjected to input motion GM_3, K_e = 5 V/in, K_p = 0.001 V/psi, f_c = 80 Hz, and τ_s = 500 μs (2000 Hz)

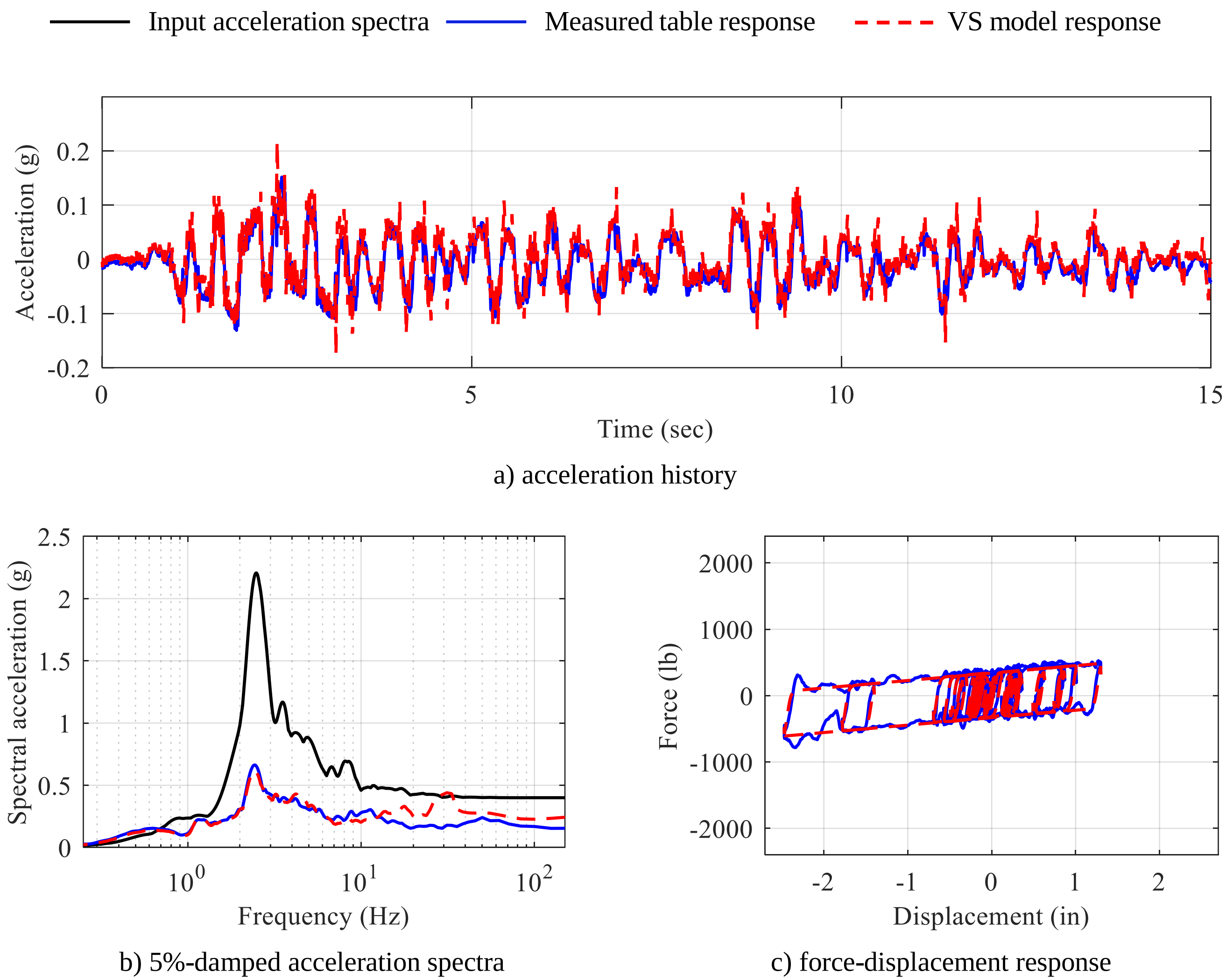

Figure 9.23. Results of MIL experiments imitating FP_2 isolation system subjected to input motion GM_1, K_e = 5 V/in, K_p = 0.001 V/psi, f_c = 80 Hz, and τ_s = 500 μs (2000 Hz)

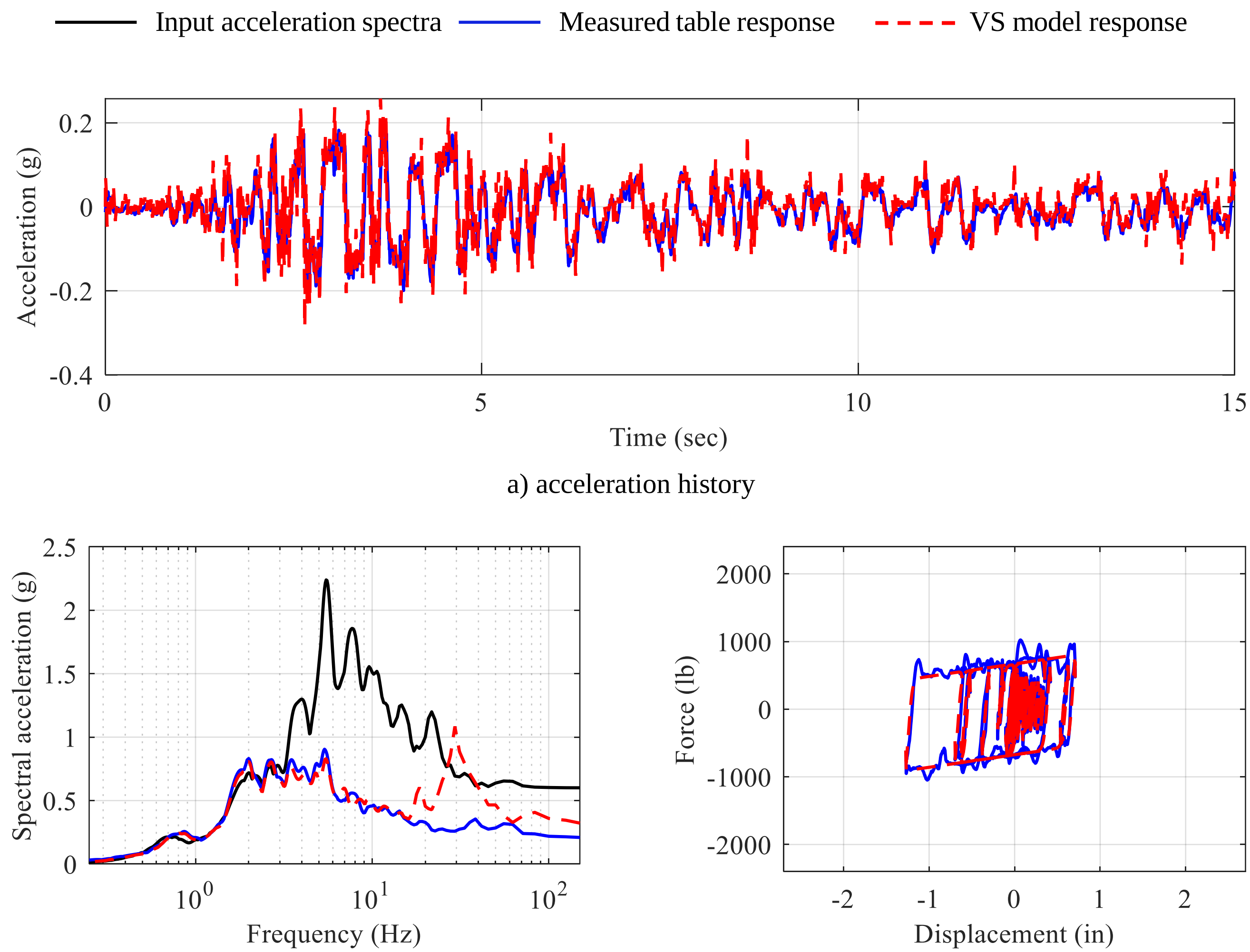

a) acceleration history

b) 5%-damped acceleration spectra

c) force-displacement response

Figure 9.24. Results of MIL experiments imitating FP_2 isolation system subjected to input motion GM_2, K_e = 5 V/in, K_p = 0.001 V/psi, f_c = 80 Hz, and τ_s = 500 μs (2000 Hz)

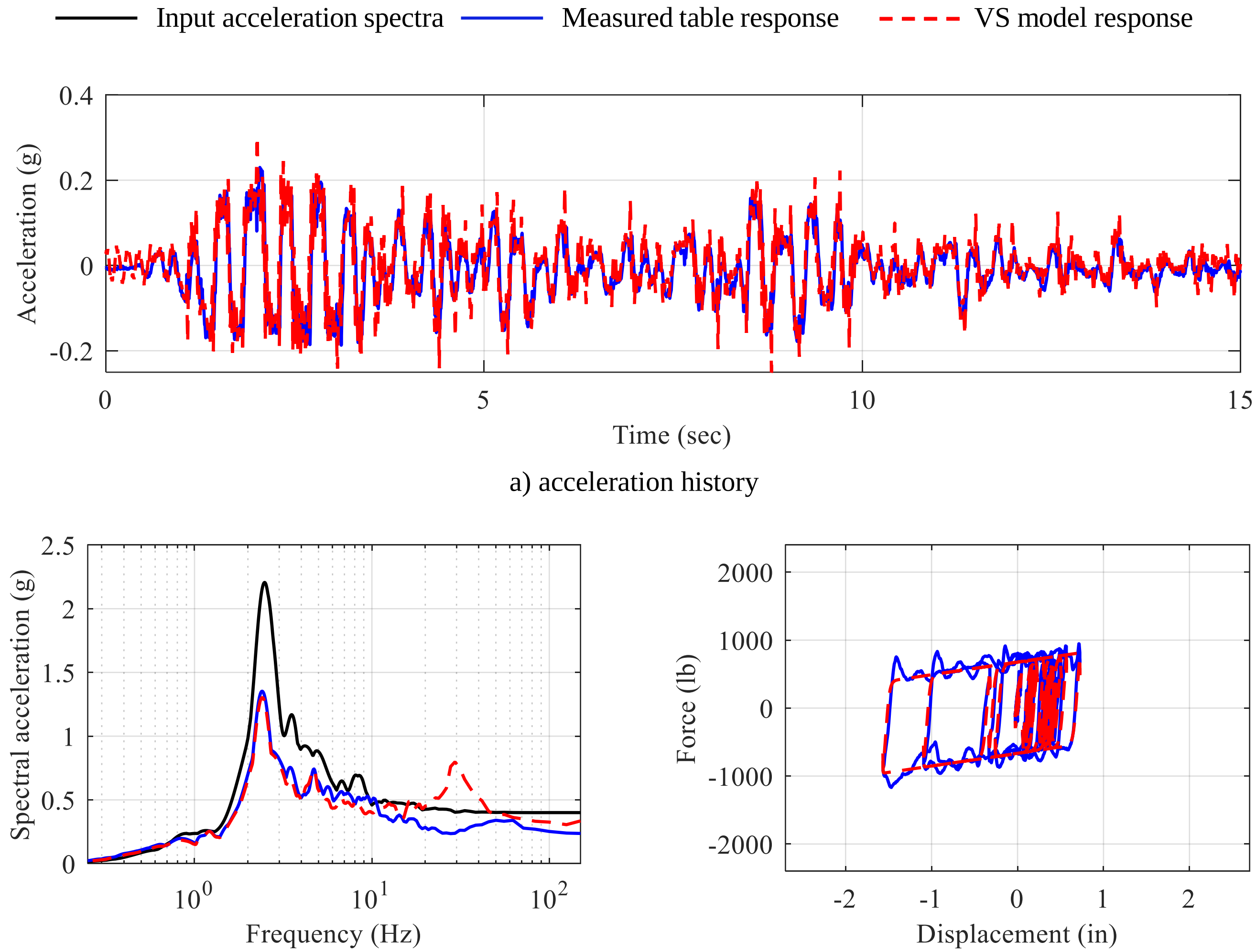

a) acceleration history

b) 5%-damped acceleration spectra

c) force-displacement response

Figure 9.25. Results of MIL experiments imitating FP_2 isolation system subjected to input motion GM_3, K_e = 5 V/in, K_p = 0.001 V/psi, f_c = 80 Hz, and τ_s = 500 µs (2000 Hz)

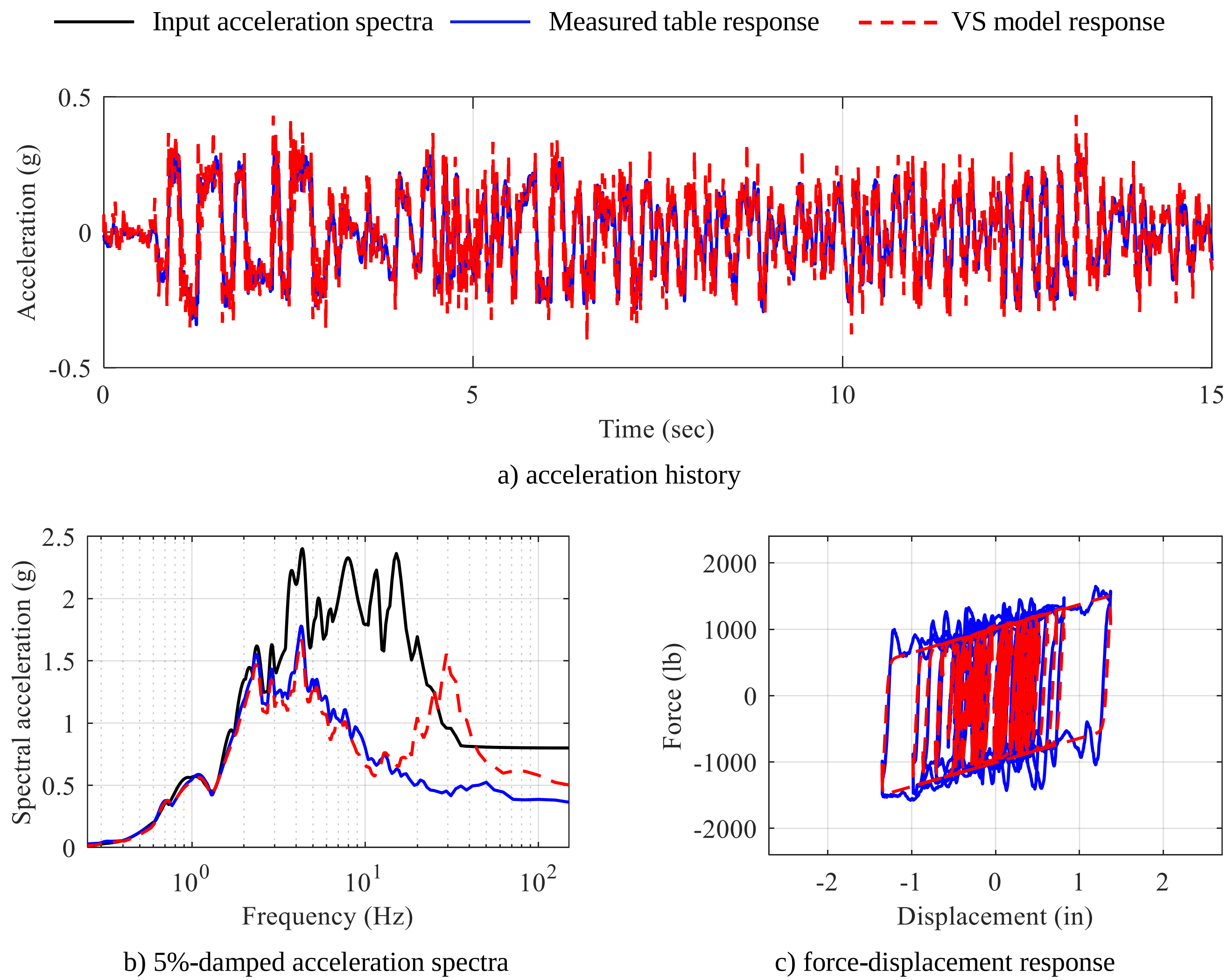

Figure 9.26. Results of MIL experiments imitating FP_3 isolation system subjected to input motion GM_1, K_e = 5 V/in, K_p = 0.001 V/psi, f_c = 80 Hz, and τ_s = 500 μs (2000 Hz)

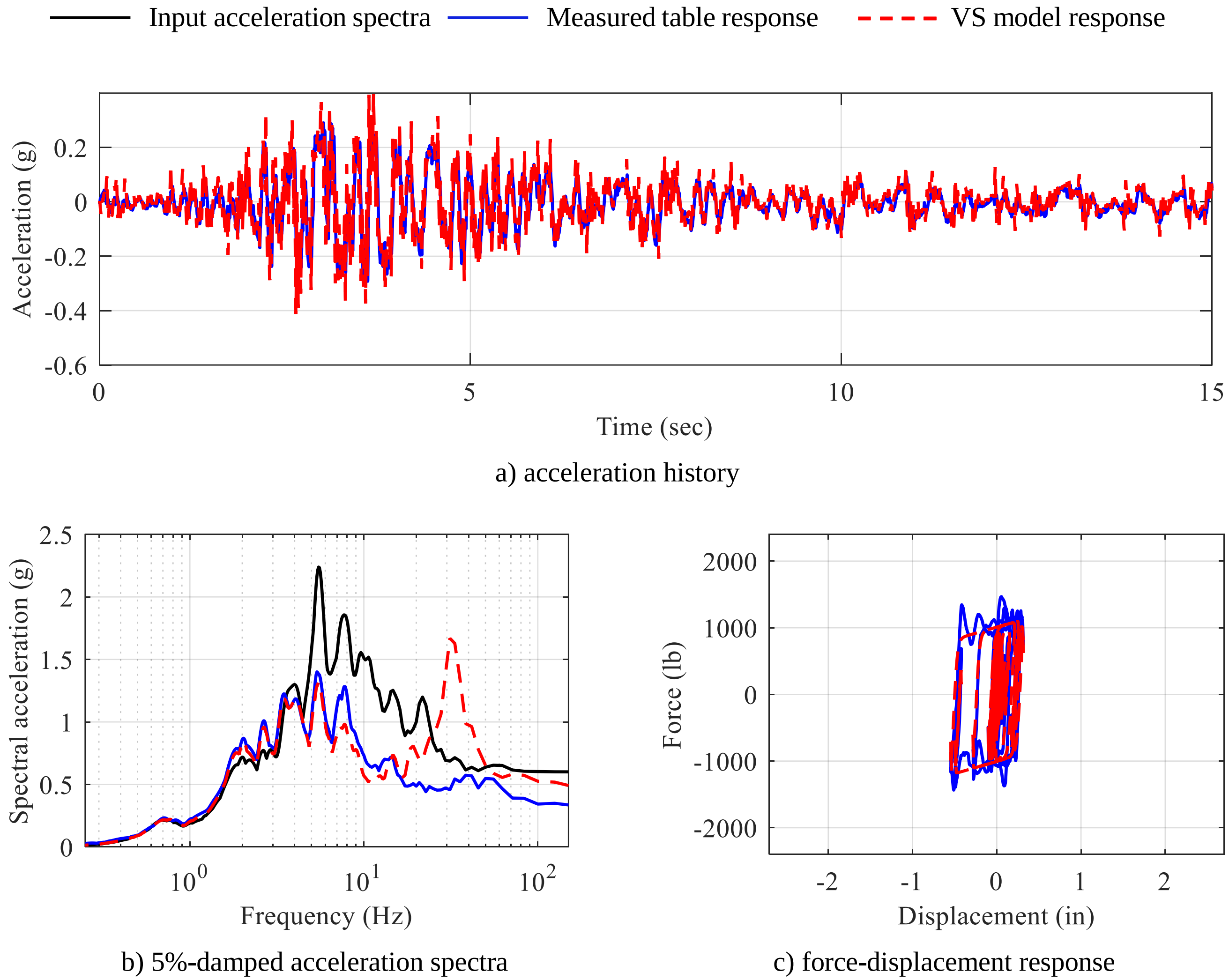

Figure 9.27. Results of MIL experiments imitating FP_3 isolation system for subjected to input motion GM_2, K_e = 5 V/in, K_p = 0.001 V/psi, f_c = 80 Hz, and τ_s = 500 µs (2000 Hz)

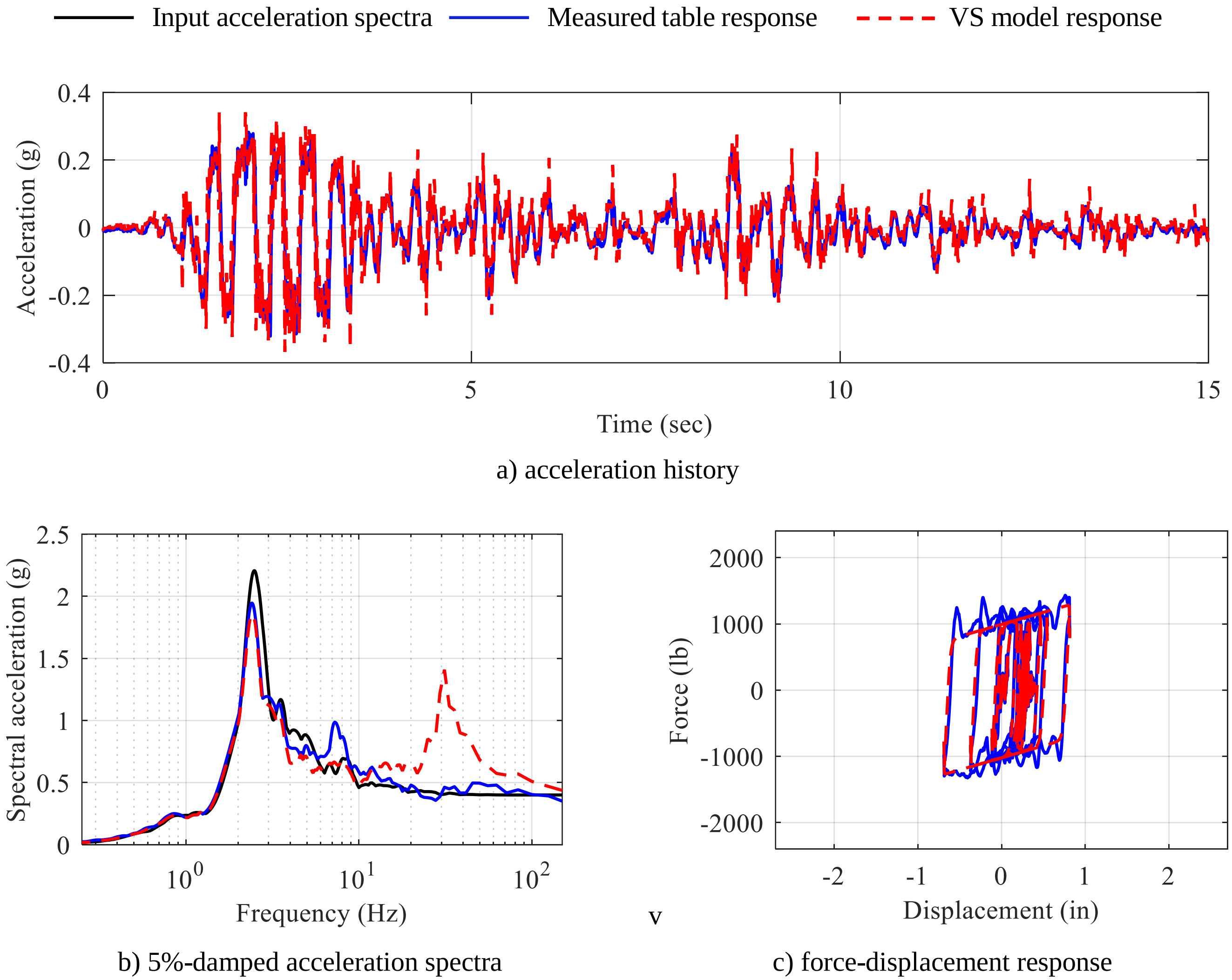

Figure 9.28. Results of MIL experiments imitating FP_3 isolation system subjected to input motion GM_3, K_e = 5 V/in, K_p = 0.001 V/psi, f_c = 80 Hz, and τ_s = 500 μs (2000 Hz)

The close agreement between the blue and red acceleration histories in Figures 9-2 through 9-28 show that the shake table with the designed MIL controls is able to imitate the target VS acceleration accurately at the base of the test article in most tests. The spectral accelerations are shown to agree well in the frequency range of 0.25 Hz to 15 Hz, but with reduced accuracy at higher frequencies (15+Hz, see Figure 9.26b for example). The difference between the two responses after 15+ Hz is small for the SD and LR systems but substantial for the FP systems. The higher the initial stiffness of the isolation system, the poorer the performance (see Figures 9-20c for FP_1 and 9-22c for FP_3 with an initial stiffness thrice that of FP_1). The reasons for these trends are examined in Section 9.3.

The results presented in Figures 9-2 through 9-29 illustrate that MIL testing enables the use of a standardized setup, herein a shake table equipped with the MIL controls, for simulating boundary conditions corresponding to different seismic isolation systems at the base of a test article. This outcome is achieved by simply changing the isolation system properties, such as k_s, μ_{max} etc., in the RMC user programs (see the block of code enclosed by the open green rectangle in Figure 7.9).

Figure 9.29 is an alternate presentation of the MIL results, wherein acceleration response spectra corresponding to the nine isolation systems, as imitated by the shake table, is plotted in one graph. Although the nine isolation systems respond very differently to the same input motion (herein GM_1), these boundary conditions are imitated at the base of the test article using one standardized MIL test setup and standardized controller (enabled by the impedance-matching pathway). Accordingly, using appropriate MIL controls, structures, systems, or components can be tested and qualified for multiple boundary environments without physically constructing the components of the environment, and importantly, the testing accounts for the real-time interaction between the test article and its environment.

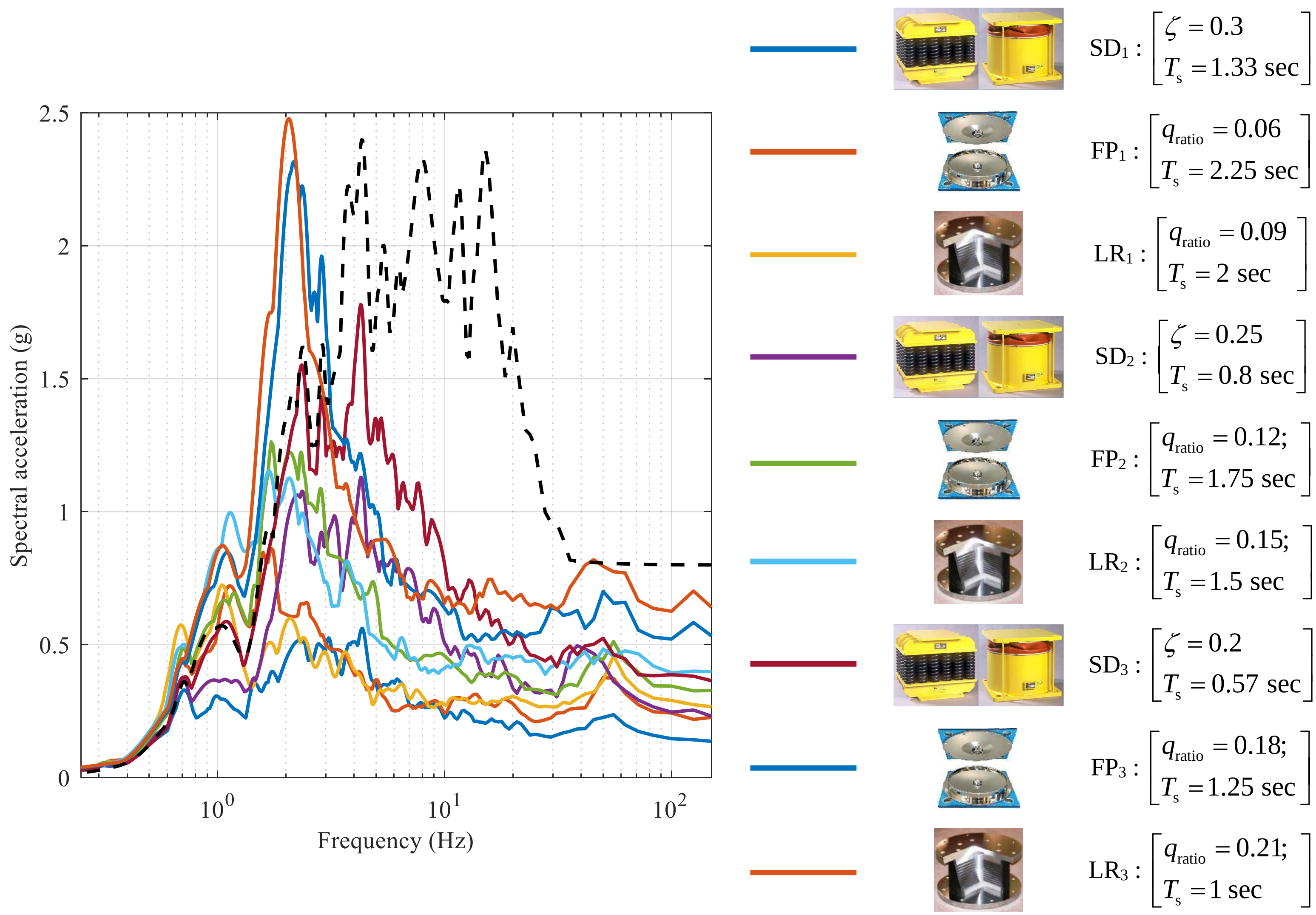

Figure 9.29. Response spectra (5% damped) of the measured shake-table acceleration imitating different seismic isolation systems; GM_1

9.4 Fundamental limitations to MIL testing

9.4.1 Overview

In Section 9.3, the poorer MIL performance at high frequencies (> 15 Hz) backstops the fact that it is practically challenging (and often impossible) to control one dynamic system to imitate the impedance of another accurately across all frequencies. This is because the two systems will generally have different dynamic characteristics. For the designed MIL controls, the shake table may represent an isolation system accurately over a certain frequency range and with reduced (or poorer) accuracy at other frequencies.

Additionally, there are some fundamental limitations to what can be achieved with controls, which are framed herein as tradeoffs between performance and stability. In the presentation to follow, performance is assessed by qualitative evaluation of how closely the shake table equipped with the designed MIL controls (hereafter referred to as 'controlled shake table') imitates the impedance of the desired VS, and stability of the shake table-test article feedback system is assessed using the notion of passivity.

9.4.2 Passivity and its assessment for linear systems

9.4.2.1 Passivity

In a MIL test, the shake table and the test article are a coupled feedback system. The shake table controls acceleration (applied condition) at the interface and the test article controls force (feedback condition). Conventionally, stability of this coupled feedback system is ensured by designing a MIL controller (using nominal properties of the test article) with sufficiently large gain and phase margins. However, this approach makes necessary knowledge of the dynamics of the test article.

In this report (and in the impedance-matching approach in general), stability of the coupled shake table-test article system is ensured using the notion of passivity. A system is said to be passive if it cannot generate more energy than what has been input to it. When two passive systems are in feedback interaction, the coupled system is guaranteed to be stable (Brogliato *et al.*, 2007). In the MIL experiments, the test article is passive because it cannot generate energy. Therefore, the feedback system will be stable if the shake table+controller is passive, making it an important design criterion for the MIL controller. The advantage of enforcing passivity is that stability can be ensured independent of knowledge of the dynamics of the test article – a prime contrast between the traditional approaches to MIL (Section 2.1) and the way MIL is implemented herein.

9.4.2.2 Assessment of passivity for linear systems

As noted above, a passive system cannot generate more energy than what has been input to it. This is true for a linear system if the work done over one cycle at steady state, at any frequency, is positive. Positive work is guaranteed if the phase difference between the force and velocity (work conjugate variables) at the system interface, at steady state, does not exceed 90°. To understand this, let the interface force and velocity, at steady state, at frequency ω, be $F_{\mathrm{o}} \sin(\omega t)$ and $v_{\mathrm{o}} \sin(\omega t + \varphi)$, respectively. The work done over one cycle is:

$$W_{\mathrm{cycle}} = \int_0^T \left(F_{\mathrm{o}} \sin(\omega t)\right)\left(v_{\mathrm{o}} \sin(\omega t + \varphi)\right) \, \mathrm{dt} \tag{9-1a}$$

$$W_{\mathrm{cycle}} = \frac{F_{\mathrm{o}} v_{\mathrm{o}}}{2} \int_0^T \left(\cos(\varphi) - \cos(\omega t + \varphi)\right) \, \mathrm{dt} \tag{9-1b}$$

$$W_{\mathrm{cycle}} = \frac{F_{\mathrm{o}} v_{\mathrm{o}}}{2} \left[\cos(\varphi) T - \frac{1}{2\omega}\left[\sin(\omega t + \varphi)\right]_0^{\frac{2\pi}{\omega}}\right] \tag{9-1c}$$

$$W_{\mathrm{cycle}} = \frac{\pi F_{\mathrm{o}} v_{\mathrm{o}}}{\omega} \cos(\varphi) \tag{9-1d}$$

From above, the work done is positive if $\cos(\varphi) > 0$, meaning that φ must be between -90° and +90°. Therefore, a system is passive if the phase difference between the interface force and velocity, at steady state, is within $\pm 90°$. For linear systems, this condition can be evaluated using Bode or Nyquist plots of the corresponding force-velocity transfer function. The Bode phase response must not exceed the $\pm 90°$ bounds and/or the Nyquist plot must completely lie in the right half-plane.

As an example, Figures 9-30a and 9-30b present Bode and Nyquist plots of the force-velocity[32] transfer function of the SD2 system, namely, $H_{vw}^{\mathrm{vs}} = s \big/ \left(m_{\mathrm{vs}} s^2 + cs + k_{\mathrm{s}}\right)$, wherein $m_{\mathrm{vs}} = 1.25\, m_{\mathrm{st}}$, $k_{\mathrm{s}} = 894$ lb/in, and $c = 57$ lb-s/in. The Nyquist plot of this transfer function is shown to lie in the right half-plane confirming passivity of the VS.

---

[32] The impedance (i.e., force-acceleration transfer function) of the spring-damper isolation system is given by Equation 5-2b, as $H_{zw}^{\mathrm{vs}} = s^2 \big/ \left(m_{\mathrm{vs}} s^2 + cs + k_{\mathrm{s}}\right)$. The corresponding force-velocity transfer function is obtained by multiplying the integrator operator ($1/s$ in the frequency domain) to this transfer function.

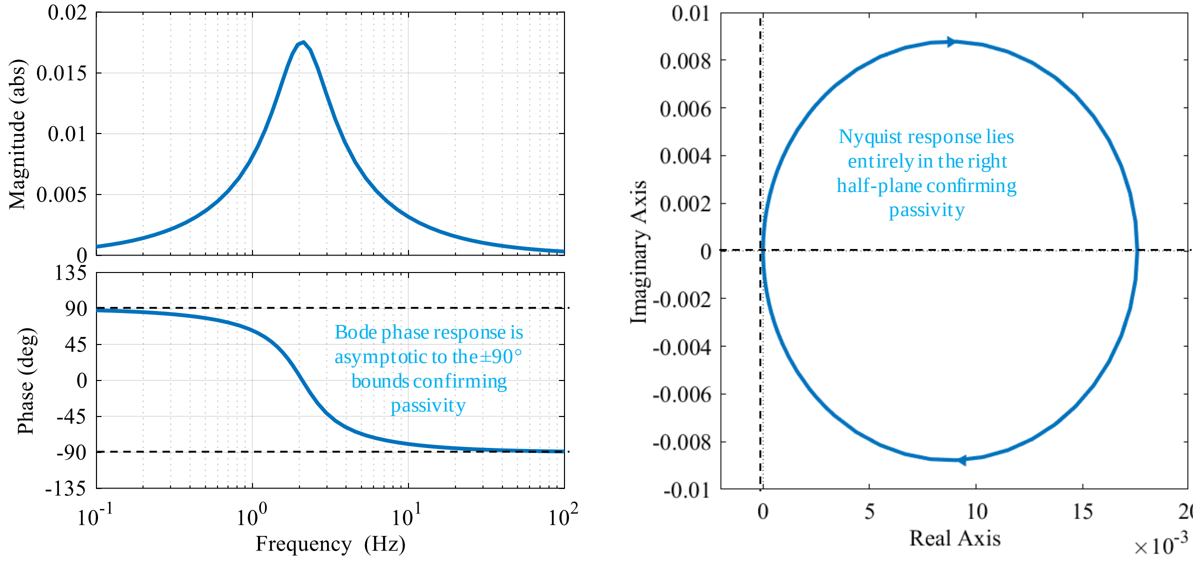

a) Bode plot b) Nyquist plot

Figure 9.30. Bode and Nyquist plots of the force-velocity transfer function of the SD_2 system

9.4.2.3 Force-velocity transfer function of the controller shake table

As conceptualized in Section 1, the acceleration of the shake-table platform can be written in the linear form as: $z_{\mathrm{st}} = H_{zu}^{\mathrm{st}} u + H_{zw}^{\mathrm{st}} w$. In the absence of a_{g}, the control input to the actuator is given by $u = H_{uw} w$. Combining the two expressions, the force-acceleration relationship of the controlled shake table is: $z_{\mathrm{st}} = \left(H_{zw}^{\mathrm{st}} + H_{zu}^{\mathrm{st}} H_{uw} \right) w$. For imitating a linear virtual system with an impedance of H_{zw}^{vs}, the controller H_{uw} takes the form: $H_{uw} = \left(H_{zu}^{\mathrm{st}} \right)^{-1} H_{w}^{\mathrm{filter}} \left(H_{zw}^{\mathrm{vs}} - H_{zw}^{\mathrm{st}} \right) w$.

From above, the force-acceleration transfer function of the controlled shake table is reduced to the form: $z_{\mathrm{st}} = \left(H_{zw}^{\mathrm{st}} + \left(H_{zw}^{\mathrm{vs}} - H_{zw}^{\mathrm{st}} \right) H_{w}^{\mathrm{filter}} \right) w$. The corresponding force-velocity transfer function is obtained by multiplying the integrator operator ($1/s$, in the frequency domain) as:

$$H_{vw}^{\mathrm{st}} = \frac{v_{\mathrm{st}}}{w} = \frac{1}{s} \left(H_{zw}^{\mathrm{st}} + \left(H_{zw}^{\mathrm{vs}} - H_{zw}^{\mathrm{st}} \right) H_{w}^{\mathrm{filter}} \right) \tag{9-2}$$

The controlled shake table system is passive if the Nyquist plot of the above transfer function lies in the right half-plane. The Nyquist response, and by extension passivity of the controlled shake table, depends on: (i) the VS properties (e.g., m_{vs}, k_{s}), which appear in the term H_{zw}^{vs}, (ii) the shake-table properties (e.g., m_{st}, K_{e}, K_{p}), which appear in the term H_{zw}^{st}, and (iii) filter properties (e.g., order, cutoff frequency), which define the form of H_{w}^{filter}.

9.4.3 Understanding performance tradeoffs introduced by the lowpass filters

In this report, the MIL controller is approximated using lowpass filters. Typically, the order of the filter is selected based on the degree of non-causality of $\left(H_{zu}^{\mathrm{st}}\right)^{-1}$, thus leaving its cutoff frequency, f_{c}, as the only design parameter. The cutoff frequency of the filter, f_{c}, needs to be small enough to limit the controller response at high frequencies where the shake-table model is poor and the measurement noise in w is large. However, reducing the value of f_{c} too much penalizes performance, that is, the output of the controlled shake table differs substantially from that of the VS. In some cases, this deviation may be large enough that although the VS is passive, the controlled shake-table system can inject energy into the system (violating passivity), again leading to instability. Thus, there is range of cutoff frequencies in which both acceptable performance and stability can be achieved.

Figure 9.31 makes clear these tradeoffs of f_{c}. Herein, important responses of the VS (SD_2 isolation system) and the controlled shake table are plotted for decreasing values of filter cutoff frequency: 1000 Hz, 250 Hz, 100 Hz, and 50 Hz. The column to the left presents Bode plots of the VS and the shake-table impedances (i.e., their force-acceleration transfer functions). The central column presents the frequency response of the MIL controller, $H_{uw}^{\mathrm{controller}} = H_{w}^{\mathrm{filter}}\left(H_{zu}^{\mathrm{st}}\right)^{-1}\left(H_{zw}^{\mathrm{vs}} - H_{zw}^{\mathrm{st}}\right)$. The column to the right presents Nyquist plots of the force-velocity transfer function for the controlled shake table, namely, $\left(H_{zw}^{\mathrm{st}} + \left(H_{zw}^{\mathrm{vs}} - H_{zw}^{\mathrm{st}}\right)H_{w}^{\mathrm{filter}}\right)/s$. These figures illustrate the three design for the controller filters: (i) *performance:* close resemblance to the VS impedance (left column), (ii) *desired control effort:* low controller response at high frequencies (middle column), and (iii) *stability:* passivity of the controlled shake table (right column).

For $f_{\mathrm{c}} = 1000$ Hz, the performance tradeoff introduced by the filter is small, as indicated by the excellent agreement between the shake-table and the VS impedances in Figure 9.31a; the Nyquist plot also lies in the right half-plane, confirming passivity[33]. The downside of achieving such a close match to the VS is greater controller response at high frequencies (see Figure 9.31b**),** where the shake-table model is poorly characterized and noise in the feedback measurement is large. As f_{c} is decreased to 50 Hz, the controller response is significantly curtailed near high frequencies (see Figure 9.31k) but the tradeoff is poorer agreement between the VS and the shake-table impedances, as shown in Figure 9.31j.

[33] This assumes that the shake-table model is accurately known across all frequencies and the feedback signal contains no measurement noise, both of which are not true. The closer the Nyquist plot to the imaginary axis, the smaller will be the margin for such assumptions and other modeling uncertainties to ensure passivity, and by extension, stability.

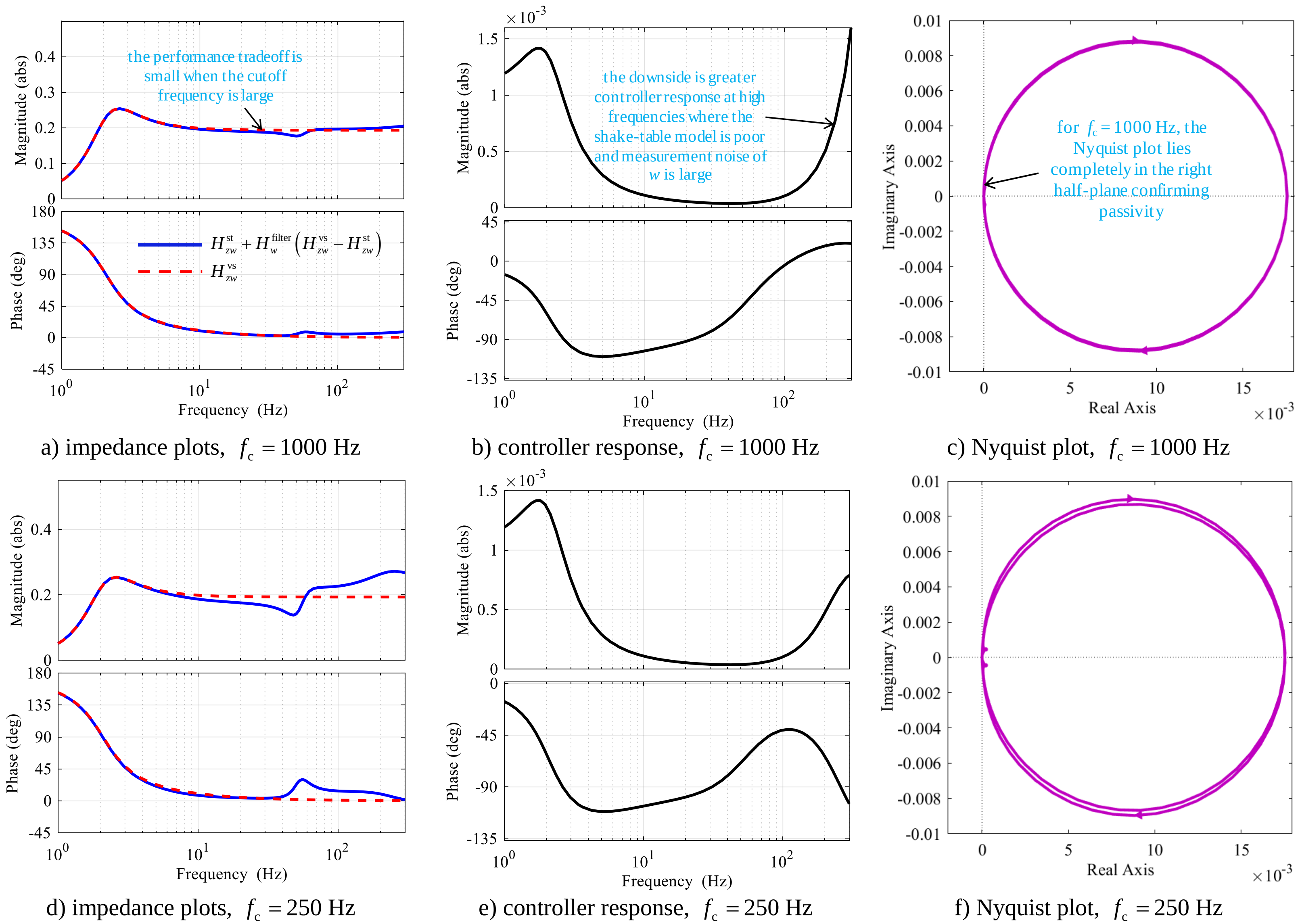

a) impedance plots, $f_c = 1000$ Hz
b) controller response, $f_c = 1000$ Hz
c) Nyquist plot, $f_c = 1000$ Hz
d) impedance plots, $f_c = 250$ Hz
e) controller response, $f_c = 250$ Hz
f) Nyquist plot, $f_c = 250$ Hz

Figure 9.31. Design criteria for the lowpass filter, K_e = 5 V/in, K_p = 0.001 V/psi, and τ_s = 500 µs (2000 Hz)

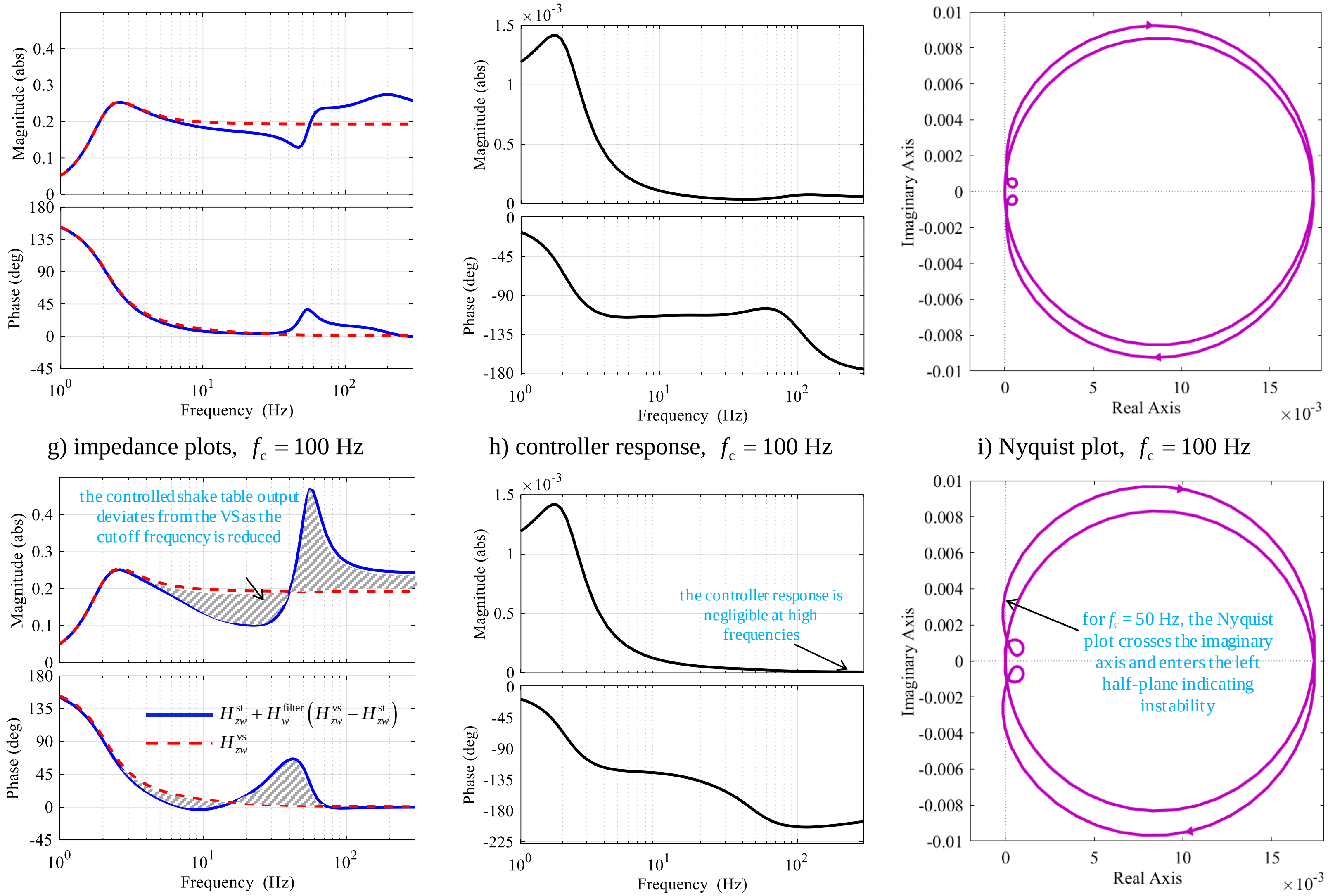

g) impedance plots, $f_c = 100$ Hz h) controller response, $f_c = 100$ Hz i) Nyquist plot, $f_c = 100$ Hz

j) impedance plots, $f_c = 50$ Hz k) controller response, $f_c = 50$ Hz l) Nyquist plot, $f_c = 50$ Hz

Figure 9-31. Performance tradeoffs introduced by the lowpass filter, K_e = 5 V/in, K_p = 0.001 V/psi, and τ_s = 500 μs (cont'd)

Also, for smaller values of f_c (herein less than 50 Hz), the Nyquist plot crosses the imaginary axis into the left half-plane (see Figure 9.31l), implying that the controlled shake-table is non passive, failing Constraint III. For the example case of Figure 9.31, Constraint II is not satisfied for $f_c = 1000$ Hz, whereas Constraints I and III are shown to fail for $f_c = 50$ Hz. Thus, there is a range of f_c in which all three design constraints are satisfied, as indicated in Table 9.5. For the SD_2 isolation system, this range is identified as 100-250 Hz and will vary depending on the VS properties, as discussed next.

Table 9.5. Understanding the tradeoffs for different values of filter cutoff frequency

f_c	Constraint I: close imitation of the VS impedance	Constraint II: low controller response to high-frequency w	Constraint III: passivity of the controlled shake table
1000 Hz	Satisfied	Not satisfied	Satisfied
250 Hz	Satisfied	Satisfied	Satisfied
100 Hz	Satisfied	Satisfied	Satisfied
50 Hz	Not satisfied	Satisfied	Not satisfied

9.4.4 Effect of the ratio of the VS basemat mass relative to the shake-table mass

In the above subsection, the effects f_c are analyzed for the SD_2 isolation system wherein the basemat mass is taken as $m_{vs} = 1.25 m_{st}$. Figure 9.32 presents Bode plots of the VS and the shake-table impedances for decreasing values of the basemat mass: m_{st}, $0.75\, m_{st}$, and $0.5\, m_{st}$. Note that only m_{vs} is varied for this exercise; the properties of the SD_2 system are per Table 9.1.

The plots show that for the same value of f_c, the smaller the VS basemat mass, the poorer the agreement between the VS and the shake-table impedances (see the difference in the hatched areas in Figure 9-32a for $m_{vs} = m_{st}$ and 9-32c for $m_{vs} = 0.5 m_{st}$). As the basemat mass is decreased, the Nyquist response of the controlled shake table moves closer to the imaginary axis (indicating a reduced stability margin), and into the left half-plane when m_{vs} is reduced below a threshold value. For test cases with $m_{vs} << m_{st}$, although the VS is passive, the controlled shake table is capable of introducing energy into the system, leading to instability, and thereby limiting implementation of MIL. This phenomenon of instability is demonstrated next using experimental results.

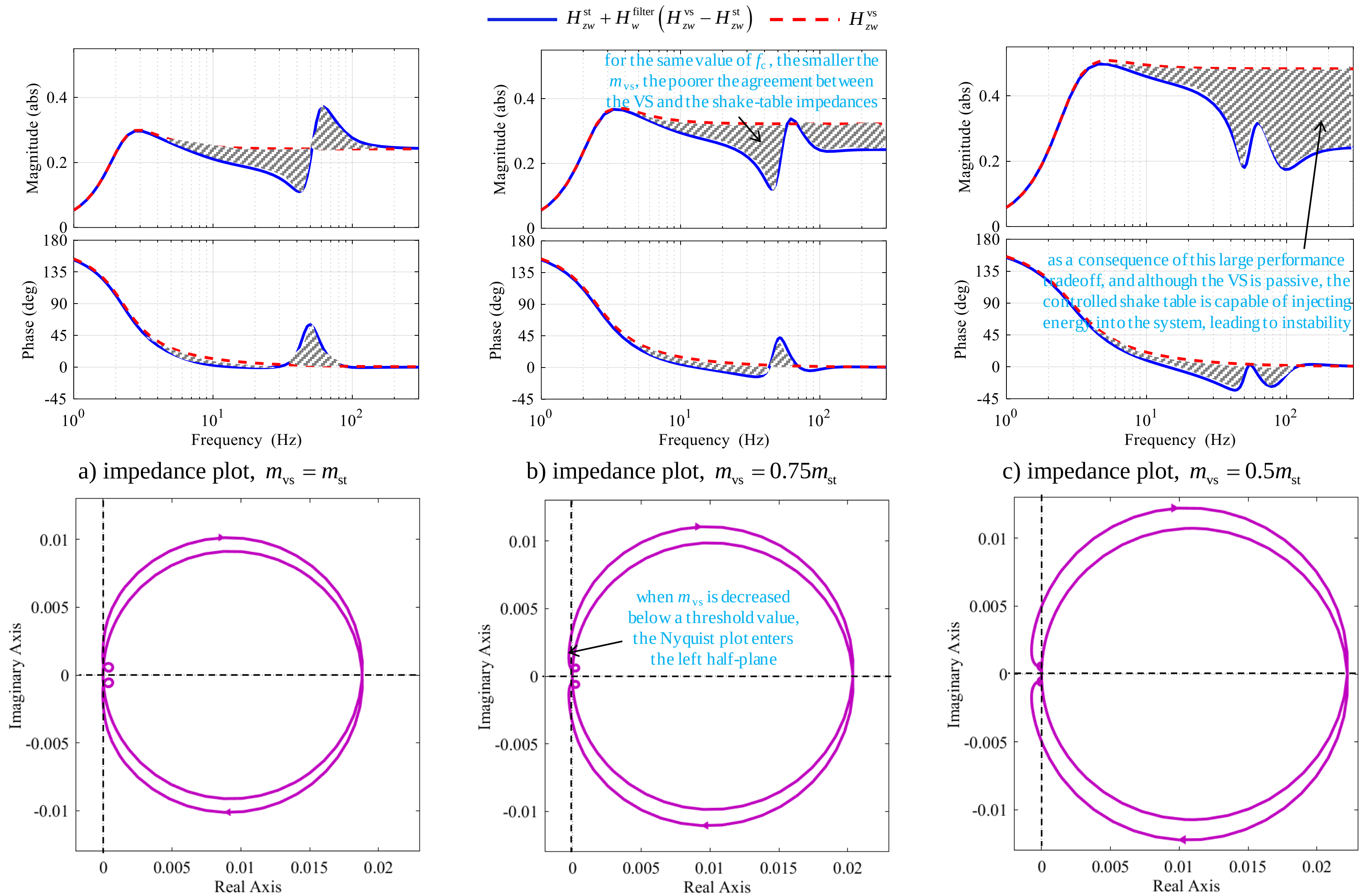

a) impedance plot, $m_{vs} = m_{st}$ b) impedance plot, $m_{vs} = 0.75m_{st}$ c) impedance plot, $m_{vs} = 0.5m_{st}$

d) Nyquist plot, $m_{vs} = m_{st}$ e) Nyquist plot, $m_{vs} = 0.75m_{st}$ f) Nyquist plot, $m_{vs} = 0.5m_{st}$

Figure 9.32. Understanding the effect of VS basemat mass, K_e = 5 V/in, K_p = 0.001 V/psi, τ_s = 500 μs (2000 Hz), and f_c = 80 Hz

9.4.5 Supplemental experimental results to understand the filter tradeoffs

Figure 9.33 presents MIL experimental results imitating SD_2 isolation system (for input motion GM_2) for decreasing values of the VS basemat mass: $m_{vs} = 1.25m_{st}$, m_{st}, $0.9m_{st}$, and $0.8m_{st}$. Only the basemat mass is varied in these tests; the stiffness, damping, and other properties of the SD_2 system are per Table 9.1 The control parameters in the experiments are set to: $K_e = 5$ V/in, $K_p = 0.001$ V/psi, $\tau_s = 500\ \mu s$ [2000 Hz], and $f_c = 80$ Hz. Results illustrate that for smaller basemat mass ratios, m_{vs}/m_{st} (herein < 1), the acceleration responses of the VS (dashed red lines), and consequently[34] those of the shake-table (solid blue lines), are dominated by high-frequency oscillations (see Figures 9-33e and 9-33g). The smaller the mass ratios, the greater the amplitude of these oscillations (see the red peaks at 15+ Hz in Figures 9-33b through 9-33h). The MIL performance, however, is unaffected at frequencies less than 10 Hz.

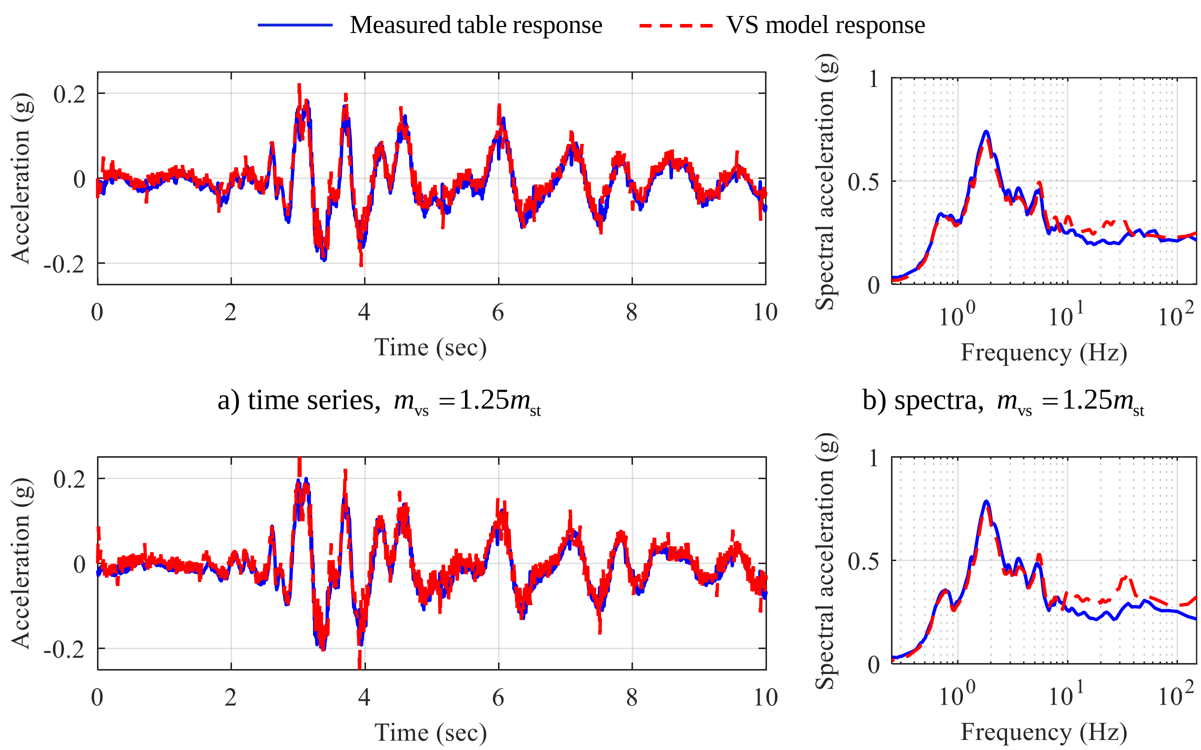

a) time series, $m_{vs} = 1.25m_{st}$

b) spectra, $m_{vs} = 1.25m_{st}$

c) time series, $m_{vs} = m_{st}$

d) spectra, $m_{vs} = m_{st}$

Figure 9.33. Effect of decreasing VS basemat mass ratio for imitating SD_2 system subjected to motion GM_2, $f_c = 80$ Hz, $K_e = 5$ V/in, $K_p = 0.001$ V/psi, $\tau_s = 500$ μs (2000 Hz)

[34] The MIL controller commands the shake-table actuator to imitate the target VS acceleration at the base of the test article. If the target z_{vs} is dominated by high-frequency content, the effect is propagated through the feedback system.

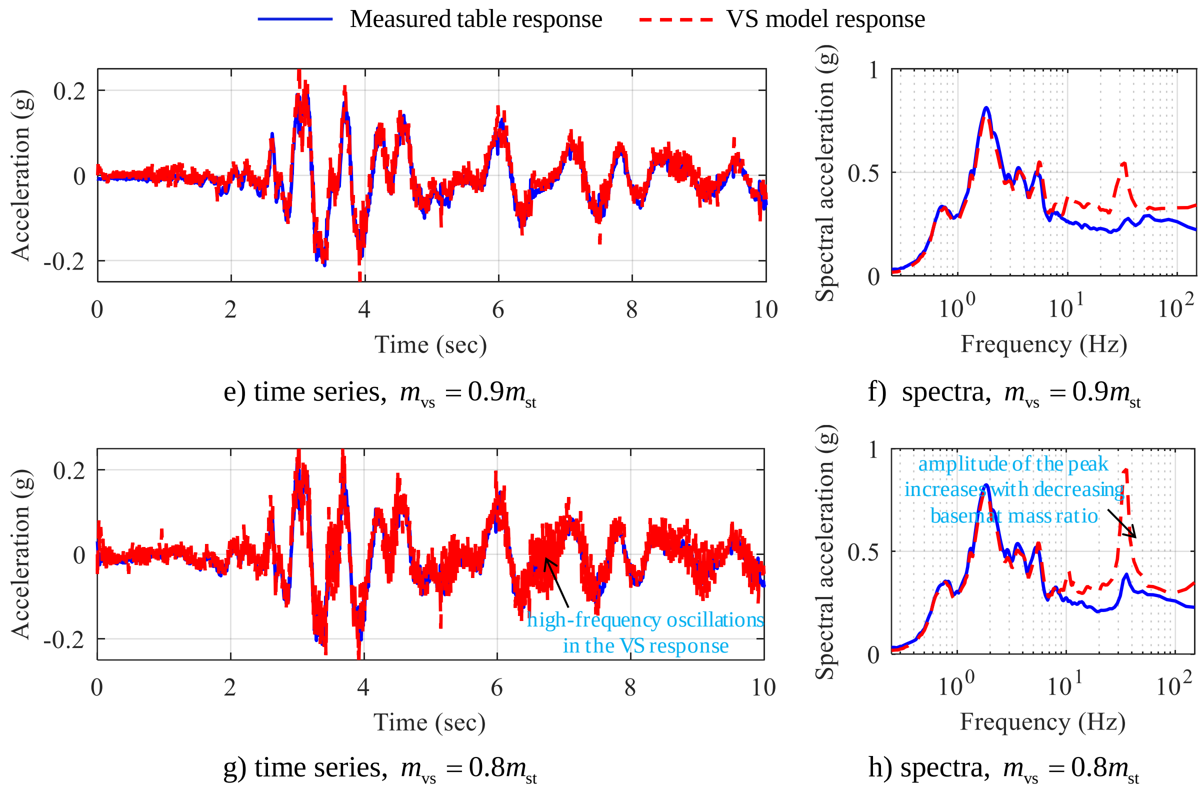

Figure 9-33. Effect of decreasing VS basemat mass ratio for imitating SD_2 system subjected to motion GM_2, f_c = 80 Hz, K_e = 5 V/in, K_p = 0.001 V/psi, τ_s = 500 μs (2000 Hz) (cont'd)

When the basemat mass is reduced to $0.7m_{st}$, the feedback system becomes unstable with large-amplitude high-frequency acceleration response, as shown in Figure 9-34. The threshold m_{vs} triggering instability varies with the isolation system properties and the cutoff frequency of the filter, and must be determined on a case-by-case basis. For example, for $f_c = 80$ Hz, the threshold m_{vs} triggering instability for the SD_2, LR_2 and FP_2 systems are identified from the experiments as $0.7m_{st}$, $0.8m_{st}$ and $0.9m_{st}$, respectively.

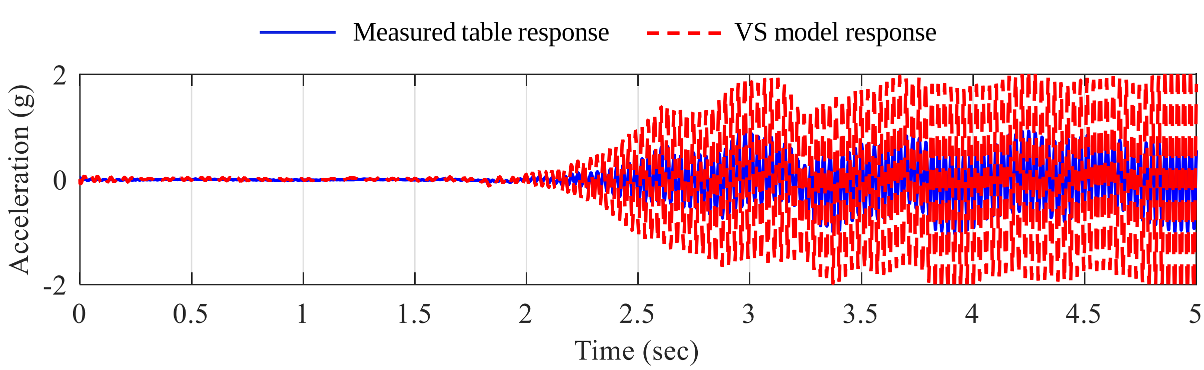

Figure 9.34. Unstable MIL simulation imitating SD_2 system subjected to motion GM_2, $m_{vs} = 0.7m_{st}$, f_c = 80 Hz, K_e = 5 V/in, K_p = 0.001 V/psi, τ_s = 500 μs [2000 Hz]

The poorer MIL performance when imitating virtual systems with a smaller basemat mass can be improved somewhat by adjusting the filter cutoff frequency. Figure 9.35 presents MIL experimental results for the test case of Figure 9.34 (i.e., $m_{vs} = 0.7m_{st}$) but for increasing values of the cutoff frequency. As f_c is increased from 80 Hz (Figure 9.34) to 200 Hz (Figure 9.35e), the performance tradeoff introduced by the filter decreases, and consequently the high-frequency oscillations in the VS response are reduced resulting in improved MIL performance.

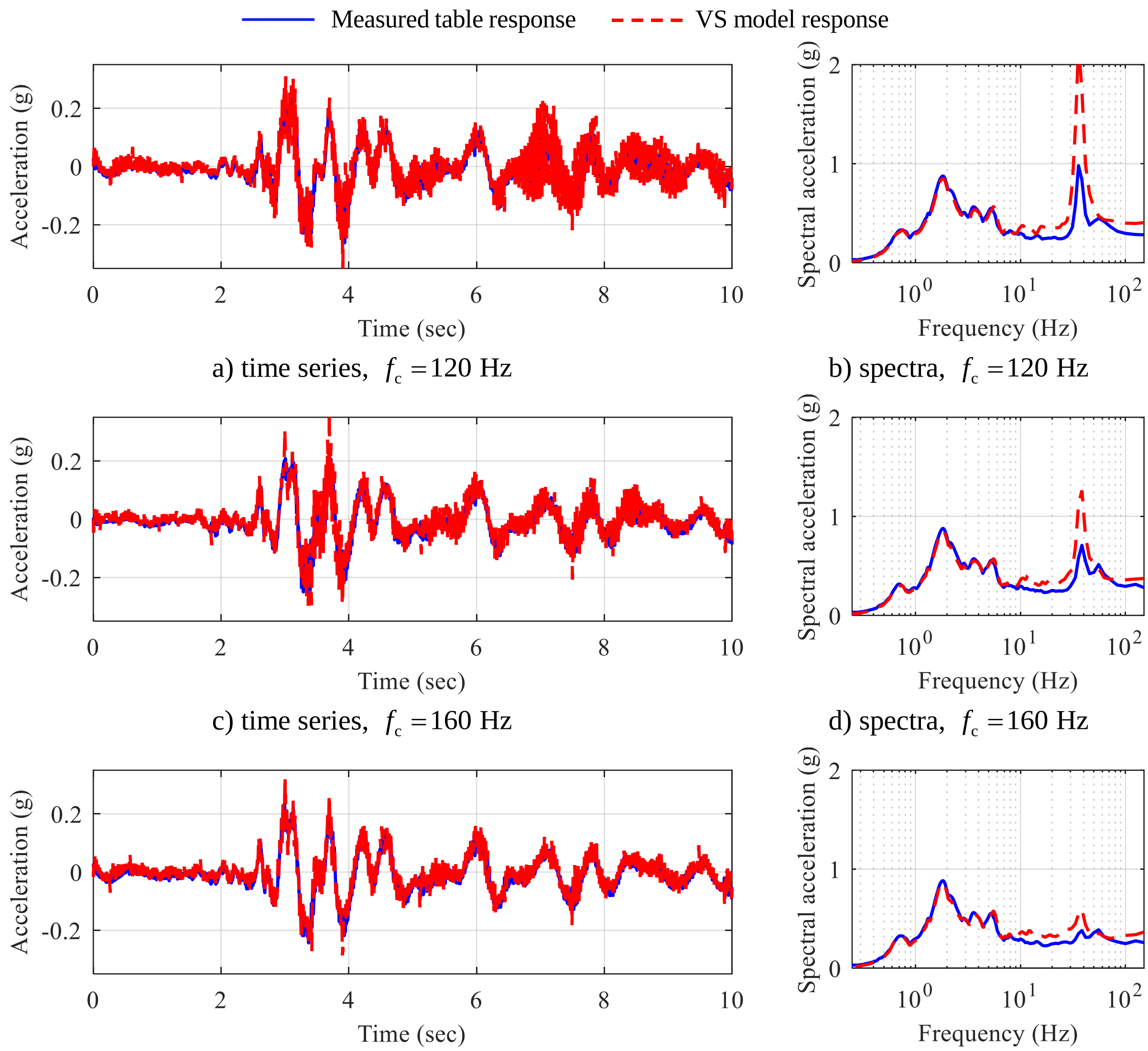

a) time series, $f_c = 120$ Hz
b) spectra, $f_c = 120$ Hz
c) time series, $f_c = 160$ Hz
d) spectra, $f_c = 160$ Hz
e) time series, $f_c = 200$ Hz
f) spectra, $f_c = 200$ Hz

Figure 9.35. Effect of the filter cutoff frequency for imitating SD_2 isolation system subjected to motion GM_2, $m_{vs} = 0.7m_{st}$, $K_e = 5$ V/in, $K_p = 0.001$ V/psi, $\tau_s = 500$ μs (2000 Hz)

The presentation in the above subsections helps the reader appreciate the limitations of implementing MIL, namely, that it is simply not possible to design MIL controls that make a given shake table imitate all possible isolation systems. The controlled shake-table system may be capable of imitating some isolation systems with great accuracy (e.g., SD_2 system with $m_{vs} = 1.25m_{st}$ and $f_c = 80$ Hz), and some systems with reduced accuracy but ensuring stability (e.g., SD_2 system with $m_{vs} = 0.7m_{st}$ and $f_c = 200$ Hz), whereas it may not be possible to imitate some systems regardless of what filter properties are used (e.g., SD_2 system with $m_{vs} = 0.4m_{st}$), thus limiting the application of MIL. Note that these limitations are not a feature of a particular approach to control design (e.g., impedance matching) but are driven by how different the shake-table and the VS dynamics are.

SECTION 10
CLOSING THE LOOP

10.1 Merits of the impedance-matching approach to model-in-the-loop simulations

The impedance-matching approach to model-in-the-loop (MIL) simulations, as described in this report, provides a pathway for standardizing MIL procedures because:

- The resulting controller causes the loading device (e.g., shake table) to imitate the impedance (force-motion response) of different virtual systems independently of the test article: fundamentally different from the traditional MIL algorithms (Section 2.1).
- Control design is not viewed as a tracking problem but rather to match the impedance of the controlled actuator system, as closely as possible, with that of the simulated environment of the test article. This fundamentally different approach eliminates the need for tracking controllers[35], and simplifies implementation of force- and acceleration-controlled MIL.
- High-fidelity mathematical models are developed for the actuators to predict their responses over a broad range of frequencies. These models, when used together with the techniques of impedance matching, enable explicit treatment of test article-actuator interaction through the term $u_w = H_{zw}^{\text{as}} w,$ thus eliminating the need for compensators[36] that are often designed for a specific test article.
- Commercial off-the-shelf controller hardware is used, facilitating ready and widespread deployment of MIL. The controller is implemented as a state-space system with a few lines of mathematical code, thus making implementation of MIL less dependent on the type (and make) of the hardware.

10.2 Generic process for implementing MIL using impedance matching

The work presented in this report helps document a generic process for implementing impedance-matching MIL for qualification testing of structural systems and other applications. This generic process can be parsed into five phases, as outlined below. The sections of this report are organized in sequential order describing these phases for the example MIL configuration of 1D base-isolated cylindrical vessel:

---

[35] Tracking controllers enable an actuator to follow a reference displacement/force command.

[36] Actuators are dynamic systems and cannot track a reference command accurately at all frequencies. Compensators are often used to address actuator dynamics and improve tracking performance.

1. **Conceptualization – Section 3**: Conceptualizing the MIL system, that is: (i) substructuring the dynamic system into components that are to be tested physically and components of the surrounding environment that are to be represented virtually, (ii) devising a system of actuators to impose boundary conditions representative of the simulated environment on the test article, and (iii) identifying feedback and drive signals at the interface.

2. **Characterization – Sections 4 and 5:** Characterizing the dynamics of the actuator system and the simulated environment. Robust mathematical models can be developed or experimental measurements may be used, as applicable. For simulating environments with multiple degrees-of-freedom, reduced-order models can be developed and only those dynamics of the environment that are significant at the interface with the test article need to be considered in modeling the environment.

3. **Design – Section 6:** In this report, lowpass filters are used to approximate the MIL controller and subsequently enabling its implementation. Alternate pathways to control design may be considered, for example, using optimization algorithms to minimize the error in impedance matching (i.e., actuator impedance minus environment impedance). Such approaches are being developed by Sivaselvan and other co-workers (e.g., control design using linear matrix inequalities by Verma *et al.* (2019), frequency-domain linear programming by Verma *et al.* (*forthcoming*)). However, regardless of the approach used, the MIL controller must satisfy the three design criteria: (i) the impedance of the controlled actuator system (e.g., $H_{zw}^{\text{as}} + H_{zu}^{\text{as}} H_{uw}$) matches, as closely as possible, that of the simulated environment (H_{zw}^{vs}), (ii) minimize the controller response at high frequencies where measurement noise is typically large and actuator models are of low fidelity, and (iii) the controlled actuator system is passive so that the actuator-test article feedback system is stable..

4. **Implementation – Section 7:** Procurement, configuring, and installation of controller hardware, and writing MIL programs. When a single piece of hardware is configured to perform both hydraulic control and execute MIL programs, as demonstrated in this report, both operations are performed at a rate equal to the sampling (or loop) frequency of the controller. Alternately, two different controller hardware, one with larger sampling frequency (> 4000 Hz, e.g., NI controllers) and the other with a relatively smaller sampling rate (1000 to 4000 Hz, e.g., RMC75E), may be used. This dual-controller configuration enables performing only time-critical operations such as hydraulic control on the hardware with a larger sampling rate. (The results presented in Section 4 demonstrated that large sampling rates are required to fully realize the benefits of ΔP feedback in hydraulic control). The other

controller may be used for executing tasks that can afford computations at relatively smaller sampling rates (e.g., solving VS equations).

5. **Validation – Sections 8 and 9:** Validating the MIL system, which can be accomplished by directly testing the loading device, as considered in Stefanaki (2017), or by coupling the loading device with the test article, as demonstrated in this report. The impedance (force-motion response) of the loading device at the interface is compared with that of several target virtual systems. Once the controller is validated, the focus shifts from the MIL system to the test article. This next phase can be referred to as production phase where the test article is subjected to a range of inputs enveloping its likely boundary conditions.

10.3 Key contributions of this report

This report is a cradle-to-grave demonstration of the impedance-matching approach, for an example configuration of 1D base-isolated equipment, from conceptualization, through design, verification, implementation, and validation. The main contributions of this research, as identified in Section 1.3, are revisited in this subsection for completeness: closing the loop.

Contribution #1 *Advancing impedance-matching MIL framework*

In this report, the impedance-matching approach is extended to perform robustly in a motion (acceleration)-controlled setting. The challenges for implementing the MIL controller are identified, solutions are proposed, the usefulness of these solutions is evaluated by extensive testing, and a framework is developed to identify limitations of such testing.

Contribution #2 *Servovalve dynamics deduced from valve specifications*

A practical approach to model servovalve dynamics is adopted in this report. The valve frequency response (performance) curve from the MTS specification manual is approximated with a second-order transfer function by curve-fitting, as described in Section 4.3.2. The second-order model is seen to predict the valve response with sufficient accuracy up to 100 Hz, as indicated by the close agreement between the blue and red lines in Figure 4.3b, reproduced below as Figure 10.1. This valve approximation, when integrated into the actuator model, resulted in a robust mathematical model of the combined servo-actuator shake table system (see Section 4.5). The use of higher-order servovalve models is not recommended, particularly for the motion-controlled settings, because the greater the order of the servovalve model, the greater the relative degree of $\left(H_{zu}^{\mathrm{st}}\right)^{-1}$, and consequently, the more the controller needs to be approximated, which compromises performance

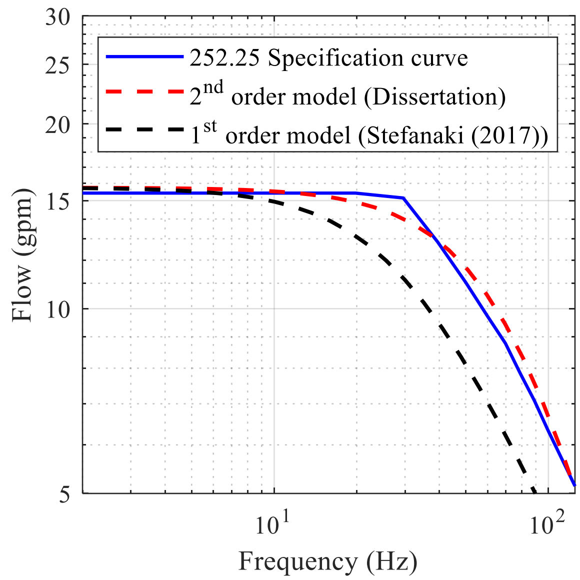

Figure 10.1. Modeling of servovalve dynamics using MTS specification curve (MTS, 2003)

Contribution #3 *Usefulness of ΔP feedback in improving model fidelity*

Differential pressure, ΔP, feedback has long been recognized as a stabilizing measure in hydraulic actuator control (e.g., Blondet and Esparza (1988); Rinawi and Clough (1991); Conte and Trombetti (2000)). However, in these applications, the ΔP gain, along with other control gains, was tuned for accurate tracking of a reference displacement command. Its potential benefit in terms of added damping to the oil-column resonance was not fully utilized. This key feature of the ΔP feedback is exploited in this report and it has been demonstrated that for a sufficiently large value of the ΔP gain, the effects of hydraulic-related (i.e., oil-column) nonlinearities are significantly reduced because of increased oil-column damping, thus enabling a linear model to predict the system response with high fidelity. Figure 4.16, reproduced below as Figure 10.2, illustrates the usefulness of ΔP feedback (with a sufficiently large gain) in improving the fidelity of the linear model. For $K_{\mathrm{p}} = 0.0002$ V/psi, the agreement between the measured and the model responses is poor in the frequency range of 10-40 Hz. As K_{p} is increased to 0.001 V/psi, the accuracy of the linear model is significantly improved.

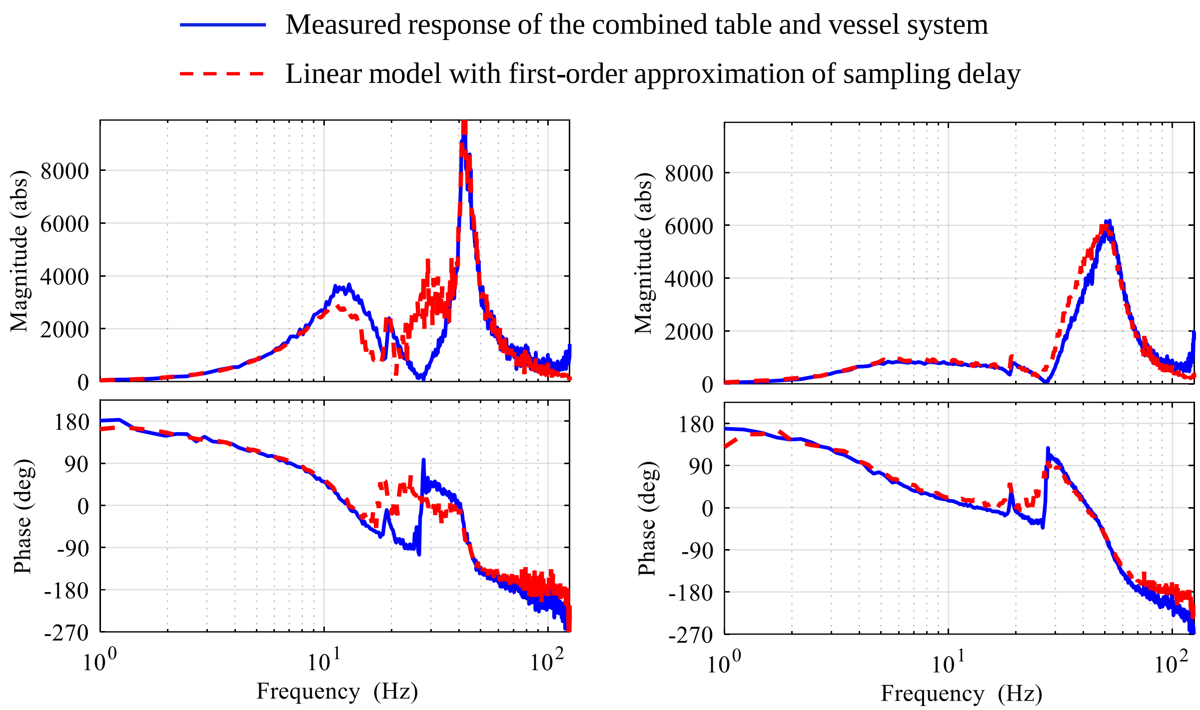

a) K_p = 0.0002 V/psi b) K_p = 0.001 V/psi

Figure 10.2. Experimental evaluation of the table and vessel system, acceleration responses, different values of K_p, water depth 36 inches, K_e = 5 V/in, and τ_s = 500 μs

Contribution #4 *Characterizing effects of controller loop (sampling) frequency*

It was demonstrated in Sections 4.3 and 4.4 that the bandwidth over which the ΔP feedback is beneficial is severely limited by the controller loop frequency, f_s. Figure 4.10, reproduced below as Figure 10.3, illustrate the effect of f_s on the frequency response of the shake table, H^{st}_{zu}. For smaller sampling rates (< 2000 Hz, the operating range for most commercial shake tables in the United States), the shake-table response is amplified near the oil-column resonance frequencies, counteracting the benefits of added damping achieved by the ΔP stabilization. This outcome is counterintuitive because the loop frequencies considered herein are at least 30 times greater than the oil-column frequency and are generally thought to not affect table response in this frequency range. Controller loop frequency is an important consideration for actuator control because (i) the fidelity of the linear model is greater when f_s is large, and (ii) higher oil-column damping can be achieved.

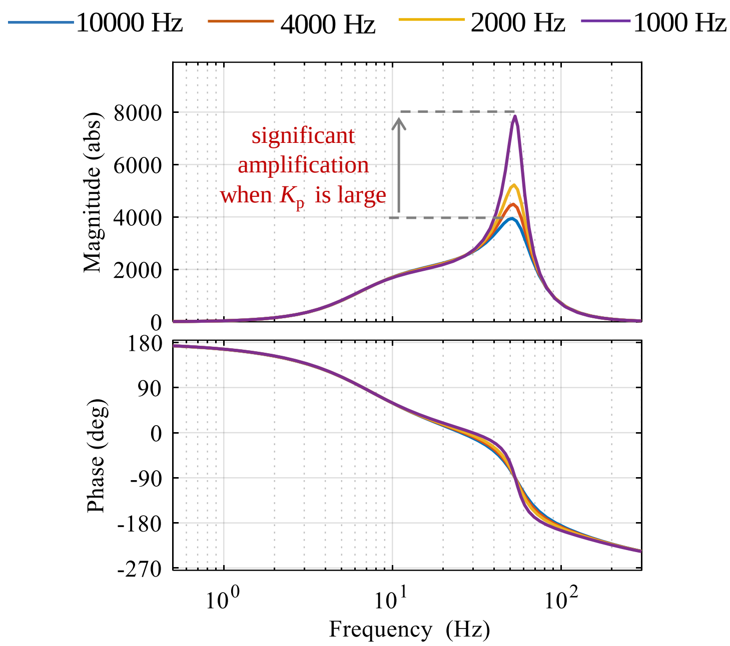

Figure 10.3. Effect of the controller loop frequency, K_e = 5 V/in, K_p = 0.001 V/psi

Contribution #5 *Developing a rational procedure for designing MIL controller*

Some fundamental limitations, such as causality of $\left(H_{zu}^{st}\right)^{-1}$ and measurement noise necessitate approximations to the MIL controller, which were addressed in this report using lowpass filters. A framework was developed for designing the filters based on three criteria: (i) the impedance of the controlled actuator system matches, as closely as possible, that of the simulated environment: Constraint I, (ii) the controller response is small at high frequencies: Constraint II, and (iii) the controlled actuator system must be passive: Constraint III.

The cutoff frequency of the filter, f_c, needs to be small enough to limit the controller response at high frequencies. However, reducing the value of f_c too much penalizes performance, that is, the output of the controlled shake table differs substantially from that of the VS: violating Constraint I. In some cases, this deviation may be large enough that although the VS is passive, the controlled shake-table system can add energy into the system (violating passivity, Constraint III), again leading to instability. Thus, there is range of cutoff frequencies in which both acceptable performance (determined by Constraints I) and stability (determined by Constraints II and II) can be achieved. Parts of Figure 9.31, reproduced below as Figure 10.4, makes clear these tradeoffs for two filter values: f_c = 1000 Hz and 50 Hz.

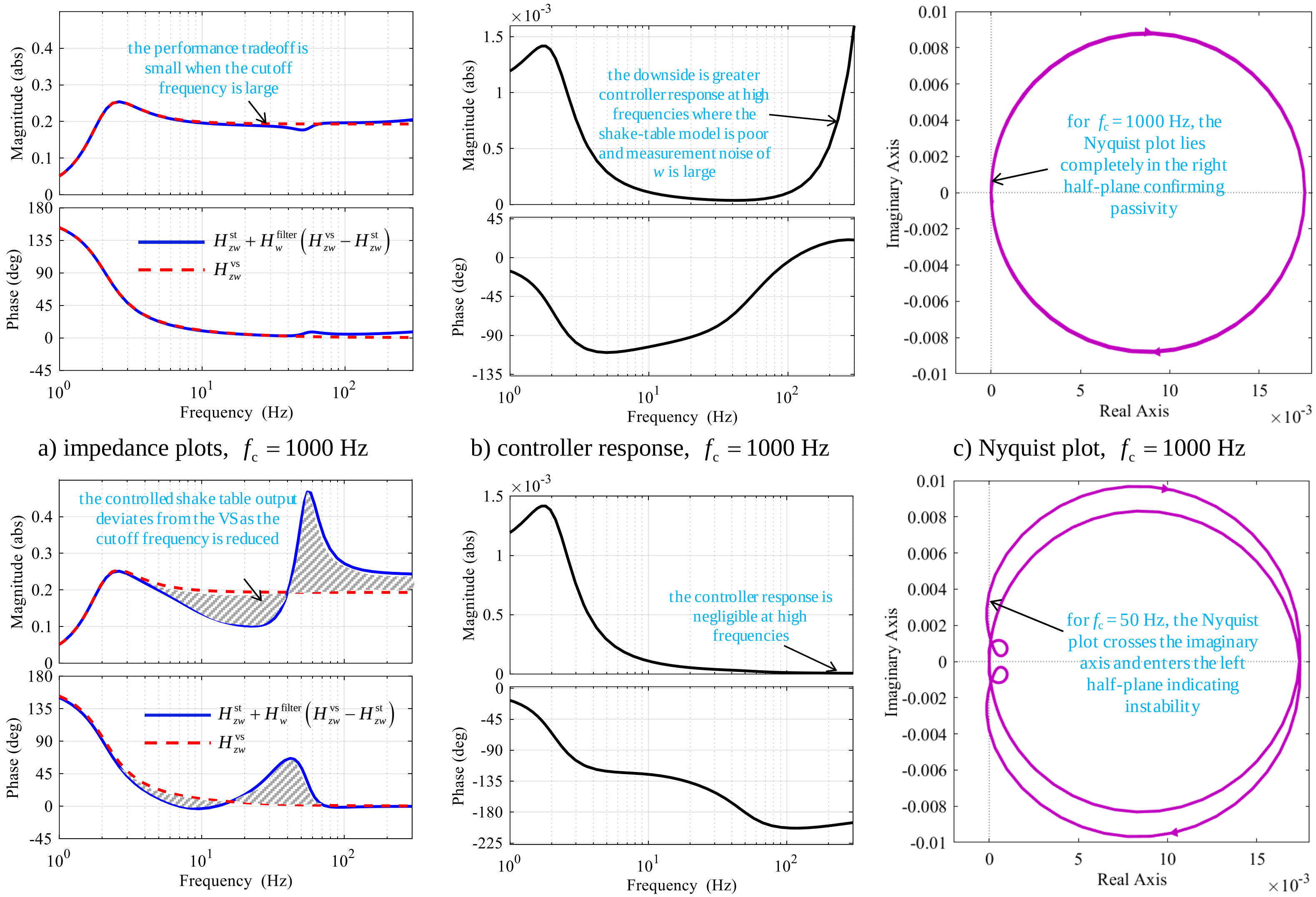

a) impedance plots, $f_c = 1000$ Hz   b) controller response, $f_c = 1000$ Hz   c) Nyquist plot, $f_c = 1000$ Hz

d) impedance plots, $f_c = 50$ Hz   e) controller response, $f_c = 50$ Hz   f) Nyquist plot, $f_c = 50$ Hz

Figure 10.4. Performance tradeoffs introduced by the lowpass filter, K_e = 5 V/in, K_p = 0.001 V/psi, and f_s = 2000 Hz

Contribution #6 *Simplifying implementation of MIL*

In this report, a single piece of commercial off-the-shelf hardware is used for both hydraulic control and executing MIL programs, thus minimizing the hardware, streamlining implementation, and importantly making the technology readily deployable at many laboratories. A part of the MIL user program of Figure 7.9 is reproduced below in Figure 10.5. The code enclosed within dashed red and blue lines is the state-space implementation of the MIL controller, meaning that the essence of the impedance-matching approach is embodied within these few lines of code, which enables control the actuator system (herein a shake table) to imitate the impedance of different virtual systems.

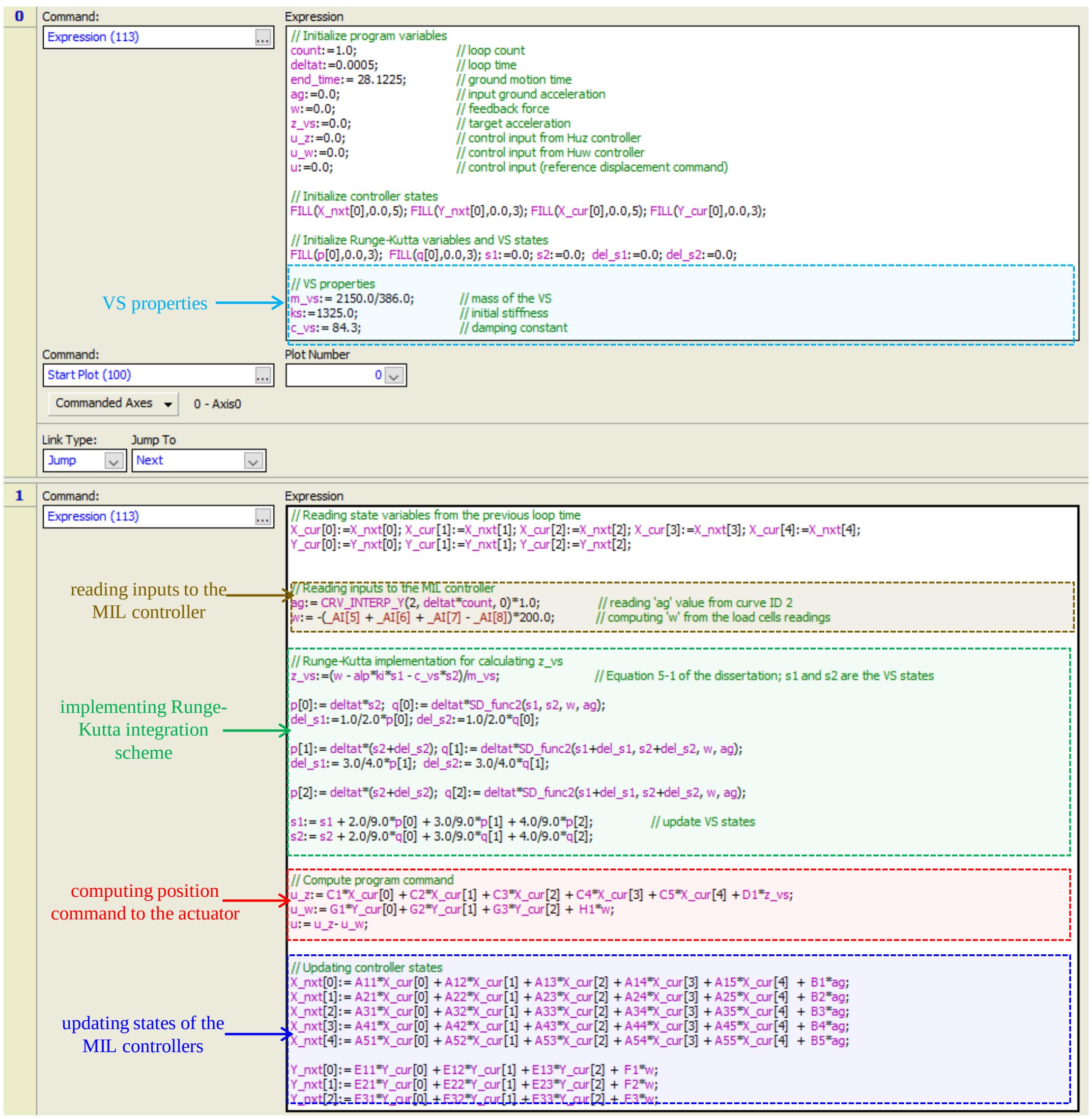

Figure 10.5. User program for executing MIL experiments for linear spring-damper systems

Contribution #7 *Applying techniques of impedance matching for shake-table testing*

The techniques of impedance-matching are applied for shake-table testing of structural system wherein the goal is to track a prescribed acceleration history, a_g, at the base of the test article. For such testing, the controller is reduced to the form: $u = H_{a_g}^{\text{filter}} \left(H_{zu}^{\text{st}} \right)^{-1} a_g - H_w^{\text{filter}} H_{zw}^{\text{st}} \left(H_{zu}^{\text{st}} \right)^{-1} w$, wherein the first component, $u_{a_g} = H_{a_g}^{\text{filter}} \left(H_{zu}^{\text{st}} \right)^{-1} a_g$, is the control input required for driving the bare shake table (without the test article) with an acceleration a_g. The second component, $u_w = H_w^{\text{filter}} H_{zw}^{\text{st}} \left(H_{zu}^{\text{st}} \right)^{-1} w$, compensates for the table-structure interaction and ensures tracking of a_g. Parts of Figure 8.5 are reproduced below in Figure 10.6 to illustrate the efficacy of the impedance-matching controller for shake-table testing. The tracking performance (agreement between the blue and red lines) is excellent even when the mass of the test specimen is approximately three times the mass of the shake table: an outcome that is difficult to achieve using conventional tuning of shake tables.

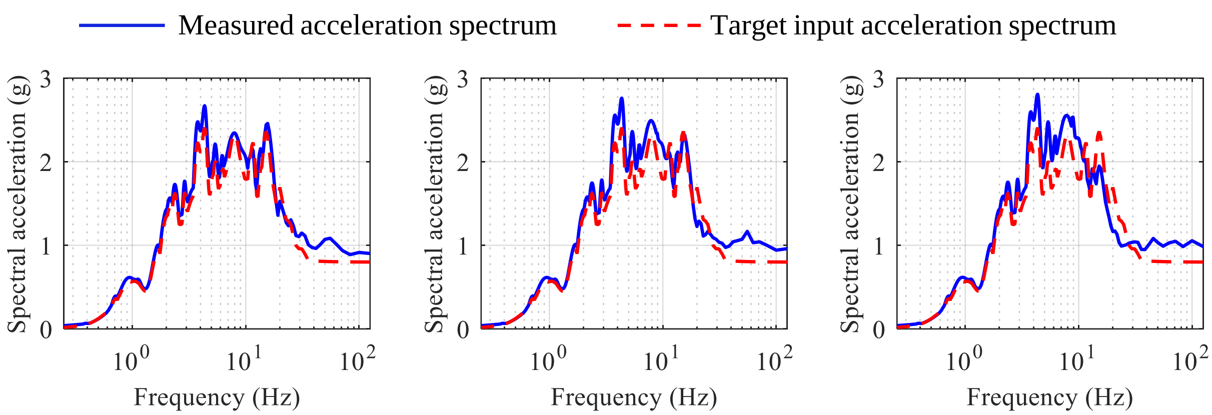

a) m_{ratio} = 1.5, GM$_1$ b) m_{ratio} = 2, GM$_1$ c) m_{ratio} = 2.5, GM$_1$

Figure 10.6. Results of acceleration-tracking experiments, different water depths, K_e = 5 V/in, K_p = 0.001 V/psi, f_c = 80 Hz, τ_s = 500 μs [2000 Hz]

Contribution #8 *Validating impedance-matching controls for motion-controlled setting*

The results presented in Section 9 illustrate that the impedance-matching MIL controller designed herein enables the use of a standardized setup (shake table equipped with the MIL controller) for simulating boundary conditions corresponding to different seismic isolation systems at the base of a test article: the overarching goal of this report. However, accuracy of MIL simulations reduced at high frequencies (> 15 Hz) backstopping the fact that it is not practically possible to control one dynamic system to imitate the impedance (i.e., force-motion behavior) of another across all frequencies. Additionally, there are some fundamental limitations to what can be achieved with controls. These limitations to MIL control design are framed in Section 9.3 as tradeoffs between performance and stability. The controlled shake-table system may be capable of imitating some isolation systems with great accuracy, and some systems with reduced accuracy but ensuring stability, whereas it may not be possible to imitate some systems regardless of what filter properties (or other form of approximations) are used. These limitations are not a feature of a particular approach to control design (e.g., impedance matching) but are driven by how different the shake-table and the VS dynamics are.

10.4 Closing remarks, open questions, and avenues for future enhancement

Despite careful analysis in this report of robust performance as well as limitations of the impedance-matching approach, there remain some open questions. The foundation laid in this report also opens avenues for advancing the impedance approach. These are outlined below.

- *Passivity analysis for nonlinear virtual systems*: The concept of passivity was introduced in this report as a framework for stability analysis of a MIL system. However, it was applied explicitly to only linear virtual systems. This concept could be extended to nonlinear virtual systems by considering a linear model of the shake table in feedback with (i) the physical test article, and (ii) the nonlinear part of the VS model (an extension of the idea illustrated in Figure 5-3). Extending the passivity-based analysis to nonlinear VS would help characterize the associated stability margins and tradeoffs.

- *Oscillatory response when imitating stiff isolation systems:* Experimental results presented in Section 9.3 showed that larger initial stiffness, k_i, of the isolation system is associated with greater likelihood of oscillatory shake-table response. This explains the more oscillatory (high frequency) behavior of the table when imitating Friction Pendulum bearings than lead-rubber or spring-damper bearings. It is likely that these effects could be characterized using passivity analysis. Although passivity has been discussed in this report as a binary concept (i.e., a system is either passive or not), there are degrees of passivity denoted using passivity indices. The “more” passive a system is, the more likely its approximation will remain passive. A question to explore is whether greater oscillatory response corresponds to less passivity.

- *Source of reaction feedback measurement and goodness of MIL*: Figures C-1 through C-3 show that both direct measurement of reaction feedback via load cells and indirect estimation based on a free-body diagram of the shake table are both effective for MIL. In this report, close agreement (qualitative) between the VS and the shake-table responses for a given w has been used as an indicator for 'correctness' or 'goodness' of MIL. However, these two sources of feedback measurement result in slightly different w for MIL computations, and consequently, a slightly different response of the VS. Test results in Figures C-1 through C-3 allow a reader to conclude that MIL performance (agreement between the VS and the shake table response) is good in both cases although the target response of the VS is slightly different. This raises a question of whether a more quantitative-based indicator is needed to assess the correctness (or goodness) of a MIL simulation.

- *Damping of virtual systems:* The virtual systems considered in this report are highly damped. It would be beneficial to understand the implications of using lightly damped VS on the kinds of tradeoffs (between performance and stability) discussed in Section 9, again in terms of passivity.
- *Optimization-based control design:* In this report, the MIL controller was designed using filter approximations. Alternate approaches to control design such as linear-programming optimization (Verma *et al.*, forthcoming) could be developed to design a MIL controller as an optimal tradeoff between performance and stability. The manual filter-based design approach presented herein serves as a good starting point to help establish meaningful objective functions and constraint parameters for such optimization-based methods.
- *Fundamental limitations to controls:* It has been emphasized throughout this report that there are fundamental limitations to what can be achieved using controls. It is not possible to control a given actuator system to imitate any desired virtual system with great accuracy across a broad frequency range. There may be virtual systems that cannot be imitated by a given actuator regardless of the control design approach (e.g., filter, optimization) because at least one of the three design constraints (i.e., close resemblance to the VS, low controller response at high frequencies, and passivity of the controlled actuator system) is violated. The options then are either to accept a very poor approximation of the VS or change the physical parameters of the shake table (i.e., use a different shake table).
- *Extension and validation of the impedance-matching approach to multi-axis configurations:* An important extension of the impedance-matching approach is to multi-axis configurations (e.g., 2DOF shakers of Kote (2019) connecting electrical bus conductors (see Figure 2-3), 6DOF shake tables at the University at Buffalo). Implementation and validation in multi-axis configurations will be an important step towards widespread and general use of MIL in qualification testing applications.

SECTION 11
REFERENCES

Blondet, M., and Esparza, C. (1988). "Analysis of shaking table-structure interaction effects during seismic simulation tests." *Earthquake Engineering & Structural Dynamics*, 16(4), 473-490.

Bouc, B. (1967). "Forced vibration of mechanical system with hysteresis." *Proceedings: 4th Conference on Nonlinear Oscillation*, September 1967, Prague, Czechoslovakia.

Bracci, J. M., Reinhorn, A. M., and Mander, J. B. (1992). "Seismic resistance of reinforced concrete frame structures designed only for gravity loads: Part I - Design and properties of a one-third scale model structure." Technical Report NCEER-92-0027, University at Buffalo, The State University of New York, Buffalo, NY.

Brogliato, B., Lozano, G., Maschke, B., and Egeland, O. (2007). "Dissipative systems analysis and control: Theory and Applications." *Springer*, London.

Bursi, O. S., He, L., Lamarche, C., and Bonelli, A. (2010). "Linearly implicit time integration methods for real‐time dynamic substructure testing." *Journal of Engineering Mechanics*, 136(11), 1380-1389.

Bursi, O. S., Jia, C., Vulcan, L., Neild, S. A., and Wagg, D. J. (2011). "Rosenbrock‐based algorithms and subcycling strategies for real‐time nonlinear substructure testing." *Earthquake Engineering & Structural Dynamics*, 40(1), 1-19.

Carl, J., and Sivaselvan, M. V. (2011). "Improved dynamic testing by impedance control." *Earthquake Engineering and Engineering Vibration*, 423(10).

Carl, J., and Sivaselvan, M. (2012). "Impedance control as a strategy for alleviating actuator-structure interaction in dynamic testing." *Proceedings: 2012 Structures Congress*, Chicago, IL.

Carrion, J. E., and Spencer, B. F. (2007). "Model-based strategies for real-time hybrid testing." Technical Report NSEL-07-0006, University of Illinois at Urbana-Champaign.

Chae, Y., Kazemibidokthi, K., and Ricles, J. M. (2013). "Adaptive time series compensator for delay compensation of servo‐hydraulic actuator systems for real‐time hybrid simulation." *Earthquake Engineering & Structural Dynamics*, 42(11), 1697-1715.

Chen, C., and Ricles, J. M. (2008). "Development of direct integration algorithms for structural dynamics using discrete control theory." *Journal of Engineering Mechanics*, 134(8), 676-683.

Chen, C., Ricles, J. M., Marullo, T. M., and Mercan, O. (2009). "Real-time hybrid testing using the unconditionally stable explicit CR integration algorithm." *Earthquake Engineering & Structural Dynamics*, 38(1), 23-44.

Chen, C., and Ricles, J. M. (2012). "Analysis of implicit HHT‐α integration algorithm for real‐time hybrid simulation." *Earthquake Engineering & Structural Dynamics*, 41(5), 1021-1041.

Chen, P.-C., and Tsai, K.-C. (2013). "Dual compensation strategy for real‐time hybrid testing." *Earthquake Engineering & Structural Dynamics*, 42(1), 1-23.

Chen, P.-C., Lai, C.-T., and Tsai, K.-C. (2017). "A control framework for uniaxial shaking tables considering tracking performance and system robustness." *Structural Control Health Monitoring*, 24(11), e2015.

Colgate, J. E. (1988). "The control of dynamically interacting systems." Ph.D. dissertation, Massachusetts Institute of Technology, PA.

Combescure, D., and Pegon, P. (1997). "α - Operator splitting time integration technique for pseudodynamic testing - Error propagation analysis." *Soil Dynamics and Earthquake Engineering*, 16(7), 427-443.

Constantinou, M. C., Whittaker, A. S., Kalpakidis, Y., Fenz, D. M., and Warn, G. P. (2007). "Performance of seismic isolation hardware under service and seismic loading." Technical Report MCEER-07-0012, University at Buffalo, The State University of New York, Buffalo, NY.

Conte, J. P., and Trombetti, T. L. (2000). "Linear dynamic modeling of a uni-axial servo-hydraulic shaking table system." *Earthquake Engineering & Structural Dynamics*, 29(9), 1375-1404.

Darby, A. P., Williams, M. S., and Blakeborough, A. (2002). "Stability and delay compensation for real - time substructure testing." *Journal of Engineering Mechanics*, 128(12), 1276-1284.

Delta Computer Systems Inc (Delta). (2020a). "RMC70 series datasheet." Battle Ground, WA.

Delta Computer Systems Inc (Delta). (2020b). "VC2124: Two axis voltage-to-current converter datasheet." Battle Ground, WA.

Delta Computer Systems Inc (Delta). (2021a). Computer Program RMC Tools (Version 4.18.4), Battle Ground, WA.

Delta Computer Systems Inc (Delta). (2021b). "RMC70/150/200 motion controllers and RMCTools software user manual." *Version 4.18.0*, Battle Ground, WA.

Dertimanis, V. K., Mouzakis, H. P., and Psycharis, I. N. (2015). "On the acceleration-based adaptive inverse control of shaking tables." *Earthquake Engineering & Structural Dynamics*, 44(9), 1329-1350.

Dimig, J., Shield, C., French, C., Bailey, F., and Clark, A. (1999). "Effective force testing: A method of seismic simulation for structural testing." *Journal of Structural Engineering*, 125(9), 1028-1037.

Dyke, S. J., Gomez, D., and Spencer, B. F. (2020). "Editorial: Special issue on the real-time hybrid simulation benchmark problem." *Mechanical Systems and Signal Processing*, 142, 106804.

Fermandois, C. G., and Spencer, B. F. (2017). "Model-based framework for multi-axial real-time hybrid simulation testing." *Earthquake Engineering and Engineering Vibration*, 16, 671-691.

Fu, Y. (2020). "Seismic interaction of high-voltage substation equipment interconnected by flexible-bus conductors." Ph.D. dissertation, University at Buffalo, The State University of New York, Buffalo, NY.

Galmez, C., and Fermandois, G. (2022). "Robust adaptive model-based compensator for the real-time hybrid simulation benchmark." *Structural Control & Health Monitoring*, 29(7), e2962.

Gao, X. S., and You, S. (2019). "Dynamical stability analysis of MDOF real-time hybrid system." *Mechanical Systems and Signal Processing*, 133, 106261.

Gui, Y., Wang, J. T., Jin, F., Chen, C., and Zhou, M. (2014). "Development of a family of explicit algorithms for structural dynamics with unconditional stability." *Nonlinear Dynamics*, 77, 1157-1170.

Gunay, S., Mosalam, K., and Takhirov, S. (2015). "Real-time hybrid simulation in a shaking table configuration for parametric studies of high-voltage equipment and IEEE693 development." *Nuclear Engineering and Design*, 295, 901-919.

Gutierrez, E., and Lopez Cela, J. J. (1998). "Improving explicit time integration by modal truncation techniques." *Earthquake Engineering & Structural Dynamics*, 27(12), 1541-1557.

Hauser, J., and Sivaselvan, M. V. (2009). "On the computation of compatible trajectories for hydraulic shake tables." *Proceedings: 2009 American Control Conference*, St. Louis, MO.

Hayati, S., and Song, W. (2016). "Discrete-time compensation technique for real-time hybrid simulation." *Proceedings: Conference on Society for Experimental Mechanics Series*, https://doi.org/10.1007/978-3-319-30084-9_33.

Hogan, N. (1985). "Impedance control: An approach to manipulation: Part I - Theory; Part II - Implementation; Part III - Applications." *Journal of Dynamic Systems, Measurement, and Control*, 107(1), 1-7; 8-16; 17-24.

Horiuchi, T., Inoue, M., Konno, T., and Namita, Y. (1999). "Real‐time hybrid experimental system with actuator delay compensation and its application to a piping system with energy absorber." *Earthquake Engineering & Structural Dynamics*, 28(10), 1121-1141.

Hwang, S. J., Chang, K. C., and Lee, G. C. (1987). "The system characteristics and performance of a shaking table." Technical Report NCEER-87-0004, University at Buffalo, The State University of New York, Buffalo, NY.

Kalpakidis , I., V, and Constantinou, M. C. (2008). "Effects of heating and load history on the behavior of lead-rubber isolators." Technical Report MCEER-08-0027, University at Buffalo, The State University of New York, Buffalo, NY.

Kalpakidis, I. V., and Constantinou, M. C. (2009). "Effects of heating on the behavior of lead-rubber bearings. I: Theory." *Journal of Structural Engineering*, 135(12), 1440-1449.

Kim, D. H., and Tsao, T. C. (2000). "A linearized electro-hydraulic servo valve model for valve dynamics sensitivity analysis and control system design." *ASME Journal of Dynamic Systems Measurement and Control*, 122(1), 179-187.

Koh, C. G., and Kelly, J. M. (1987). "Effects of axial load on elastomeric bearings." Technical Report EERC/UBC-86/12, Earthquake Engineering Research Center, University of California, Berkeley, CA.

Kolay, C., and Ricles, J. M. (2014). "Development of a family of unconditionally stable explicit direct integration algorithms with controllable numerical energy dissipation." *Earthquake Engineering & Structural Dynamics*, 43(9), 1361-1380.

Kolay, C., Ricles, J. M., Marullo, T. M., Mahvashmohammadi, A., and Sause, R. (2015). "Implementation and application of the unconditionally stable explicit parametrically dissipative KR-α method for real-time hybrid simulation." *Earthquake Engineering & Structural Dynamics*, 44(5), 735-755.

Kolay, C., and Ricles, J. M. (2016). "Assessment of explicit and semi-explicit classes of model-based algorithms for direct integration in structural dynamics." *International Journal for Numerical Methods in Engineering*, 107(1), 49-73.

Kolay, C., and Ricles, J. M. (2019). "Improved explicit integration algorithms for structural dynamic analysis with unconditional stability and controllable numerical dissipation." *Journal of Earthquake Engineering*, 23(5), 771-792.

Kote, V. B. (2019). "Model-in-the-loop testing of flexible-bus conductors interconnecting substation equipment." Ph.D. dissertation, University at Buffalo, The State University of New York, Buffalo, NY.

Kumar, M., Whittaker, A. S., and Constantinou, M. C. (2019a). "Seismic isolation of nuclear power plants using elastomeric bearings." NUREG/CR-7255, United States Nuclear Regulatory Commission, Washington, D.C. (ML19063A541).

Kumar, M., Whittaker, A. S., and Constantinou, M. C. (2019b). "Seismic isolation of nuclear power plants using sliding bearings." NUREG/CR-7254, United States Nuclear Regulatory Commission, Washington, D.C. (ML19158A513).

Lal, K. M., Constantinou, M. C., and Whittaker, A. S. (2021). "Seismic isolation of safety-class equipment in advanced nuclear reactors." *Proceedings: 17th World Conference on Earthquake Engineering (17WCEE)*, September, Sendai, Japan.

Lee, S.-K., Park, E. C., Min, K.-W., and Park, J.-H. (2007). "Real‐time substructuring technique for the shaking table test of upper substructures." *Engineering Structures*, 29(9), 2219-2232.

Lin, S. J., and Akers, A. (1989). "A dynamics model of the flapper-nozzle component of an electrohydraulic servovalve." *ASME Journal of Dynamic Systems Measurement and Control*, 111(1), 105-109.

Liu, C., and Jiang, H. (2014). "A seventh-order model for dynamic response of an electro-hydraulic servovalve." *Chinese Journal of Aeronautics*, 27(6), 1605-1611.

Ma, O., Flores-Abad, A., and Boge, T. (2012). "Use of industrial robots for hardware-in-the-loop simulation of satellite rendezvous and docking." *Acta Astronautica*, 81(1), 335-347.

Mahin, S. A., Shing, P. B., Thewalt, C. R., and Hanson, R. D. (1989). "Pseudodynamic test method - current status and future directions." *Journal of Structural Engineering*, 115(8), 2113-2128.

The Mathworks Inc (Mathworks). (2020). Computer Program MATLAB R2020b (Version 9.9.0.1495850).

McCrum, D. P., and Williams, M. S. (2016). "An overview of seismic hybrid testing of engineering structures." *Engineering Structures*, 118, 240-261.

Merritt, H. E. (1967). "Hydraulic control systems." *Wiley*, New York.

Mir, F. U. H., Yu, C. C., and Whittaker, A. S. (2020). "Experimental and numerical studies of seismic fluid‐structure interaction in a base‐supported cylindrical vessel." *Earthquake Engineering & Structural Dynamics*, 50(5), 1395-1413.

Mokha, A., Constantinou, M. C., and Reinhorn, A. M. (1988). "Teflon bearings in aseismic base isolation: Experimental studies and mathematical modeling." Technical Report NCEER-88-0038, University at Buffalo, The State University of New York, Buffalo, NY.

MOOG Industrial Controls Division (MOOG). (2007). "MOOG 760 series servovalves ISO 10372 Size 04." East Aurora, NY.

Mosqueda, G., and Ahmadizadeh, M. (2011). "Iterative implicit integration procedure for hybrid simulation of large nonlinear structures." *Earthquake Engineering & Structural Dynamics*, 40(9), 945-960.

MTS Systems Corporation (MTS). (2003). "Series 252 servovalves product information." *011-182-906 J*, Eden Prairie, MN.

MTS Systems Corporation (MTS). (2010). "469D seismic digital control software." Eden Prairie, MN.

MTS Systems Corporation (MTS). (2017). "MTS DuraGlide™ hydraulic actuators." *100-361-218 A*, Eden Prairie, MN.

Muhlenkamp, M., Conte, J. P., Hudgings, T. R., and Durrani, A. J. (1997). "Analysis, design, and construction of a shaking table facility." Structural Research at Rice, Report No 46, Department of Civil Engineering, Rice University, Houston, Texas.

Nagarajaiah, S., Reinhorn, A. M., and Constantinou, M. C. (1989). "Nonlinear dynamic analysis of three-dimensional base isolated structures (3D-BASIS)." Technical Report NCEER-89-0019, University at Buffalo, The State University of New York, Buffalo, NY.

Najafi, A., and Spencer, B. F. (2019). "Adaptive model reference control method for real-time hybrid simulation." *Mechanical Systems and Signal Processing*, 132, 183-193.

Najafi, A., and Spencer, B. F. (2020). "Modified model-based control of shake tables for online acceleration tracking." *Earthquake Engineering & Structural Dynamics*, 49(15), 1721-1737.

Najafi, A., and Spencer, B. F. (2021). "Validation of model-based real-time hybrid simulation for a lightly-damped and highly-nonlinear structural system." *Journal of Applied and Computational Mechanics*, 7, 1252-1265.

Nakashima, M., Kaminosomo, T., Ishida, M., and Ando, K. (1990). "Integration techniques for substructuring pseudodynamic test." *Proceedings: 4th National Conference on Earthquake Engineering (4NCEE)*, Palm Springs, CA.

Nakashima, M., Kato, H., and Takaoka, E. (1992). "Development of real - time pseudo dynamic testing." *Earthquake Engineering & Structural Dynamics*, 21(1), 79-92.

Nakashima, M., and Masaoka, N. (1999). "Real - time on - line test for MDOF systems." *Earthquake Engineering & Structural Dynamics*, 28(4), 393-420.

Nakashima, M. (2020). "Hybrid simulation: An early history." *Earthquake Engineering & Structural Dynamics*, 49(10), 949-962.

Nakata, N. (2013). "Effective force testing using a robust loop shaping controller." *Earthquake Engineering & Structural Dynamics*, 42(2), 261-275.

Nakata, N., Erb, R., and Stehman, M. (2017). "Mixed force and displacement control for testing base - isolated bearings in real - time hybrid simulation." *Journal of Earthquake Engineering*, 23(6), 1055-1071.

Narutoshi, N., and Matthew, S. (2014). "Compensation techniques for experimental errors in real - time hybrid simulation using shake tables." *Smart Structures and Systems*, 14(6), 1055-1079.

Neild, S. A., Stoten, D. P., and Wagg, D. J. (2005). "Control issues relating to real - time substructuring experiments using a shaking table." *Earthquake Engineering & Structural Dynamics*, 34(9), 1171-1192.

Ning, X., Wang, Z., Zhou, H., Wu, B., Ding, Y., and Xu, B. (2019). "Robust actuator dynamics compensation method for real-time hybrid simulation." *Mechanical Systems and Signal Processing*, 131, 49-70.

Ogata, K. (2010). "Modern control engineering." *Pearson Education*, New Jersey.

Ou, G., Prakash, A., and Dyke, S. J. (2015). "Modified Runge - Kutta integration algorithm for improved stability and accuracy in real time hybrid simulation." *Journal of Earthquake Engineering*, 19(7), 1112-1139.

Ouyang, Y., Shi, W., Shan, J., and Spencer, B. F. (2019). "Backstepping adaptive control for real-time hybrid simulation including servo-hydraulic dynamics." *Mechanical Systems and Signal Processing*, 130, 732-754.

Palacio-Betancur, A., and Gutierrez Soto, M. (2019). "Adaptive tracking control for real-time hybrid simulation of structures subjected to seismic loading." *Mechanical Systems and Signal Processing*, 134(106345).

Park, Y., Wen, Y., and Ang, A. H. S. (1986). "Random vibration of hysteretic systems under bi‐directional ground motions." *Earthquake Engineering & Structural Dynamics*, 14(4), 543-557.

Parsi, S. S. (2022). "Impedance-matching control design for shake-table testing and model-in-the-loop simulations." Ph.D. dissertation, University at Buffalo, The State University of New York, Buffalo, NY.

Peiris, L. D. H., Bartl, A., du Bois, J. L., and Plummer, A. (2020). "Passivity control with adaptive feed-forward filtering for real-time hybrid tests." *IFAC Journal of Systems and Control*, 12, 100081.

Phillips, B. M., Wierschem, N. E., and Spencer, B. F. (2014). "Model-based multi-metric control of uniaxial shake tables." *Earthquake Engineering & Structural Dynamics*, 43(5), 681-699.

Pratt, J., Krupp, B., and Morse, C. (2002). "Series elastic actuators for high fidelity force control." *Industrial Robot*, 29(3), 234-241.

Rajabi, N., Abolmasoumi, A. H., and Soleymani, M. (2018). "Sliding mode trajectory tracking control of a ball-screw-driven shake table based on online state estimations using EKF/UKF." *Structural Control & Health Monitoring*, 25(4), e2133.

Rea, D., Abedi-Hayati, S., and Takahashi, Y. (1977). "Dynamic analysis of electro-hydraulic shaking tables." Technical Report UCB/EERC-77/29, Earthquake Engineering Research Center, University of California, Berkeley, CA.

Reinhorn, A. M., Sivaselvan, M. V., Liang, Z., and Shao, X. (2004). "Real-time dynamic hybrid testing of structural systems." *Proceedings: 13th World Conference on Earthquake Engineering (13WCEE)*, Vancouver, Canada.

Rinawi, A. M., and Clough, R. W. (1991). "Shaking table-structure interaction." Technical Report UCB/EERC-91/13, Earthquake Engineering Research Center, University of California, Berkeley, CA.

Ryu, K. P., and Reinhorn, A. M. (2016). "Real-time control of shake tables for nonlinear hysteretic systems." *Structural Control & Health Monitoring*, 24(2), e1871.

Schellenberg, A. H., Mahin, S. A., and Fenves, G. L. (2009). "Advanced implementation of hybrid simulation." Technical Report PEER 2009/104, Pacific Earthquake Engineering Research Center, University of California, Berkeley, CA.

Schoukens, J., Pintelon, R., and Rolain, Y. (2012). "Mastering system identification in 100 exercises." *John Wiley & Sons, Inc.*, Hoboken, NJ.

Seto, K., Fuji, D., Hiramathu, H., and Watanabe, T. (2002). "Motion and vibration control of three-dimensional flexible shaking table using LQI control approach." *Proceedings: 2002 American Control Conference*, Anchorage, AK.

Shao, X., Reinhorn, A. M., and Sivaselvan, M. V. (2011). "Real‐time hybrid simulation using shake tables and dynamic actuators." *Journal of Structural Engineering*, 137(7), 748-760.

Shao, X., and Griffith, C. (2013). "An overview of hybrid simulation implementations in NEES projects." *Engineering Structures*, 56, 1439-1451.

Shing, P. B., Nakashima, M., and Bursi, O. S. (1996). "Application of pseudodynamic test method to structural research." *Earthquake Spectra*, 12(1), 29-56.

Sivaselvan, M. V., Reinhorn, A. M., Shao, X., and Weinreber, S. (2008). "Dynamic force control with hydraulic actuators using added compliance and displacement compensation." *Earthquake Engineering & Structural Dynamics*, 37(15), 1785-1800.

Stefanaki, A. (2017). "A simple strategy for dynamic substructuring and its application to soil-foundation-structure interaction." Ph.D. dissertation, University at Buffalo, The State University of New York, Buffalo, NY.

Stefanaki, A., and Sivaselvan, M. V. (2018a). "A simple strategy for dynamic substructuring: I. Concept and development." *Earthquake Engineering & Structural Dynamics*, 47(9), 1801-1822.

Stefanaki, A., and Sivaselvan, M. V. (2018b). "A simple strategy for dynamic substructuring: II. Experimental evaluation." *Earthquake Engineering & Structural Dynamics*, 47(9), 1823-1843.

Stoten, D. P., and Benchoubane, H. (1990). "Robustness of a minimal controller synthesis algorithm." *Interanational Journal of Control*, 51(4), 851-861.

Tao, J., and Mercan, O. (2021). "Adaptive discrete feedforward controller for tracking error compensation of servo-hydraulic actuators in real-time hybrid simulation." *Structural Control & Health Monitoring*, 29(3), e2895.

Thayer, W. J. (1958). "Transfer functions for Moog servovalves." *Moog Technical Bulletin 103*, East Aurora, Moog Inc., Controls Division, New York.

Tian, Y., Shao, X., Zhou, H., and Wang, T. (2020). "Advances in real-time hybrid testing technology for shaking table substructure testing." *Frontiers in Built Environment*, 6(123).

Verma, M., and Sivaselvan, M. V. (2019). "Impedance matching control design for the benchmark problem in real-time hybrid simulation." *Mechanical Systems and Signal Processing*, 134.

Verma, M., Sivaselvan, M. V., and Rajasankar, J. (2019). "Impedance matching for dynamic substructuring." *Structural Control and Health Monitoring*, 26(11).

Verma, M., Kote, V. B., Parsi, S. S., Weinreber, S., and Sivaselvan, M. V. (*forthcoming*). "Model-in-the-Loop control design by frequency-domain linear programming and passivity enforcement." *To be submitted*.

Wagg, D. J., and Stoten, D. P. (2001). "Substructuring of dynamical systems via the adaptive minimal control synthesis algorithm." *Earthquake Engineering & Structural Dynamics*, 30(6), 865-877.

Wallace, M. I., Wagg, D. J., and Neild, S. A. (2005). "An adaptive polynomial based forward prediction algorithm for multi-actuator real-time dynamic substructuring." *Proceedings of the Royal Society A: Mathematical, Physical and Engineering Sciences*, 461(2064), 3807-3826.

Wang, Z., Ning, X., Xu, G., Zhou, H., and Wu, B. (2019). "High performance compensation using an adaptive strategy for real-time hybrid simulation." *Structural Control & Health Monitoring*, 29(3), e2895.

Warn, G. P., and Whittaker, A. S. (2006). "A study of the coupled horizontal-vertical behavior of elastomeric and lead-rubber seismic isolation bearings." Technical Report MCEER 06-0011, University at Buffalo, The State University of New York, Buffalo, NY.

Watton, J. (1989). "Fluid power systems: Modeling, simulation, analog and microcomputer control." *Prentice Hall*, New York.

Wen, Y.-K. (1976). "Method for random vibration of hysteresis systems." *Journal of the Engineering Mechanics Division*, 102(2), 249-263.

Wu, B., Bao, H., Ou, J., and Tian, S. Z. (2005). "Stability and accuracy analysis of the central difference method for real-time substructuring testing." *Earthquake Engineering & Structural Dynamics*, 34(7), 705-718.

Wu, B., Xu, G., Wang, Q., and Williams, M. S. (2006). "Operator-splitting method for real-time substructuring testing." *Earthquake Engineering & Structural Dynamics*, 35(3), 293-314.

Wu, B., Pan, T., Xie, J., and Spencer, B. F. (2020). "Energy-consistent integration method and its application to hybrid testing." *Earthquake Engineering & Structural Dynamics*, 49(5), 415-433.

Wu, T., Li, S., and Sivaselvan, M. V. (2019). "Real-time aerodynamics hybrid simulation: a novel wind-tunnel model for flexible bridges." *Journal of Engineering Mechanics*, 145(9).

Xu, W., Chen, C., Guo, T., and Chen, M. (2019). "Evaluation of frequency evaluation index based compensation for benchmark study in real-time hybrid simulation." *Mechanical Systems and Signal Processing*, 130, 649-663.

Yang, T. Y., Li, K., Lin, J. Y., Li, Y. J., and Tung, D. P. (2015). "Development of high-performance shake tables using the heirarchial control strategy and nonlinear control techniques." *Earthquake Engineering & Structural Dynamics*, 44(11), 1717-1728.

Yu, C.-C., Mir, F. U. H., and Whittaker, A. S. (2021). "Validation of numerical models for seismic fluid-structure-interaction analysis of nuclear, safety-related equipment." *Nuclear Engineering and Design*, 379 (111179).

Zhang, Y. F., Sause, R., Ricles, J. M., and Naito, C. J. (2005). "Modified predictor - corrector numerical scheme for real - time pseudo dynamic tests using state-space formulation." *Earthquake Engineering & Structural Dynamics*, 34(3), 271-288.

Zhou, H. M., and Wu, B. (2013). "Validation study of shaking table hybrid test platform." *Journal of Vibration Engineering*, 26(4), 500-505.

Zhou, H. M., Xu, D., Shao, X. Y., Ning, X. Z., and Wang, T. (2019). "A robust Linear-Quadratic-Gaussian controller for real-time hybrid simulation on a benchmark problem." *Mechanical Systems and Signal Processing*, 133(106260).

Zhou, Z., and Li, N. (2020). "Improving model-based compensation method for real-time hybrid simulation considering error of identified model." *Journal of Vibration and Control*, 27(21), 2523-2535.

Zhu, F., Wang, J. T., Jin, F., Gui, Y., and Zhou, M. X. (2014). "Analysis of delay compensation in real-time dynamic hybrid testing with large integration time-step." *Smart Structures and Systems*, 14(6), 1269-1289.

APPENDIX A
CALIBRATION OF LOAD CELLS

A.1 Calibration setup

This appendix describes the procedure used to calibrate the reaction load cells (LCs) for the model-in-the-loop (MIL) experiments. Four load cells, numbered LC-03, LC-06, LC-08, and LC-14, were selected from the UB SEESL inventory. The load cells are fabricated from a 0.25-inch-thick cylindrical steel tube with attachment plates bolted at top and bottom. Drawings of the load cell assembly are presented in Figure 3.5. The load cells measure reaction forces and moments from strain gauges wired in a Wheatstone bridge. Bracci *et al.*, (1992) provides detailed information on the wiring of the strain gauges. The axial, shear, and moment ratings are ± 40 kip, ± 5 kip, and ± 40 kip-in, respectively.

The load cells are calibrated in horizontal shear using the Tinius Olsen Tension-Compression Testing machine at the University at Buffalo. Three units are bolted together and horizontally supported per the configuration shown in Figure A.1 The LCs to be calibrated are placed at the ends of the assembly. Steel rods are placed above and beneath the end LCs to simulate a two-point loading condition. A certified tension and compression load cell (Honeywell, Model IC48), is used as a reference LC and placed atop a thick steel plate resting on the rollers. A solid steel stub is used to transfer the load from the tension-compression machine to the reference LC. The configuration of Figure A.1 results in uniform shear force in the end LCs and uniform moment in the central LC. From equilibrium, an axial load P applied on the reference load cell will result in a shear force of $0.5P$ in the end LCs.

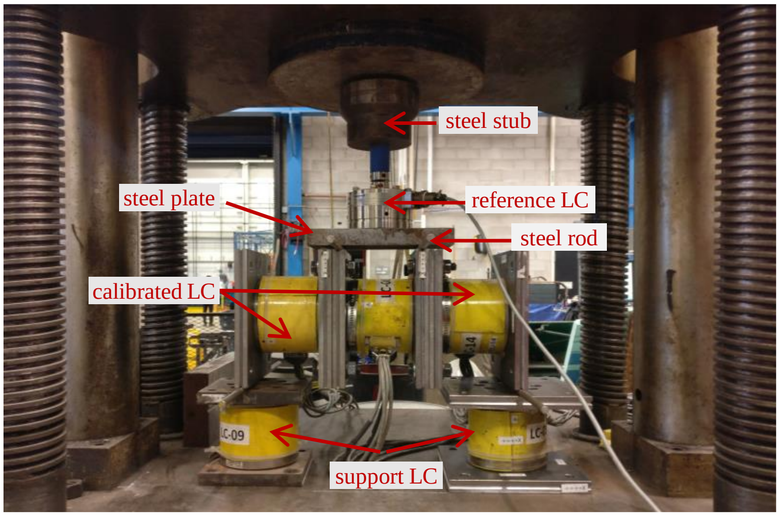

Figure A.1. Calibration setup for the load cells

A.2 Calibration procedure

The MIL experiments involved unidirectional horizontal loading, hence only the shear-x (S_x) channels were calibrated. The S_x channels were conditioned using 2310 Vishay signal conditioning amplifiers prior to connecting them to the Pacific 6000 data acquisition and control system. A two-point Engineering Unit (EU) calibration scheme was adopted as follows:

- The LC-03 and LC-06 units were calibrated first. In the unloaded configuration, the Wheatstone circuit was balanced and any residual voltage was set to zero. This corresponds to the first calibration point and an EU value of 0 kip was entered in the acquisition system.
- The load was slowly increased until the reference LC read 2 kip. (The corresponding shear force in the end LCs will be 1 kip each). At this load, the voltage from the S_x channels of the end LCs was measured using a voltmeter.
- The gain on the signal conditioners was adjusted to obtain an output voltage of 5 V for the applied 1-kip shear force, that is, a calibration factor of 0.2 kip/V. (For this gain, each LC can measure a maximum shear force of 2 kip corresponding to the maximum 10 V signal. The anticipated shear demands in the MIL experiments are less than 1.25 kip.)
- The loaded configuration is the second calibration point and an EU value of 1 kip was entered in the acquisition system. The gain on the signal conditioners was noted for use in the MIL experiments.
- After the calibration process was completed, the system was loaded to 2.5 kip and then unloaded at a speed of 0.1 kip/sec. The calibrated and reference LC readings were recorded at 0.01 sec intervals during the unloading process to generate calibration charts.
- Steps 1 through 5 were repeated for the other pair of load cells: LC-08 and LC-14.

Table A.1 reports the gain and shunt voltage values for the four LCs. The calibration data recorded during the unloading process are presented in Figure A.2. The reference LC reading is plotted on the *x*-axis and the S_x reading from the calibrated LC on the *y*-axis. The blue solid line is the calibrated slope and the red dashed line is the idealized slope. The close agreement between the two slopes implies that the calibration holds over the range of shear force anticipated in the MIL experiments, that is, 0 to 1.25 kips.

Table A.1. Gain and shunt voltage values after calibration

Load cell (S_x channel)	Gain ($\times$ 1000)	Shunt voltage (V)
LC-03	595	10.22
LC-06	586	9.90
LC-08	521	9.03
LC-14	807	9.76

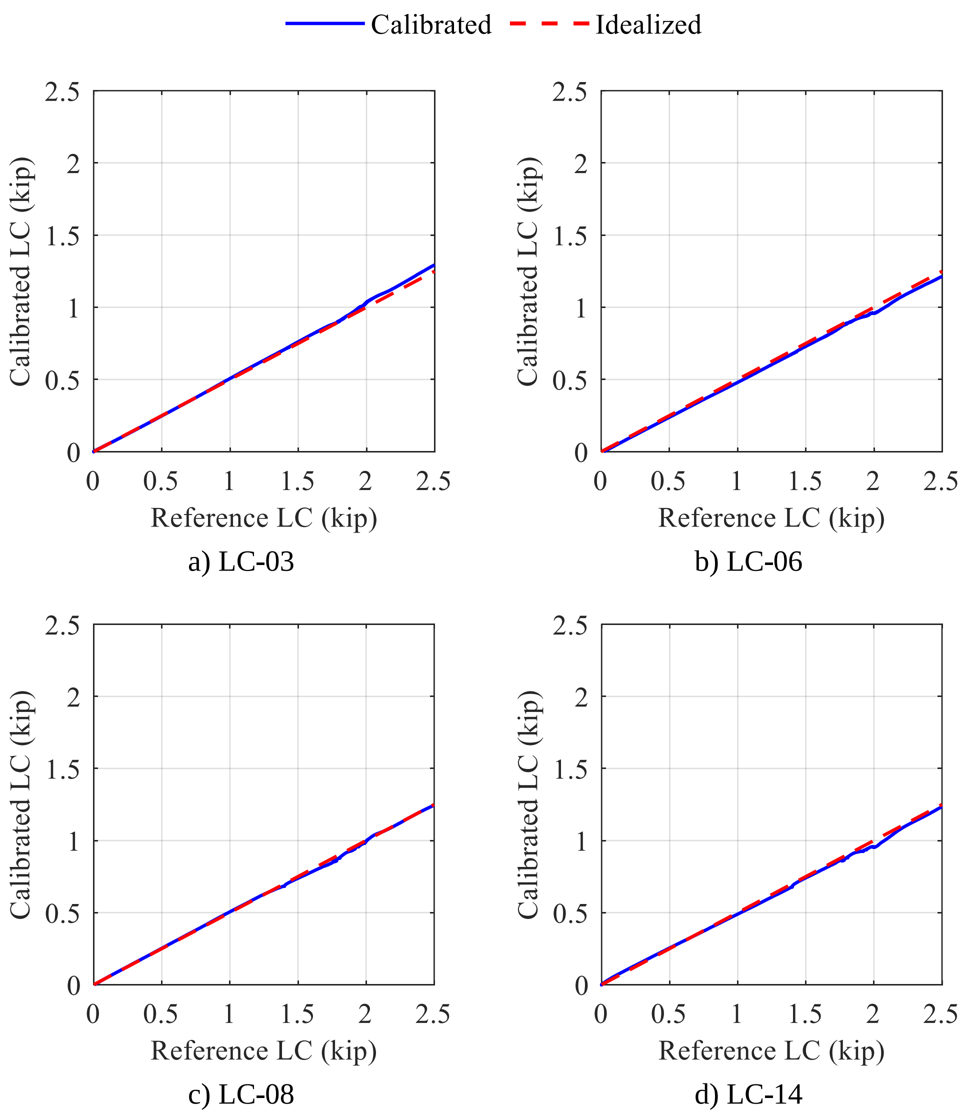

Figure A.2.Calibration charts for the shear-x channels

APPENDIX B
CONFIGURING THE CONTROLLER HARDWARE AND SOFTWARE WITH THE TEST SYSTEM

B.1 Controller hardware definitions and loop settings

This appendix presents: (i) a step-by-step procedure for configuring the RMC75E controller hardware and (ii) important control definitions in the RMCTools (software system used by the RMC controllers). Upon creating a new project in the RMCTools, a controller wizard appears on the screen to add information on the controller and its hardware modules, as shown in Figure B.1. It includes information on the controller family (RMC70 series), CPU (RMC75E), axis module (AA1), and the expansion modules (AP2 and A2). The controller is assigned automatically a name per the order in which these modules are installed, from left-to-right: RMC75E-AA1-AP2-A2-A2-A2.

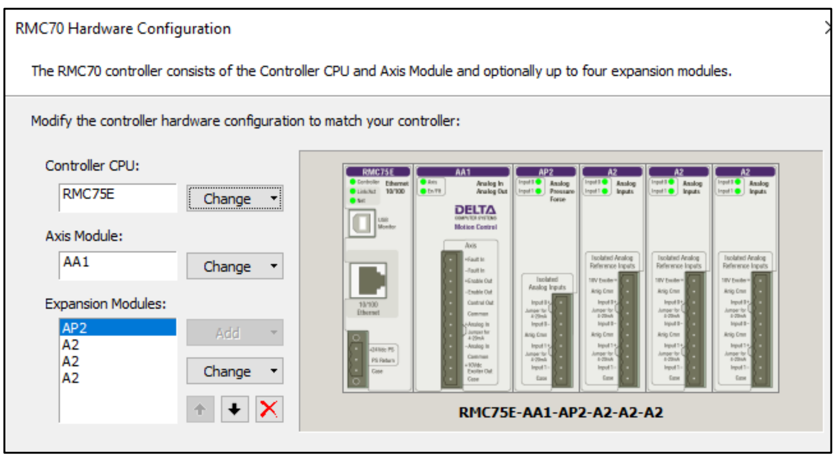

Figure B.1.Controller wizard in the RMCTools

After adding the controller information, a project pane window appears on the screen, providing an hierarchical overview of (and access to) all features of the RMCTools Project (see Figure B.2): *Modules*, *Axes*, *Programming*, *Curves*, *Plots*, *Event Log* etc. The *Modules* tab presents information on the controller hardware units, and facilitate defining key CPU properties such as loop time. The *Axes* tab is used to create/edit axis definitions (see Section 7.2.3). The *Programming* tab contains a list of user programs, user functions, and variable table editor used in the project. The *Curve* tab help upload/modify/create data curves to be used by the user programs (e.g., multisine time series or input acceleration histories).

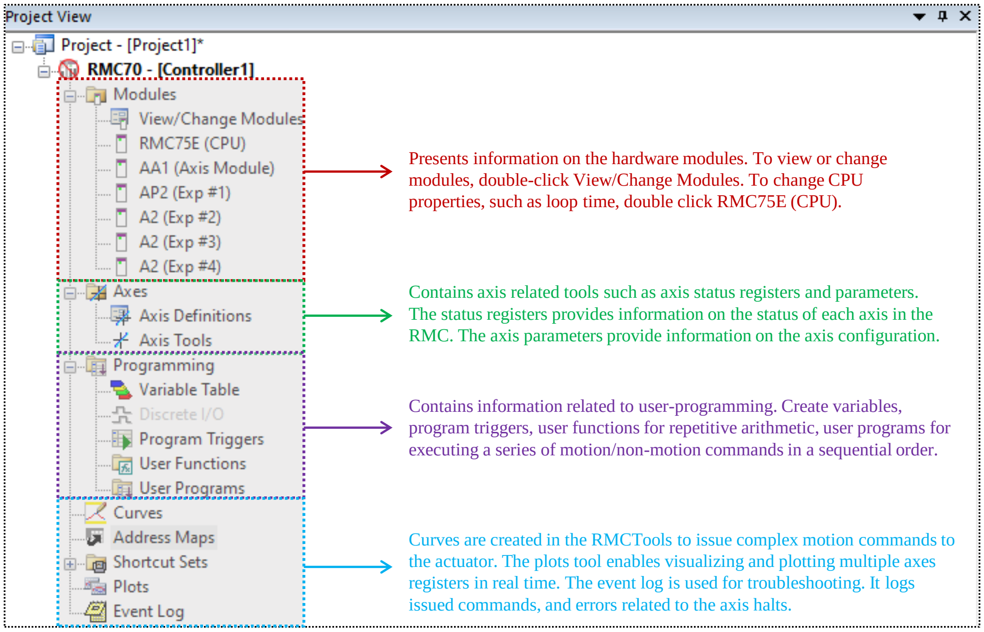

Figure B.2. Project pane window in the RMCTools

B.2 Axis Tool window

The Axis Tools window (Project pane → Axes → Axis Tools) displays status registers and parameters of each axis, as shown in Figure B.3. Axis status registers are read-only and helps monitor the actuator parameters (e.g., position, velocity). The axis parameters are read-write registers providing information on the axis configuration (e.g., display units, sensor calibration factors for converting volts to engineering units, +ve and -ve stroke limits for the control axis).

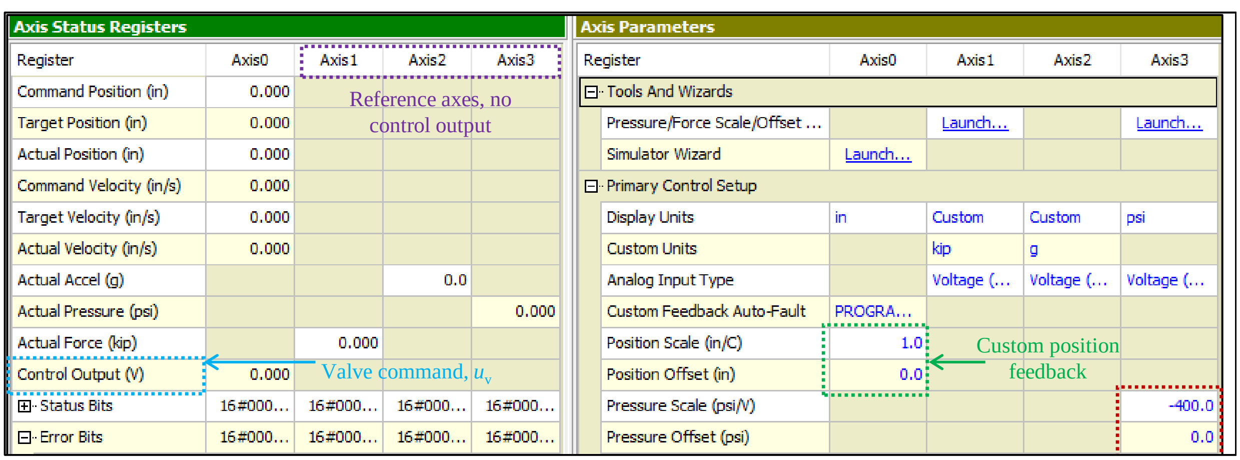

Figure B.3. Axis tools window in the RMCTools

B.3 Control gains definitions

The control gains are specified in the RMCTools using the tuning wizard (see Figure B.4). The gain values are entered as % of the maximum valve command (i.e., % of 10 V/). For example, if $K_e = 5$ V/in, the gain value is specified as 50 (i.e., 50% of 10 V). The derivative, integral, and feedforward gains are set to zero.

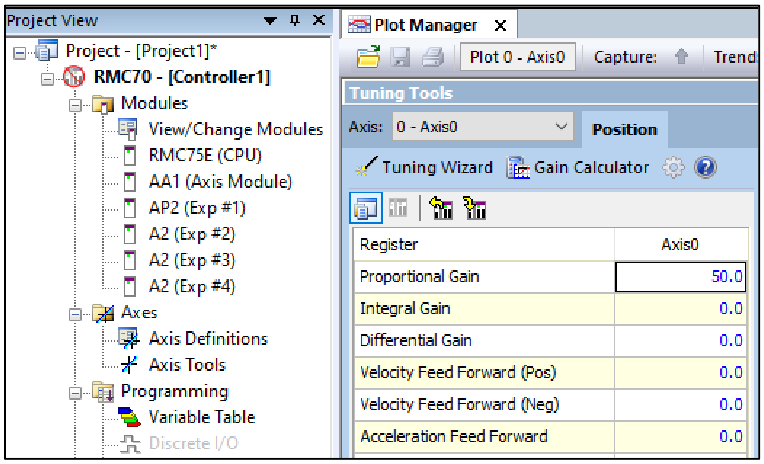

Figure B.4. Control gains definitions in the RMCTools

B.4 Issuing motion commands to the RMC

RMCTools includes a rich set of pre-programmed commands to perform simple actuator moves. Motion commands are issued to the RMC controller: (i) directly using the command tool, (ii) via user programs (see Section 7.3), and (iii) using an external PLC. Figure B.5 presents some example pre-programmed commands issued directly using the command tool. Note that motion commands can be issued only to a control axis.

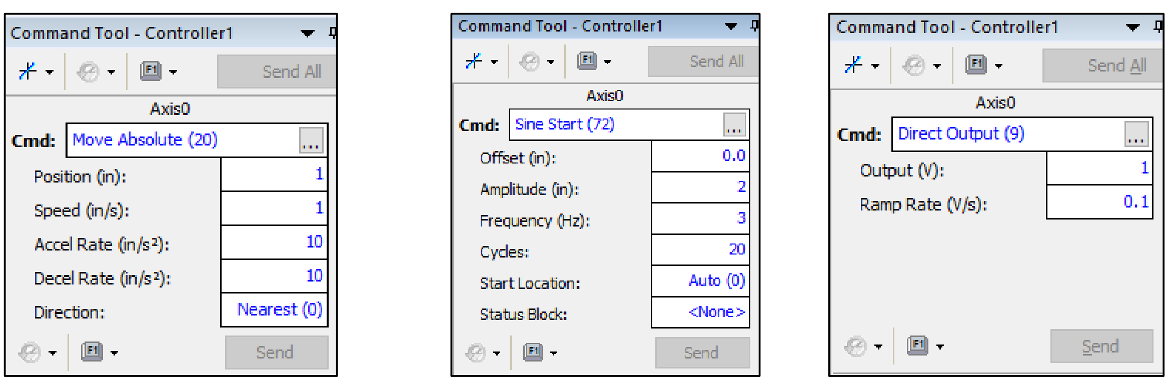

a) move absolute motion command (closed loop)

b) sine start motion command (closed loop)

c) direct output command (open loop)

Figure B.5. Issuing motion commands to the RMC using the command tool

APPENDIX C
EVALUATION OF GOODNESS OF MIL SIMULATIONS FOR DIFFERENT SOURCES OF FEEDBCK MEASUREMENTS

C.1 Different sources for feedback measurement

This appendix evaluates goodness (or correctness) of MIL simulations for different sources of feedback measurement. The presentation is similar to that of Section 8.3.2diss for the prescribed acceleration tracking experiments (i.e., $z_{\mathrm{vs}} = a_{\mathrm{g}}$). The following cases for feedback measurement are considered:

i). The feedback force from the reaction load cells, w_{LC}, is used as input to both the VS numerical model for calculating the target z_{vs} and to the MIL controller for calculating the control input, u. The MIL controller then takes the form: $u = u_z - u_w = H_z^{\mathrm{filter}} \left(H_{zu}^{\mathrm{st}} \right)^{-1} z_{\mathrm{vs}} - H_w^{\mathrm{filter}} H_{zw}^{\mathrm{st}} \left(H_{zu}^{\mathrm{st}} \right)^{-1} w_{\mathrm{LC}}$, where u_z corresponds to the control input required to apply target z_{vs}, and u_w compensates for the table-test article interaction. Experimental results for this case are presented in Section 9.3.

ii). The feedback force is calculated from force equilibrium of the shake table, as the actuator force minus the table inertia, $w_{\mathrm{FE}} = A_{\mathrm{p}} \Delta P - m_{\mathrm{st}} z_{\mathrm{exp}}$, for subsequent use in both VS and MIL-related calculations. (This equilibrium equation assumes frictional forces in the shake table are negligible.)

iii). The feedback force from the load cells, w_{LC}, is used to calculate the target VS acceleration (like case i)) but its contribution in calculating the control input is ignored (unlike case i)). Put differently, the table-test article interaction is ignored, that is $u_w = 0$ and the control input $u = u_z = H_z^{\mathrm{filter}} \left(H_{zu}^{\mathrm{st}} \right)^{-1} z_{\mathrm{vs}}$.

C.2 Results

Figures C-1, C-2, and C-3 illustrate the effect of different sources of feedback measurements for imitating spring-damper (SD), lead-rubber (LR), and Friction Pendulum (FP) isolation systems, respectively, whose properties are presented in Tables 9-1, 9-2, and 9-3, and summarized below in Table C-1 wherein isolator strength and stiffness are bracketed as either high (H), moderate (M), or low (L).

Table C.1. Bracketing of isolation systems introduced in Section 9

	SD_1	SD_2	SD_3	LR_1	LR_2	LR_3	FP_1	FP_2	FP_3
Strength	L	M	H	L	M	H	L	M	H
Stiffness	L	M	H	L	M	H	L	M	H

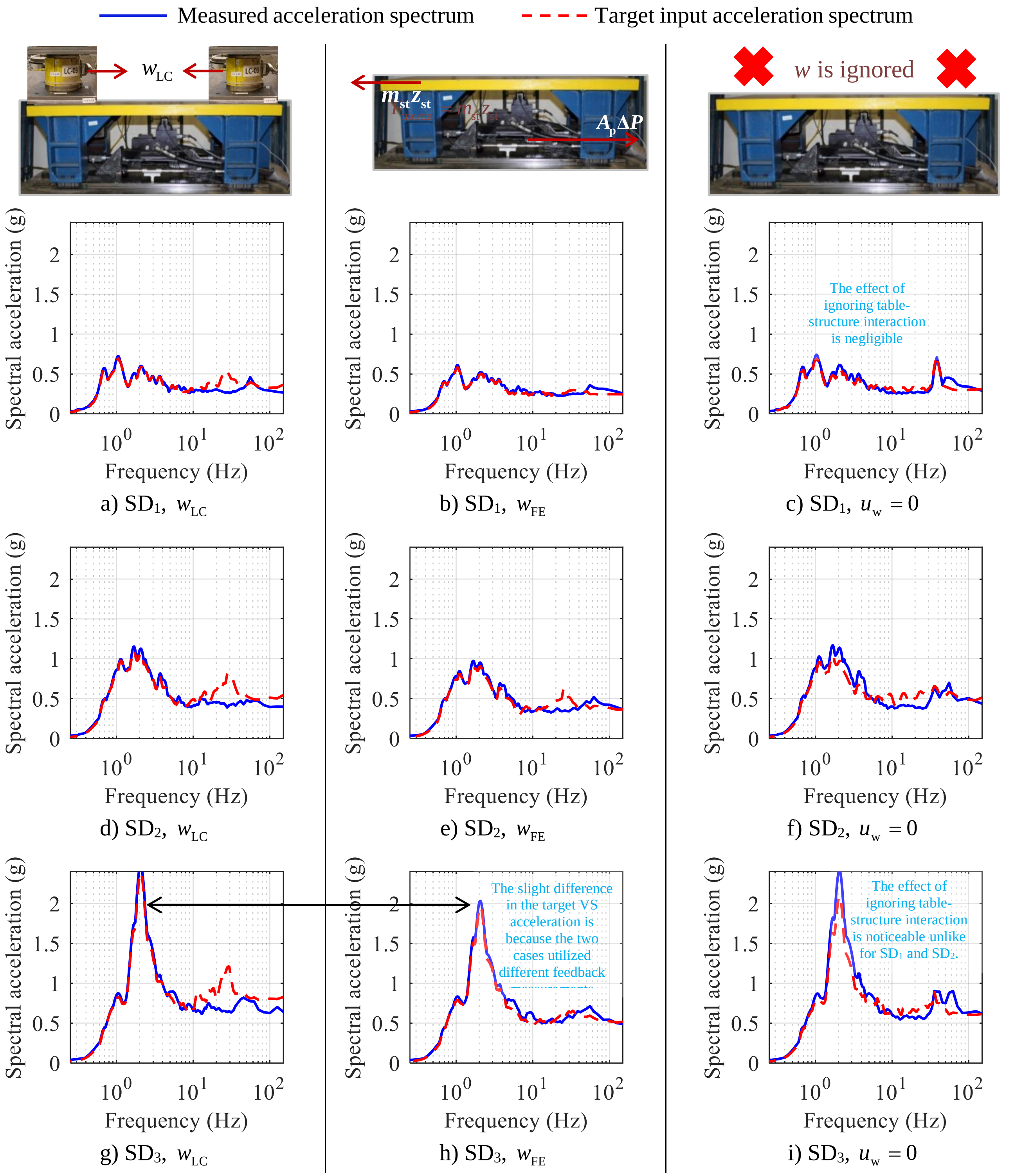

Figure C.1. Effect of different sources of feedback measurement on MIL performance imitating SD isolation systems for GM_1

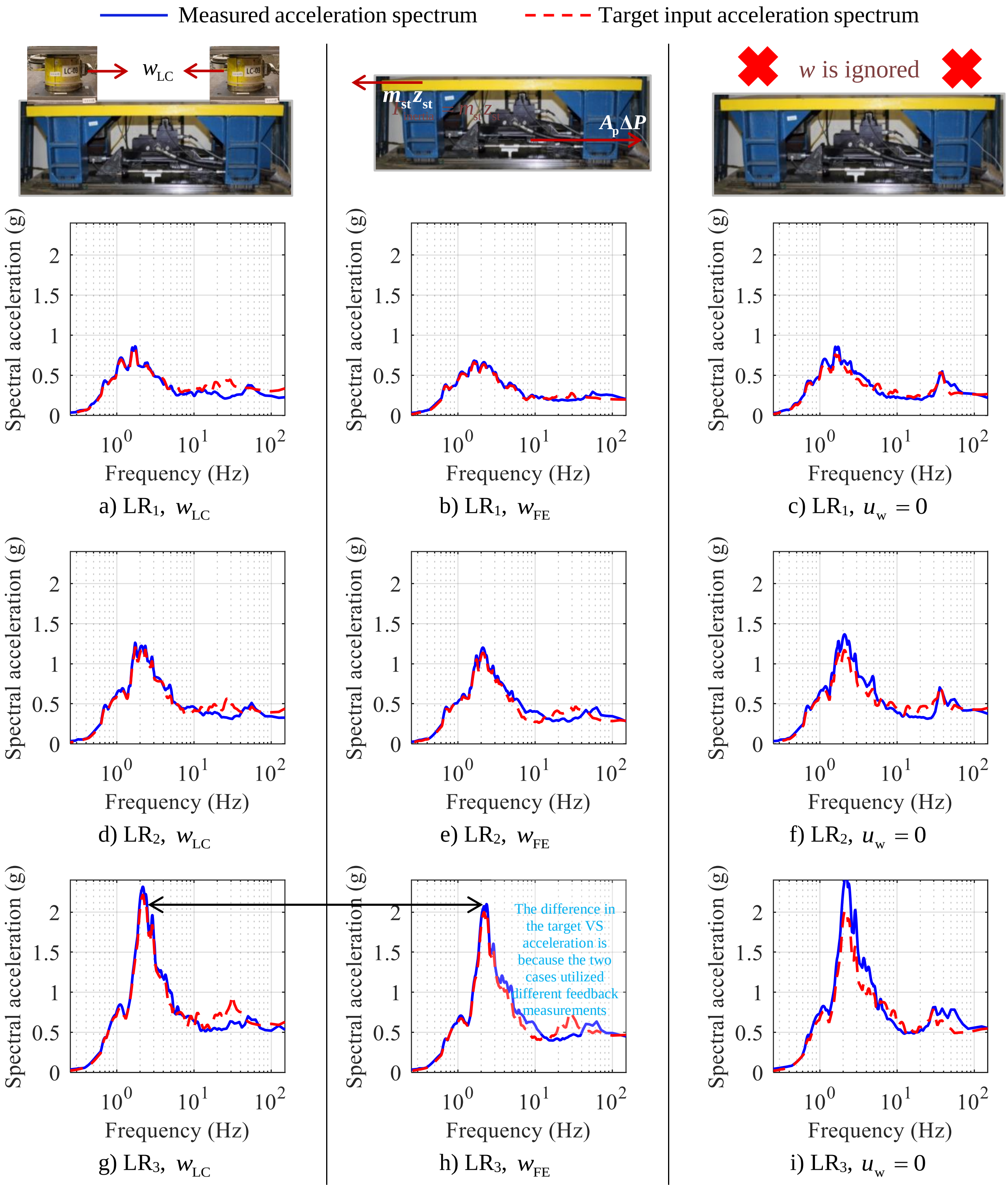

Figure C.2. Effect of different sources of feedback measurement on MIL performance imitating SD isolation systems for GM_1

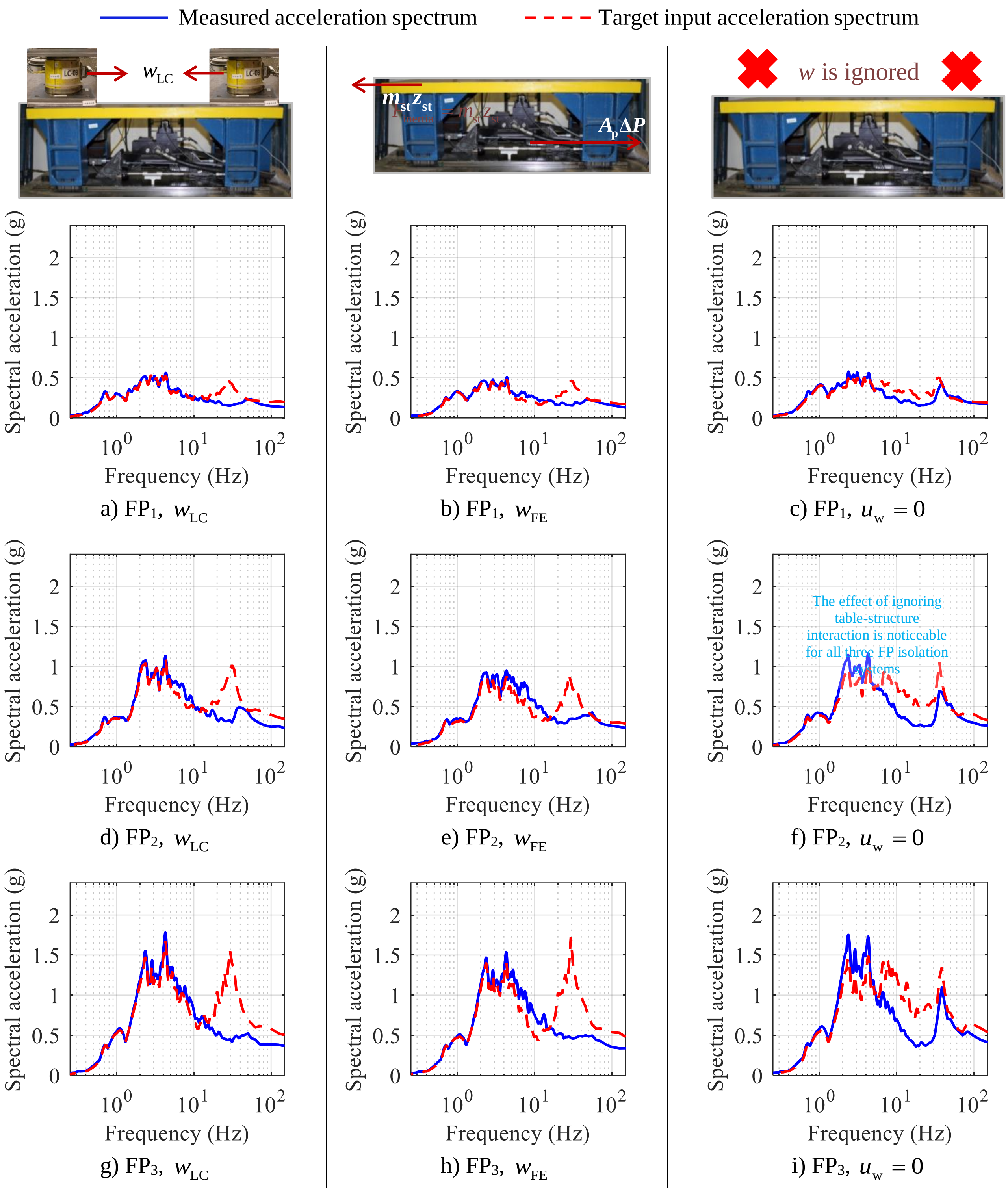

Figure C.3. Effect of different sources of feedback measurement on MIL performance imitating SD isolation systems for GM_1

The spectra in blue are generated from the measured acceleration of the shake table and the spectra in red are the target acceleration responses of the VS model. For the nine isolation systems considered herein, the MIL performance is similarly accurate for cases i) and ii), as shown by the close agreement between the blue and red spectra for frequencies less than 20 Hz in panels a), b), d), e), g), and h). An interesting observation being although the input motion and the VS properties are the same for cases i) and ii), the computed target VS acceleration, z_{vs}, is slightly different, particularly for high-strength, high-strength systems (e.g., SD_3, Figures C-1g and C-1h). The difference is because the two test cases utilized different feedback measurements, w_{LC} and w_{FE}, which are close but not identical. In this report, close agreement (qualitative) between the VS and the shake-table responses for a given w has been used as an indicator for 'correctness' or 'goodness' of MIL. Results in Figures C-1 through C-3 allow a reader to conclude that MIL performance (agreement between the VS and the shake table response) is good in both cases although the target response of the VS is slightly different. This raises a question of whether a more quantitative-based indicator is needed to assess the correctness (or goodness) of a MIL simulation.

The results presented in panels c), f), and i), where $u_{\mathrm{w}} = 0$, show that the effect of ignoring table-test article interaction is minimal when imitating low-strength, low-stiffness systems (e.g., Figure C-1c presented for the SD_1 system) but considerable when imitating high-strength, high-stiffness systems (see Figures C-1i, C-2i, and C-3i), because the interaction force is greater for high-strength, high-stiffness systems, and requires compensation for table-test article interaction via u_{w}.

MCEER Technical Reports

MCEER publishes technical reports on a variety of subjects written by authors funded through MCEER. These reports can be downloaded from the MCEER website at http://www.buffalo.edu/mceer. They can also be requested through NTIS, P.O. Box 1425, Springfield, Virginia 22151. NTIS accession numbers are shown in parenthesis, if available.

NCEER-87-0001 "First-Year Program in Research, Education and Technology Transfer," 3/5/87, (PB88-134275, A04, MF-A01).

NCEER-87-0002 "Experimental Evaluation of Instantaneous Optimal Algorithms for Structural Control," by R.C. Lin, T.T. Soong and A.M. Reinhorn, 4/20/87, (PB88-134341, A04, MF-A01).

NCEER-87-0003 "Experimentation Using the Earthquake Simulation Facilities at University at Buffalo," by A.M. Reinhorn and R.L. Ketter, not available.

NCEER-87-0004 "The System Characteristics and Performance of a Shaking Table," by J.S. Hwang, K.C. Chang and G.C. Lee, 6/1/87, (PB88-134259, A03, MF-A01). This report is available only through NTIS (see address given above).

NCEER-87-0005 "A Finite Element Formulation for Nonlinear Viscoplastic Material Using a Q Model," by O. Gyebi and G. Dasgupta, 11/2/87, (PB88-213764, A08, MF-A01).

NCEER-87-0006 "Symbolic Manipulation Program (SMP) - Algebraic Codes for Two and Three Dimensional Finite Element Formulations," by X. Lee and G. Dasgupta, 11/9/87, (PB88-218522, A05, MF-A01).

NCEER-87-0007 "Instantaneous Optimal Control Laws for Tall Buildings Under Seismic Excitations," by J.N. Yang, A. Akbarpour and P. Ghaemmaghami, 6/10/87, (PB88-134333, A06, MF-A01). This report is only available through NTIS (see address given above).

NCEER-87-0008 "IDARC: Inelastic Damage Analysis of Reinforced Concrete Frame - Shear-Wall Structures," by Y.J. Park, A.M. Reinhorn and S.K. Kunnath, 7/20/87, (PB88-134325, A09, MF-A01). This report is only available through NTIS (see address given above).

NCEER-87-0009 "Liquefaction Potential for New York State: A Preliminary Report on Sites in Manhattan and Buffalo," by M. Budhu, V. Vijayakumar, R.F. Giese and L. Baumgras, 8/31/87, (PB88-163704, A03, MF-A01). This report is available only through NTIS (see address given above).

NCEER-87-0010 "Vertical and Torsional Vibration of Foundations in Inhomogeneous Media," by A.S. Veletsos and K.W. Dotson, 6/1/87, (PB88-134291, A03, MF-A01). This report is only available through NTIS (see address given above).

NCEER-87-0011 "Seismic Probabilistic Risk Assessment and Seismic Margins Studies for Nuclear Power Plants," by Howard H.M. Hwang, 6/15/87, (PB88-134267, A03, MF-A01). This report is only available through NTIS (see address given above).

NCEER-87-0012 "Parametric Studies of Frequency Response of Secondary Systems Under Ground-Acceleration Excitations," by Y. Yong and Y.K. Lin, 6/10/87, (PB88-134309, A03, MF-A01). This report is only available through NTIS (see address given above).

NCEER-87-0013 "Frequency Response of Secondary Systems Under Seismic Excitation," by J.A. HoLung, J. Cai and Y.K. Lin, 7/31/87, (PB88-134317, A05, MF-A01). This report is only available through NTIS (see address given above).

NCEER-87-0014 "Modelling Earthquake Ground Motions in Seismically Active Regions Using Parametric Time Series Methods," by G.W. Ellis and A.S. Cakmak, 8/25/87, (PB88-134283, A08, MF-A01). This report is only available through NTIS (see address given above).

NCEER-87-0015 "Detection and Assessment of Seismic Structural Damage," by E. DiPasquale and A.S. Cakmak, 8/25/87, (PB88-163712, A05, MF-A01). This report is only available through NTIS (see address given above).

NCEER-87-0016 "Pipeline Experiment at Parkfield, California," by J. Isenberg and E. Richardson, 9/15/87, (PB88-163720, A03, MF-A01). This report is available only through NTIS (see address given above).

NCEER-87-0017 "Digital Simulation of Seismic Ground Motion," by M. Shinozuka, G. Deodatis and T. Harada, 8/31/87, (PB88-155197, A04, MF-A01). This report is available only through NTIS (see address given above).

NCEER-87-0018 "Practical Considerations for Structural Control: System Uncertainty, System Time Delay and Truncation of Small Control Forces," J.N. Yang and A. Akbarpour, 8/10/87, (PB88-163738, A08, MF-A01). This report is only available through NTIS (see address given above).

NCEER-87-0019 "Modal Analysis of Nonclassically Damped Structural Systems Using Canonical Transformation," by J.N. Yang, S. Sarkani and F.X. Long, 9/27/87, (PB88-187851, A04, MF-A01).

NCEER-87-0020 "A Nonstationary Solution in Random Vibration Theory," by J.R. Red-Horse and P.D. Spanos, 11/3/87, (PB88-163746, A03, MF-A01).

NCEER-87-0021 "Horizontal Impedances for Radially Inhomogeneous Viscoelastic Soil Layers," by A.S. Veletsos and K.W. Dotson, 10/15/87, (PB88-150859, A04, MF-A01).

NCEER-87-0022 "Seismic Damage Assessment of Reinforced Concrete Members," by Y.S. Chung, C. Meyer and M. Shinozuka, 10/9/87, (PB88-150867, A05, MF-A01). This report is available only through NTIS (see address given above).

NCEER-87-0023 "Active Structural Control in Civil Engineering," by T.T. Soong, 11/11/87, (PB88-187778, A03, MF-A01).

NCEER-87-0024 "Vertical and Torsional Impedances for Radially Inhomogeneous Viscoelastic Soil Layers," by K.W. Dotson and A.S. Veletsos, 12/87, (PB88-187786, A03, MF-A01).

NCEER-87-0025 "Proceedings from the Symposium on Seismic Hazards, Ground Motions, Soil-Liquefaction and Engineering Practice in Eastern North America," October 20-22, 1987, edited by K.H. Jacob, 12/87, (PB88-188115, A23, MF-A01). This report is available only through NTIS (see address given above).

NCEER-87-0026 "Report on the Whittier-Narrows, California, Earthquake of October 1, 1987," by J. Pantelic and A. Reinhorn, 11/87, (PB88-187752, A03, MF-A01). This report is available only through NTIS (see address given above).

NCEER-87-0027 "Design of a Modular Program for Transient Nonlinear Analysis of Large 3-D Building Structures," by S. Srivastav and J.F. Abel, 12/30/87, (PB88-187950, A05, MF-A01). This report is only available through NTIS (see address given above).

NCEER-87-0028 "Second-Year Program in Research, Education and Technology Transfer," 3/8/88, (PB88-219480, A04, MF-A01).

NCEER-88-0001 "Workshop on Seismic Computer Analysis and Design of Buildings With Interactive Graphics," by W. McGuire, J.F. Abel and C.H. Conley, 1/18/88, (PB88-187760, A03, MF-A01). This report is only available through NTIS (see address given above).

NCEER-88-0002 "Optimal Control of Nonlinear Flexible Structures," by J.N. Yang, F.X. Long and D. Wong, 1/22/88, (PB88-213772, A06, MF-A01).

NCEER-88-0003 "Substructuring Techniques in the Time Domain for Primary-Secondary Structural Systems," by G.D. Manolis and G. Juhn, 2/10/88, (PB88-213780, A04, MF-A01).

NCEER-88-0004 "Iterative Seismic Analysis of Primary-Secondary Systems," by A. Singhal, L.D. Lutes and P.D. Spanos, 2/23/88, (PB88-213798, A04, MF-A01).

NCEER-88-0005 "Stochastic Finite Element Expansion for Random Media," by P.D. Spanos and R. Ghanem, 3/14/88, (PB88-213806, A03, MF-A01).

NCEER-88-0006 "Combining Structural Optimization and Structural Control," by F.Y. Cheng and C.P. Pantelides, 1/10/88, (PB88-213814, A05, MF-A01).

NCEER-88-0007 "Seismic Performance Assessment of Code-Designed Structures," by H.H-M. Hwang, J-W. Jaw and H-J. Shau, 3/20/88, (PB88-219423, A04, MF-A01). This report is only available through NTIS (see address given above).

NCEER-88-0008 "Reliability Analysis of Code-Designed Structures Under Natural Hazards," by H.H-M. Hwang, H. Ushiba and M. Shinozuka, 2/29/88, (PB88-229471, A07, MF-A01). This report is only available through NTIS (see address given above).

NCEER-88-0009 "Seismic Fragility Analysis of Shear Wall Structures," by J-W Jaw and H.H-M. Hwang, 4/30/88, (PB89-102867, A04, MF-A01).

NCEER-88-0010 "Base Isolation of a Multi-Story Building Under a Harmonic Ground Motion - A Comparison of Performances of Various Systems," by F-G Fan, G. Ahmadi and I.G. Tadjbakhsh, 5/18/88, (PB89-122238, A06, MF-A01). This report is only available through NTIS (see address given above).

NCEER-88-0011 "Seismic Floor Response Spectra for a Combined System by Green's Functions," by F.M. Lavelle, L.A. Bergman and P.D. Spanos, 5/1/88, (PB89-102875, A03, MF-A01).

NCEER-88-0012 "A New Solution Technique for Randomly Excited Hysteretic Structures," by G.Q. Cai and Y.K. Lin, 5/16/88, (PB89-102883, A03, MF-A01).

NCEER-88-0013 "A Study of Radiation Damping and Soil-Structure Interaction Effects in the Centrifuge," by K. Weissman, supervised by J.H. Prevost, 5/24/88, (PB89-144703, A06, MF-A01).

NCEER-88-0014 "Parameter Identification and Implementation of a Kinematic Plasticity Model for Frictional Soils," by J.H. Prevost and D.V. Griffiths, not available.

NCEER-88-0015 "Two- and Three- Dimensional Dynamic Finite Element Analyses of the Long Valley Dam," by D.V. Griffiths and J.H. Prevost, 6/17/88, (PB89-144711, A04, MF-A01).

NCEER-88-0016 "Damage Assessment of Reinforced Concrete Structures in Eastern United States," by A.M. Reinhorn, M.J. Seidel, S.K. Kunnath and Y.J. Park, 6/15/88, (PB89-122220, A04, MF-A01). This report is only available through NTIS (see address given above).

NCEER-88-0017 "Dynamic Compliance of Vertically Loaded Strip Foundations in Multilayered Viscoelastic Soils," by S. Ahmad and A.S.M. Israil, 6/17/88, (PB89-102891, A04, MF-A01).

NCEER-88-0018 "An Experimental Study of Seismic Structural Response With Added Viscoelastic Dampers," by R.C. Lin, Z. Liang, T.T. Soong and R.H. Zhang, 6/30/88, (PB89-122212, A05, MF-A01). This report is available only through NTIS (see address given above).

NCEER-88-0019 "Experimental Investigation of Primary - Secondary System Interaction," by G.D. Manolis, G. Juhn and A.M. Reinhorn, 5/27/88, (PB89-122204, A04, MF-A01).

NCEER-88-0020 "A Response Spectrum Approach For Analysis of Nonclassically Damped Structures," by J.N. Yang, S. Sarkani and F.X. Long, 4/22/88, (PB89-102909, A04, MF-A01).

NCEER-88-0021 "Seismic Interaction of Structures and Soils: Stochastic Approach," by A.S. Veletsos and A.M. Prasad, 7/21/88, (PB89-122196, A04, MF-A01). This report is only available through NTIS (see address given above).

NCEER-88-0022 "Identification of the Serviceability Limit State and Detection of Seismic Structural Damage," by E. DiPasquale and A.S. Cakmak, 6/15/88, (PB89-122188, A05, MF-A01). This report is available only through NTIS (see address given above).

NCEER-88-0023 "Multi-Hazard Risk Analysis: Case of a Simple Offshore Structure," by B.K. Bhartia and E.H. Vanmarcke, 7/21/88, (PB89-145213, A05, MF-A01).

NCEER-88-0024 "Automated Seismic Design of Reinforced Concrete Buildings," by Y.S. Chung, C. Meyer and M. Shinozuka, 7/5/88, (PB89-122170, A06, MF-A01). This report is available only through NTIS (see address given above).

NCEER-88-0025 "Experimental Study of Active Control of MDOF Structures Under Seismic Excitations," by L.L. Chung, R.C. Lin, T.T. Soong and A.M. Reinhorn, 7/10/88, (PB89-122600, A04, MF-A01).

NCEER-88-0026 "Earthquake Simulation Tests of a Low-Rise Metal Structure," by J.S. Hwang, K.C. Chang, G.C. Lee and R.L. Ketter, 8/1/88, (PB89-102917, A04, MF-A01).

NCEER-88-0027 "Systems Study of Urban Response and Reconstruction Due to Catastrophic Earthquakes," by F. Kozin and H.K. Zhou, 9/22/88, (PB90-162348, A04, MF-A01).

NCEER-88-0028 "Seismic Fragility Analysis of Plane Frame Structures," by H.H-M. Hwang and Y.K. Low, 7/31/88, (PB89-131445, A06, MF-A01).

NCEER-88-0029 "Response Analysis of Stochastic Structures," by A. Kardara, C. Bucher and M. Shinozuka, 9/22/88, (PB89-174429, A04, MF-A01).

NCEER-88-0030 "Nonnormal Accelerations Due to Yielding in a Primary Structure," by D.C.K. Chen and L.D. Lutes, 9/19/88, (PB89-131437, A04, MF-A01).

NCEER-88-0031 "Design Approaches for Soil-Structure Interaction," by A.S. Veletsos, A.M. Prasad and Y. Tang, 12/30/88, (PB89-174437, A03, MF-A01). This report is available only through NTIS (see address given above).

NCEER-88-0032 "A Re-evaluation of Design Spectra for Seismic Damage Control," by C.J. Turkstra and A.G. Tallin, 11/7/88, (PB89-145221, A05, MF-A01).

NCEER-88-0033 "The Behavior and Design of Noncontact Lap Splices Subjected to Repeated Inelastic Tensile Loading," by V.E. Sagan, P. Gergely and R.N. White, 12/8/88, (PB89-163737, A08, MF-A01).

NCEER-88-0034 "Seismic Response of Pile Foundations," by S.M. Mamoon, P.K. Banerjee and S. Ahmad, 11/1/88, (PB89-145239, A04, MF-A01).

NCEER-88-0035 "Modeling of R/C Building Structures With Flexible Floor Diaphragms (IDARC2)," by A.M. Reinhorn, S.K. Kunnath and N. Panahshahi, 9/7/88, (PB89-207153, A07, MF-A01).

NCEER-88-0036 "Solution of the Dam-Reservoir Interaction Problem Using a Combination of FEM, BEM with Particular Integrals, Modal Analysis, and Substructuring," by C-S. Tsai, G.C. Lee and R.L. Ketter, 12/31/88, (PB89-207146, A04, MF-A01).

NCEER-88-0037 "Optimal Placement of Actuators for Structural Control," by F.Y. Cheng and C.P. Pantelides, 8/15/88, (PB89-162846, A05, MF-A01).

NCEER-88-0038 "Teflon Bearings in Aseismic Base Isolation: Experimental Studies and Mathematical Modeling," by A. Mokha, M.C. Constantinou and A.M. Reinhorn, 12/5/88, (PB89-218457, A10, MF-A01). This report is available only through NTIS (see address given above).

NCEER-88-0039 "Seismic Behavior of Flat Slab High-Rise Buildings in the New York City Area," by P. Weidlinger and M. Ettouney, 10/15/88, (PB90-145681, A04, MF-A01).

NCEER-88-0040 "Evaluation of the Earthquake Resistance of Existing Buildings in New York City," by P. Weidlinger and M. Ettouney, 10/15/88, not available.

NCEER-88-0041 "Small-Scale Modeling Techniques for Reinforced Concrete Structures Subjected to Seismic Loads," by W. Kim, A. El-Attar and R.N. White, 11/22/88, (PB89-189625, A05, MF-A01).

NCEER-88-0042 "Modeling Strong Ground Motion from Multiple Event Earthquakes," by G.W. Ellis and A.S. Cakmak, 10/15/88, (PB89-174445, A03, MF-A01).

NCEER-88-0043 "Nonstationary Models of Seismic Ground Acceleration," by M. Grigoriu, S.E. Ruiz and E. Rosenblueth, 7/15/88, (PB89-189617, A04, MF-A01).

NCEER-88-0044 "SARCF User's Guide: Seismic Analysis of Reinforced Concrete Frames," by Y.S. Chung, C. Meyer and M. Shinozuka, 11/9/88, (PB89-174452, A08, MF-A01).

NCEER-88-0045 "First Expert Panel Meeting on Disaster Research and Planning," edited by J. Pantelic and J. Stoyle, 9/15/88, (PB89-174460, A05, MF-A01).

NCEER-88-0046 "Preliminary Studies of the Effect of Degrading Infill Walls on the Nonlinear Seismic Response of Steel Frames," by C.Z. Chrysostomou, P. Gergely and J.F. Abel, 12/19/88, (PB89-208383, A05, MF-A01).

NCEER-88-0047 "Reinforced Concrete Frame Component Testing Facility - Design, Construction, Instrumentation and Operation," by S.P. Pessiki, C. Conley, T. Bond, P. Gergely and R.N. White, 12/16/88, (PB89-174478, A04, MF-A01).

NCEER-89-0001 "Effects of Protective Cushion and Soil Compliancy on the Response of Equipment Within a Seismically Excited Building," by J.A. HoLung, 2/16/89, (PB89-207179, A04, MF-A01).

NCEER-89-0002 "Statistical Evaluation of Response Modification Factors for Reinforced Concrete Structures," by H.H-M. Hwang and J-W. Jaw, 2/17/89, (PB89-207187, A05, MF-A01).

NCEER-89-0003 "Hysteretic Columns Under Random Excitation," by G-Q. Cai and Y.K. Lin, 1/9/89, (PB89-196513, A03, MF-A01).

NCEER-89-0004 "Experimental Study of `Elephant Foot Bulge' Instability of Thin-Walled Metal Tanks," by Z-H. Jia and R.L. Ketter, 2/22/89, (PB89-207195, A03, MF-A01).

NCEER-89-0005 "Experiment on Performance of Buried Pipelines Across San Andreas Fault," by J. Isenberg, E. Richardson and T.D. O'Rourke, 3/10/89, (PB89-218440, A04, MF-A01). This report is available only through NTIS (see address given above).

NCEER-89-0006 "A Knowledge-Based Approach to Structural Design of Earthquake-Resistant Buildings," by M. Subramani, P. Gergely, C.H. Conley, J.F. Abel and A.H. Zaghw, 1/15/89, (PB89-218465, A06, MF-A01).

NCEER-89-0007 "Liquefaction Hazards and Their Effects on Buried Pipelines," by T.D. O'Rourke and P.A. Lane, 2/1/89, (PB89-218481, A09, MF-A01).

NCEER-89-0008 "Fundamentals of System Identification in Structural Dynamics," by H. Imai, C-B. Yun, O. Maruyama and M. Shinozuka, 1/26/89, (PB89-207211, A04, MF-A01).

NCEER-89-0009 "Effects of the 1985 Michoacan Earthquake on Water Systems and Other Buried Lifelines in Mexico," by A.G. Ayala and M.J. O'Rourke, 3/8/89, (PB89-207229, A06, MF-A01).

NCEER-89-R010 "NCEER Bibliography of Earthquake Education Materials," by K.E.K. Ross, Second Revision, 9/1/89, (PB90-125352, A05, MF-A01). This report is replaced by NCEER-92-0018.

NCEER-89-0011 "Inelastic Three-Dimensional Response Analysis of Reinforced Concrete Building Structures (IDARC-3D), Part I - Modeling," by S.K. Kunnath and A.M. Reinhorn, 4/17/89, (PB90-114612, A07, MF-A01). This report is available only through NTIS (see address given above).

NCEER-89-0012 "Recommended Modifications to ATC-14," by C.D. Poland and J.O. Malley, 4/12/89, (PB90-108648, A15, MF-A01).

NCEER-89-0013 "Repair and Strengthening of Beam-to-Column Connections Subjected to Earthquake Loading," by M. Corazao and A.J. Durrani, 2/28/89, (PB90-109885, A06, MF-A01).

NCEER-89-0014 "Program EXKAL2 for Identification of Structural Dynamic Systems," by O. Maruyama, C-B. Yun, M. Hoshiya and M. Shinozuka, 5/19/89, (PB90-109877, A09, MF-A01).

NCEER-89-0015 "Response of Frames With Bolted Semi-Rigid Connections, Part I - Experimental Study and Analytical Predictions," by P.J. DiCorso, A.M. Reinhorn, J.R. Dickerson, J.B. Radziminski and W.L. Harper, 6/1/89, not available.

NCEER-89-0016 "ARMA Monte Carlo Simulation in Probabilistic Structural Analysis," by P.D. Spanos and M.P. Mignolet, 7/10/89, (PB90-109893, A03, MF-A01).

NCEER-89-P017 "Preliminary Proceedings from the Conference on Disaster Preparedness - The Place of Earthquake Education in Our Schools," Edited by K.E.K. Ross, 6/23/89, (PB90-108606, A03, MF-A01).

NCEER-89-0017 "Proceedings from the Conference on Disaster Preparedness - The Place of Earthquake Education in Our Schools," Edited by K.E.K. Ross, 12/31/89, (PB90-207895, A012, MF-A02). This report is available only through NTIS (see address given above).

NCEER-89-0018 "Multidimensional Models of Hysteretic Material Behavior for Vibration Analysis of Shape Memory Energy Absorbing Devices, by E.J. Graesser and F.A. Cozzarelli, 6/7/89, (PB90-164146, A04, MF-A01).

NCEER-89-0019 "Nonlinear Dynamic Analysis of Three-Dimensional Base Isolated Structures (3D-BASIS)," by S. Nagarajaiah, A.M. Reinhorn and M.C. Constantinou, 8/3/89, (PB90-161936, A06, MF-A01). This report has been replaced by NCEER-93-0011.

NCEER-89-0020 "Structural Control Considering Time-Rate of Control Forces and Control Rate Constraints," by F.Y. Cheng and C.P. Pantelides, 8/3/89, (PB90-120445, A04, MF-A01).

NCEER-89-0021 "Subsurface Conditions of Memphis and Shelby County," by K.W. Ng, T-S. Chang and H-H.M. Hwang, 7/26/89, (PB90-120437, A03, MF-A01).

NCEER-89-0022 "Seismic Wave Propagation Effects on Straight Jointed Buried Pipelines," by K. Elhmadi and M.J. O'Rourke, 8/24/89, (PB90-162322, A10, MF-A02).

NCEER-89-0023 "Workshop on Serviceability Analysis of Water Delivery Systems," edited by M. Grigoriu, 3/6/89, (PB90-127424, A03, MF-A01).

NCEER-89-0024 "Shaking Table Study of a 1/5 Scale Steel Frame Composed of Tapered Members," by K.C. Chang, J.S. Hwang and G.C. Lee, 9/18/89, (PB90-160169, A04, MF-A01).

NCEER-89-0025 "DYNA1D: A Computer Program for Nonlinear Seismic Site Response Analysis - Technical Documentation," by Jean H. Prevost, 9/14/89, (PB90-161944, A07, MF-A01). This report is available only through NTIS (see address given above).

NCEER-89-0026 "1:4 Scale Model Studies of Active Tendon Systems and Active Mass Dampers for Aseismic Protection," by A.M. Reinhorn, T.T. Soong, R.C. Lin, Y.P. Yang, Y. Fukao, H. Abe and M. Nakai, 9/15/89, (PB90-173246, A10, MF-A02). This report is available only through NTIS (see address given above).

NCEER-89-0027 "Scattering of Waves by Inclusions in a Nonhomogeneous Elastic Half Space Solved by Boundary Element Methods," by P.K. Hadley, A. Askar and A.S. Cakmak, 6/15/89, (PB90-145699, A07, MF-A01).

NCEER-89-0028 "Statistical Evaluation of Deflection Amplification Factors for Reinforced Concrete Structures," by H.H.M. Hwang, J-W. Jaw and A.L. Ch'ng, 8/31/89, (PB90-164633, A05, MF-A01).

NCEER-89-0029 "Bedrock Accelerations in Memphis Area Due to Large New Madrid Earthquakes," by H.H.M. Hwang, C.H.S. Chen and G. Yu, 11/7/89, (PB90-162330, A04, MF-A01).

NCEER-89-0030 "Seismic Behavior and Response Sensitivity of Secondary Structural Systems," by Y.Q. Chen and T.T. Soong, 10/23/89, (PB90-164658, A08, MF-A01).

NCEER-89-0031 "Random Vibration and Reliability Analysis of Primary-Secondary Structural Systems," by Y. Ibrahim, M. Grigoriu and T.T. Soong, 11/10/89, (PB90-161951, A04, MF-A01).

NCEER-89-0032 "Proceedings from the Second U.S. - Japan Workshop on Liquefaction, Large Ground Deformation and Their Effects on Lifelines, September 26-29, 1989," Edited by T.D. O'Rourke and M. Hamada, 12/1/89, (PB90-209388, A22, MF-A03).

NCEER-89-0033 "Deterministic Model for Seismic Damage Evaluation of Reinforced Concrete Structures," by J.M. Bracci, A.M. Reinhorn, J.B. Mander and S.K. Kunnath, 9/27/89, (PB91-108803, A06, MF-A01).

NCEER-89-0034 "On the Relation Between Local and Global Damage Indices," by E. DiPasquale and A.S. Cakmak, 8/15/89, (PB90-173865, A05, MF-A01).

NCEER-89-0035 "Cyclic Undrained Behavior of Nonplastic and Low Plasticity Silts," by A.J. Walker and H.E. Stewart, 7/26/89, (PB90-183518, A10, MF-A01).

NCEER-89-0036 "Liquefaction Potential of Surficial Deposits in the City of Buffalo, New York," by M. Budhu, R. Giese and L. Baumgrass, 1/17/89, (PB90-208455, A04, MF-A01).

NCEER-89-0037 "A Deterministic Assessment of Effects of Ground Motion Incoherence," by A.S. Veletsos and Y. Tang, 7/15/89, (PB90-164294, A03, MF-A01).

NCEER-89-0038 "Workshop on Ground Motion Parameters for Seismic Hazard Mapping," July 17-18, 1989, edited by R.V. Whitman, 12/1/89, (PB90-173923, A04, MF-A01).

NCEER-89-0039 "Seismic Effects on Elevated Transit Lines of the New York City Transit Authority," by C.J. Costantino, C.A. Miller and E. Heymsfield, 12/26/89, (PB90-207887, A06, MF-A01).

NCEER-89-0040 "Centrifugal Modeling of Dynamic Soil-Structure Interaction," by K. Weissman, Supervised by J.H. Prevost, 5/10/89, (PB90-207879, A07, MF-A01).

NCEER-89-0041 "Linearized Identification of Buildings With Cores for Seismic Vulnerability Assessment," by I-K. Ho and A.E. Aktan, 11/1/89, (PB90-251943, A07, MF-A01).

NCEER-90-0001 "Geotechnical and Lifeline Aspects of the October 17, 1989 Loma Prieta Earthquake in San Francisco," by T.D. O'Rourke, H.E. Stewart, F.T. Blackburn and T.S. Dickerman, 1/90, (PB90-208596, A05, MF-A01).

NCEER-90-0002 "Nonnormal Secondary Response Due to Yielding in a Primary Structure," by D.C.K. Chen and L.D. Lutes, 2/28/90, (PB90-251976, A07, MF-A01).

NCEER-90-0003 "Earthquake Education Materials for Grades K-12," by K.E.K. Ross, 4/16/90, (PB91-251984, A05, MF-A05). This report has been replaced by NCEER-92-0018.

NCEER-90-0004 "Catalog of Strong Motion Stations in Eastern North America," by R.W. Busby, 4/3/90, (PB90-251984, A05, MF-A01).

NCEER-90-0005 "NCEER Strong-Motion Data Base: A User Manual for the GeoBase Release (Version 1.0 for the Sun3)," by P. Friberg and K. Jacob, 3/31/90 (PB90-258062, A04, MF-A01).

NCEER-90-0006 "Seismic Hazard Along a Crude Oil Pipeline in the Event of an 1811-1812 Type New Madrid Earthquake," by H.H.M. Hwang and C-H.S. Chen, 4/16/90, (PB90-258054, A04, MF-A01).

NCEER-90-0007 "Site-Specific Response Spectra for Memphis Sheahan Pumping Station," by H.H.M. Hwang and C.S. Lee, 5/15/90, (PB91-108811, A05, MF-A01).

NCEER-90-0008 "Pilot Study on Seismic Vulnerability of Crude Oil Transmission Systems," by T. Ariman, R. Dobry, M. Grigoriu, F. Kozin, M. O'Rourke, T. O'Rourke and M. Shinozuka, 5/25/90, (PB91-108837, A06, MF-A01).

NCEER-90-0009 "A Program to Generate Site Dependent Time Histories: EQGEN," by G.W. Ellis, M. Srinivasan and A.S. Cakmak, 1/30/90, (PB91-108829, A04, MF-A01).

NCEER-90-0010 "Active Isolation for Seismic Protection of Operating Rooms," by M.E. Talbott, Supervised by M. Shinozuka, 6/8/9, (PB91-110205, A05, MF-A01).

NCEER-90-0011 "Program LINEARID for Identification of Linear Structural Dynamic Systems," by C-B. Yun and M. Shinozuka, 6/25/90, (PB91-110312, A08, MF-A01).

NCEER-90-0012 "Two-Dimensional Two-Phase Elasto-Plastic Seismic Response of Earth Dams," by A.N. Yiagos, Supervised by J.H. Prevost, 6/20/90, (PB91-110197, A13, MF-A02).

NCEER-90-0013 "Secondary Systems in Base-Isolated Structures: Experimental Investigation, Stochastic Response and Stochastic Sensitivity," by G.D. Manolis, G. Juhn, M.C. Constantinou and A.M. Reinhorn, 7/1/90, (PB91-110320, A08, MF-A01).

NCEER-90-0014 "Seismic Behavior of Lightly-Reinforced Concrete Column and Beam-Column Joint Details," by S.P. Pessiki, C.H. Conley, P. Gergely and R.N. White, 8/22/90, (PB91-108795, A11, MF-A02).

NCEER-90-0015 "Two Hybrid Control Systems for Building Structures Under Strong Earthquakes," by J.N. Yang and A. Danielians, 6/29/90, (PB91-125393, A04, MF-A01).

NCEER-90-0016 "Instantaneous Optimal Control with Acceleration and Velocity Feedback," by J.N. Yang and Z. Li, 6/29/90, (PB91-125401, A03, MF-A01).

NCEER-90-0017 "Reconnaissance Report on the Northern Iran Earthquake of June 21, 1990," by M. Mehrain, 10/4/90, (PB91-125377, A03, MF-A01).

NCEER-90-0018 "Evaluation of Liquefaction Potential in Memphis and Shelby County," by T.S. Chang, P.S. Tang, C.S. Lee and H. Hwang, 8/10/90, (PB91-125427, A09, MF-A01).

NCEER-90-0019 "Experimental and Analytical Study of a Combined Sliding Disc Bearing and Helical Steel Spring Isolation System," by M.C. Constantinou, A.S. Mokha and A.M. Reinhorn, 10/4/90, (PB91-125385, A06, MF-A01). This report is available only through NTIS (see address given above).

NCEER-90-0020 "Experimental Study and Analytical Prediction of Earthquake Response of a Sliding Isolation System with a Spherical Surface," by A.S. Mokha, M.C. Constantinou and A.M. Reinhorn, 10/11/90, (PB91-125419, A05, MF-A01).

NCEER-90-0021 "Dynamic Interaction Factors for Floating Pile Groups," by G. Gazetas, K. Fan, A. Kaynia and E. Kausel, 9/10/90, (PB91-170381, A05, MF-A01).

NCEER-90-0022 "Evaluation of Seismic Damage Indices for Reinforced Concrete Structures," by S. Rodriguez-Gomez and A.S. Cakmak, 9/30/90, PB91-171322, A06, MF-A01).

NCEER-90-0023 "Study of Site Response at a Selected Memphis Site," by H. Desai, S. Ahmad, E.S. Gazetas and M.R. Oh, 10/11/90, (PB91-196857, A03, MF-A01).

NCEER-90-0024 "A User's Guide to Strongmo: Version 1.0 of NCEER's Strong-Motion Data Access Tool for PCs and Terminals," by P.A. Friberg and C.A.T. Susch, 11/15/90, (PB91-171272, A03, MF-A01).

NCEER-90-0025 "A Three-Dimensional Analytical Study of Spatial Variability of Seismic Ground Motions," by L-L. Hong and A.H.-S. Ang, 10/30/90, (PB91-170399, A09, MF-A01).

NCEER-90-0026 "MUMOID User's Guide - A Program for the Identification of Modal Parameters," by S. Rodriguez-Gomez and E. DiPasquale, 9/30/90, (PB91-171298, A04, MF-A01).

NCEER-90-0027 "SARCF-II User's Guide - Seismic Analysis of Reinforced Concrete Frames," by S. Rodriguez-Gomez, Y.S. Chung and C. Meyer, 9/30/90, (PB91-171280, A05, MF-A01).

NCEER-90-0028 "Viscous Dampers: Testing, Modeling and Application in Vibration and Seismic Isolation," by N. Makris and M.C. Constantinou, 12/20/90 (PB91-190561, A06, MF-A01).

NCEER-90-0029 "Soil Effects on Earthquake Ground Motions in the Memphis Area," by H. Hwang, C.S. Lee, K.W. Ng and T.S. Chang, 8/2/90, (PB91-190751, A05, MF-A01).

NCEER-91-0001 "Proceedings from the Third Japan-U.S. Workshop on Earthquake Resistant Design of Lifeline Facilities and Countermeasures for Soil Liquefaction, December 17-19, 1990," edited by T.D. O'Rourke and M. Hamada, 2/1/91, (PB91-179259, A99, MF-A04).

NCEER-91-0002 "Physical Space Solutions of Non-Proportionally Damped Systems," by M. Tong, Z. Liang and G.C. Lee, 1/15/91, (PB91-179242, A04, MF-A01).

NCEER-91-0003 "Seismic Response of Single Piles and Pile Groups," by K. Fan and G. Gazetas, 1/10/91, (PB92-174994, A04, MF-A01).

NCEER-91-0004 "Damping of Structures: Part 1 - Theory of Complex Damping," by Z. Liang and G. Lee, 10/10/91, (PB92-197235, A12, MF-A03).

NCEER-91-0005 "3D-BASIS - Nonlinear Dynamic Analysis of Three Dimensional Base Isolated Structures: Part II," by S. Nagarajaiah, A.M. Reinhorn and M.C. Constantinou, 2/28/91, (PB91-190553, A07, MF-A01). This report has been replaced by NCEER-93-0011.

NCEER-91-0006 "A Multidimensional Hysteretic Model for Plasticity Deforming Metals in Energy Absorbing Devices," by E.J. Graesser and F.A. Cozzarelli, 4/9/91, (PB92-108364, A04, MF-A01).

NCEER-91-0007 "A Framework for Customizable Knowledge-Based Expert Systems with an Application to a KBES for Evaluating the Seismic Resistance of Existing Buildings," by E.G. Ibarra-Anaya and S.J. Fenves, 4/9/91, (PB91-210930, A08, MF-A01).

NCEER-91-0008 "Nonlinear Analysis of Steel Frames with Semi-Rigid Connections Using the Capacity Spectrum Method," by G.G. Deierlein, S-H. Hsieh, Y-J. Shen and J.F. Abel, 7/2/91, (PB92-113828, A05, MF-A01).

NCEER-91-0009 "Earthquake Education Materials for Grades K-12," by K.E.K. Ross, 4/30/91, (PB91-212142, A06, MF-A01). This report has been replaced by NCEER-92-0018.

NCEER-91-0010 "Phase Wave Velocities and Displacement Phase Differences in a Harmonically Oscillating Pile," by N. Makris and G. Gazetas, 7/8/91, (PB92-108356, A04, MF-A01).

NCEER-91-0011 "Dynamic Characteristics of a Full-Size Five-Story Steel Structure and a 2/5 Scale Model," by K.C. Chang, G.C. Yao, G.C. Lee, D.S. Hao and Y.C. Yeh," 7/2/91, (PB93-116648, A06, MF-A02).

NCEER-91-0012 "Seismic Response of a 2/5 Scale Steel Structure with Added Viscoelastic Dampers," by K.C. Chang, T.T. Soong, S-T. Oh and M.L. Lai, 5/17/91, (PB92-110816, A05, MF-A01).

NCEER-91-0013 "Earthquake Response of Retaining Walls; Full-Scale Testing and Computational Modeling," by S. Alampalli and A-W.M. Elgamal, 6/20/91, not available.

NCEER-91-0014 "3D-BASIS-M: Nonlinear Dynamic Analysis of Multiple Building Base Isolated Structures," by P.C. Tsopelas, S. Nagarajaiah, M.C. Constantinou and A.M. Reinhorn, 5/28/91, (PB92-113885, A09, MF-A02).

NCEER-91-0015 "Evaluation of SEAOC Design Requirements for Sliding Isolated Structures," by D. Theodossiou and M.C. Constantinou, 6/10/91, (PB92-114602, A11, MF-A03).

NCEER-91-0016 "Closed-Loop Modal Testing of a 27-Story Reinforced Concrete Flat Plate-Core Building," by H.R. Somaprasad, T. Toksoy, H. Yoshiyuki and A.E. Aktan, 7/15/91, (PB92-129980, A07, MF-A02).

NCEER-91-0017 "Shake Table Test of a 1/6 Scale Two-Story Lightly Reinforced Concrete Building," by A.G. El-Attar, R.N. White and P. Gergely, 2/28/91, (PB92-222447, A06, MF-A02).

NCEER-91-0018 "Shake Table Test of a 1/8 Scale Three-Story Lightly Reinforced Concrete Building," by A.G. El-Attar, R.N. White and P. Gergely, 2/28/91, (PB93-116630, A08, MF-A02).

NCEER-91-0019 "Transfer Functions for Rigid Rectangular Foundations," by A.S. Veletsos, A.M. Prasad and W.H. Wu, 7/31/91, not available.

NCEER-91-0020 "Hybrid Control of Seismic-Excited Nonlinear and Inelastic Structural Systems," by J.N. Yang, Z. Li and A. Danielians, 8/1/91, (PB92-143171, A06, MF-A02).

NCEER-91-0021 "The NCEER-91 Earthquake Catalog: Improved Intensity-Based Magnitudes and Recurrence Relations for U.S. Earthquakes East of New Madrid," by L. Seeber and J.G. Armbruster, 8/28/91, (PB92-176742, A06, MF-A02).

NCEER-91-0022 "Proceedings from the Implementation of Earthquake Planning and Education in Schools: The Need for Change - The Roles of the Changemakers," by K.E.K. Ross and F. Winslow, 7/23/91, (PB92-129998, A12, MF-A03).

NCEER-91-0023 "A Study of Reliability-Based Criteria for Seismic Design of Reinforced Concrete Frame Buildings," by H.H.M. Hwang and H-M. Hsu, 8/10/91, (PB92-140235, A09, MF-A02).

NCEER-91-0024 "Experimental Verification of a Number of Structural System Identification Algorithms," by R.G. Ghanem, H. Gavin and M. Shinozuka, 9/18/91, (PB92-176577, A18, MF-A04).

NCEER-91-0025 "Probabilistic Evaluation of Liquefaction Potential," by H.H.M. Hwang and C.S. Lee," 11/25/91, (PB92-143429, A05, MF-A01).

NCEER-91-0026 "Instantaneous Optimal Control for Linear, Nonlinear and Hysteretic Structures - Stable Controllers," by J.N. Yang and Z. Li, 11/15/91, (PB92-163807, A04, MF-A01).

NCEER-91-0027 "Experimental and Theoretical Study of a Sliding Isolation System for Bridges," by M.C. Constantinou, A. Kartoum, A.M. Reinhorn and P. Bradford, 11/15/91, (PB92-176973, A10, MF-A03).

NCEER-92-0001 "Case Studies of Liquefaction and Lifeline Performance During Past Earthquakes, Volume 1: Japanese Case Studies," Edited by M. Hamada and T. O'Rourke, 2/17/92, (PB92-197243, A18, MF-A04).

NCEER-92-0002 "Case Studies of Liquefaction and Lifeline Performance During Past Earthquakes, Volume 2: United States Case Studies," Edited by T. O'Rourke and M. Hamada, 2/17/92, (PB92-197250, A20, MF-A04).

NCEER-92-0003 "Issues in Earthquake Education," Edited by K. Ross, 2/3/92, (PB92-222389, A07, MF-A02).

NCEER-92-0004 "Proceedings from the First U.S. - Japan Workshop on Earthquake Protective Systems for Bridges," Edited by I.G. Buckle, 2/4/92, (PB94-142239, A99, MF-A06).

NCEER-92-0005 "Seismic Ground Motion from a Haskell-Type Source in a Multiple-Layered Half-Space," A.P. Theoharis, G. Deodatis and M. Shinozuka, 1/2/92, not available.

NCEER-92-0006 "Proceedings from the Site Effects Workshop," Edited by R. Whitman, 2/29/92, (PB92-197201, A04, MF-A01).

NCEER-92-0007 "Engineering Evaluation of Permanent Ground Deformations Due to Seismically-Induced Liquefaction," by M.H. Baziar, R. Dobry and A-W.M. Elgamal, 3/24/92, (PB92-222421, A13, MF-A03).

NCEER-92-0008 "A Procedure for the Seismic Evaluation of Buildings in the Central and Eastern United States," by C.D. Poland and J.O. Malley, 4/2/92, (PB92-222439, A20, MF-A04).

NCEER-92-0009 "Experimental and Analytical Study of a Hybrid Isolation System Using Friction Controllable Sliding Bearings," by M.Q. Feng, S. Fujii and M. Shinozuka, 5/15/92, (PB93-150282, A06, MF-A02).

NCEER-92-0010 "Seismic Resistance of Slab-Column Connections in Existing Non-Ductile Flat-Plate Buildings," by A.J. Durrani and Y. Du, 5/18/92, (PB93-116812, A06, MF-A02).

NCEER-92-0011 "The Hysteretic and Dynamic Behavior of Brick Masonry Walls Upgraded by Ferrocement Coatings Under Cyclic Loading and Strong Simulated Ground Motion," by H. Lee and S.P. Prawel, 5/11/92, not available.

NCEER-92-0012 "Study of Wire Rope Systems for Seismic Protection of Equipment in Buildings," by G.F. Demetriades, M.C. Constantinou and A.M. Reinhorn, 5/20/92, (PB93-116655, A08, MF-A02).

NCEER-92-0013 "Shape Memory Structural Dampers: Material Properties, Design and Seismic Testing," by P.R. Witting and F.A. Cozzarelli, 5/26/92, (PB93-116663, A05, MF-A01).

NCEER-92-0014 "Longitudinal Permanent Ground Deformation Effects on Buried Continuous Pipelines," by M.J. O'Rourke, and C. Nordberg, 6/15/92, (PB93-116671, A08, MF-A02).

NCEER-92-0015 "A Simulation Method for Stationary Gaussian Random Functions Based on the Sampling Theorem," by M. Grigoriu and S. Balopoulou, 6/11/92, (PB93-127496, A05, MF-A01).

NCEER-92-0016 "Gravity-Load-Designed Reinforced Concrete Buildings: Seismic Evaluation of Existing Construction and Detailing Strategies for Improved Seismic Resistance," by G.W. Hoffmann, S.K. Kunnath, A.M. Reinhorn and J.B. Mander, 7/15/92, (PB94-142007, A08, MF-A02).

NCEER-92-0017 "Observations on Water System and Pipeline Performance in the Limón Area of Costa Rica Due to the April 22, 1991 Earthquake," by M. O'Rourke and D. Ballantyne, 6/30/92, (PB93-126811, A06, MF-A02).

NCEER-92-0018 "Fourth Edition of Earthquake Education Materials for Grades K-12," Edited by K.E.K. Ross, 8/10/92, (PB93-114023, A07, MF-A02).

NCEER-92-0019 "Proceedings from the Fourth Japan-U.S. Workshop on Earthquake Resistant Design of Lifeline Facilities and Countermeasures for Soil Liquefaction," Edited by M. Hamada and T.D. O'Rourke, 8/12/92, (PB93-163939, A99, MF-E11).

NCEER-92-0020 "Active Bracing System: A Full Scale Implementation of Active Control," by A.M. Reinhorn, T.T. Soong, R.C. Lin, M.A. Riley, Y.P. Wang, S. Aizawa and M. Higashino, 8/14/92, (PB93-127512, A06, MF-A02).

NCEER-92-0021 "Empirical Analysis of Horizontal Ground Displacement Generated by Liquefaction-Induced Lateral Spreads," by S.F. Bartlett and T.L. Youd, 8/17/92, (PB93-188241, A06, MF-A02).

NCEER-92-0022 "IDARC Version 3.0: Inelastic Damage Analysis of Reinforced Concrete Structures," by S.K. Kunnath, A.M. Reinhorn and R.F. Lobo, 8/31/92, (PB93-227502, A07, MF-A02).

NCEER-92-0023 "A Semi-Empirical Analysis of Strong-Motion Peaks in Terms of Seismic Source, Propagation Path and Local Site Conditions, by M. Kamiyama, M.J. O'Rourke and R. Flores-Berrones, 9/9/92, (PB93-150266, A08, MF-A02).

NCEER-92-0024 "Seismic Behavior of Reinforced Concrete Frame Structures with Nonductile Details, Part I: Summary of Experimental Findings of Full Scale Beam-Column Joint Tests," by A. Beres, R.N. White and P. Gergely, 9/30/92, (PB93-227783, A05, MF-A01).

NCEER-92-0025 "Experimental Results of Repaired and Retrofitted Beam-Column Joint Tests in Lightly Reinforced Concrete Frame Buildings," by A. Beres, S. El-Borgi, R.N. White and P. Gergely, 10/29/92, (PB93-227791, A05, MF-A01).

NCEER-92-0026 "A Generalization of Optimal Control Theory: Linear and Nonlinear Structures," by J.N. Yang, Z. Li and S. Vongchavalitkul, 11/2/92, (PB93-188621, A05, MF-A01).

NCEER-92-0027 "Seismic Resistance of Reinforced Concrete Frame Structures Designed Only for Gravity Loads: Part I - Design and Properties of a One-Third Scale Model Structure," by J.M. Bracci, A.M. Reinhorn and J.B. Mander, 12/1/92, (PB94-104502, A08, MF-A02).

NCEER-92-0028 "Seismic Resistance of Reinforced Concrete Frame Structures Designed Only for Gravity Loads: Part II - Experimental Performance of Subassemblages," by L.E. Aycardi, J.B. Mander and A.M. Reinhorn, 12/1/92, (PB94-104510, A08, MF-A02).

NCEER-92-0029 "Seismic Resistance of Reinforced Concrete Frame Structures Designed Only for Gravity Loads: Part III - Experimental Performance and Analytical Study of a Structural Model," by J.M. Bracci, A.M. Reinhorn and J.B. Mander, 12/1/92, (PB93-227528, A09, MF-A01).

NCEER-92-0030 "Evaluation of Seismic Retrofit of Reinforced Concrete Frame Structures: Part I - Experimental Performance of Retrofitted Subassemblages," by D. Choudhuri, J.B. Mander and A.M. Reinhorn, 12/8/92, (PB93-198307, A07, MF-A02).

NCEER-92-0031 "Evaluation of Seismic Retrofit of Reinforced Concrete Frame Structures: Part II - Experimental Performance and Analytical Study of a Retrofitted Structural Model," by J.M. Bracci, A.M. Reinhorn and J.B. Mander, 12/8/92, (PB93-198315, A09, MF-A03).

NCEER-92-0032 "Experimental and Analytical Investigation of Seismic Response of Structures with Supplemental Fluid Viscous Dampers," by M.C. Constantinou and M.D. Symans, 12/21/92, (PB93-191435, A10, MF-A03). This report is available only through NTIS (see address given above).

NCEER-92-0033 "Reconnaissance Report on the Cairo, Egypt Earthquake of October 12, 1992," by M. Khater, 12/23/92, (PB93-188621, A03, MF-A01).

NCEER-92-0034 "Low-Level Dynamic Characteristics of Four Tall Flat-Plate Buildings in New York City," by H. Gavin, S. Yuan, J. Grossman, E. Pekelis and K. Jacob, 12/28/92, (PB93-188217, A07, MF-A02).

NCEER-93-0001 "An Experimental Study on the Seismic Performance of Brick-Infilled Steel Frames With and Without Retrofit," by J.B. Mander, B. Nair, K. Wojtkowski and J. Ma, 1/29/93, (PB93-227510, A07, MF-A02).

NCEER-93-0002 "Social Accounting for Disaster Preparedness and Recovery Planning," by S. Cole, E. Pantoja and V. Razak, 2/22/93, (PB94-142114, A12, MF-A03).

NCEER-93-0003 "Assessment of 1991 NEHRP Provisions for Nonstructural Components and Recommended Revisions," by T.T. Soong, G. Chen, Z. Wu, R-H. Zhang and M. Grigoriu, 3/1/93, (PB93-188639, A06, MF-A02).

NCEER-93-0004 "Evaluation of Static and Response Spectrum Analysis Procedures of SEAOC/UBC for Seismic Isolated Structures," by C.W. Winters and M.C. Constantinou, 3/23/93, (PB93-198299, A10, MF-A03).

NCEER-93-0005 "Earthquakes in the Northeast - Are We Ignoring the Hazard? A Workshop on Earthquake Science and Safety for Educators," edited by K.E.K. Ross, 4/2/93, (PB94-103066, A09, MF-A02).

NCEER-93-0006 "Inelastic Response of Reinforced Concrete Structures with Viscoelastic Braces," by R.F. Lobo, J.M. Bracci, K.L. Shen, A.M. Reinhorn and T.T. Soong, 4/5/93, (PB93-227486, A05, MF-A02).

NCEER-93-0007 "Seismic Testing of Installation Methods for Computers and Data Processing Equipment," by K. Kosar, T.T. Soong, K.L. Shen, J.A. HoLung and Y.K. Lin, 4/12/93, (PB93-198299, A07, MF-A02).

NCEER-93-0008 "Retrofit of Reinforced Concrete Frames Using Added Dampers," by A. Reinhorn, M. Constantinou and C. Li, not available.

NCEER-93-0009 "Seismic Behavior and Design Guidelines for Steel Frame Structures with Added Viscoelastic Dampers," by K.C. Chang, M.L. Lai, T.T. Soong, D.S. Hao and Y.C. Yeh, 5/1/93, (PB94-141959, A07, MF-A02).

NCEER-93-0010 "Seismic Performance of Shear-Critical Reinforced Concrete Bridge Piers," by J.B. Mander, S.M. Waheed, M.T.A. Chaudhary and S.S. Chen, 5/12/93, (PB93-227494, A08, MF-A02).

NCEER-93-0011 "3D-BASIS-TABS: Computer Program for Nonlinear Dynamic Analysis of Three Dimensional Base Isolated Structures," by S. Nagarajaiah, C. Li, A.M. Reinhorn and M.C. Constantinou, 8/2/93, (PB94-141819, A09, MF-A02).

NCEER-93-0012 "Effects of Hydrocarbon Spills from an Oil Pipeline Break on Ground Water," by O.J. Helweg and H.H.M. Hwang, 8/3/93, (PB94-141942, A06, MF-A02).

NCEER-93-0013 "Simplified Procedures for Seismic Design of Nonstructural Components and Assessment of Current Code Provisions," by M.P. Singh, L.E. Suarez, E.E. Matheu and G.O. Maldonado, 8/4/93, (PB94-141827, A09, MF-A02).

NCEER-93-0014 "An Energy Approach to Seismic Analysis and Design of Secondary Systems," by G. Chen and T.T. Soong, 8/6/93, (PB94-142767, A11, MF-A03).

NCEER-93-0015 "Proceedings from School Sites: Becoming Prepared for Earthquakes - Commemorating the Third Anniversary of the Loma Prieta Earthquake," Edited by F.E. Winslow and K.E.K. Ross, 8/16/93, (PB94-154275, A16, MF-A02).

NCEER-93-0016 "Reconnaissance Report of Damage to Historic Monuments in Cairo, Egypt Following the October 12, 1992 Dahshur Earthquake," by D. Sykora, D. Look, G. Croci, E. Karaesmen and E. Karaesmen, 8/19/93, (PB94-142221, A08, MF-A02).

NCEER-93-0017 "The Island of Guam Earthquake of August 8, 1993," by S.W. Swan and S.K. Harris, 9/30/93, (PB94-141843, A04, MF-A01).

NCEER-93-0018 "Engineering Aspects of the October 12, 1992 Egyptian Earthquake," by A.W. Elgamal, M. Amer, K. Adalier and A. Abul-Fadl, 10/7/93, (PB94-141983, A05, MF-A01).

NCEER-93-0019 "Development of an Earthquake Motion Simulator and its Application in Dynamic Centrifuge Testing," by I. Krstelj, Supervised by J.H. Prevost, 10/23/93, (PB94-181773, A-10, MF-A03).

NCEER-93-0020 "NCEER-Taisei Corporation Research Program on Sliding Seismic Isolation Systems for Bridges: Experimental and Analytical Study of a Friction Pendulum System (FPS)," by M.C. Constantinou, P. Tsopelas, Y-S. Kim and S. Okamoto, 11/1/93, (PB94-142775, A08, MF-A02).

NCEER-93-0021 "Finite Element Modeling of Elastomeric Seismic Isolation Bearings," by L.J. Billings, Supervised by R. Shepherd, 11/8/93, not available.

NCEER-93-0022 "Seismic Vulnerability of Equipment in Critical Facilities: Life-Safety and Operational Consequences," by K. Porter, G.S. Johnson, M.M. Zadeh, C. Scawthorn and S. Eder, 11/24/93, (PB94-181765, A16, MF-A03).

NCEER-93-0023 "Hokkaido Nansei-oki, Japan Earthquake of July 12, 1993, by P.I. Yanev and C.R. Scawthorn, 12/23/93, (PB94-181500, A07, MF-A01).

NCEER-94-0001 "An Evaluation of Seismic Serviceability of Water Supply Networks with Application to the San Francisco Auxiliary Water Supply System," by I. Markov, Supervised by M. Grigoriu and T. O'Rourke, 1/21/94, (PB94-204013, A07, MF-A02).

NCEER-94-0002 "NCEER-Taisei Corporation Research Program on Sliding Seismic Isolation Systems for Bridges: Experimental and Analytical Study of Systems Consisting of Sliding Bearings, Rubber Restoring Force Devices and Fluid Dampers," Volumes I and II, by P. Tsopelas, S. Okamoto, M.C. Constantinou, D. Ozaki and S. Fujii, 2/4/94, (PB94-181740, A09, MF-A02 and PB94-181757, A12, MF-A03).

NCEER-94-0003 "A Markov Model for Local and Global Damage Indices in Seismic Analysis," by S. Rahman and M. Grigoriu, 2/18/94, (PB94-206000, A12, MF-A03).

NCEER-94-0004 "Proceedings from the NCEER Workshop on Seismic Response of Masonry Infills," edited by D.P. Abrams, 3/1/94, (PB94-180783, A07, MF-A02).

NCEER-94-0005 "The Northridge, California Earthquake of January 17, 1994: General Reconnaissance Report," edited by J.D. Goltz, 3/11/94, (PB94-193943, A10, MF-A03).

NCEER-94-0006 "Seismic Energy Based Fatigue Damage Analysis of Bridge Columns: Part I - Evaluation of Seismic Capacity," by G.A. Chang and J.B. Mander, 3/14/94, (PB94-219185, A11, MF-A03).

NCEER-94-0007 "Seismic Isolation of Multi-Story Frame Structures Using Spherical Sliding Isolation Systems," by T.M. Al-Hussaini, V.A. Zayas and M.C. Constantinou, 3/17/94, (PB94-193745, A09, MF-A02).

NCEER-94-0008 "The Northridge, California Earthquake of January 17, 1994: Performance of Highway Bridges," edited by I.G. Buckle, 3/24/94, (PB94-193851, A06, MF-A02).

NCEER-94-0009 "Proceedings of the Third U.S.-Japan Workshop on Earthquake Protective Systems for Bridges," edited by I.G. Buckle and I. Friedland, 3/31/94, (PB94-195815, A99, MF-A06).

NCEER-94-0010 "3D-BASIS-ME: Computer Program for Nonlinear Dynamic Analysis of Seismically Isolated Single and Multiple Structures and Liquid Storage Tanks," by P.C. Tsopelas, M.C. Constantinou and A.M. Reinhorn, 4/12/94, (PB94-204922, A09, MF-A02).

NCEER-94-0011 "The Northridge, California Earthquake of January 17, 1994: Performance of Gas Transmission Pipelines," by T.D. O'Rourke and M.C. Palmer, 5/16/94, (PB94-204989, A05, MF-A01).

NCEER-94-0012 "Feasibility Study of Replacement Procedures and Earthquake Performance Related to Gas Transmission Pipelines," by T.D. O'Rourke and M.C. Palmer, 5/25/94, (PB94-206638, A09, MF-A02).

NCEER-94-0013 "Seismic Energy Based Fatigue Damage Analysis of Bridge Columns: Part II - Evaluation of Seismic Demand," by G.A. Chang and J.B. Mander, 6/1/94, (PB95-18106, A08, MF-A02).

NCEER-94-0014 "NCEER-Taisei Corporation Research Program on Sliding Seismic Isolation Systems for Bridges: Experimental and Analytical Study of a System Consisting of Sliding Bearings and Fluid Restoring Force/Damping Devices," by P. Tsopelas and M.C. Constantinou, 6/13/94, (PB94-219144, A10, MF-A03).

NCEER-94-0015 "Generation of Hazard-Consistent Fragility Curves for Seismic Loss Estimation Studies," by H. Hwang and J-R. Huo, 6/14/94, (PB95-181996, A09, MF-A02).

NCEER-94-0016 "Seismic Study of Building Frames with Added Energy-Absorbing Devices," by W.S. Pong, C.S. Tsai and G.C. Lee, 6/20/94, (PB94-219136, A10, A03).

NCEER-94-0017 "Sliding Mode Control for Seismic-Excited Linear and Nonlinear Civil Engineering Structures," by J. Yang, J. Wu, A. Agrawal and Z. Li, 6/21/94, (PB95-138483, A06, MF-A02).

NCEER-94-0018 "3D-BASIS-TABS Version 2.0: Computer Program for Nonlinear Dynamic Analysis of Three Dimensional Base Isolated Structures," by A.M. Reinhorn, S. Nagarajaiah, M.C. Constantinou, P. Tsopelas and R. Li, 6/22/94, (PB95-182176, A08, MF-A02).

NCEER-94-0019 "Proceedings of the International Workshop on Civil Infrastructure Systems: Application of Intelligent Systems and Advanced Materials on Bridge Systems," Edited by G.C. Lee and K.C. Chang, 7/18/94, (PB95-252474, A20, MF-A04).

NCEER-94-0020 "Study of Seismic Isolation Systems for Computer Floors," by V. Lambrou and M.C. Constantinou, 7/19/94, (PB95-138533, A10, MF-A03).

NCEER-94-0021 "Proceedings of the U.S.-Italian Workshop on Guidelines for Seismic Evaluation and Rehabilitation of Unreinforced Masonry Buildings," Edited by D.P. Abrams and G.M. Calvi, 7/20/94, (PB95-138749, A13, MF-A03).

NCEER-94-0022 "NCEER-Taisei Corporation Research Program on Sliding Seismic Isolation Systems for Bridges: Experimental and Analytical Study of a System Consisting of Lubricated PTFE Sliding Bearings and Mild Steel Dampers," by P. Tsopelas and M.C. Constantinou, 7/22/94, (PB95-182184, A08, MF-A02).

NCEER-94-0023 “Development of Reliability-Based Design Criteria for Buildings Under Seismic Load,” by Y.K. Wen, H. Hwang and M. Shinozuka, 8/1/94, (PB95-211934, A08, MF-A02).

NCEER-94-0024 “Experimental Verification of Acceleration Feedback Control Strategies for an Active Tendon System,” by S.J. Dyke, B.F. Spencer, Jr., P. Quast, M.K. Sain, D.C. Kaspari, Jr. and T.T. Soong, 8/29/94, (PB95-212320, A05, MF-A01).

NCEER-94-0025 “Seismic Retrofitting Manual for Highway Bridges,” Edited by I.G. Buckle and I.F. Friedland, published by the Federal Highway Administration (PB95-212676, A15, MF-A03).

NCEER-94-0026 “Proceedings from the Fifth U.S.-Japan Workshop on Earthquake Resistant Design of Lifeline Facilities and Countermeasures Against Soil Liquefaction,” Edited by T.D. O’Rourke and M. Hamada, 11/7/94, (PB95-220802, A99, MF-E08).

NCEER-95-0001 "Experimental and Analytical Investigation of Seismic Retrofit of Structures with Supplemental Damping: Part 1 - Fluid Viscous Damping Devices," by A.M. Reinhorn, C. Li and M.C. Constantinou, 1/3/95, (PB95-266599, A09, MF-A02).

NCEER-95-0002 "Experimental and Analytical Study of Low-Cycle Fatigue Behavior of Semi-Rigid Top-And-Seat Angle Connections," by G. Pekcan, J.B. Mander and S.S. Chen, 1/5/95, (PB95-220042, A07, MF-A02).

NCEER-95-0003 "NCEER-ATC Joint Study on Fragility of Buildings," by T. Anagnos, C. Rojahn and A.S. Kiremidjian, 1/20/95, (PB95-220026, A06, MF-A02).

NCEER-95-0004 "Nonlinear Control Algorithms for Peak Response Reduction," by Z. Wu, T.T. Soong, V. Gattulli and R.C. Lin, 2/16/95, (PB95-220349, A05, MF-A01).

NCEER-95-0005 "Pipeline Replacement Feasibility Study: A Methodology for Minimizing Seismic and Corrosion Risks to Underground Natural Gas Pipelines," by R.T. Eguchi, H.A. Seligson and D.G. Honegger, 3/2/95, (PB95-252326, A06, MF-A02).

NCEER-95-0006 "Evaluation of Seismic Performance of an 11-Story Frame Building During the 1994 Northridge Earthquake," by F. Naeim, R. DiSulio, K. Benuska, A. Reinhorn and C. Li, not available.

NCEER-95-0007 "Prioritization of Bridges for Seismic Retrofitting," by N. Basöz and A.S. Kiremidjian, 4/24/95, (PB95-252300, A08, MF-A02).

NCEER-95-0008 "Method for Developing Motion Damage Relationships for Reinforced Concrete Frames," by A. Singhal and A.S. Kiremidjian, 5/11/95, (PB95-266607, A06, MF-A02).

NCEER-95-0009 "Experimental and Analytical Investigation of Seismic Retrofit of Structures with Supplemental Damping: Part II - Friction Devices," by C. Li and A.M. Reinhorn, 7/6/95, (PB96-128087, A11, MF-A03).

NCEER-95-0010 "Experimental Performance and Analytical Study of a Non-Ductile Reinforced Concrete Frame Structure Retrofitted with Elastomeric Spring Dampers," by G. Pekcan, J.B. Mander and S.S. Chen, 7/14/95, (PB96-137161, A08, MF-A02).

NCEER-95-0011 "Development and Experimental Study of Semi-Active Fluid Damping Devices for Seismic Protection of Structures," by M.D. Symans and M.C. Constantinou, 8/3/95, (PB96-136940, A23, MF-A04).

NCEER-95-0012 "Real-Time Structural Parameter Modification (RSPM): Development of Innervated Structures," by Z. Liang, M. Tong and G.C. Lee, 4/11/95, (PB96-137153, A06, MF-A01).

NCEER-95-0013 "Experimental and Analytical Investigation of Seismic Retrofit of Structures with Supplemental Damping: Part III - Viscous Damping Walls," by A.M. Reinhorn and C. Li, 10/1/95, (PB96-176409, A11, MF-A03).

NCEER-95-0014 "Seismic Fragility Analysis of Equipment and Structures in a Memphis Electric Substation," by J-R. Huo and H.H.M. Hwang, 8/10/95, (PB96-128087, A09, MF-A02).

NCEER-95-0015 "The Hanshin-Awaji Earthquake of January 17, 1995: Performance of Lifelines," Edited by M. Shinozuka, 11/3/95, (PB96-176383, A15, MF-A03).

NCEER-95-0016 "Highway Culvert Performance During Earthquakes," by T.L. Youd and C.J. Beckman, available as NCEER-96-0015.

NCEER-95-0017 "The Hanshin-Awaji Earthquake of January 17, 1995: Performance of Highway Bridges," Edited by I.G. Buckle, 12/1/95, not available.

NCEER-95-0018 "Modeling of Masonry Infill Panels for Structural Analysis," by A.M. Reinhorn, A. Madan, R.E. Valles, Y. Reichmann and J.B. Mander, 12/8/95, (PB97-110886, MF-A01, A06).

NCEER-95-0019 "Optimal Polynomial Control for Linear and Nonlinear Structures," by A.K. Agrawal and J.N. Yang, 12/11/95, (PB96-168737, A07, MF-A02).

NCEER-95-0020 "Retrofit of Non-Ductile Reinforced Concrete Frames Using Friction Dampers," by R.S. Rao, P. Gergely and R.N. White, 12/22/95, (PB97-133508, A10, MF-A02).

NCEER-95-0021 "Parametric Results for Seismic Response of Pile-Supported Bridge Bents," by G. Mylonakis, A. Nikolaou and G. Gazetas, 12/22/95, (PB97-100242, A12, MF-A03).

NCEER-95-0022 "Kinematic Bending Moments in Seismically Stressed Piles," by A. Nikolaou, G. Mylonakis and G. Gazetas, 12/23/95, (PB97-113914, MF-A03, A13).

NCEER-96-0001 "Dynamic Response of Unreinforced Masonry Buildings with Flexible Diaphragms," by A.C. Costley and D.P. Abrams," 10/10/96, (PB97-133573, MF-A03, A15).

NCEER-96-0002 "State of the Art Review: Foundations and Retaining Structures," by I. Po Lam, not available.

NCEER-96-0003 "Ductility of Rectangular Reinforced Concrete Bridge Columns with Moderate Confinement," by N. Wehbe, M. Saiidi, D. Sanders and B. Douglas, 11/7/96, (PB97-133557, A06, MF-A02).

NCEER-96-0004 "Proceedings of the Long-Span Bridge Seismic Research Workshop," edited by I.G. Buckle and I.M. Friedland, not available.

NCEER-96-0005 "Establish Representative Pier Types for Comprehensive Study: Eastern United States," by J. Kulicki and Z. Prucz, 5/28/96, (PB98-119217, A07, MF-A02).

NCEER-96-0006 "Establish Representative Pier Types for Comprehensive Study: Western United States," by R. Imbsen, R.A. Schamber and T.A. Osterkamp, 5/28/96, (PB98-118607, A07, MF-A02).

NCEER-96-0007 "Nonlinear Control Techniques for Dynamical Systems with Uncertain Parameters," by R.G. Ghanem and M.I. Bujakov, 5/27/96, (PB97-100259, A17, MF-A03).

NCEER-96-0008 "Seismic Evaluation of a 30-Year Old Non-Ductile Highway Bridge Pier and Its Retrofit," by J.B. Mander, B. Mahmoodzadegan, S. Bhadra and S.S. Chen, 5/31/96, (PB97-110902, MF-A03, A10).

NCEER-96-0009 "Seismic Performance of a Model Reinforced Concrete Bridge Pier Before and After Retrofit," by J.B. Mander, J.H. Kim and C.A. Ligozio, 5/31/96, (PB97-110910, MF-A02, A10).

NCEER-96-0010 "IDARC2D Version 4.0: A Computer Program for the Inelastic Damage Analysis of Buildings," by R.E. Valles, A.M. Reinhorn, S.K. Kunnath, C. Li and A. Madan, 6/3/96, (PB97-100234, A17, MF-A03).

NCEER-96-0011 "Estimation of the Economic Impact of Multiple Lifeline Disruption: Memphis Light, Gas and Water Division Case Study," by S.E. Chang, H.A. Seligson and R.T. Eguchi, 8/16/96, (PB97-133490, A11, MF-A03).

NCEER-96-0012 "Proceedings from the Sixth Japan-U.S. Workshop on Earthquake Resistant Design of Lifeline Facilities and Countermeasures Against Soil Liquefaction, Edited by M. Hamada and T. O'Rourke, 9/11/96, (PB97-133581, A99, MF-A06).

NCEER-96-0013 "Chemical Hazards, Mitigation and Preparedness in Areas of High Seismic Risk: A Methodology for Estimating the Risk of Post-Earthquake Hazardous Materials Release," by H.A. Seligson, R.T. Eguchi, K.J. Tierney and K. Richmond, 11/7/96, (PB97-133565, MF-A02, A08).

NCEER-96-0014 "Response of Steel Bridge Bearings to Reversed Cyclic Loading," by J.B. Mander, D-K. Kim, S.S. Chen and G.J. Premus, 11/13/96, (PB97-140735, A12, MF-A03).

NCEER-96-0015 "Highway Culvert Performance During Past Earthquakes," by T.L. Youd and C.J. Beckman, 11/25/96, (PB97-133532, A06, MF-A01).

NCEER-97-0001 "Evaluation, Prevention and Mitigation of Pounding Effects in Building Structures," by R.E. Valles and A.M. Reinhorn, 2/20/97, (PB97-159552, A14, MF-A03).

NCEER-97-0002 "Seismic Design Criteria for Bridges and Other Highway Structures," by C. Rojahn, R. Mayes, D.G. Anderson, J. Clark, J.H. Hom, R.V. Nutt and M.J. O'Rourke, 4/30/97, (PB97-194658, A06, MF-A03).

NCEER-97-0003 "Proceedings of the U.S.-Italian Workshop on Seismic Evaluation and Retrofit," Edited by D.P. Abrams and G.M. Calvi, 3/19/97, (PB97-194666, A13, MF-A03).

NCEER-97-0004 "Investigation of Seismic Response of Buildings with Linear and Nonlinear Fluid Viscous Dampers," by A.A. Seleemah and M.C. Constantinou, 5/21/97, (PB98-109002, A15, MF-A03).

NCEER-97-0005 "Proceedings of the Workshop on Earthquake Engineering Frontiers in Transportation Facilities," edited by G.C. Lee and I.M. Friedland, 8/29/97, (PB98-128911, A25, MR-A04).

NCEER-97-0006 "Cumulative Seismic Damage of Reinforced Concrete Bridge Piers," by S.K. Kunnath, A. El-Bahy, A. Taylor and W. Stone, 9/2/97, (PB98-108814, A11, MF-A03).

NCEER-97-0007 "Structural Details to Accommodate Seismic Movements of Highway Bridges and Retaining Walls," by R.A. Imbsen, R.A. Schamber, E. Thorkildsen, A. Kartoum, B.T. Martin, T.N. Rosser and J.M. Kulicki, 9/3/97, (PB98-108996, A09, MF-A02).

NCEER-97-0008 "A Method for Earthquake Motion-Damage Relationships with Application to Reinforced Concrete Frames," by A. Singhal and A.S. Kiremidjian, 9/10/97, (PB98-108988, A13, MF-A03).

NCEER-97-0009 "Seismic Analysis and Design of Bridge Abutments Considering Sliding and Rotation," by K. Fishman and R. Richards, Jr., 9/15/97, (PB98-108897, A06, MF-A02).

NCEER-97-0010 "Proceedings of the FHWA/NCEER Workshop on the National Representation of Seismic Ground Motion for New and Existing Highway Facilities," edited by I.M. Friedland, M.S. Power and R.L. Mayes, 9/22/97, (PB98-128903, A21, MF-A04).

NCEER-97-0011 "Seismic Analysis for Design or Retrofit of Gravity Bridge Abutments," by K.L. Fishman, R. Richards, Jr. and R.C. Divito, 10/2/97, (PB98-128937, A08, MF-A02).

NCEER-97-0012 "Evaluation of Simplified Methods of Analysis for Yielding Structures," by P. Tsopelas, M.C. Constantinou, C.A. Kircher and A.S. Whittaker, 10/31/97, (PB98-128929, A10, MF-A03).

NCEER-97-0013 "Seismic Design of Bridge Columns Based on Control and Repairability of Damage," by C-T. Cheng and J.B. Mander, 12/8/97, (PB98-144249, A11, MF-A03).

NCEER-97-0014 "Seismic Resistance of Bridge Piers Based on Damage Avoidance Design," by J.B. Mander and C-T. Cheng, 12/10/97, (PB98-144223, A09, MF-A02).

NCEER-97-0015 "Seismic Response of Nominally Symmetric Systems with Strength Uncertainty," by S. Balopoulou and M. Grigoriu, 12/23/97, (PB98-153422, A11, MF-A03).

NCEER-97-0016 "Evaluation of Seismic Retrofit Methods for Reinforced Concrete Bridge Columns," by T.J. Wipf, F.W. Klaiber and F.M. Russo, 12/28/97, (PB98-144215, A12, MF-A03).

NCEER-97-0017 "Seismic Fragility of Existing Conventional Reinforced Concrete Highway Bridges," by C.L. Mullen and A.S. Cakmak, 12/30/97, (PB98-153406, A08, MF-A02).

NCEER-97-0018 "Loss Asssessment of Memphis Buildings," edited by D.P. Abrams and M. Shinozuka, 12/31/97, (PB98-144231, A13, MF-A03).

NCEER-97-0019 "Seismic Evaluation of Frames with Infill Walls Using Quasi-static Experiments," by K.M. Mosalam, R.N. White and P. Gergely, 12/31/97, (PB98-153455, A07, MF-A02).

NCEER-97-0020 "Seismic Evaluation of Frames with Infill Walls Using Pseudo-dynamic Experiments," by K.M. Mosalam, R.N. White and P. Gergely, 12/31/97, (PB98-153430, A07, MF-A02).

NCEER-97-0021 "Computational Strategies for Frames with Infill Walls: Discrete and Smeared Crack Analyses and Seismic Fragility," by K.M. Mosalam, R.N. White and P. Gergely, 12/31/97, (PB98-153414, A10, MF-A02).

NCEER-97-0022 "Proceedings of the NCEER Workshop on Evaluation of Liquefaction Resistance of Soils," edited by T.L. Youd and I.M. Idriss, 12/31/97, (PB98-155617, A15, MF-A03).

MCEER-98-0001 "Extraction of Nonlinear Hysteretic Properties of Seismically Isolated Bridges from Quick-Release Field Tests," by Q. Chen, B.M. Douglas, E.M. Maragakis and I.G. Buckle, 5/26/98, (PB99-118838, A06, MF-A01).

MCEER-98-0002 "Methodologies for Evaluating the Importance of Highway Bridges," by A. Thomas, S. Eshenaur and J. Kulicki, 5/29/98, (PB99-118846, A10, MF-A02).

MCEER-98-0003 "Capacity Design of Bridge Piers and the Analysis of Overstrength," by J.B. Mander, A. Dutta and P. Goel, 6/1/98, (PB99-118853, A09, MF-A02).

MCEER-98-0004 "Evaluation of Bridge Damage Data from the Loma Prieta and Northridge, California Earthquakes," by N. Basoz and A. Kiremidjian, 6/2/98, (PB99-118861, A15, MF-A03).

MCEER-98-0005 "Screening Guide for Rapid Assessment of Liquefaction Hazard at Highway Bridge Sites," by T. L. Youd, 6/16/98, (PB99-118879, A06, not available on microfiche).

MCEER-98-0006 "Structural Steel and Steel/Concrete Interface Details for Bridges," by P. Ritchie, N. Kauhl and J. Kulicki, 7/13/98, (PB99-118945, A06, MF-A01).

MCEER-98-0007 "Capacity Design and Fatigue Analysis of Confined Concrete Columns," by A. Dutta and J.B. Mander, 7/14/98, (PB99-118960, A14, MF-A03).

MCEER-98-0008 "Proceedings of the Workshop on Performance Criteria for Telecommunication Services Under Earthquake Conditions," edited by A.J. Schiff, 7/15/98, (PB99-118952, A08, MF-A02).

MCEER-98-0009 "Fatigue Analysis of Unconfined Concrete Columns," by J.B. Mander, A. Dutta and J.H. Kim, 9/12/98, (PB99-123655, A10, MF-A02).

MCEER-98-0010 "Centrifuge Modeling of Cyclic Lateral Response of Pile-Cap Systems and Seat-Type Abutments in Dry Sands," by A.D. Gadre and R. Dobry, 10/2/98, (PB99-123606, A13, MF-A03).

MCEER-98-0011 "IDARC-BRIDGE: A Computational Platform for Seismic Damage Assessment of Bridge Structures," by A.M. Reinhorn, V. Simeonov, G. Mylonakis and Y. Reichman, 10/2/98, (PB99-162919, A15, MF-A03).

MCEER-98-0012 "Experimental Investigation of the Dynamic Response of Two Bridges Before and After Retrofitting with Elastomeric Bearings," by D.A. Wendichansky, S.S. Chen and J.B. Mander, 10/2/98, (PB99-162927, A15, MF-A03).

MCEER-98-0013 "Design Procedures for Hinge Restrainers and Hinge Sear Width for Multiple-Frame Bridges," by R. Des Roches and G.L. Fenves, 11/3/98, (PB99-140477, A13, MF-A03).

MCEER-98-0014 "Response Modification Factors for Seismically Isolated Bridges," by M.C. Constantinou and J.K. Quarshie, 11/3/98, (PB99-140485, A14, MF-A03).

MCEER-98-0015 "Proceedings of the U.S.-Italy Workshop on Seismic Protective Systems for Bridges," edited by I.M. Friedland and M.C. Constantinou, 11/3/98, (PB2000-101711, A22, MF-A04).

MCEER-98-0016 "Appropriate Seismic Reliability for Critical Equipment Systems: Recommendations Based on Regional Analysis of Financial and Life Loss," by K. Porter, C. Scawthorn, C. Taylor and N. Blais, 11/10/98, (PB99-157265, A08, MF-A02).

MCEER-98-0017 "Proceedings of the U.S. Japan Joint Seminar on Civil Infrastructure Systems Research," edited by M. Shinozuka and A. Rose, 11/12/98, (PB99-156713, A16, MF-A03).

MCEER-98-0018 "Modeling of Pile Footings and Drilled Shafts for Seismic Design," by I. PoLam, M. Kapuskar and D. Chaudhuri, 12/21/98, (PB99-157257, A09, MF-A02).

MCEER-99-0001 "Seismic Evaluation of a Masonry Infilled Reinforced Concrete Frame by Pseudodynamic Testing," by S.G. Buonopane and R.N. White, 2/16/99, (PB99-162851, A09, MF-A02).

MCEER-99-0002 "Response History Analysis of Structures with Seismic Isolation and Energy Dissipation Systems: Verification Examples for Program SAP2000," by J. Scheller and M.C. Constantinou, 2/22/99, (PB99-162869, A08, MF-A02).

MCEER-99-0003 "Experimental Study on the Seismic Design and Retrofit of Bridge Columns Including Axial Load Effects," by A. Dutta, T. Kokorina and J.B. Mander, 2/22/99, (PB99-162877, A09, MF-A02).

MCEER-99-0004 "Experimental Study of Bridge Elastomeric and Other Isolation and Energy Dissipation Systems with Emphasis on Uplift Prevention and High Velocity Near-source Seismic Excitation," by A. Kasalanati and M. C. Constantinou, 2/26/99, (PB99-162885, A12, MF-A03).

MCEER-99-0005 "Truss Modeling of Reinforced Concrete Shear-flexure Behavior," by J.H. Kim and J.B. Mander, 3/8/99, (PB99-163693, A12, MF-A03).

MCEER-99-0006 "Experimental Investigation and Computational Modeling of Seismic Response of a 1:4 Scale Model Steel Structure with a Load Balancing Supplemental Damping System," by G. Pekcan, J.B. Mander and S.S. Chen, 4/2/99, (PB99-162893, A11, MF-A03).

MCEER-99-0007 "Effect of Vertical Ground Motions on the Structural Response of Highway Bridges," by M.R. Button, C.J. Cronin and R.L. Mayes, 4/10/99, (PB2000-101411, A10, MF-A03).

MCEER-99-0008 "Seismic Reliability Assessment of Critical Facilities: A Handbook, Supporting Documentation, and Model Code Provisions," by G.S. Johnson, R.E. Sheppard, M.D. Quilici, S.J. Eder and C.R. Scawthorn, 4/12/99, (PB2000-101701, A18, MF-A04).

MCEER-99-0009 "Impact Assessment of Selected MCEER Highway Project Research on the Seismic Design of Highway Structures," by C. Rojahn, R. Mayes, D.G. Anderson, J.H. Clark, D'Appolonia Engineering, S. Gloyd and R.V. Nutt, 4/14/99, (PB99-162901, A10, MF-A02).

MCEER-99-0010 "Site Factors and Site Categories in Seismic Codes," by R. Dobry, R. Ramos and M.S. Power, 7/19/99, (PB2000-101705, A08, MF-A02).

MCEER-99-0011 "Restrainer Design Procedures for Multi-Span Simply-Supported Bridges," by M.J. Randall, M. Saiidi, E. Maragakis and T. Isakovic, 7/20/99, (PB2000-101702, A10, MF-A02).

MCEER-99-0012 "Property Modification Factors for Seismic Isolation Bearings," by M.C. Constantinou, P. Tsopelas, A. Kasalanati and E. Wolff, 7/20/99, (PB2000-103387, A11, MF-A03).

MCEER-99-0013 "Critical Seismic Issues for Existing Steel Bridges," by P. Ritchie, N. Kauhl and J. Kulicki, 7/20/99, (PB2000-101697, A09, MF-A02).

MCEER-99-0014 "Nonstructural Damage Database," by A. Kao, T.T. Soong and A. Vender, 7/24/99, (PB2000-101407, A06, MF-A01).

MCEER-99-0015 "Guide to Remedial Measures for Liquefaction Mitigation at Existing Highway Bridge Sites," by H.G. Cooke and J. K. Mitchell, 7/26/99, (PB2000-101703, A11, MF-A03).

MCEER-99-0016 "Proceedings of the MCEER Workshop on Ground Motion Methodologies for the Eastern United States," edited by N. Abrahamson and A. Becker, 8/11/99, (PB2000-103385, A07, MF-A02).

MCEER-99-0017 "Quindío, Colombia Earthquake of January 25, 1999: Reconnaissance Report," by A.P. Asfura and P.J. Flores, 10/4/99, (PB2000-106893, A06, MF-A01).

MCEER-99-0018 "Hysteretic Models for Cyclic Behavior of Deteriorating Inelastic Structures," by M.V. Sivaselvan and A.M. Reinhorn, 11/5/99, (PB2000-103386, A08, MF-A02).

MCEER-99-0019 "Proceedings of the 7th U.S.- Japan Workshop on Earthquake Resistant Design of Lifeline Facilities and Countermeasures Against Soil Liquefaction," edited by T.D. O'Rourke, J.P. Bardet and M. Hamada, 11/19/99, (PB2000-103354, A99, MF-A06).

MCEER-99-0020 "Development of Measurement Capability for Micro-Vibration Evaluations with Application to Chip Fabrication Facilities," by G.C. Lee, Z. Liang, J.W. Song, J.D. Shen and W.C. Liu, 12/1/99, (PB2000-105993, A08, MF-A02).

MCEER-99-0021 "Design and Retrofit Methodology for Building Structures with Supplemental Energy Dissipating Systems," by G. Pekcan, J.B. Mander and S.S. Chen, 12/31/99, (PB2000-105994, A11, MF-A03).

MCEER-00-0001 "The Marmara, Turkey Earthquake of August 17, 1999: Reconnaissance Report," edited by C. Scawthorn; with major contributions by M. Bruneau, R. Eguchi, T. Holzer, G. Johnson, J. Mander, J. Mitchell, W. Mitchell, A. Papageorgiou, C. Scaethorn, and G. Webb, 3/23/00, (PB2000-106200, A11, MF-A03).

MCEER-00-0002 "Proceedings of the MCEER Workshop for Seismic Hazard Mitigation of Health Care Facilities," edited by G.C. Lee, M. Ettouney, M. Grigoriu, J. Hauer and J. Nigg, 3/29/00, (PB2000-106892, A08, MF-A02).

MCEER-00-0003 "The Chi-Chi, Taiwan Earthquake of September 21, 1999: Reconnaissance Report," edited by G.C. Lee and C.H. Loh, with major contributions by G.C. Lee, M. Bruneau, I.G. Buckle, S.E. Chang, P.J. Flores, T.D. O'Rourke, M. Shinozuka, T.T. Soong, C-H. Loh, K-C. Chang, Z-J. Chen, J-S. Hwang, M-L. Lin, G-Y. Liu, K-C. Tsai, G.C. Yao and C-L. Yen, 4/30/00, (PB2001-100980, A10, MF-A02).

MCEER-00-0004 "Seismic Retrofit of End-Sway Frames of Steel Deck-Truss Bridges with a Supplemental Tendon System: Experimental and Analytical Investigation," by G. Pekcan, J.B. Mander and S.S. Chen, 7/1/00, (PB2001-100982, A10, MF-A02).

MCEER-00-0005 "Sliding Fragility of Unrestrained Equipment in Critical Facilities," by W.H. Chong and T.T. Soong, 7/5/00, (PB2001-100983, A08, MF-A02).

MCEER-00-0006 "Seismic Response of Reinforced Concrete Bridge Pier Walls in the Weak Direction," by N. Abo-Shadi, M. Saiidi and D. Sanders, 7/17/00, (PB2001-100981, A17, MF-A03).

MCEER-00-0007 "Low-Cycle Fatigue Behavior of Longitudinal Reinforcement in Reinforced Concrete Bridge Columns," by J. Brown and S.K. Kunnath, 7/23/00, (PB2001-104392, A08, MF-A02).

MCEER-00-0008 "Soil Structure Interaction of Bridges for Seismic Analysis," I. PoLam and H. Law, 9/25/00, (PB2001-105397, A08, MF-A02).

MCEER-00-0009 "Proceedings of the First MCEER Workshop on Mitigation of Earthquake Disaster by Advanced Technologies (MEDAT-1), edited by M. Shinozuka, D.J. Inman and T.D. O'Rourke, 11/10/00, (PB2001-105399, A14, MF-A03).

MCEER-00-0010 "Development and Evaluation of Simplified Procedures for Analysis and Design of Buildings with Passive Energy Dissipation Systems, Revision 01," by O.M. Ramirez, M.C. Constantinou, C.A. Kircher, A.S. Whittaker, M.W. Johnson, J.D. Gomez and C. Chrysostomou, 11/16/01, (PB2001-105523, A23, MF-A04).

MCEER-00-0011 "Dynamic Soil-Foundation-Structure Interaction Analyses of Large Caissons," by C-Y. Chang, C-M. Mok, Z-L. Wang, R. Settgast, F. Waggoner, M.A. Ketchum, H.M. Gonnermann and C-C. Chin, 12/30/00, (PB2001-104373, A07, MF-A02).

MCEER-00-0012 "Experimental Evaluation of Seismic Performance of Bridge Restrainers," by A.G. Vlassis, E.M. Maragakis and M. Saiid Saiidi, 12/30/00, (PB2001-104354, A09, MF-A02).

MCEER-00-0013 "Effect of Spatial Variation of Ground Motion on Highway Structures," by M. Shinozuka, V. Saxena and G. Deodatis, 12/31/00, (PB2001-108755, A13, MF-A03).

MCEER-00-0014 "A Risk-Based Methodology for Assessing the Seismic Performance of Highway Systems," by S.D. Werner, C.E. Taylor, J.E. Moore, II, J.S. Walton and S. Cho, 12/31/00, (PB2001-108756, A14, MF-A03).

MCEER-01-0001 "Experimental Investigation of P-Delta Effects to Collapse During Earthquakes," by D. Vian and M. Bruneau, 6/25/01, (PB2002-100534, A17, MF-A03).

MCEER-01-0002 "Proceedings of the Second MCEER Workshop on Mitigation of Earthquake Disaster by Advanced Technologies (MEDAT-2)," edited by M. Bruneau and D.J. Inman, 7/23/01, (PB2002-100434, A16, MF-A03).

MCEER-01-0003 "Sensitivity Analysis of Dynamic Systems Subjected to Seismic Loads," by C. Roth and M. Grigoriu, 9/18/01, (PB2003-100884, A12, MF-A03).

MCEER-01-0004 "Overcoming Obstacles to Implementing Earthquake Hazard Mitigation Policies: Stage 1 Report," by D.J. Alesch and W.J. Petak, 12/17/01, (PB2002-107949, A07, MF-A02).

MCEER-01-0005 "Updating Real-Time Earthquake Loss Estimates: Methods, Problems and Insights," by C.E. Taylor, S.E. Chang and R.T. Eguchi, 12/17/01, (PB2002-107948, A05, MF-A01).

MCEER-01-0006 "Experimental Investigation and Retrofit of Steel Pile Foundations and Pile Bents Under Cyclic Lateral Loadings," by A. Shama, J. Mander, B. Blabac and S. Chen, 12/31/01, (PB2002-107950, A13, MF-A03).

MCEER-02-0001 "Assessment of Performance of Bolu Viaduct in the 1999 Duzce Earthquake in Turkey" by P.C. Roussis, M.C. Constantinou, M. Erdik, E. Durukal and M. Dicleli, 5/8/02, (PB2003-100883, A08, MF-A02).

MCEER-02-0002 "Seismic Behavior of Rail Counterweight Systems of Elevators in Buildings," by M.P. Singh, Rildova and L.E. Suarez, 5/27/02. (PB2003-100882, A11, MF-A03).

MCEER-02-0003 "Development of Analysis and Design Procedures for Spread Footings," by G. Mylonakis, G. Gazetas, S. Nikolaou and A. Chauncey, 10/02/02, (PB2004-101636, A13, MF-A03, CD-A13).

MCEER-02-0004 "Bare-Earth Algorithms for Use with SAR and LIDAR Digital Elevation Models," by C.K. Huyck, R.T. Eguchi and B. Houshmand, 10/16/02, (PB2004-101637, A07, CD-A07).

MCEER-02-0005 "Review of Energy Dissipation of Compression Members in Concentrically Braced Frames," by K.Lee and M. Bruneau, 10/18/02, (PB2004-101638, A10, CD-A10).

MCEER-03-0001 "Experimental Investigation of Light-Gauge Steel Plate Shear Walls for the Seismic Retrofit of Buildings" by J. Berman and M. Bruneau, 5/2/03, (PB2004-101622, A10, MF-A03, CD-A10).

MCEER-03-0002 "Statistical Analysis of Fragility Curves," by M. Shinozuka, M.Q. Feng, H. Kim, T. Uzawa and T. Ueda, 6/16/03, (PB2004-101849, A09, CD-A09).

MCEER-03-0003 "Proceedings of the Eighth U.S.-Japan Workshop on Earthquake Resistant Design f Lifeline Facilities and Countermeasures Against Liquefaction," edited by M. Hamada, J.P. Bardet and T.D. O'Rourke, 6/30/03, (PB2004-104386, A99, CD-A99).

MCEER-03-0004 "Proceedings of the PRC-US Workshop on Seismic Analysis and Design of Special Bridges," edited by L.C. Fan and G.C. Lee, 7/15/03, (PB2004-104387, A14, CD-A14).

MCEER-03-0005 "Urban Disaster Recovery: A Framework and Simulation Model," by S.B. Miles and S.E. Chang, 7/25/03, (PB2004-104388, A07, CD-A07).

MCEER-03-0006 "Behavior of Underground Piping Joints Due to Static and Dynamic Loading," by R.D. Meis, M. Maragakis and R. Siddharthan, 11/17/03, (PB2005-102194, A13, MF-A03, CD-A00).

MCEER-04-0001 "Experimental Study of Seismic Isolation Systems with Emphasis on Secondary System Response and Verification of Accuracy of Dynamic Response History Analysis Methods," by E. Wolff and M. Constantinou, 1/16/04 (PB2005-102195, A99, MF-E08, CD-A00).

MCEER-04-0002 "Tension, Compression and Cyclic Testing of Engineered Cementitious Composite Materials," by K. Kesner and S.L. Billington, 3/1/04, (PB2005-102196, A08, CD-A08).

MCEER-04-0003 "Cyclic Testing of Braces Laterally Restrained by Steel Studs to Enhance Performance During Earthquakes," by O.C. Celik, J.W. Berman and M. Bruneau, 3/16/04, (PB2005-102197, A13, MF-A03, CD-A00).

MCEER-04-0004 "Methodologies for Post Earthquake Building Damage Detection Using SAR and Optical Remote Sensing: Application to the August 17, 1999 Marmara, Turkey Earthquake," by C.K. Huyck, B.J. Adams, S. Cho, R.T. Eguchi, B. Mansouri and B. Houshmand, 6/15/04, (PB2005-104888, A10, CD-A00).

MCEER-04-0005 "Nonlinear Structural Analysis Towards Collapse Simulation: A Dynamical Systems Approach," by M.V. Sivaselvan and A.M. Reinhorn, 6/16/04, (PB2005-104889, A11, MF-A03, CD-A00).

MCEER-04-0006 "Proceedings of the Second PRC-US Workshop on Seismic Analysis and Design of Special Bridges," edited by G.C. Lee and L.C. Fan, 6/25/04, (PB2005-104890, A16, CD-A00).

MCEER-04-0007 "Seismic Vulnerability Evaluation of Axially Loaded Steel Built-up Laced Members," by K. Lee and M. Bruneau, 6/30/04, (PB2005-104891, A16, CD-A00).

MCEER-04-0008 "Evaluation of Accuracy of Simplified Methods of Analysis and Design of Buildings with Damping Systems for Near-Fault and for Soft-Soil Seismic Motions," by E.A. Pavlou and M.C. Constantinou, 8/16/04, (PB2005-104892, A08, MF-A02, CD-A00).

MCEER-04-0009 "Assessment of Geotechnical Issues in Acute Care Facilities in California," by M. Lew, T.D. O'Rourke, R. Dobry and M. Koch, 9/15/04, (PB2005-104893, A08, CD-A00).

MCEER-04-0010 "Scissor-Jack-Damper Energy Dissipation System," by A.N. Sigaher-Boyle and M.C. Constantinou, 12/1/04 (PB2005-108221).

MCEER-04-0011 "Seismic Retrofit of Bridge Steel Truss Piers Using a Controlled Rocking Approach," by M. Pollino and M. Bruneau, 12/20/04 (PB2006-105795).

MCEER-05-0001 "Experimental and Analytical Studies of Structures Seismically Isolated with an Uplift-Restraint Isolation System," by P.C. Roussis and M.C. Constantinou, 1/10/05 (PB2005-108222).

MCEER-05-0002 "A Versatile Experimentation Model for Study of Structures Near Collapse Applied to Seismic Evaluation of Irregular Structures," by D. Kusumastuti, A.M. Reinhorn and A. Rutenberg, 3/31/05 (PB2006-101523).

MCEER-05-0003 "Proceedings of the Third PRC-US Workshop on Seismic Analysis and Design of Special Bridges," edited by L.C. Fan and G.C. Lee, 4/20/05, (PB2006-105796).

MCEER-05-0004 "Approaches for the Seismic Retrofit of Braced Steel Bridge Piers and Proof-of-Concept Testing of an Eccentrically Braced Frame with Tubular Link," by J.W. Berman and M. Bruneau, 4/21/05 (PB2006-101524).

MCEER-05-0005 "Simulation of Strong Ground Motions for Seismic Fragility Evaluation of Nonstructural Components in Hospitals," by A. Wanitkorkul and A. Filiatrault, 5/26/05 (PB2006-500027).

MCEER-05-0006 "Seismic Safety in California Hospitals: Assessing an Attempt to Accelerate the Replacement or Seismic Retrofit of Older Hospital Facilities," by D.J. Alesch, L.A. Arendt and W.J. Petak, 6/6/05 (PB2006-105794).

MCEER-05-0007 "Development of Seismic Strengthening and Retrofit Strategies for Critical Facilities Using Engineered Cementitious Composite Materials," by K. Kesner and S.L. Billington, 8/29/05 (PB2006-111701).

MCEER-05-0008 "Experimental and Analytical Studies of Base Isolation Systems for Seismic Protection of Power Transformers," by N. Murota, M.Q. Feng and G-Y. Liu, 9/30/05 (PB2006-111702).

MCEER-05-0009 "3D-BASIS-ME-MB: Computer Program for Nonlinear Dynamic Analysis of Seismically Isolated Structures," by P.C. Tsopelas, P.C. Roussis, M.C. Constantinou, R. Buchanan and A.M. Reinhorn, 10/3/05 (PB2006-111703).

MCEER-05-0010 "Steel Plate Shear Walls for Seismic Design and Retrofit of Building Structures," by D. Vian and M. Bruneau, 12/15/05 (PB2006-111704).

MCEER-05-0011 "The Performance-Based Design Paradigm," by M.J. Astrella and A. Whittaker, 12/15/05 (PB2006-111705).

MCEER-06-0001 "Seismic Fragility of Suspended Ceiling Systems," H. Badillo-Almaraz, A.S. Whittaker, A.M. Reinhorn and G.P. Cimellaro, 2/4/06 (PB2006-111706).

MCEER-06-0002 "Multi-Dimensional Fragility of Structures," by G.P. Cimellaro, A.M. Reinhorn and M. Bruneau, 3/1/06 (PB2007-106974, A09, MF-A02, CD A00).

MCEER-06-0003 "Built-Up Shear Links as Energy Dissipators for Seismic Protection of Bridges," by P. Dusicka, A.M. Itani and I.G. Buckle, 3/15/06 (PB2006-111708).

MCEER-06-0004 "Analytical Investigation of the Structural Fuse Concept," by R.E. Vargas and M. Bruneau, 3/16/06 (PB2006-111709).

MCEER-06-0005 "Experimental Investigation of the Structural Fuse Concept," by R.E. Vargas and M. Bruneau, 3/17/06 (PB2006-111710).

MCEER-06-0006 "Further Development of Tubular Eccentrically Braced Frame Links for the Seismic Retrofit of Braced Steel Truss Bridge Piers," by J.W. Berman and M. Bruneau, 3/27/06 (PB2007-105147).

MCEER-06-0007 "REDARS Validation Report," by S. Cho, C.K. Huyck, S. Ghosh and R.T. Eguchi, 8/8/06 (PB2007-106983).

MCEER-06-0008 "Review of Current NDE Technologies for Post-Earthquake Assessment of Retrofitted Bridge Columns," by J.W. Song, Z. Liang and G.C. Lee, 8/21/06 (PB2007-106984).

MCEER-06-0009 "Liquefaction Remediation in Silty Soils Using Dynamic Compaction and Stone Columns," by S. Thevanayagam, G.R. Martin, R. Nashed, T. Shenthan, T. Kanagalingam and N. Ecemis, 8/28/06 (PB2007-106985).

MCEER-06-0010 "Conceptual Design and Experimental Investigation of Polymer Matrix Composite Infill Panels for Seismic Retrofitting," by W. Jung, M. Chiewanichakorn and A.J. Aref, 9/21/06 (PB2007-106986).

MCEER-06-0011 "A Study of the Coupled Horizontal-Vertical Behavior of Elastomeric and Lead-Rubber Seismic Isolation Bearings," by G.P. Warn and A.S. Whittaker, 9/22/06 (PB2007-108679).

MCEER-06-0012 "Proceedings of the Fourth PRC-US Workshop on Seismic Analysis and Design of Special Bridges: Advancing Bridge Technologies in Research, Design, Construction and Preservation," Edited by L.C. Fan, G.C. Lee and L. Ziang, 10/12/06 (PB2007-109042).

MCEER-06-0013 "Cyclic Response and Low Cycle Fatigue Characteristics of Plate Steels," by P. Dusicka, A.M. Itani and I.G. Buckle, 11/1/06 06 (PB2007-106987).

MCEER-06-0014 "Proceedings of the Second US-Taiwan Bridge Engineering Workshop," edited by W.P. Yen, J. Shen, J-Y. Chen and M. Wang, 11/15/06 (PB2008-500041).

MCEER-06-0015 "User Manual and Technical Documentation for the REDARS™ Import Wizard," by S. Cho, S. Ghosh, C.K. Huyck and S.D. Werner, 11/30/06 (PB2007-114766).

MCEER-06-0016 "Hazard Mitigation Strategy and Monitoring Technologies for Urban and Infrastructure Public Buildings: Proceedings of the China-US Workshops," edited by X.Y. Zhou, A.L. Zhang, G.C. Lee and M. Tong, 12/12/06 (PB2008-500018).

MCEER-07-0001 "Static and Kinetic Coefficients of Friction for Rigid Blocks," by C. Kafali, S. Fathali, M. Grigoriu and A.S. Whittaker, 3/20/07 (PB2007-114767).

MCEER-07-0002 "Hazard Mitigation Investment Decision Making: Organizational Response to Legislative Mandate," by L.A. Arendt, D.J. Alesch and W.J. Petak, 4/9/07 (PB2007-114768).

MCEER-07-0003 "Seismic Behavior of Bidirectional-Resistant Ductile End Diaphragms with Unbonded Braces in Straight or Skewed Steel Bridges," by O. Celik and M. Bruneau, 4/11/07 (PB2008-105141).

MCEER-07-0004 "Modeling Pile Behavior in Large Pile Groups Under Lateral Loading," by A.M. Dodds and G.R. Martin, 4/16/07(PB2008-105142).

MCEER-07-0005 "Experimental Investigation of Blast Performance of Seismically Resistant Concrete-Filled Steel Tube Bridge Piers," by S. Fujikura, M. Bruneau and D. Lopez-Garcia, 4/20/07 (PB2008-105143).

MCEER-07-0006 "Seismic Analysis of Conventional and Isolated Liquefied Natural Gas Tanks Using Mechanical Analogs," by I.P. Christovasilis and A.S. Whittaker, 5/1/07, not available.

MCEER-07-0007 "Experimental Seismic Performance Evaluation of Isolation/Restraint Systems for Mechanical Equipment – Part 1: Heavy Equipment Study," by S. Fathali and A. Filiatrault, 6/6/07 (PB2008-105144).

MCEER-07-0008 "Seismic Vulnerability of Timber Bridges and Timber Substructures," by A.A. Sharma, J.B. Mander, I.M. Friedland and D.R. Allicock, 6/7/07 (PB2008-105145).

MCEER-07-0009 "Experimental and Analytical Study of the XY-Friction Pendulum (XY-FP) Bearing for Bridge Applications," by C.C. Marin-Artieda, A.S. Whittaker and M.C. Constantinou, 6/7/07 (PB2008-105191).

MCEER-07-0010 "Proceedings of the PRC-US Earthquake Engineering Forum for Young Researchers," Edited by G.C. Lee and X.Z. Qi, 6/8/07 (PB2008-500058).

MCEER-07-0011 "Design Recommendations for Perforated Steel Plate Shear Walls," by R. Purba and M. Bruneau, 6/18/07, (PB2008-105192).

MCEER-07-0012 "Performance of Seismic Isolation Hardware Under Service and Seismic Loading," by M.C. Constantinou, A.S. Whittaker, Y. Kalpakidis, D.M. Fenz and G.P. Warn, 8/27/07, (PB2008-105193).

MCEER-07-0013 "Experimental Evaluation of the Seismic Performance of Hospital Piping Subassemblies," by E.R. Goodwin, E. Maragakis and A.M. Itani, 9/4/07, (PB2008-105194).

MCEER-07-0014 "A Simulation Model of Urban Disaster Recovery and Resilience: Implementation for the 1994 Northridge Earthquake," by S. Miles and S.E. Chang, 9/7/07, (PB2008-106426).

MCEER-07-0015 "Statistical and Mechanistic Fragility Analysis of Concrete Bridges," by M. Shinozuka, S. Banerjee and S-H. Kim, 9/10/07, (PB2008-106427).

MCEER-07-0016 "Three-Dimensional Modeling of Inelastic Buckling in Frame Structures," by M. Schachter and AM. Reinhorn, 9/13/07, (PB2008-108125).

MCEER-07-0017 "Modeling of Seismic Wave Scattering on Pile Groups and Caissons," by I. Po Lam, H. Law and C.T. Yang, 9/17/07 (PB2008-108150).

MCEER-07-0018 "Bridge Foundations: Modeling Large Pile Groups and Caissons for Seismic Design," by I. Po Lam, H. Law and G.R. Martin (Coordinating Author), 12/1/07 (PB2008-111190).

MCEER-07-0019 "Principles and Performance of Roller Seismic Isolation Bearings for Highway Bridges," by G.C. Lee, Y.C. Ou, Z. Liang, T.C. Niu and J. Song, 12/10/07 (PB2009-110466).

MCEER-07-0020 "Centrifuge Modeling of Permeability and Pinning Reinforcement Effects on Pile Response to Lateral Spreading," by L.L Gonzalez-Lagos, T. Abdoun and R. Dobry, 12/10/07 (PB2008-111191).

MCEER-07-0021 "Damage to the Highway System from the Pisco, Perú Earthquake of August 15, 2007," by J.S. O'Connor, L. Mesa and M. Nykamp, 12/10/07, (PB2008-108126).

MCEER-07-0022 "Experimental Seismic Performance Evaluation of Isolation/Restraint Systems for Mechanical Equipment – Part 2: Light Equipment Study," by S. Fathali and A. Filiatrault, 12/13/07 (PB2008-111192).

MCEER-07-0023 "Fragility Considerations in Highway Bridge Design," by M. Shinozuka, S. Banerjee and S.H. Kim, 12/14/07 (PB2008-111193).

MCEER-07-0024 "Performance Estimates for Seismically Isolated Bridges," by G.P. Warn and A.S. Whittaker, 12/30/07 (PB2008-112230).

MCEER-08-0001 "Seismic Performance of Steel Girder Bridge Superstructures with Conventional Cross Frames," by L.P. Carden, A.M. Itani and I.G. Buckle, 1/7/08, (PB2008-112231).

MCEER-08-0002 "Seismic Performance of Steel Girder Bridge Superstructures with Ductile End Cross Frames with Seismic Isolators," by L.P. Carden, A.M. Itani and I.G. Buckle, 1/7/08 (PB2008-112232).

MCEER-08-0003 "Analytical and Experimental Investigation of a Controlled Rocking Approach for Seismic Protection of Bridge Steel Truss Piers," by M. Pollino and M. Bruneau, 1/21/08 (PB2008-112233).

MCEER-08-0004 "Linking Lifeline Infrastructure Performance and Community Disaster Resilience: Models and Multi-Stakeholder Processes," by S.E. Chang, C. Pasion, K. Tatebe and R. Ahmad, 3/3/08 (PB2008-112234).

MCEER-08-0005 "Modal Analysis of Generally Damped Linear Structures Subjected to Seismic Excitations," by J. Song, Y-L. Chu, Z. Liang and G.C. Lee, 3/4/08 (PB2009-102311).

MCEER-08-0006 "System Performance Under Multi-Hazard Environments," by C. Kafali and M. Grigoriu, 3/4/08 (PB2008-112235).

MCEER-08-0007 "Mechanical Behavior of Multi-Spherical Sliding Bearings," by D.M. Fenz and M.C. Constantinou, 3/6/08 (PB2008-112236).

MCEER-08-0008 "Post-Earthquake Restoration of the Los Angeles Water Supply System," by T.H.P. Tabucchi and R.A. Davidson, 3/7/08 (PB2008-112237).

MCEER-08-0009 "Fragility Analysis of Water Supply Systems," by A. Jacobson and M. Grigoriu, 3/10/08 (PB2009-105545).

MCEER-08-0010 "Experimental Investigation of Full-Scale Two-Story Steel Plate Shear Walls with Reduced Beam Section Connections," by B. Qu, M. Bruneau, C-H. Lin and K-C. Tsai, 3/17/08 (PB2009-106368).

MCEER-08-0011 "Seismic Evaluation and Rehabilitation of Critical Components of Electrical Power Systems," S. Ersoy, B. Feizi, A. Ashrafi and M. Ala Saadeghvaziri, 3/17/08 (PB2009-105546).

MCEER-08-0012 "Seismic Behavior and Design of Boundary Frame Members of Steel Plate Shear Walls," by B. Qu and M. Bruneau, 4/26/08 . (PB2009-106744).

MCEER-08-0013 "Development and Appraisal of a Numerical Cyclic Loading Protocol for Quantifying Building System Performance," by A. Filiatrault, A. Wanitkorkul and M. Constantinou, 4/27/08 (PB2009-107906).

MCEER-08-0014 "Structural and Nonstructural Earthquake Design: The Challenge of Integrating Specialty Areas in Designing Complex, Critical Facilities," by W.J. Petak and D.J. Alesch, 4/30/08 (PB2009-107907).

MCEER-08-0015 "Seismic Performance Evaluation of Water Systems," by Y. Wang and T.D. O'Rourke, 5/5/08 (PB2009-107908).

MCEER-08-0016 "Seismic Response Modeling of Water Supply Systems," by P. Shi and T.D. O'Rourke, 5/5/08 (PB2009-107910).

MCEER-08-0017 "Numerical and Experimental Studies of Self-Centering Post-Tensioned Steel Frames," by D. Wang and A. Filiatrault, 5/12/08 (PB2009-110479).

MCEER-08-0018 "Development, Implementation and Verification of Dynamic Analysis Models for Multi-Spherical Sliding Bearings," by D.M. Fenz and M.C. Constantinou, 8/15/08 (PB2009-107911).

MCEER-08-0019 "Performance Assessment of Conventional and Base Isolated Nuclear Power Plants for Earthquake Blast Loadings," by Y.N. Huang, A.S. Whittaker and N. Luco, 10/28/08 (PB2009-107912).

MCEER-08-0020 "Remote Sensing for Resilient Multi-Hazard Disaster Response – Volume I: Introduction to Damage Assessment Methodologies," by B.J. Adams and R.T. Eguchi, 11/17/08 (PB2010-102695).

MCEER-08-0021 "Remote Sensing for Resilient Multi-Hazard Disaster Response – Volume II: Counting the Number of Collapsed Buildings Using an Object-Oriented Analysis: Case Study of the 2003 Bam Earthquake," by L. Gusella, C.K. Huyck and B.J. Adams, 11/17/08 (PB2010-100925).

MCEER-08-0022 "Remote Sensing for Resilient Multi-Hazard Disaster Response – Volume III: Multi-Sensor Image Fusion Techniques for Robust Neighborhood-Scale Urban Damage Assessment," by B.J. Adams and A. McMillan, 11/17/08 (PB2010-100926).

MCEER-08-0023 "Remote Sensing for Resilient Multi-Hazard Disaster Response – Volume IV: A Study of Multi-Temporal and Multi-Resolution SAR Imagery for Post-Katrina Flood Monitoring in New Orleans," by A. McMillan, J.G. Morley, B.J. Adams and S. Chesworth, 11/17/08 (PB2010-100927).

MCEER-08-0024 "Remote Sensing for Resilient Multi-Hazard Disaster Response – Volume V: Integration of Remote Sensing Imagery and VIEWS^{TM} Field Data for Post-Hurricane Charley Building Damage Assessment," by J.A. Womble, K. Mehta and B.J. Adams, 11/17/08 (PB2009-115532).

MCEER-08-0025 "Building Inventory Compilation for Disaster Management: Application of Remote Sensing and Statistical Modeling," by P. Sarabandi, A.S. Kiremidjian, R.T. Eguchi and B. J. Adams, 11/20/08 (PB2009-110484).

MCEER-08-0026 "New Experimental Capabilities and Loading Protocols for Seismic Qualification and Fragility Assessment of Nonstructural Systems," by R. Retamales, G. Mosqueda, A. Filiatrault and A. Reinhorn, 11/24/08 (PB2009-110485).

MCEER-08-0027 "Effects of Heating and Load History on the Behavior of Lead-Rubber Bearings," by I.V. Kalpakidis and M.C. Constantinou, 12/1/08 (PB2009-115533).

MCEER-08-0028 "Experimental and Analytical Investigation of Blast Performance of Seismically Resistant Bridge Piers," by S.Fujikura and M. Bruneau, 12/8/08 (PB2009-115534).

MCEER-08-0029 "Evolutionary Methodology for Aseismic Decision Support," by Y. Hu and G. Dargush, 12/15/08.

MCEER-08-0030 "Development of a Steel Plate Shear Wall Bridge Pier System Conceived from a Multi-Hazard Perspective," by D. Keller and M. Bruneau, 12/19/08 (PB2010-102696).

MCEER-09-0001 "Modal Analysis of Arbitrarily Damped Three-Dimensional Linear Structures Subjected to Seismic Excitations," by Y.L. Chu, J. Song and G.C. Lee, 1/31/09 (PB2010-100922).

MCEER-09-0002 "Air-Blast Effects on Structural Shapes," by G. Ballantyne, A.S. Whittaker, A.J. Aref and G.F. Dargush, 2/2/09 (PB2010-102697).

MCEER-09-0003 "Water Supply Performance During Earthquakes and Extreme Events," by A.L. Bonneau and T.D. O'Rourke, 2/16/09 (PB2010-100923).

MCEER-09-0004 "Generalized Linear (Mixed) Models of Post-Earthquake Ignitions," by R.A. Davidson, 7/20/09 (PB2010-102698).

MCEER-09-0005 "Seismic Testing of a Full-Scale Two-Story Light-Frame Wood Building: NEESWood Benchmark Test," by I.P. Christovasilis, A. Filiatrault and A. Wanitkorkul, 7/22/09 (PB2012-102401).

MCEER-09-0006 "IDARC2D Version 7.0: A Program for the Inelastic Damage Analysis of Structures," by A.M. Reinhorn, H. Roh, M. Sivaselvan, S.K. Kunnath, R.E. Valles, A. Madan, C. Li, R. Lobo and Y.J. Park, 7/28/09 (PB2010-103199).

MCEER-09-0007 "Enhancements to Hospital Resiliency: Improving Emergency Planning for and Response to Hurricanes," by D.B. Hess and L.A. Arendt, 7/30/09 (PB2010-100924).

MCEER-09-0008 "Assessment of Base-Isolated Nuclear Structures for Design and Beyond-Design Basis Earthquake Shaking," by Y.N. Huang, A.S. Whittaker, R.P. Kennedy and R.L. Mayes, 8/20/09 (PB2010-102699).

MCEER-09-0009 "Quantification of Disaster Resilience of Health Care Facilities," by G.P. Cimellaro, C. Fumo, A.M Reinhorn and M. Bruneau, 9/14/09 (PB2010-105384).

MCEER-09-0010 "Performance-Based Assessment and Design of Squat Reinforced Concrete Shear Walls," by C.K. Gulec and A.S. Whittaker, 9/15/09 (PB2010-102700).

MCEER-09-0011 "Proceedings of the Fourth US-Taiwan Bridge Engineering Workshop," edited by W.P. Yen, J.J. Shen, T.M. Lee and R.B. Zheng, 10/27/09 (PB2010-500009).

MCEER-09-0012 "Proceedings of the Special International Workshop on Seismic Connection Details for Segmental Bridge Construction," edited by W. Phillip Yen and George C. Lee, 12/21/09 (PB2012-102402).

MCEER-10-0001 "Direct Displacement Procedure for Performance-Based Seismic Design of Multistory Woodframe Structures," by W. Pang and D. Rosowsky, 4/26/10 (PB2012-102403).

MCEER-10-0002 "Simplified Direct Displacement Design of Six-Story NEESWood Capstone Building and Pre-Test Seismic Performance Assessment," by W. Pang, D. Rosowsky, J. van de Lindt and S. Pei, 5/28/10 (PB2012-102404).

MCEER-10-0003 "Integration of Seismic Protection Systems in Performance-Based Seismic Design of Woodframed Structures," by J.K. Shinde and M.D. Symans, 6/18/10 (PB2012-102405).

MCEER-10-0004 "Modeling and Seismic Evaluation of Nonstructural Components: Testing Frame for Experimental Evaluation of Suspended Ceiling Systems," by A.M. Reinhorn, K.P. Ryu and G. Maddaloni, 6/30/10 (PB2012-102406).

MCEER-10-0005 "Analytical Development and Experimental Validation of a Structural-Fuse Bridge Pier Concept," by S. El-Bahey and M. Bruneau, 10/1/10 (PB2012-102407).

MCEER-10-0006 "A Framework for Defining and Measuring Resilience at the Community Scale: The PEOPLES Resilience Framework," by C.S. Renschler, A.E. Frazier, L.A. Arendt, G.P. Cimellaro, A.M. Reinhorn and M. Bruneau, 10/8/10 (PB2012-102408).

MCEER-10-0007 "Impact of Horizontal Boundary Elements Design on Seismic Behavior of Steel Plate Shear Walls," by R. Purba and M. Bruneau, 11/14/10 (PB2012-102409).

MCEER-10-0008 "Seismic Testing of a Full-Scale Mid-Rise Building: The NEESWood Capstone Test," by S. Pei, J.W. van de Lindt, S.E. Pryor, H. Shimizu, H. Isoda and D.R. Rammer, 12/1/10 (PB2012-102410).

MCEER-10-0009 "Modeling the Effects of Detonations of High Explosives to Inform Blast-Resistant Design," by P. Sherkar, A.S. Whittaker and A.J. Aref, 12/1/10 (PB2012-102411).

MCEER-10-0010 "L'Aquila Earthquake of April 6, 2009 in Italy: Rebuilding a Resilient City to Withstand Multiple Hazards," by G.P. Cimellaro, I.P. Christovasilis, A.M. Reinhorn, A. De Stefano and T. Kirova, 12/29/10.

MCEER-11-0001 "Numerical and Experimental Investigation of the Seismic Response of Light-Frame Wood Structures," by I.P. Christovasilis and A. Filiatrault, 8/8/11 (PB2012-102412).

MCEER-11-0002 "Seismic Design and Analysis of a Precast Segmental Concrete Bridge Model," by M. Anagnostopoulou, A. Filiatrault and A. Aref, 9/15/11.

MCEER-11-0003 'Proceedings of the Workshop on Improving Earthquake Response of Substation Equipment," Edited by A.M. Reinhorn, 9/19/11 (PB2012-102413).

MCEER-11-0004 "LRFD-Based Analysis and Design Procedures for Bridge Bearings and Seismic Isolators," by M.C. Constantinou, I. Kalpakidis, A. Filiatrault and R.A. Ecker Lay, 9/26/11.

MCEER-11-0005 "Experimental Seismic Evaluation, Model Parameterization, and Effects of Cold-Formed Steel-Framed Gypsum Partition Walls on the Seismic Performance of an Essential Facility," by R. Davies, R. Retamales, G. Mosqueda and A. Filiatrault, 10/12/11.

MCEER-11-0006 "Modeling and Seismic Performance Evaluation of High Voltage Transformers and Bushings," by A.M. Reinhorn, K. Oikonomou, H. Roh, A. Schiff and L. Kempner, Jr., 10/3/11.

MCEER-11-0007 "Extreme Load Combinations: A Survey of State Bridge Engineers," by G.C. Lee, Z. Liang, J.J. Shen and J.S. O'Connor, 10/14/11.

MCEER-12-0001 "Simplified Analysis Procedures in Support of Performance Based Seismic Design," by Y.N. Huang and A.S. Whittaker.

MCEER-12-0002 "Seismic Protection of Electrical Transformer Bushing Systems by Stiffening Techniques," by M. Koliou, A. Filiatrault, A.M. Reinhorn and N. Oliveto, 6/1/12.

MCEER-12-0003 "Post-Earthquake Bridge Inspection Guidelines," by J.S. O'Connor and S. Alampalli, 6/8/12.

MCEER-12-0004 "Integrated Design Methodology for Isolated Floor Systems in Single-Degree-of-Freedom Structural Fuse Systems," by S. Cui, M. Bruneau and M.C. Constantinou, 6/13/12.

MCEER-12-0005 "Characterizing the Rotational Components of Earthquake Ground Motion," by D. Basu, A.S. Whittaker and M.C. Constantinou, 6/15/12.

MCEER-12-0006 "Bayesian Fragility for Nonstructural Systems," by C.H. Lee and M.D. Grigoriu, 9/12/12.

MCEER-12-0007 "A Numerical Model for Capturing the In-Plane Seismic Response of Interior Metal Stud Partition Walls," by R.L. Wood and T.C. Hutchinson, 9/12/12.

MCEER-12-0008 "Assessment of Floor Accelerations in Yielding Buildings," by J.D. Wieser, G. Pekcan, A.E. Zaghi, A.M. Itani and E. Maragakis, 10/5/12.

MCEER-13-0001 "Experimental Seismic Study of Pressurized Fire Sprinkler Piping Systems," by Y. Tian, A. Filiatrault and G. Mosqueda, 4/8/13.

MCEER-13-0002 "Enhancing Resource Coordination for Multi-Modal Evacuation Planning," by D.B. Hess, B.W. Conley and C.M. Farrell, 2/8/13.

MCEER-13-0003 "Seismic Response of Base Isolated Buildings Considering Pounding to Moat Walls," by A. Masroor and G. Mosqueda, 2/26/13.

MCEER-13-0004 "Seismic Response Control of Structures Using a Novel Adaptive Passive Negative Stiffness Device," by D.T.R. Pasala, A.A. Sarlis, S. Nagarajaiah, A.M. Reinhorn, M.C. Constantinou and D.P. Taylor, 6/10/13.

MCEER-13-0005 "Negative Stiffness Device for Seismic Protection of Structures," by A.A. Sarlis, D.T.R. Pasala, M.C. Constantinou, A.M. Reinhorn, S. Nagarajaiah and D.P. Taylor, 6/12/13.

MCEER-13-0006 "Emilia Earthquake of May 20, 2012 in Northern Italy: Rebuilding a Resilient Community to Withstand Multiple Hazards," by G.P. Cimellaro, M. Chiriatti, A.M. Reinhorn and L. Tirca, June 30, 2013.

MCEER-13-0007 "Precast Concrete Segmental Components and Systems for Accelerated Bridge Construction in Seismic Regions," by A.J. Aref, G.C. Lee, Y.C. Ou and P. Sideris, with contributions from K.C. Chang, S. Chen, A. Filiatrault and Y. Zhou, June 13, 2013.

MCEER-13-0008 "A Study of U.S. Bridge Failures (1980-2012)," by G.C. Lee, S.B. Mohan, C. Huang and B.N. Fard, June 15, 2013.

MCEER-13-0009 "Development of a Database Framework for Modeling Damaged Bridges," by G.C. Lee, J.C. Qi and C. Huang, June 16, 2013.

MCEER-13-0010 “Model of Triple Friction Pendulum Bearing for General Geometric and Frictional Parameters and for Uplift Conditions,” by A.A. Sarlis and M.C. Constantinou, July 1, 2013.

MCEER-13-0011 “Shake Table Testing of Triple Friction Pendulum Isolators under Extreme Conditions,” by A.A. Sarlis, M.C. Constantinou and A.M. Reinhorn, July 2, 2013.

MCEER-13-0012 “Theoretical Framework for the Development of MH-LRFD,” by G.C. Lee (coordinating author), H.A Capers, Jr., C. Huang, J.M. Kulicki, Z. Liang, T. Murphy, J.J.D. Shen, M. Shinozuka and P.W.H. Yen, July 31, 2013.

MCEER-13-0013 “Seismic Protection of Highway Bridges with Negative Stiffness Devices,” by N.K.A. Attary, M.D. Symans, S. Nagarajaiah, A.M. Reinhorn, M.C. Constantinou, A.A. Sarlis, D.T.R. Pasala, and D.P. Taylor, September 3, 2014.

MCEER-14-0001 “Simplified Seismic Collapse Capacity-Based Evaluation and Design of Frame Buildings with and without Supplemental Damping Systems,” by M. Hamidia, A. Filiatrault, and A. Aref, May 19, 2014.

MCEER-14-0002 “Comprehensive Analytical Seismic Fragility of Fire Sprinkler Piping Systems,” by Siavash Soroushian, Emmanuel “Manos” Maragakis, Arash E. Zaghi, Alicia Echevarria, Yuan Tian and Andre Filiatrault, August 26, 2014.

MCEER-14-0003 “Hybrid Simulation of the Seismic Response of a Steel Moment Frame Building Structure through Collapse,” by M. Del Carpio Ramos, G. Mosqueda and D.G. Lignos, October 30, 2014.

MCEER-14-0004 “Blast and Seismic Resistant Concrete-Filled Double Skin Tubes and Modified Steel Jacketed Bridge Columns,” by P.P. Fouche and M. Bruneau, June 30, 2015.

MCEER-14-0005 “Seismic Performance of Steel Plate Shear Walls Considering Various Design Approaches,” by R. Purba and M. Bruneau, October 31, 2014.

MCEER-14-0006 “Air-Blast Effects on Civil Structures,” by Jinwon Shin, Andrew S. Whittaker, Amjad J. Aref and David Cormie, October 30, 2014.

MCEER-14-0007 “Seismic Performance Evaluation of Precast Girders with Field-Cast Ultra High Performance Concrete (UHPC) Connections,” by G.C. Lee, C. Huang, J. Song, and J. S. O’Connor, July 31, 2014.

MCEER-14-0008 “Post-Earthquake Fire Resistance of Ductile Concrete-Filled Double-Skin Tube Columns,” by Reza Imani, Gilberto Mosqueda and Michel Bruneau, December 1, 2014.

MCEER-14-0009 “Cyclic Inelastic Behavior of Concrete Filled Sandwich Panel Walls Subjected to In-Plane Flexure,” by Y. Alzeni and M. Bruneau, December 19, 2014.

MCEER-14-0010 “Analytical and Experimental Investigation of Self-Centering Steel Plate Shear Walls,” by D.M. Dowden and M. Bruneau, December 19, 2014.

MCEER-15-0001 “Seismic Analysis of Multi-story Unreinforced Masonry Buildings with Flexible Diaphragms,” by J. Aleman, G. Mosqueda and A.S. Whittaker, June 12, 2015.

MCEER-15-0002 “Site Response, Soil-Structure Interaction and Structure-Soil-Structure Interaction for Performance Assessment of Buildings and Nuclear Structures,” by C. Bolisetti and A.S. Whittaker, June 15, 2015.

MCEER-15-0003 “Stress Wave Attenuation in Solids for Mitigating Impulsive Loadings,” by R. Rafiee-Dehkharghani, A.J. Aref and G. Dargush, August 15, 2015.

MCEER-15-0004 “Computational, Analytical, and Experimental Modeling of Masonry Structures,” by K.M. Dolatshahi and A.J. Aref, November 16, 2015.

MCEER-15-0005 “Property Modification Factors for Seismic Isolators: Design Guidance for Buildings,” by W.J. McVitty and M.C. Constantinou, June 30, 2015.

MCEER-15-0006 "Seismic Isolation of Nuclear Power Plants using Sliding Bearings," by Manish Kumar, Andrew S. Whittaker and Michael C. Constantinou, December 27, 2015.

MCEER-15-0007 "Quintuple Friction Pendulum Isolator Behavior, Modeling and Validation," by Donghun Lee and Michael C. Constantinou, December 28, 2015.

MCEER-15-0008 "Seismic Isolation of Nuclear Power Plants using Elastomeric Bearings," by Manish Kumar, Andrew S. Whittaker and Michael C. Constantinou, December 29, 2015.

MCEER-16-0001 "Experimental, Numerical and Analytical Studies on the Seismic Response of Steel-Plate Concrete (SC) Composite Shear Walls," by Siamak Epackachi and Andrew S. Whittaker, June 15, 2016.

MCEER-16-0002 "Seismic Demand in Columns of Steel Frames," by Lisa Shrestha and Michel Bruneau, June 17, 2016.

MCEER-16-0003 "Development and Evaluation of Procedures for Analysis and Design of Buildings with Fluidic Self-Centering Systems" by Shoma Kitayama and Michael C. Constantinou, July 21, 2016.

MCEER-16-0004 "Real Time Control of Shake Tables for Nonlinear Hysteretic Systems," by Ki Pung Ryu and Andrei M. Reinhorn, October 22, 2016.

MCEER-16-0006 "Seismic Isolation of High Voltage Electrical Power Transformers," by Kostis Oikonomou, Michael C. Constantinou, Andrei M. Reinhorn and Leon Kemper, Jr., November 2, 2016.

MCEER-16-0007 "Open Space Damping System Theory and Experimental Validation," by Erkan Polat and Michael C. Constantinou, December 13, 2016.

MCEER-16-0008 "Seismic Response of Low Aspect Ratio Reinforced Concrete Walls for Buildings and Safety-Related Nuclear Applications," by Bismarck N. Luna and Andrew S. Whittaker.

MCEER-16-0009 "Buckling Restrained Braces Applications for Superstructure and Substructure Protection in Bridges," by Xiaone Wei and Michel Bruneau, December 28, 2016.

MCEER-16-0010 "Procedures and Results of Assessment of Seismic Performance of Seismically Isolated Electrical Transformers with Due Consideration for Vertical Isolation and Vertical Ground Motion Effects," by Shoma Kitayama, Michael C. Constantinou and Donghun Lee, December 31, 2016.

MCEER-17-0001 "Diagonal Tension Field Inclination Angle in Steel Plate Shear Walls," by Yushan Fu, Fangbo Wang and Michel Bruneau, February 10, 2017.

MCEER-17-0002 "Behavior of Steel Plate Shear Walls Subjected to Long Duration Earthquakes," by Ramla Qureshi and Michel Bruneau, September 1, 2017.

MCEER-17-0003 "Response of Steel-plate Concrete (SC) Wall Piers to Combined In-plane and Out-of-plane Seismic Loadings," by Brian Terranova, Andrew S. Whittaker, Siamak Epackachi and Nebojsa Orbovic, July 17, 2017.

MCEER-17-0004 "Design of Reinforced Concrete Panels for Wind-borne Missile Impact," by Brian Terranova, Andrew S. Whittaker and Len Schwer, July 18, 2017.

MCEER-17-0005 "A Simple Strategy for Dynamic Substructuring and its Application to Soil-Foundation-Structure Interaction," by Aikaterini Stefanaki and Metttupalayam V. Sivaselvan, December 15, 2017.

MCEER-17-0006 "Dynamics of Cable Structures: Modeling and Applications," by Nicholas D. Oliveto and Mettupalayam V. Sivaselvan, December 1, 2017.

MCEER-17-0007 "Development and Validation of a Combined Horizontal-Vertical Seismic Isolation System for High-Voltage-Power Transformers," by Donghun Lee and Michael C. Constantinou, November 3, 2017.

MCEER-18-0001 "Reduction of Seismic Acceleration Parameters for Temporary Bridge Design," by Conor Stucki and Michel Bruneau, March 22, 2018.

MCEER-18-0002 "Seismic Response of Low Aspect Ratio Reinforced Concrete Walls," by Bismarck N. Luna, Jonathan P. Rivera, Siamak Epackachi and Andrew S. Whittaker, April 21, 2018.

MCEER-18-0003 "Seismic Damage Assessment of Low Aspect Ratio Reinforced Concrete Shear Walls," by Jonathan P. Rivera, Bismarck N. Luna and Andrew S. Whittaker, April 16, 2018.

MCEER-18-0004 "Seismic Performance Assessment of Seismically Isolated Buildings Designed by the Procedures of ASCE/SEI 7," by Shoma Kitayama and Michael C. Constantinou, April 14, 2018.

MCEER-19-0001 MCEER-19-0001 "Development and Validation of a Seismic Isolation System for Lightweight Residential Construction," by Huseyin Cisalar and Michael C. Constantinou, March 24, 2019.

MCEER-20-0001 "A Multiscale Study of Reinforced Concrete Shear Walls Subjected to Elevated Temperatures," by Alok Deshpande and Andrew S. Whittaker, June 26, 2020.

MCEER-20-0002 "Further Results on the Assessment of Performance of Seismically Isolated Electrical Transformers," by Shoma Kitayama and Michael C. Constantinou, June 30, 2020.

MCEER-20-0003 "Analytical and Numerical Studies of Seismic Fluid-Structure Interaction in Liquid-Filled Vessels," by Ching-Ching Yu and Andrew S. Whittaker, August 1, 2020.

MCEER-22-0001 "Modeling Triple Friction Pendulum Bearings in Program OpenSees Including Frictional Heating Effects," by Hyun-Myung Kim and Michael C. Constantinou, April 18, 2022.

MCEER-22-0002 "Physical and Numerical Simulations of Seismic Fluid-Structure Interaction in Advanced Nuclear Reactors," by Faizan Ul Haq Mir, Ching-Ching Yu, Andrew S. Whittaker and Michael C. Constantinou, July 8, 2022.

MCEER-22-0003 "Impedance-Matching Control Design for Shake-Table Testing and Model-in-the-Loop Simulations," by Sai Sharath Parsi, Mettupalayam V. Sivaselvan and Andrew S. Whittaker, September 30, 2022.

MCEER: Earthquake Engineering to Extreme Events

University at Buffalo, The State University of New York
133A Ketter Hall | Buffalo, NY 14260
mceer@buffalo.edu; buffalo.edu/mceer

ISSN 1520-295X